NASA-CR-201528

Title of the Grant: Applications of Quantum Theory of Atomic and
Molecular Scattering to Problems in
Hypersonic Flow

Type of Report: Final Report

Principal Invest.: F. Bary Malik

Period Report: December 17, 1993-December 16, 1995

Name and Address
of Institution: Southern Illinois University at Carbondale
Carbondale, Illinois 62901-4709

Grant Number: NAG 1 1563

The grant period was for two years: from January 1994 to
December 1995. The grant, basically, supported the salary of a
senior research associate and provided some travel money to
attend conference and 25% salary of a graduate student for one
year. No salary money was allocated to the principal
investigator (PI). Dr. Ram Tripathi was selected to be the
senior research associate. Although the grant was initially
approved for three years subject to availability of funds, it was
discontinued after two years because of (a) a lack of funds and
(b) reorganization within NASA, which eliminated the branch and
the research program.

Despite the short duration, the grant has been very
productive. There have been five following short communications:
as shown in attachment 1.

1. Bose condensation of nuclei in heavy-ion collision: finite system effects by L.W. Townsend and R.K. Tripathi, Bull. Am. Phys. Soc. 39, 1395 (1994).

2. Observation of Bose condensation of nuclei in heavy-ion collision by R.K. Tripathi and L.W. Townsend, Bull. Am. Phys. Soc. 39, 1395 (1994).

3. Evaporation of strange particles in anti-proton nucleus reactions by F. B. Malik, L.W. Townsend and R.K. Tripathi, Bull.Am. Phys.Soc. 39, 1426 (1994).

4. Nuclear fragmentation of heavy-ion by protons, by L.W. Townsend, and R.K. Tripathi, Bull.Am.Phys.Soc. 39, 1426 1(1994).

5. On nucleon removal cross sections in light and medium nuclei by R.K. Tripathi, J.W. Wilson, F.A. Cucinotta, J.L. Shinn, F.F. Badavi and S.Y. Chun, Bull.Am.Phys.Soc. 40, 1632(1995).

In addition, eleven full length articles have appeared as publications or reports or been submitted for publication. These are listed below and attached in Attachment 2.

1. Accurate universal parameterization of absorption cross section by R.K. Tripathi,. F.A. Cucinotta and J.W. Wilson, accepted for publication in N.I.M-B (1996).

2. Universal parameterization of absorption cross sections by R.K., Tripathi, F.A. Cucinotta and J.W. Wilson, NASA Report: NASA-TP-17580, (1996).

3. Emission of light fragments as an indicator of equilibrated populations in nuclear collisions by R.K. Tripathi and L.W. Townsend (submitted for publication 1996).

4. Transport of light ions in matter by J.W. Wilson, F.A. Cucinotta, H. Tai, J.L. Shinn, S.Y. Chun, R.K. Tripathi and L. Sihver (submitted for publication).

5. Bose-Einstein condensation of nuclei by L.W. Townsend and R.K. Tripathi (Accepted for publication in Condensed Matter Theories Vol. 11, 1996).

6. Theoretical model of HZE particle fragmentation by hydrogen targets by L.W. Townsend, F.A. Cucinotta, R. Bagga and R. K. Tripathi, Adv. Space Research 17, 109 (1996).

7. Liquid drop model considerations in HZE particle fragmentation by hydrogen by L.W. Townsend, R.K. Tripathi, F.A. Cucinotta, and R. Bagga (submitted for publication, 1996).

8. NUCFRGZ: An evaluation of the semi-empirical nuclear fragmentation database by J.W. Wilson, R.K. Tripathi, F.A. Cucinotta, J.L. Shinn, F. F. Badavi, S.Y. Chun, J.W. Norbury, C. J. Zeitlin, H. Heilbronn and J. Miller. NASA Technical Report 3533.

9. Atomic electron correlation and particle and anti-particle induced single and double-ionization by T. Das and F. B. Malik (Accepted for publication in Condensed Matter Theories, vol 11 (1996)).

10. On the ionization of He by proton and anti-proton: I. Single ionization by T. Das and F. B Malik (submitted for publication, 1996).

11. On the ionization of He by proton and anti-proton: II. Double ionization by T. Das and F. B. Malik (submitted for publication, 1996).

The research done under the grant is recognized to be important and Dr. Townsend, one of R.K. Tripathi's collaborators and F. B. Malik were invited to present their research done under the grant in plenary sessions at XIX International Workshop on Condensed Matter Theories held in Caracas, Venezuela in June 1995.

Attachment 1
Short Articles

of grid points in proportion to dependent variable. The three-dimensional results presented are for ultra relativistic condition, with a steep density gradient in initial density distribution. An elliptic generation system was solved by SOR iteration technique, to control grid skewness, by smoothing grid. Results of this simulation were compared with the available simulations.

14:30
AE 6 Kaon Flow as a Probe of Kaon Mean-Field Potential in Dense Matter G. Q. LI, B. A. LI and C. M. KO, Texas A&M U.*–Kaon flow in heavy-ion collisions is studied in the relativistic transport model and is found to be sensitive to the kaon mean-field potential in dense matter. With an attractive kaon mean-field potential, kaon flow is in the same direction as the nucleon flow, while with a repulsive mean-field potential, it is opposite to that of nucleons. Kaon flow in heavy-ion collisions is thus a useful observable for studying kaon properties in dense matter.

*Supported by NSF Grant No. 9212209 and the Robert A. Welch Foundation Grant No. A-1110

14:42
AE 7 Bose Condensation of Nuclei in Heavy Ion Collisions: Finite System Effects. L. W. TOWNSEND, NASA Langley Research Center, and R. K. TRIPATHI, Southern Illinois University*. —In previous work the possibility of Bose condensation of nuclei in heavy ion collisions was demonstrated[1] by using quantum statistics to model an equilibrated system consisting of a finite number of nucleons. The existence of a concomitant total phase transition, however, was affected by the relatively small numbers of nucleons involved in the collision (~ 80). In this work we investigate the effects of finite nucleon numbers on the observation of a possible total phase transition.

*Supported by NASA Grant.

[1] R. K. Tripathi and L. W. Townsend, Phys. Rev. C (1994, in press)

14:54
AE 8 S-Wave π-π Correlations in Cold Nuclear Matter. R. RAPP, Z. AOUISSAT, J. WAMBACH, G. CHANFRAY[1], P. SCHUCK[2], KFA Jülich, [1]IPN Lyon, [2]ISN Grenoble. — Starting from a standard treatment of the single pion selfenergy in terms of particle-hole and Δ-hole Lindhard functions we examine π-π s-wave correlations in cold nuclear matter. When calculating the in-medium π-π T-matrix we take into account the full off-shell properties of the pion selfenergy. The latter enters the scattering equation of Lippmann-Schwinger type through the uncorrelated 2π propagator of the intermediate state. Using a well tested phenomenological π-π interaction (the Jülich meson exchange model) we find a π-π pairing instability in slightly compressed nuclear matter ($\rho \approx 1.3\rho_0$). This model, however, does not respect constraints from chiral symmetry which are known to govern the near threshold behaviour of π-π scattering. Additionally imposing chiral constraints on the Jülich model in fact inhibits the instability leading to more moderate effects in the subthreshold region of the in-medium scattering amplitude.

15:06
AE 9 Neutron-Neutron Correlation Functions. C. M. Mader, R. S. Bennink and P. A. DeYoung, Hope College - The structure of two-proton correlation functions measured at small relative angles is dominated by the ^{2}He resonance peak. The height of this peak is then related to the size of the emitting system. In the two-neutron system, the Coulomb interaction is no longer a factor, and thus only the nuclear interaction and Pauli exclusion principle will play a role in the correlation function. It is expected that without a 2-neutron resonance, the correlation peak will shift to zero relative momentum and the source size will be determined by the width of the peak. We use the Koonin formalism to calculate the two-neutron correlation function. We explore the effects of the short-ranged nuclear potential as well as the parameterization of the neutron source and compare with recent experimental results for 210 MeV ^{16}O + ^{27}Al reactions.

15:18
AE 10 Observation of Bose Condensation of Nuclei in Heavy Ion Collisions: R. K. TRIPATHI, Southern Illinois University*, and L. W. TOWNSEND, NASA Langley Research Center –We have demonstrated[1] the presence of Bose condensed nuclei in heavy ion collisions. Here, we present results identifying the optimum conditions for their observations and focus on the ways of experimental verification of this new, exciting phenomenon.

*Supported by NASA Grant.

[1] R. K. Tripathi and L. W. Townsend, Phys. Rev. C 50, R1 (1994)

15:30
AE 11 Self-consistent momentum-dependence in hot and dense nuclear matter.* VINOD K. MISHRA and G. FAI, Kent State U., — The momentum dependence of the nucleon-nucleon interaction and of the mean field has important consequences for the properties of nuclear matter[1] and for collision simulations[2]. In particular, momentum-dependent interactions (such as the Momentum-Dependent Yukawa Interaction or MDYI[3]) lead to a stiffer equation of state (EOS) for nuclear matter than the corresponding momentum-independent ones. We have carried out in the past couple of years a study of local and global observables of hot and dense nuclear matter with the MDYI in successively better approximations. To complete this program we now examine the same observables in a self-consistent Hartree approximation which moves the project from a largely analytical domain to a purely numerical study. We use the earlier analytical approximations as input to the self-consistent calculation. We present results on the optical potential, the effective-mass, pressure (EOS), and the incompressibility for the Maxwell-Boltzmann distribution and compare them with the momentum-independent results and results of the earlier analytical approximations.
* Work supported by DOE Grant DE-FG02-86ER40251.

1. V.K. Mishra, et al, PRC47, 1519 (1993).
2. C. Gale, G.F. Bertsch and S. Das Gupta, PRC25, 1666 (1987).
3. G.F. Bertsch and S. Das Gupta, Phys. Rep. 160, 189 (1988).

15:42
AE 12
Toroidal Structures in BUU-Predictions for ^{36}Ar + ^{45}Sc at E/A=80 MeV viewed by Proton-Proton Correlations [†]
G.J. KUNDE, S.J. GAFF, C.K. GELBKE, T. GLASMACHER, D.O. HANDZY, L. MARTIN, W. BAUER, F.C.DAFFIN NSCL, Michigan State University.
For central (b=0 fm) collisions BUU-predictions suggest that a

In first order the use of a free NN t-matrix accounts for the short-range interaction between the projectile and a target nucleon. The effect of the nuclear medium can be interpreted as higher order correction and arises from the difference between the free NN propagator and the propagator in the nuclear medium. A formal framework consistent with a multiple scattering expansion has been constructed to include these contributions by using nuclear mean field potentials, which when applied to p-nucleus scattering gives a significant improvement of the elastic scattering observables at energies less than 200 MeV[†]. The influence of these medium modifications on the free NN t-matrix will be discussed in detail for different nuclei, together with its energy dependence between 100 and 800 MeV and its influence on the off-shell structure of the NN t-matrix.

* Supported by the U.S. Department of Energy.
† C.R. Chinn, Ch. Elster, R.M. Thaler, Phys. Rev. C48 (1993), 2956.

14:30
EB 6 Causality with Noncausal Potentials in the Many-Body Approach to Elastic Nuclear Scattering.* V.A. MADSEN, Oregon State University*- It has been shown by Bell and Squires [1] that the self-energy operator of the one-particle time ordered Green's function can be interpreted as the optical potential for nucleon-nucleus scattering. However, Mahaux and Sartor [2] have demonstrated that this time nonlocal potential is noncausal in the sense that $V(t,t') \neq 0$ for $t' > t$, where t is the current time and t', the nonlocal time. We shall demonstrate, making use of the retarded Green's function, that the time depe   Lippmann-Schwinger equation for the elastic scattering nevertheless causal.

* Research supported in part by the U.S. Department of Energy under Contract FG06-86ER40283 at Oregon State University.
1. J.S. Bell and E.J. Squires. Phys. Rev. Lett. 3, 96 (1959).
2. C. Mahaux and R. Sartor, Nuclear Physics, A530, 303 (1991).

14:42
EB 7 Validity of Sinha's local approximation to the exchange nonlocality. D. LUKASZEK and G.H. RAWITSCHER, Univ. of Connecticut.- - Several methods for replacing exchange nonlocalities with local equivalent potentials exist in the literature. In testing the validity of Sinha's method [1], Georgiev et al [2] suggested an improved version which includes the imaginary part of the local momentum. In the present study we apply their [2] version to the case of n-^{16}O scattering at several energies from 20 to 100 MeV. In a prior investigation [3], we obtained the n-^{16}O nonlocal potential by the folding of a complex g-matrix and now use the corresponding phase equivalent inversion potential [3] for comparison with Sinha's approximation. Results will be presented and discussed.

[1] B. Sinha, Phys. Reports 20 C, 1 (1975).
[2] B. L. Georgiev and R. S. Mackintosh, Phys. Lett. B 73, 250 (1978).
[3] G. H. Rawitscher, D. Lukaszek, R. S. Mackintosh, and S. G. Cooper, Phys. Rev. C 49, 1621 (1994).

14:54
EB 8 An Inverse Scattering Theory at a Fixed Energy for Klein-Gordon Equation. Z. F. SHEHADEH and F. Bary MALIK, Southern Illinois Univ. at Carbondale.---The inverse scattering formalism of Alam and Malik [1] at a fixed energy for potential scattering using

Schrödinger equation has been extended to scattering involving Klein-Gordon equation with a view of determining complex potentials for scattering of spinless particle by a spinless target at relativistic energies. The formalism replaces the differential equation by difference equation and the inversion results into solving a continued fraction equation and provides number of points of the potential equal to the number of partial waves. In case the number of partial waves is large i.e., about 10 or more and the knowledge of logarithmic derivative is accurate, the potential is determined very well. A few model cases for determining potentials from phase shifts as well as logarithmic derivatives will be presented with a view of applying the method for the pion-nucleus case.

[1] M.M. Alam and F.B. Malik, Phys. Lett. B 237, 14 (1990) and Nucl. Phys. A 524, 88 (1991)

15:06
EB 9 Evaporation of Strange Particles in Antiproton Nucleus Reactions: F. B. MALIK, Southern Illinois University*, L. W. TOWNSEND, NASA Langley Research Center, and R. K. TRIPATHI, Southern Illinois University* --We have investigated the production of neutral strange particles in antiproton - nucleus collisions, and found that an evaporation - like model provides better explanation for their emission. New systematics about their production will be discussed. Detailed comparisons will be made with the available experimental data.

*Supported by NASA Grant.

15:18
EB 10 Nuclear Fragmentation of Heavy Ions by Protons. R. BAGGA, Old Dominion University, L.W. TOWNSEND, NASA Langley Research Center, R. K. TRIPATHI, Southern Illinois University. --- Optical Model methods for calculating cross sections for the breakup of heavy nuclei by protons are presented. The fragmentation cross sections are calculated with a modified abrasion-ablation collision formalism where the abrasion stage is treated as a quantum-mechanical knockout process and the ablation stage incorporates excitation energy from particle-hole and frictional-spectator-interaction (FSI) processes. Comparisons with recently published cross section results will be presented.

SESSION EC: HEAVY-ION REACTIONS III: CORRELATIONS AND COLLECTIVE PHENOMENA
Saturday afternoon, 29 October 1994
Gen Hooker's Redoubt at 13:30
T. C. Sangster, presiding

13:30
EC 1 Systematic Study of Highly Excited Nuclear Matter Systems with an Exclusive Impact-parameter Trigger G.C. BALL, D. HORN, D.R. BOWMAN, D. FOX, A. GALINDO-URIBARRI and E. HAGBERG, AECL Research, Chalk River Laboratories; L. BEAULIEU, R. LAFOREST, Y. LAROCHELLE and R. ROY, Université Laval and T. LI, A. VANDER MOLEN, G.D. WESTFALL, J.S. WINFIELD, J. YEE AND S.J. YENELLO, Michigan State University --- Symmetric heavy-ion collisions were studied at TASCC and NSCL with 22-80A MeV beams of ^{20}Ne ^{35,37}Cl and ^{36}Ar. The 4π

14:42
EA 3
Structure of Neutron Rich Nuclei.*
I. Y. LEE, Lawrence Berkeley National Laboratory.

Neutron rich nuclei are of particular interest since they might reveal new aspects of nuclear structure associated with an excess of neutrons, such as new region of deformation, shell effects and modes of excitation. Deep-Inelastic reactions have been shown to produce neutron-rich nuclei with a high multiplicity of gamma-rays. However, since these reactions produce many final nuclei, it has been very difficult to study them until now, due to the lack of sensitivity of the available gamma-ray detector arrays. We have carried out gamma-spectroscopy studies of neutron rich nuclei using the reaction ^{48}Ca+^{176}Yb. A Si-strip detector was used to detect the projectile-like fragments and the coincident gamma rays were detected in the Gammasphere. States with spin as high as 20 in neutron-rich nuclei such ^{177,178}Yb and ^{173}Tm were observed from 2- and 3-fold gamma-ray coincidence data. We will discuss results on the variation of nuclear structure over a wide range of neutron numbers. For example, the study of pairing strength as a function of spin, and the variation of the interaction strength of the first backbending.

15:18
EA 4   New Insights from Studies of Spontaneous Fission: Yields and Neutron Multiplicities, Cold Fission, and Structure of Neutron-Rich Nuclei.*
J. H. HAMILTON, Vanderbilt University.

An overview of many of the new insights extracted from γ,γ and γ-γ-γ coincidence studies of spontaneous fission of ^{252}Cf and ^{242}Pu with large detector arrays at ORNL and Gammasphere will be presented. These include direct measurements of yields and neutron multiplicities from 0 to 10ν for five correlated pairs, identification of a number of cold fission (cluster radioactivity) channels, identification of new structures and behaviors in many neutron-rich nuclei from ^{94}Sr to ^{160}Sm. From the yields of the correlated pairs, a new, second mode of SF is observed in the Mo-Ba pairs with much lower total kinetic energy. This mode goes via a hyperdeformed shape (3:1 axis ratio) for ^{144}Ba, ^{145}Ba, or ^{146}Ba. Calculations indicate a third minima in ^{252}Cf at $\beta_3 \sim 0.7$ and $\beta_2 \sim 0.9$. The zero neutron cluster radioactivity yields for odd-odd Mo-Ba pairs are about four times larger than for the even-even ones in agreement with recent cluster radioactivity predictions. Identical bands are observed in ^{98,100}Sr, ^{108,110}Ru, ^{144,146}Ba, and ^{152,154}Nd nuclei and new types of identical bands in ^{156,158,160}Sm nuclei, and the first identical octupole bands. Octupole deformation is seen in N=86, ^{142}Ba, ^{144}Ce and the new high spin octupole states to 19⁻ exhibit the first backbending and quenching of the static octupole strength as predicted by theory. Selected examples of the new physics being seen will be presented.

SESSION EB: HEAVY IONS IV: NUCLEON-NUCLEON CORRELATIONS AND INTERMEDIATE ENERGY
Saturday afternoon, 28 October 1995
Oak Room at 13:30
T. C. Sangster, presiding

13:30
EB 1 Proton–Proton Correlation Functions for ^{16}O + ^{197}Au collisions at E/A = 200 MeV S.J. GAFF, D.O. HANDZY, W. BAUER, F.C. DAFFIN, J.D. DINIUS, C.K. GELBKE, T. GLASMACHER, E. GUALTIERI, S. HANNUSCHKE, M.J. HUANG, W.C. HSI, G.J. KUNDE, M.A. LISA, W.J. LLOPE, W.G. LYNCH, L. MARTIN, C.P. MONTOYA, R. PAK, L. PHAIR, S. PRATT, C. SCHWARZ, N. STONE, M.B. TSANG, A.M. VANDER MOLEN, G.D. WESTFALL, J. YEE, AND S.J. YENNELLO, *National Superconducting Cyclotron Laboratory, Michigan State University* — Using a high-resolution hodoscope, coincident protons were measured from the reaction ^{16}O + ^{197}Au at E/A = 200 MeV. The experiment was preformed at the National Superconducting Cyclotron Laboratory. The results to be presented include the correlation functions, both integrated and gated on total momentum, and the proton energy spectra. These experimental results will be compared with BUU calculations. Consistent with other measurements, discrepencies with BUU predictions will be shown. [1]

[1]Supported in part by the National Science Foundation.

13:42
EB 2   Proton-proton correlations in peripheral collisions.
H.M.Xu, G.K. Ajupova, C.A. Gagliardi, Y.W. Lui, A.A. Reid and R.P. Schmitt *Texas A&M U.*—We have measured proton-proton correlation functions in ^{14}N induced reactions on ^{27}Al and ^{116}Sn targets at average angles $\theta_{ave} = 10^0$ and $\theta_{ave} = 25^0$ with the Texas A&M University Proton Spectrometer. The spectrometer data will be compared to earlier multi-detector data and the dependence of proton-proton correlations on the emission angles and the momenta of the proton pairs will be discussed.

13:54
EB 3   One Nucleon Removal Cross Sections in Light and Medium Nuclei: R. K. TRIPATHI, *Southern Illinois University*, J. W. WILSON, F. A. CUCINOTTA, J. L. SHINN, *NASA Langley Research Center*, F. F. BADAVI, *Christopher Newport University*, and S. Y. CHUN, *Old Dominion*

University --Using a semiempirical nuclear fragmentation model developed[1] at NASA Langley Research Center (NUCFRG2), we analyze one nucleon removal cross sections in terms of nuclear and coulomb cross sections. We find there is a need for structure effects in light and medium nuclei. The interesting cases of one neutron and one proton removal cross sections in ^{40}Ar and ^{56}Fe will be discussed. Within a simple single particle shell model picture, both these nuclei can be described by 2p-2h states with respect to sd and fp shells, respectively. Experimentally, one neutron removal cross sections for these nuclei are approximately three times larger than one proton removal cross sections reflecting to the neutron shells to be "farther" than proton shells.

14:06
EB 4   Nuclear Dissipation from Measurements of Light Charged Particle Emission in Fusion – Fission Reactions R.C. LEMMON, NSCL, Michigan State U. , D.J. HINDE, J.R. LEIGH, C.R. MORTON, J.O. NEWTON, M. DASGUPTA, Australian National U., J.P. LESTONE, U. of Washington. — At moderate excitation energies, the dynamics of nuclear fission are determined by the dissipative coupling of collective and internal single-particle degrees of freedom. One of the foremost problems in nuclear physics is understanding the mechanism and magnitude of this dissipation. The alpha particle and proton multiplicities from the reactions ^{19}F+^{169}Tm, ^{28}Si+^{160}Gd and ^{34}S+^{154}Sm have been measured. Pre- and post-saddle timescales for the fission of ^{188}Pt were then extracted from these multiplicities using a statistical model modified to include fission delay times and a Kramers factor [1]. The timescales have now been interpreted within the framework of a Langevin collective transport model to give values of the dissipation as a function of deformation. These results will be presented and comparisons made with different microscopic models of nuclear dissipation [2,3].

[1] J.P. Lestone, Phys. Rev. Lett. 70, (1991) 2245
[2] J.R. Nix and A.J. Sierk, Proc. International School-Seminar on Heavy Ion Physics, Dubna, 1986, Joint Institute for Nuclear Research Report No. JINR-D7-87-68 (1987)
[3] P. Fröbrich, I.I. Gontchar and N.D. Mavlitov, Nuclear Physics A556 (1993) 281

14:18
EB 5   Characterizing the Two Stage Reaction Dynamics in 1 AGeV Projectile Fragmentation of Gold Nuclei J.A. HAUGER[1], S. ALBERGO[2], F. BIESER[3], F.P. BRADY[4], Z. CACCIA[2], D.A. CEBRA[4], A.D. CHACON[5], J.L. CHANCE[4], Y. CHOI[1], S. COSTA[2], J.B. ELLIOTT[1], M.L. GILKES[8], A.S. HIRSCH[1], E.L. HJORT[1], A. INSOLIA[2], M. JUSTICE[6], D. KEANE[6], J.C. KITNER[4], V. LINDENSTRUTH[7], M. A. LISA[3], U. LYNEN[7], H.S. MATIS[3], M. MCMAHAN[3], C. MCPARLAND[3], W.F.J. MUELLER[7], D.L. OLSON[3], M.D. PARTLAN[4], N.T. PORILE[1], R. POTENZA[2], G. RAI[3], J. RASMUSSEN[3], H.G. RITTER[3], J. ROMANSKI[2], J.L. ROMERO[4], G.V. RUSSO[2], H. SANN[7], R.P. SCHARENBERG[1], A. SCOTT[6], Y. SHAO[6], B. SRIVASTAVA[1], T.J.M. SYMONS[3], M.L. TINCKNELL[1], C. TUVE[2], S. WANG[6], P. WARREN[1], D. WEERASUNDARA[6], H.H. WIEMAN[3], K.L. WOLF[5], [1]Purdue U., [2]INFN, Catania, [3]Lawrence Berkeley Lab., [4]UC - Davis, [5]Texas A&M U., [6]Kent State U., [7]GSI, Darmstadt, [8]SUNY -Stony Brook. — By studying protons from the multifragmentation of 1AGeV Au + C

collisions, we can distinguish two stages in the reaction process. A method for separating these two components will be presented.

14:30
EB 6   Cavitation and Penetration in Central Collisions Induced by Light Ions. G. WANG, K. KWIATKOWSKI, and V. E. VIOLA, Indiana University; and W. BAUER and P. DANIELEWICZ, Michigan State University. Two different BUU calculations are employed to examine the dynamics of central collisions induced by light-ion projectiles. For projectile energies above about one GeV incident on heavy target nuclei, a region of low density develops in the core of the nucleus at times of the order of 30 fm/c. The simulations predict penetration of the target by the projectile momentum front above energies of 4-6 GeV, leading to a saturation of deposition energy. These results are examined in the context of marked changes in reaction observables for such collisions.

14:42
EB 7   One Step Production of 6 Alpha Particles by ^{12}C + ^{12}C →6 ^{4}He. E. NORBECK, Y.W. CHENG, L.B. YANG, U. of Iowa, F.D. INGRAM, Rock Valley College. According to the Born approximation, the cross section for ^{12}C + ^{12}C → 6 ^{4}He is proportional to $\rho (p^*)^n |\langle \psi_f |V| \psi_i \rangle |^2$ in which n = 14 is the number of independent parameters, and V is the potential acting between α clusters in the beam with the α clusters in the target. ψ_f is the final state with each cluster expressed as a plane wave. ψ_i is the initial state consisting of α cluster ^{12}C wave functions times plane waves for the relative motion. The phase space factor, ρ, is slowly varying. The matrix element, $\langle \psi_f |V| \psi_i \rangle$, is large if the momentum of one or more clusters are spectators which have the same momentum after, as before the reaction. If two α particles in the target and two in the beam are spectators, the threshold for the reaction is 88 Mev, and the sum of the energies of the two remaining α particles is 1/3 of the beam energy less about 14 Mev binding energy. Such peaks in the sum of the energies of two α particles have been observed for ^{12}C energies from 660 to 1860 Mev.

SUPPLEMENTARY

14:54
EB 8

Quantum field description of high energy multiple sequential collisions in dense media. Jicai Pan, Dept. of Physics, McGill University, Montreal, Canada. High energy sequential collisions in dense media have, so far, been discussed in the framework of classical kinetic theory. In this picture, quantum fluctuation is not taken into account. As a result, inteference between sequential collisions is usually overestimated. We propose here generalized Lagrangians that consist of fields with different initial space-time coordinates to develop a full quantum description of sequential collisions in dense electromagnetic and strong interacting media. Unlike Glauber theory that is a quantum mechanical description of elastic and quasielastic hadron-nucleus scatterings, the present formulation provides a unified quantum field description of particle production, radiation, scattering, and particularly the interference in high energy sequential collisions in dense matter that may be produced in high energy nuclear collisions. The destructive interference of soft dilepton and photon productions, known as Landau-Permoranchuk-Migdal effect, in both hadronic gas and quark-gluon plasma is weaker than that obtained in classical kinetic theory.

Attachment 2
Full Length Articles

Accurate Universal Parameterization of Absorption Cross Sections

R. K. Tripathi

Southern Illinois University, Carbondale, Illinois 62901

Hampton University, Hampton, VA 23668

Francis A. Cucinotta and John W. Wilson

NASA Langley Research Center, Hampton, VA 23681

Abstract

We present a simple universal parameterization of total reaction cross sections for any system of colliding nuclei valid for the entire energy range from a few A MeV to a few A GeV. The universal picture presented here treats proton-nucleus collision as a special case of nucleus-nucleus collision, where the projectile has charge and mass number of one. The parameters are associated with the physics of the collision system. In general terms Coulomb interaction modifies cross sections at lower energies and the effects of Pauli blocking is important at higher energies. The agreement between the calculated and experimental data is better than all earlier published results.

1. Introduction

The transportation of energetic ions in bulk matter is of direct interest in several areas [1] including shielding against ions originating from either space radiations or terrestrial accelerators, cosmic ray propagation studies in galactic medium or radiobiological effects resulting from the work place or clinical exposures. For carcinogenesis, terrestrial radiation therapy, and radiobiological research; knowledge of the beam composition and interactions is necessary to properly evaluate the effects on human and animal tissues. For the proper assessment of radiation exposures both reliable transport codes and accurate input parameters are needed.

One such important input is the total reaction cross section, defined as the total minus the elastic cross sections for two colliding ions:

$$\sigma_R = \sigma_T - \sigma_{el} \tag{1}$$

In view of its importance the total reaction cross section has been extensively studied both theoretically [1-14] and experimentally [15-20] for the past five decades. A detailed list of references is given in Ref.[1, 13, 16]. Empirical prescriptions have been developed [2-4, 10, 11, 13] for the total reaction cross sections working in various energy ranges and combination of interacting ions. The present model works in all energy ranges for any combination of interacting ions including proton-nucleus collisions and is more accurate than earlier reported empirical models.

2.Model Description

The present model is an updated and revised version of the empirical model developed at NASA Langley Research Center and reported earlier [10].Most of the empirical models approximate total reaction cross section of Bradt-Peters form:

$$\sigma_{abs} = \pi r_0^2 (A_P^{1/3} + A_T^{1/3} - \delta)^2 \qquad (2)$$

where r_0 is energy independent and δ is either energy-independent or energy dependent parameter, and A_P and A_t are the projectile and target mass numbers, respectively. This form of parameterization works nicely for higher energies. However, for lower energies Coulomb interaction becomes important and modifies reaction cross sections significantly. In addition, strong absorption models suggest energy dependence of the interaction radius. Incorporating these effects, and other effects discussed latter in the text, we propose the following form for the reaction cross section:

$$\sigma_R = \pi r_0^2 (A_P^{1/3} + A_T^{1/3} + \delta_E)^2 (1 - \frac{B}{E_{cm}}) \qquad (3)$$

We notice that Coulomb interaction, where $r_0 = 1.1$ fm, and Ecm is in MeV, modifies cross sections at lower energies and gets less important as the energy increases (typically after several tens of A MeV). In Eq. (3) B is the energy dependent Coulomb interaction barrier (right hand factor in Eq. 3), and is given by,

$$B = \frac{1.44 Z_P Z_T}{R} \qquad (4)$$

where,

$$R = r_P + r_T + \frac{1.2 (A_P^{1/3} + A_T^{1/3})}{E_{cm}^{1/3}} \qquad (5)$$

with (i = P,T),

$$r_i = 1.29 (r_i)_{rms} \qquad (6)$$

There is energy dependence in the reaction cross section at intermediate and higher energies mainly due to two effects -- transparency and Pauli blocking. This is taken into account in δ_E , which is given by,

$$\delta_E = 1.85S + 0.16S/E_{cm}^{1/3} - C_E \\ +0.91 (A_T - 2Z_T) Z_P / (A_T A_P) \qquad (7)$$

where S is the mass asymmetry term and is given by,

$$S = \frac{A_P^{1/3} A_T^{1/3}}{A_P^{1/3} + A_T^{1/3}} \qquad (8)$$

and is related to the volume overlap of the collision system. The last term on the right hand side of Eq. (7) accounts for the isotope dependence of the reaction cross section. The term C_E is related to the transparency and Pauli blocking and is given by,

4

$$C_E = D(1-\exp(-E/40))-0.292\exp(-E/792)$$
$$\times \cos(0.229E^{0.453})$$
(9)

Here D is related to the density dependence of the colliding system scaled with respect to the density of C + C system, ie:

$$D = 1.75\frac{\rho_{A_P} + \rho_{A_T}}{\rho_{A_C} + \rho_{A_C}}$$
(10)

The density of a nucleus is calculated in the hard sphere model [24], and for a nucleus of mass number A_i is given by,

$$\rho_{A_i} = \frac{A_i}{\frac{4\pi}{3}r_i^3}$$
(11)

where the radius of the nucleus r_i is defined in Eq. (6) with root-mean-square radius, $(r_i)_{rms}$, obtained directly from experiment [25]. There is interesting physics associated with constant D. This in effect simulates the modifications of the reaction cross sections due to Pauli blocking. This effect is new and has not been taken into account in other empirical calculations. This helps present a universal picture of the reaction cross sections.

At lower energies (below several tens of A MeV) where the overlap of interacting nuclei is small (and where Coulomb interaction modifies the reaction cross sections significantly) the modifications of the cross sections due to Pauli blocking are small, and gradually play an increasing role as the energy increases,

since this leads to higher densities where Pauli blocking gets increasingly important. Interestingly enough for the proton-nucleus case,since there is not much compression effect, a single constant value of D=2.05 gives very good results for all proton-nucleus collisions. For alpha - nucleus collisions, where there is a little compression, the best value of D is given by,

$$D = 2.77 - 8.0 \times 10^{-3} A_T + 1.8 \times 10^{-5} A_T^2$$
$$-0.8/(1+\exp(250-E)/75) \qquad (12)$$

For lithium nuclei because of the 'halos', compression is less and hence the Pauli blocking effect is less important and a reduced value of D/3 gives better results for the reaction cross sections at the intermediate and higher energies.

There are no adjustable parameters in the model except that for proton nucleus collisions this method of calculating the Coulomb energy underestimates its value for the very light closed shell nuclei of alpha and carbon, and these should be increased by a factor of 27 and 3.5 respectively for a better fit.

3.Results/Conclusions:

Typical results obtained from the model are shown in Figures 1 through 5. Agreement with experimental data is excellent and is better than all other empirical models reported earlier. This is particularly important in view of the fact that the agreement is excellent throughout the whole energy range - upto a few A GeV. The model has been tested with all the available data for projectiles

6

proton through krypton and targets alpha through bismuth for the energy range from a few A MeV upto a few A GeV and is found to give excellent results for all the systems throughout the energy range. In view of the simplicity and accuracy of the model it is a welcome improvement for transport calculations.

It will be interesting to see how the model compares with the new experimental data as and when these become available.

Acknowlegement

Figure Captions:

Figures 1 :   Absorption cross sections for proton - beryllium collision as a function of proton kinetic energy. Solid line represents present model and the experimental data are from [15].

Figures 2 :   Absorption cross sections for proton - aluminum collision as a function of proton kinetic energy. Solid line represents present model and the experimental data are from [15].

Figures 3:   Absorption cross sections for alpha - carbon collision as a function of incident ion kinetic energy. Solid line represents present model and the experimental data are from [21 - 22].
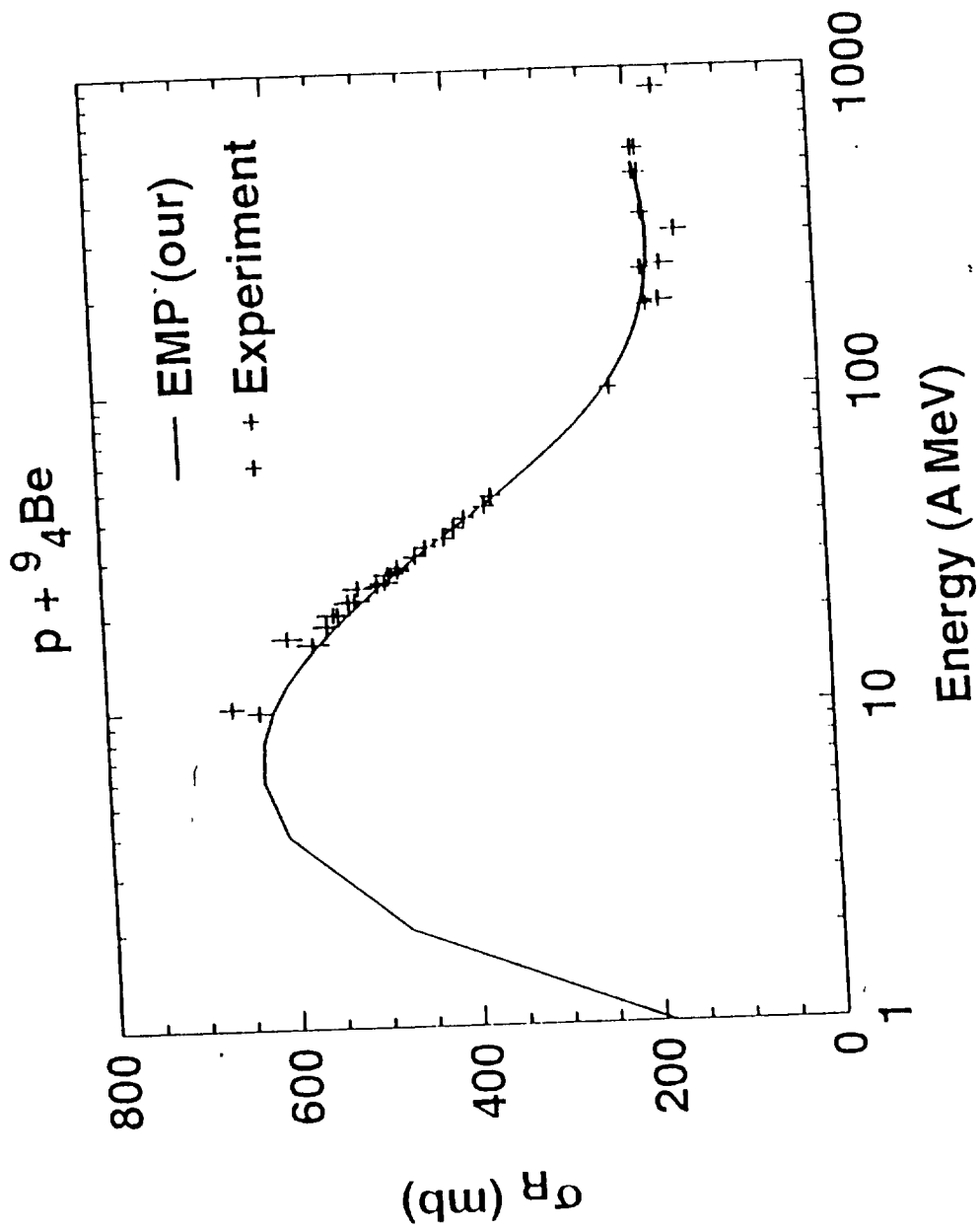
Figures 4 :   Absorption cross sections for carbon - carbon collision as a function of incident ion kinetic energy. Solid line represents present model and the experimental data are from [1,9,13,16].
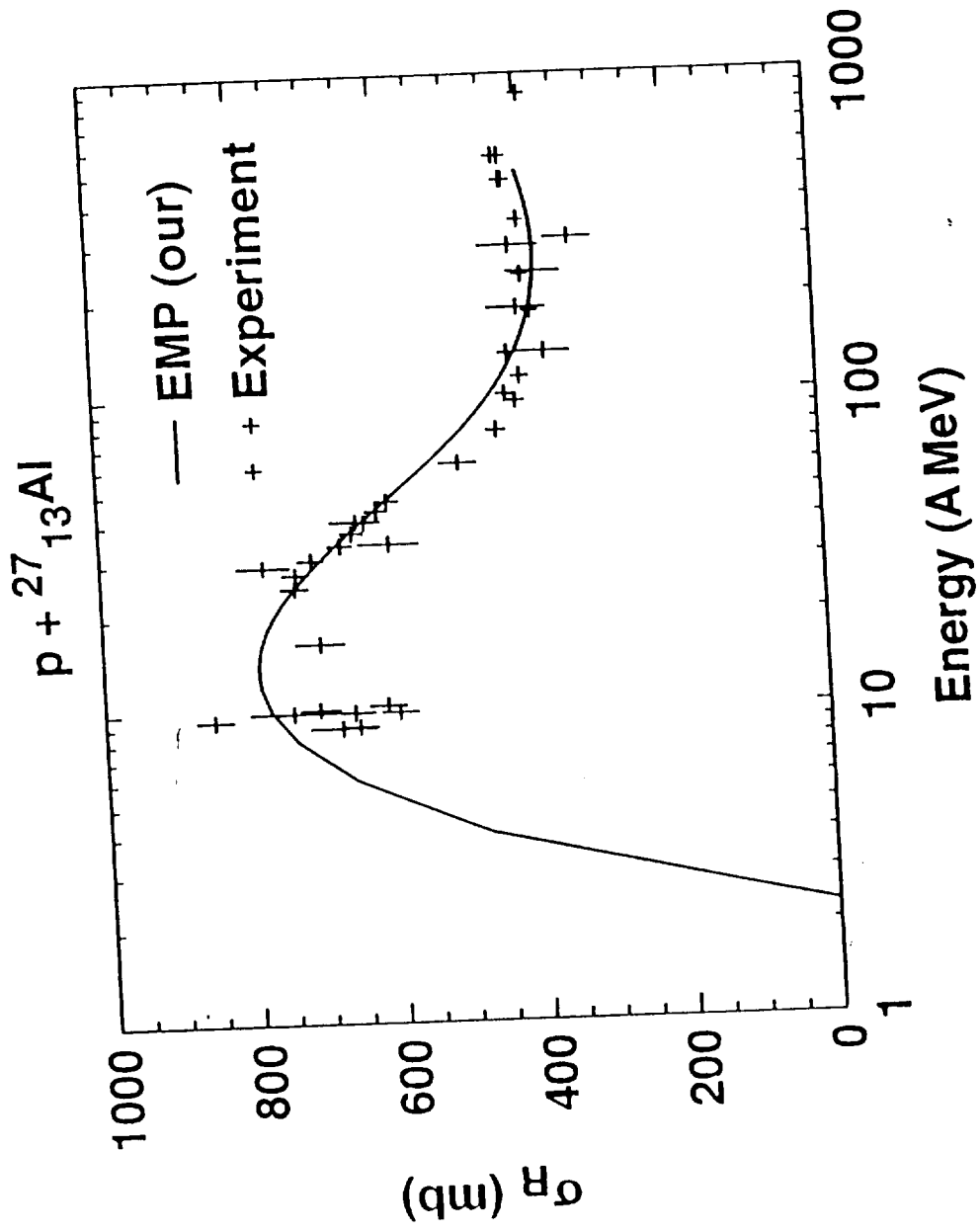
Figures 5 :   Absorption cross sections for calcium - calcium collision as a function of incident ion kinetic energy. Solid line represents present model and the experimental data are from [1,9,13,16].
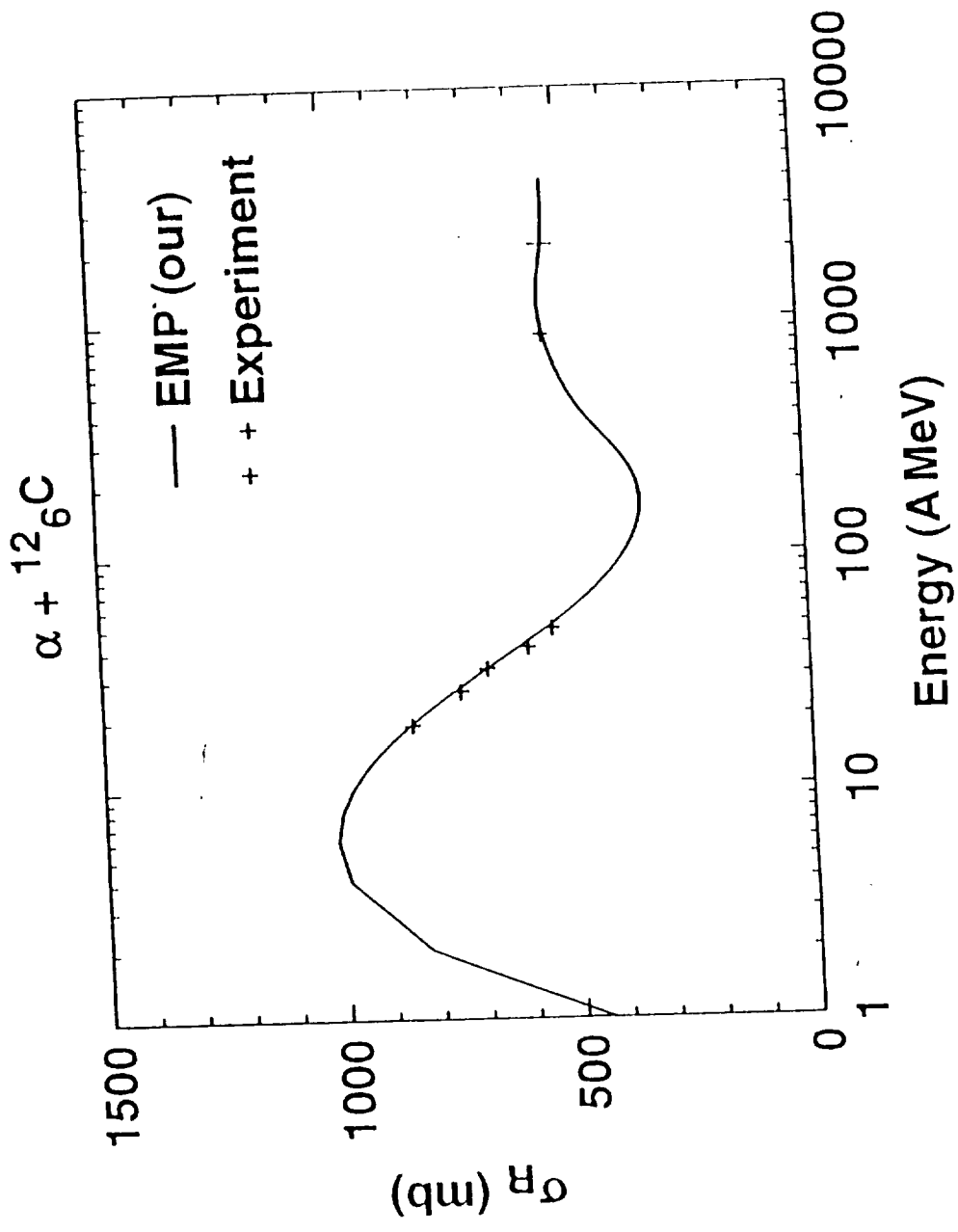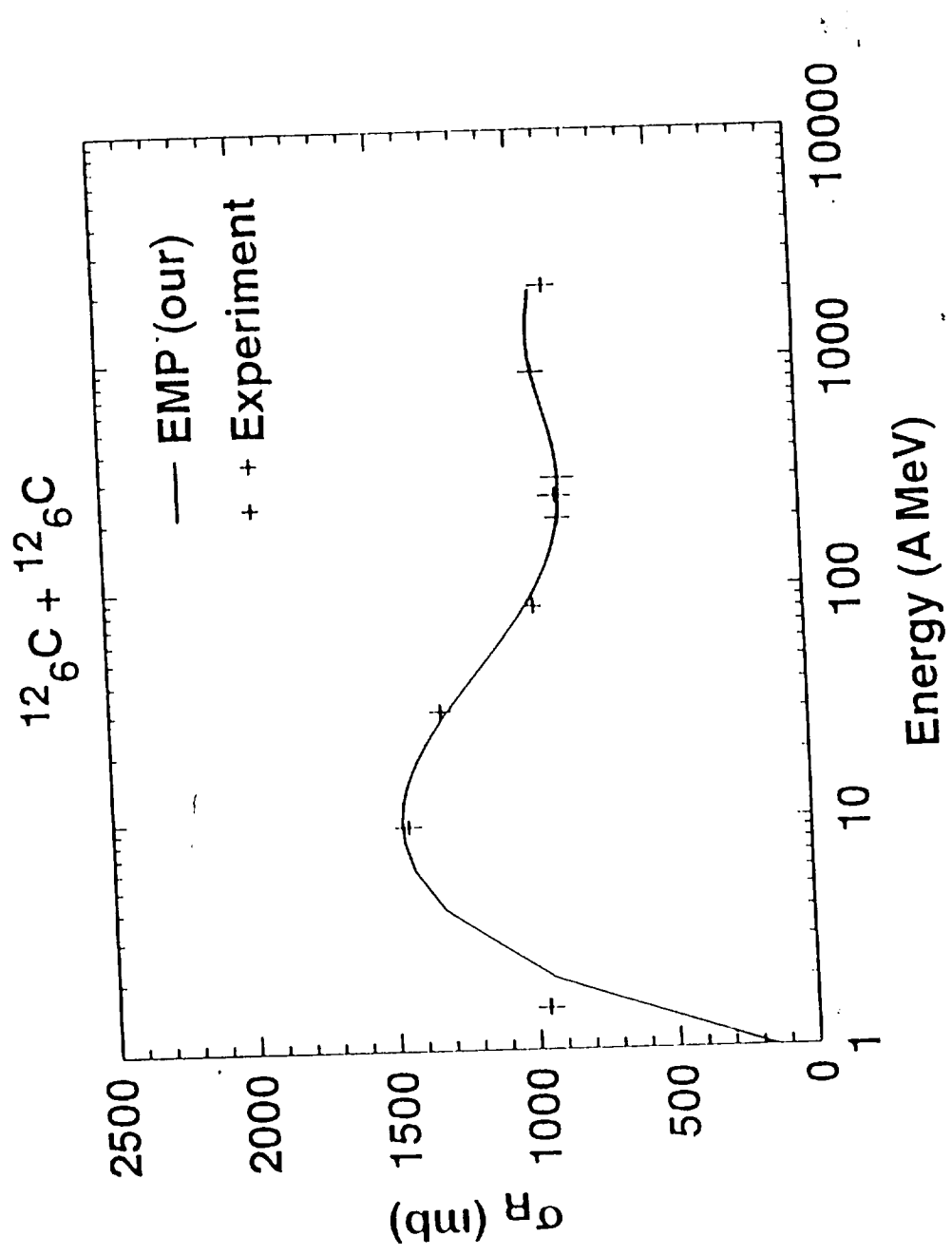
References:

1. J.W. Wilson et al., NASA RP-1257,December 1991.

2. R. Bass, Nuclear Reactions with Heavy Ions, Springer Verlag Berlin,1980.

3. H. L. Bradt and B. Peters, Physical Rev. 77 (1950) 54.

4. P.J. Karol Physical Rev. C 11 (1975) 1203.

5. R.J. Glauber Lectures in Theoretical Physics, ed. Brittin Interscience New York, Vol. I (1959) 315.

6. J.W. Wilson,Composite Particle Reaction Theory, Ph.D. dissertation, College of William and Mary in Virginia, June 1975.

7. J.W. Wilson and L.W. Townsend, Can. J. Phys. 59 (1981) 1569.

8. D.J. Ernst, Physical Rev. C19 (1979) 896.

9. S.K. Gupta and S. Kailash, Z. Phys. 317 (1984) 75; S.K. Gupta and P. Shukla, Physical Rev. C 52 (1995) 3212.

10. L.W. Townsend and J.W. Wilson, Rad. Res. 106 (1986) 283.

11. W. Shen, B. Wang, J. Feng, W. Zhan, Y. Zhu and E. Feng, Nucl. Phys. A491 (1989) 130.

12. A. Vituri and F. Zardi, Physical Rev. C36 (1987) 1404,

13. L. Sihver, C.H.Tsao, C.H.,R. Silberberg, T. Kanai and A.F. Barghourty, Physical Rev. C47 (1993) 1225.

14. R.M. DeVries and J.C. Peng, Physical Rev. 22 (1980) 527.

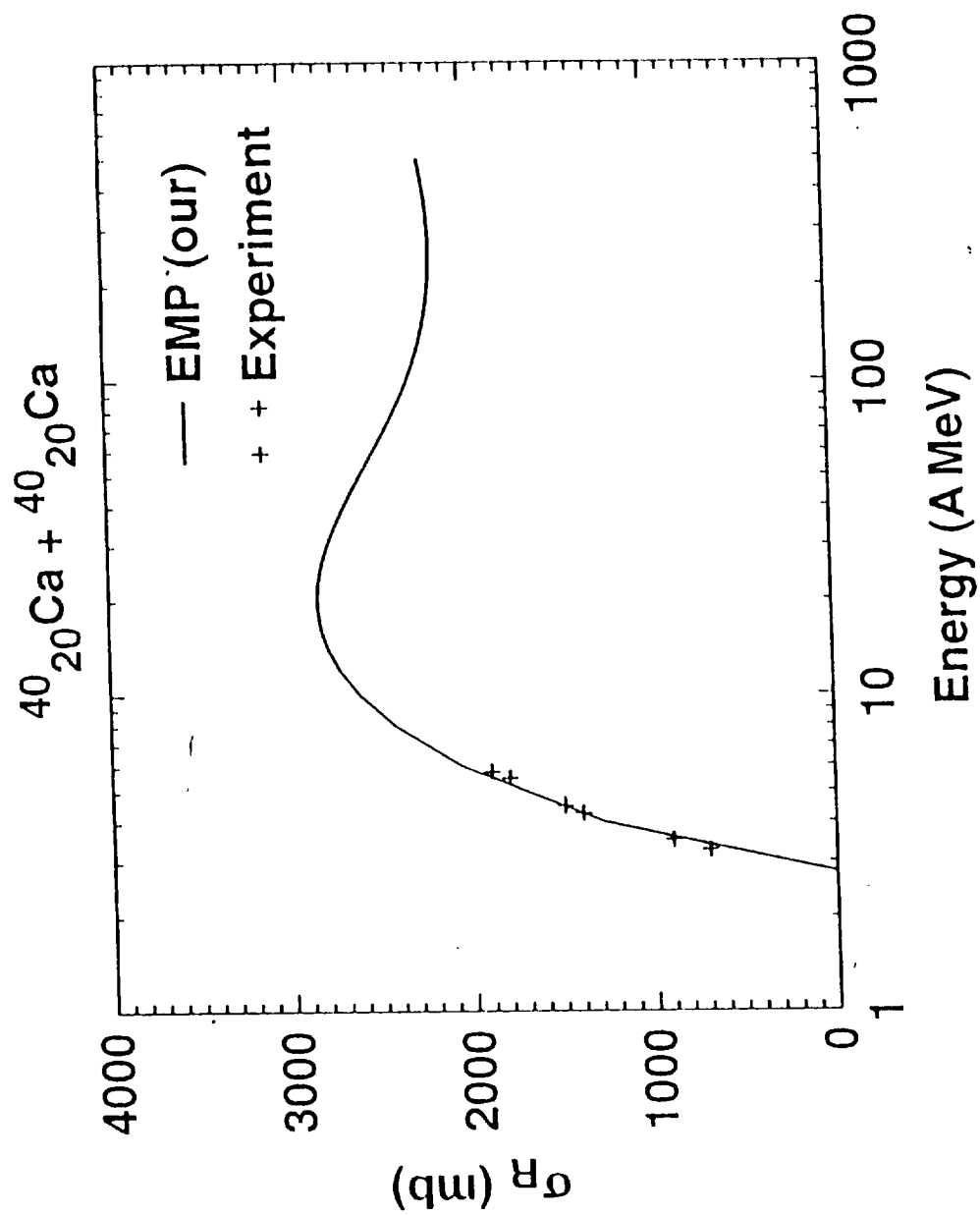15. W. Bauhoff,At. Data Nucl. Data Tables 35 (1986) 429.

16. S. Kox, A. Gamp, C. Perrin, J. Arvieux, R. Bertholet, J.F. Bruandet, M. Buenerd, R. Cherkaoui, A.J. Cole, Y. El-Masri, N. Longequeue, J. Menet, F. Merchez and J.B. Viano, Physical Rev. C35 (1987) 1678; and references there in.

17. V. S. Barashenkov, K.K. Gudima and V.D. Toneev, Prog. Phys. 17 (1969) 693.

18. W.R. Webber, J.C. Kish and D.A. Schrier, Physical Rev.C 41 (1990) 547.

19. L.V. Dubar, D. Sh.Eeukenov, L.I. Slyusarenko and N.P. Yurkuts,Sov. J. Nucl.Phys. 49 (1989) 771.

20. J. J. Menet, E.E. Gross, J.J. Malanify and A. Zucker, Physical Rev. C4 (1971) 1114.

21. J. Jaros, A. Wagner, L. Anderson, O. Chamberlain, R. Z. Fuzesy, J. Gallop, W. Gorn, L. Schroeder, S. Shannon, G. Shapiro and H. Steiner, Phys. Rev. C18 (1978) 2273.

22. A. Auce, R.F. Carlson, A.J. Cox, A. Ingemarsson, R. Johansson, P.U. Renberg, O. Sundber, G. Tibell and R. Zorno, Phys. Rev. C50 (1994) 871.

23. R.K. Tripathi, F.A. Cucinotta and J.W. Wilson, NASA TP, under preparation.

24. R.K. Tripathi, L. W. Townsend and F.W. Khan, Phys. Rev. C47 (1993) R935.

25. H. DeVries, C.W. DeJager and C. DeVries, At. Data Nucl. Data Tables 36 (1987) 495.

$p + \, ^9_4\text{Be}$

— EMP (our)

+ + Experiment

Energy (A MeV)

σ_R (mb)

$p + {}^{27}_{13}Al$

—— EMP (our)

+ + Experiment

σ_R (mb)

Energy (A MeV)

$\alpha + ^{12}_6C$

EMP (our)

+ + Experiment

Energy (A MeV)

σ_R (mb)

$^{12}_{6}C + ^{12}_{6}C$

— EMP (our)

+ + Experiment

Energy (A MeV)

σ_R (mb)

$^{40}_{20}Ca + ^{40}_{20}Ca$

— EMP (our)
+ + Experiment

σ_R (mb)

Energy (A MeV)

Universal Parameterization of Absorption Cross Sections

R. K. Tripathi

Southern Illinois University, Carbondale, Illinois 62901

Francis A. Cucinotta and John W. Wilson

NASA Langley Research Center, Hampton, VA 23681

Abstract:

We present a simple universal parameterization of total reaction cross sections for any system of colliding nuclei valid for the entire energy range from a few A MeV to a few A GeV. The universal picture presented here treats proton-nucleus collision as a special case of nucleus-nucleus collision, where the projectile has charge and mass number of one. The parameters are associated with the physics of the collision system. In general terms Coulomb interaction modifies cross sections at lower energies and the effects of Pauli blocking is important at higher energies. The agreement between the calculated and experimental data is better than all earlier published results.

Introduction:

The transportation of energetic ions in bulk matter is of direct interest in several areas [1] including shielding against ions originating from either space radiations or terrestrial accelerators, cosmic ray propagation studies in galactic medium or radiobiological effects resulting from the work place or clinical exposures. For carcinogenesis, terrestrial radiation therapy, and radiobiological research; knowledge of the beam composition and interactions is necessary to properly evaluate the effects on human and animal tissues. For the proper assessment to radiation exposures both reliable transport codes and accurate input parameters are needed.

One such important input is the total reaction cross section, defined as the total minus the elastic cross sections for two colliding ions:

$$\sigma_R = \sigma_T - \sigma_{el} \tag{1}$$

In view of its importance the total reaction cross section has been extensively studied both theoretically [1-14] and experimentally [15-24] for the past five decades. A detailed list of references is given in Ref.[1, 13, 16]. Empirical prescriptions have been developed [2-4, 10, 11, 13] for the total reaction cross sections working in various energy ranges and combination of interacting ions. The present model works in all energy ranges with uniform accuracy for any combination of'interacting ions including proton-nucleus collisions and is more accurate than earlier reported empirical models [10] which were accurate above

2

100 A MeV but showed large errors upto 25 percent at lower energies.

Model Description:

Most of the empirical models approximate total reaction cross section of Bradt-Peters form:

$$\sigma_R = \pi r_0^2 (A_P^{1/3} + A_T^{1/3} - \delta)^2 \qquad (2)$$

where r_0 is energy independent and δ is either energy-independent or energy dependent parameter, and A_P and A_T are the projectile and target mass numbers, respectively. This form of parameterization works nicely for higher energies. However, for lower energies Coulomb interaction becomes important and modifies reaction cross sections significantly. In addition, strong absorption models suggest energy dependence of the interaction radius. Incorporating these effects, and other effects discussed latter in the text, we propose the following form for the reaction cross section:

$$\sigma_R = \pi r_0^2 (A_P^{1/3} + A_T^{1/3} + \delta_E)^2 \left(1 - \frac{B}{E_{cm}}\right) \qquad (3)$$

Where $r_0 = 1.1$ fm, and Ecm is colliding system center of mass energy in MeV. The last term is the Coulomb interaction term which modifies the cross section at lower energies and gets less important as the energy increases (typically after several tens of A MeV). In Eq. (3) B is the energy dependent Coulomb interaction barrier (right hand factor in Eq. 3), and is given by,

3

$$B = \frac{1.44 Z_P Z_T}{R} \qquad (4)$$

where Z_P (Z_T) is atomic number of the projectile (target) and radius for evaluating the Coulomb barrier height is,

$$R = r_P + r_T + \frac{1.2 (A_P^{1/3} + A_T^{1/3})}{E_{cm}^{1/3}}. \qquad (5)$$

where r_i is equivalent sphere radius and is related to the $r_{rms,i}$ radius by ,

$$r_i = 1.29 r_{rms,i} \qquad (6)$$

with ($i = P,T$).

There is energy dependence in the reaction cross section at intermediate and higher energies mainly due to two effects -- transparency and Pauli blocking. This is taken into account in δ_E , which is given by,

$$\delta_E = 1.85S + 0.16S/E_{cm}^{1/3} - C_E$$
$$+0.91 (A_T - 2Z_T) Z_P / (A_T A_P) \qquad (7)$$

where S is the mass asymmetry term and is given by,

$$S = \frac{A_P^{1/3} A_T^{1/3}}{A_P^{1/3} + A_T^{1/3}} \qquad (8)$$

and is related to the volume overlap of the collision system. The last term on the right hand side of Eq. (7) accounts for the isotope dependence of the reaction

4

cross section. The term C_E is related to the transparency and Pauli blocking and is given by,

$$C_E = D(1-\exp(-E/40))-0.292\exp(-E/792)$$
$$\times \cos(0.229E^{0.453})$$

(9)

Where the collision kinetic energy E is in units of A MeV. Here D is related to the density dependence of the colliding system scaled with respect to the density of $^{12}C +^{12}C$ colliding system, ie:

$$D = 1.75\frac{\rho_{A_P} + \rho_{A_T}}{\rho_{A_C} + \rho_{A_C}}$$

(10)

The density of a nucleus is calculated in the hard sphere model. There is interesting physics associated with constant D. This in effect simulates the modifications of the reaction cross sections due to Pauli blocking. This effect is new and has not been taken into account in other empirical calculations. This helps present a universal picture of the reaction cross sections.

At lower energies (below several tens of A MeV) where the overlap of interacting nuclei is small (and where Coulomb interaction modifies the reaction cross sections significantly) the modifications of the cross sections due to Pauli blocking are small, and gradually play an increasing role as the energy increases, since this leads to higher densities where Pauli blocking gets increasingly important. Interestingly enough for the proton-nucleus case,since there is not much compression effect, a single constant value of D=2.05 gives very good

5

results for all proton-nucleus collisions. For alpha - nucleus collisions, where there is a little compression, the best value of D is given by,

$$D = 2.77 - 8.0 \times 10^{-3} A_T + 1.8 \times 10^{-5} A_T^2$$
$$-0.8/(1 + \exp(250 - E)/75) \tag{11}$$

For lithium nuclei because of the 'halos' [2], compression is less and hence the Pauli blocking effect is less important and a reduced value of D/3 gives better results for the reaction cross sections at the intermediate and higher energies.

There are no adjustable parameters in the model except that for proton nucleus collisions this method of calculating the Coulomb interaction barrier underestimates its value for the very light closed shell nuclei of alpha and carbon, which are very lightly bound and hence compact. Consequently, for these two cases Coulomb barrier should be increased by a factor of 27 and 3.5 respectively for a better fit.

Results/Conclusions:

Figures (1-45) show the plot of available results for proton-nucleus, alpha-nucleus, and nucleus-nucleus collisions. Figures (6,18) also show comparison with Ref. [10]. The data set used for figures (1-5) has been collected from Refs. [15, 23] and for figures (6-14) has been obtained from Refs. [16, 17, 22, 23]. There is extensive data set available for C + C system (Fig. 18) and has been taken from Refs. [16, 17, 23, 24]. For the remaining figures data has been collected from the

6

compilation of data set from Refs. [9, 16-20]. The agreement with experiment is excellent and is better than all other empirical models reported earlier. This is particularly important in view of the fact that the agreement is excellent throughout the whole energy range -- up to a few A GeV. We notice again that at lower energy end the cross sections are modified by the Coulomb interaction and at the intermediate and high energy end Pauli blocking effects become increasingly important. It will be interesting to see how the model compares with the new experimental data as and when these become available.

Figure Captions:

Figures (1-5) :   Reaction cross sections as a function of energy for proton-nucleus collisions. Solid line represents present model.

Figures (6-14) :   Reaction cross sections as a function of energy for alpha-nucleus collisions. Solid line represents present model. The dashed line in Fig. 6 is from Ref. [10].

Figures (15-45) :   Reaction cross sections as a function of energy for nucleus-nucleus collisions. Solid line represents present model. The dashed line in Fig. 18 is from Ref. [18].

References:

1. Wilson, J.W.; et al., NASA RP-1257,December 1991.

2. Bass, R.; Nuclear Reactions with Heavy Ions, Springer Verlag Berlin,1980.

3. Bradt, H.L.; and Peters, B.: Physical Rev. 77,54,1950.

4. Karol, P.J.; Physical Rev. C 11,1203,1975.

5. Glauber, R.J.; Lectures in Theoretical Physics, ed. Brittin Interscience New York, Vol. I, 315, 1959.

6. Wilson, J.W.; Composite Particle Reaction Theory, Ph.D. dissertation, College of William and Mary in Virginia, June 1975.

7. Wilson, J.W.; and Townsend, L.W.; Can. J. Phys. 59,1569, 1981.

8. Ernst, D.J.; Physical Rev. C19,896,1979.

9. Gupta, S.K.; and Kallash, S.; Z. Phys. 317,75,1984: Gupta, S.K.; and Shukla, P.; Physical Rev. C 52,3212,1995.

10. Townsend, L.W.; and Wilson, J.W.; Rad. Res. 106,283,1986

11. Shen, W.; Wang, B.; Feng, J.; Zhan, W.; Zhu, Y.; and Feng, E.;Nucl. Phys. A491,130,1989.

12. Vituri, A.;and Zardi, F.; Physical Rev. C36,1404,1987,

13. Sihver, L.; Tsao, C.H.; Silberberg, R.; Kanai, T.; and Barghourty, A.F.; Physical Rev. C47,1225,1993.

14. DeVries, R.M.; and Peng, J.C.; Physical Rev. 22,527,1980.

15. Bauhoff, W.; At. Data Nucl. Data Tables 35,429,1986.

16. Kox, S.; Gamp, A.; Perrin, C.; Arvieux, J.; Bertholet, R..; Bruandet, J.F.; Buenerd, M.; Cherkaoui, R.; Cole, A.J.; El-Masri, Y.; Longequeue, N.; Menet, J.; Merchez, F.; and Viano, J.B.; Physical Rev. C35,1678,1987; and references there in.

17. Barashenkov, V.S.; Gudima, K. K.; and Toneev, V.D.; Prog. Phys. 17, 693, 1969.

18. Webber, W.R.; Kish, J. C.; and Schrier, D.A.; Physical Rev.C 41,547,1990.

19. Dubar, L.V.; Eeukenov, D. Sh.; Slyusarenko, L.I.; and Yurkuts, N.P.; Sov. J. Nucl. Phys. 49,771,1989.

20. Menet, J.J.; Gross, E.E.; Malanify, J.J.; and Zucker, A.; Physical Rev. C4, 1114,1971

21. Riisagar, K.; Rev. Mod. Phys. 66,1105,1994: and references there in.

22. Auce,A.; Carlson, R.F.; Cox, A.J.; Ingemarsson, A.; Johansson, R.; Renberg, P.U.; Sundberg, O.; and Tibell, G.; Physical Rev. C 50, 871, 1994.

23. Joros, J.; Wagner, A.; Anderson, L.; Chamberlain, O.; Fuzesy, R.Z.; Gallup, J.; Gorn, W.; Schroeder, L.; Shannon, S.; Shapiro, G.; and Steiner, H.; Physical rev. c18, 2273, 1978.

24. Heckman, H.H.; Greiner, D.E.; Lindslrom, P.H.; and Shewe, H.; Physical Rev. C17, 1735, 1978.

p + $^{9}_{4}$Be

Fig. 1

$p + {}^{12}_{6}C$

Fig. 2

$p + {}^{27}_{13}Al$

Fig. 3

$$p + {}^{nat}_{26}Fe$$

Fig. 4

$\alpha + {}^1_1 H$

.150

100

σ_R (mb)

50

0

1   10   100   1000   10000

Energy (A MeV)

Fig. 5

$\alpha + {}^{12}_{6}C$

Fig. 6

Fig. 7

DL>

$\alpha + {}^{28}_{14}Si$

1500

1000

σ_R (mb)

500

0

1   10   100   1000

Energy (A MeV)

Fig. 8

$\alpha + {}^{40}_{20}Ca$

Fig. 9

$\alpha + {}^{48}_{20}Ca$

Fig. 10

$\alpha + ^{58}_{28}Ni$

Fig. 11

$$\alpha + {}^{60}_{28}\text{Ni}$$

Fig. 12.

Fig. 13

Fig. 14

Fig. 15

$^{6}_{3}Li + ^{90}_{40}Zr$

Fig. 16

$^9_4Be\ +\ ^{90}_{14}Si$

Fig. 17

Fig. 18

Fig. 19

$^{12}_{6}C + ^{40}_{20}Ca$

Fig. 2 m

$$^{12}_{6}C + ^{58}_{26}Fe$$

Fig. 21

$$^{12}_{6}C + {}^{64}_{30}Zn$$

Fig. 22

Fig. 23

$$^{16}_{8}O \ + \ ^{40}_{20}Ca$$

Fig. 24

$$^{16}_{8}O \ +^{59}_{27}Co$$

Fig. 25

$^{16}_{8}O$ + $^{58}_{28}Ni$

Fig. 26

$^{16}_{8}O \; + \; ^{208}_{82}Pb$

Fig.27

$$^{20}_{10}Ne + ^{12}_{6}C$$

Fig. 28

$^{20}_{10}Ne + ^{27}_{13}Al$

Fig. 29

$^{20}_{10}Ne + ^{40}_{20}Ca$

Energy (A MeV)

fig. 30

$^{20}_{10}$Ne $+ ^{208}_{82}$Pb

Fig. 31

$$^{20}_{10}\text{Ne} + {}^{235}_{92}\text{U}$$

Fig 32

$^{32}_{16}S + ^{24}_{12}Mg$

Fig. 33

$$^{32}_{16}S + ^{27}_{13}Al$$

Fig. 34

σL>

$^{35}_{17}Cl + ^{58}_{28}Ni$

4000

3000

σ_R (mb)

2000

1000

0

1   10   100   1000

Energy (A MeV)

Fig. 35

Fig. 36

$^{40}_{18}$Ar + $^{109}_{47}$Ag

σ_R (mb)

5000

4000

3000

2000

1000

0

1   10   100   1000

Energy (A MeV)

Fig. 37

$^{40}_{18}Ar \ + \ ^{209}_{83}Bi$

Fig. 38

$^{40}_{18}Ar + {}^{238}_{82}U$

Fig. 39

IDL>

$^{40}_{20}Ca + {}^{40}_{20}Ca$

Fig. 40

$$^{84}_{36}Kr + {}^{65}_{28}Cu$$

Fig. 41

$^{86}_{36}$Kr + $^{139}_{57}$La

Fig. 42

Fig. 43

$$^{84}_{36}Kr \; + \; ^{208}_{82}Pb$$

Fig. 44

$$^{84}_{36}Kr \ + \ ^{209}_{83}Bi$$
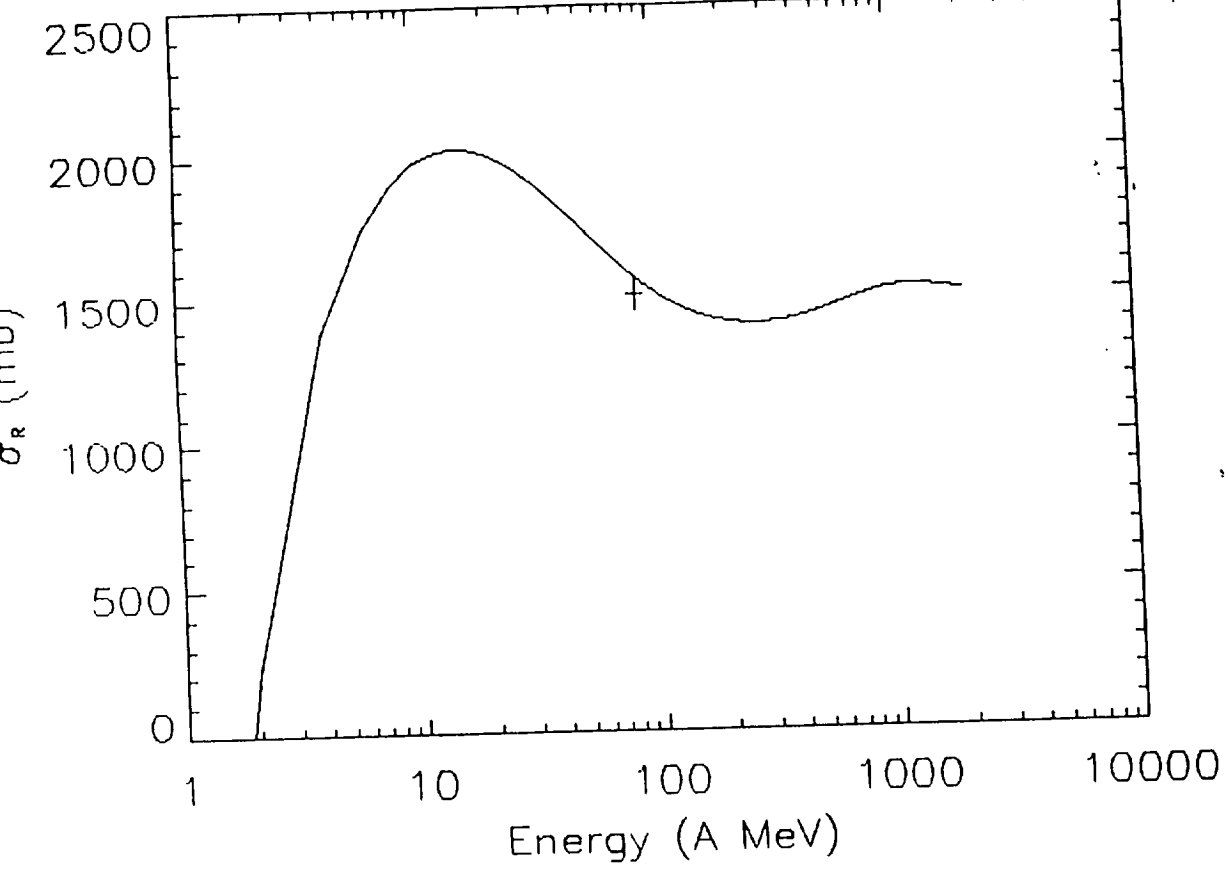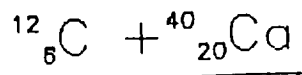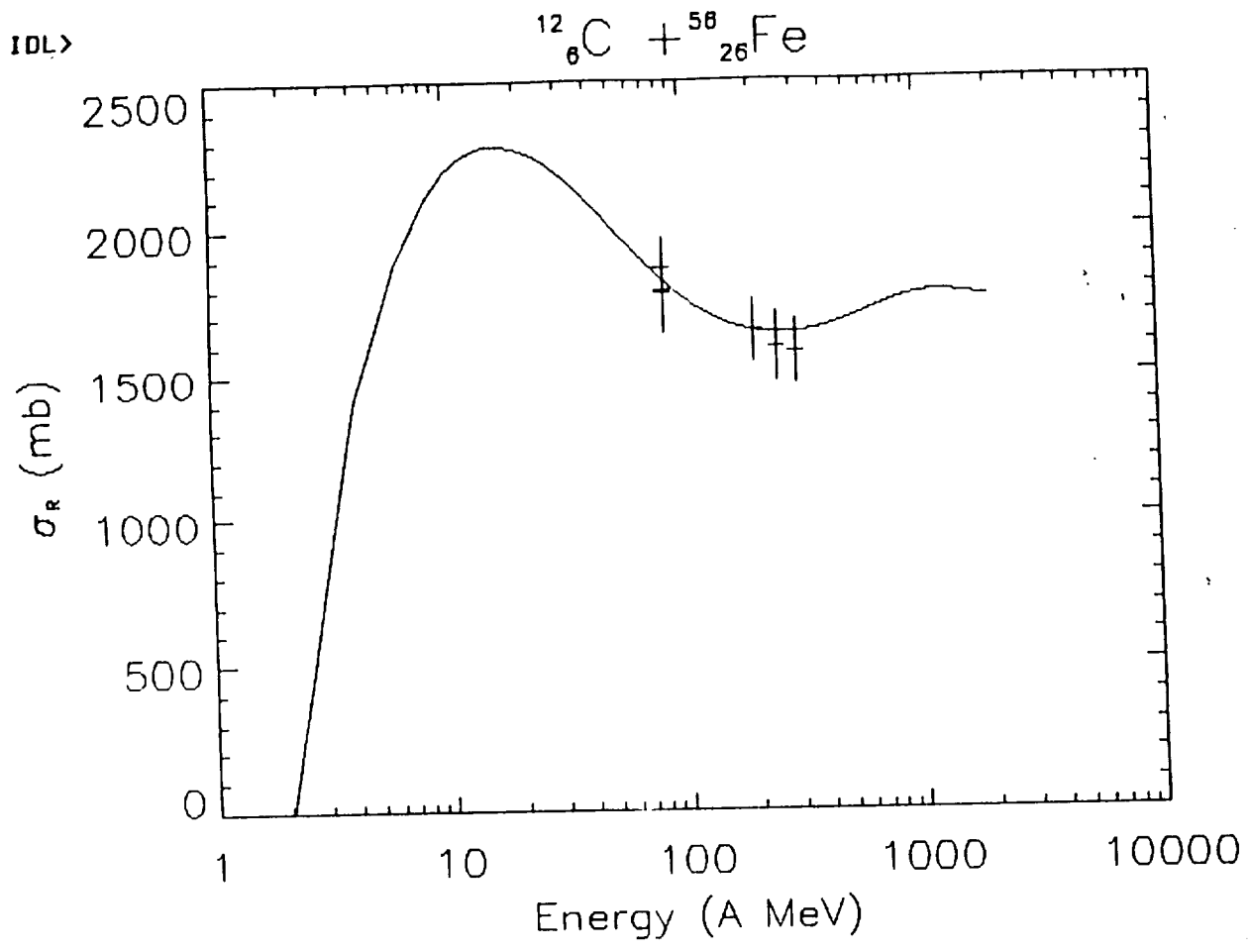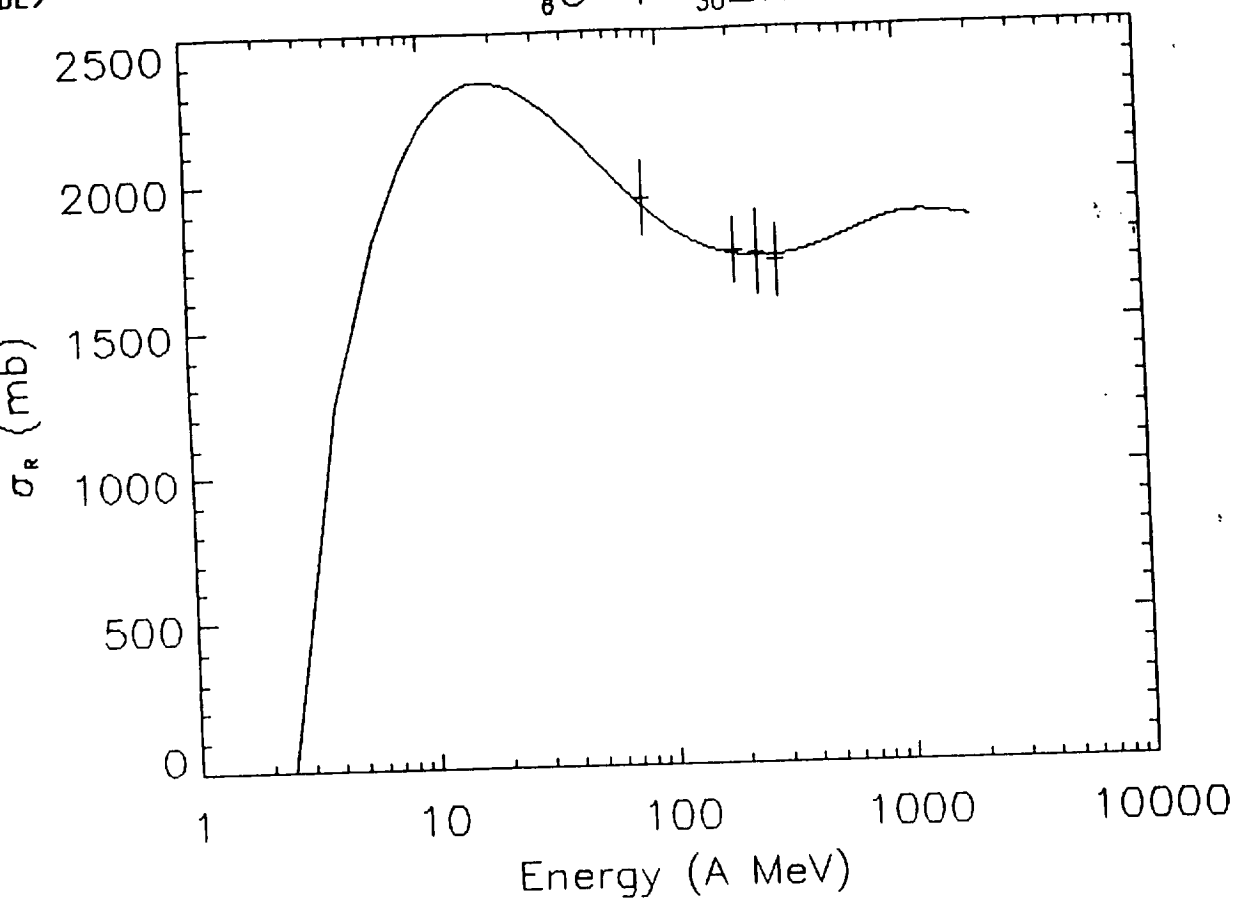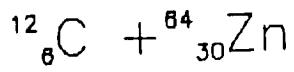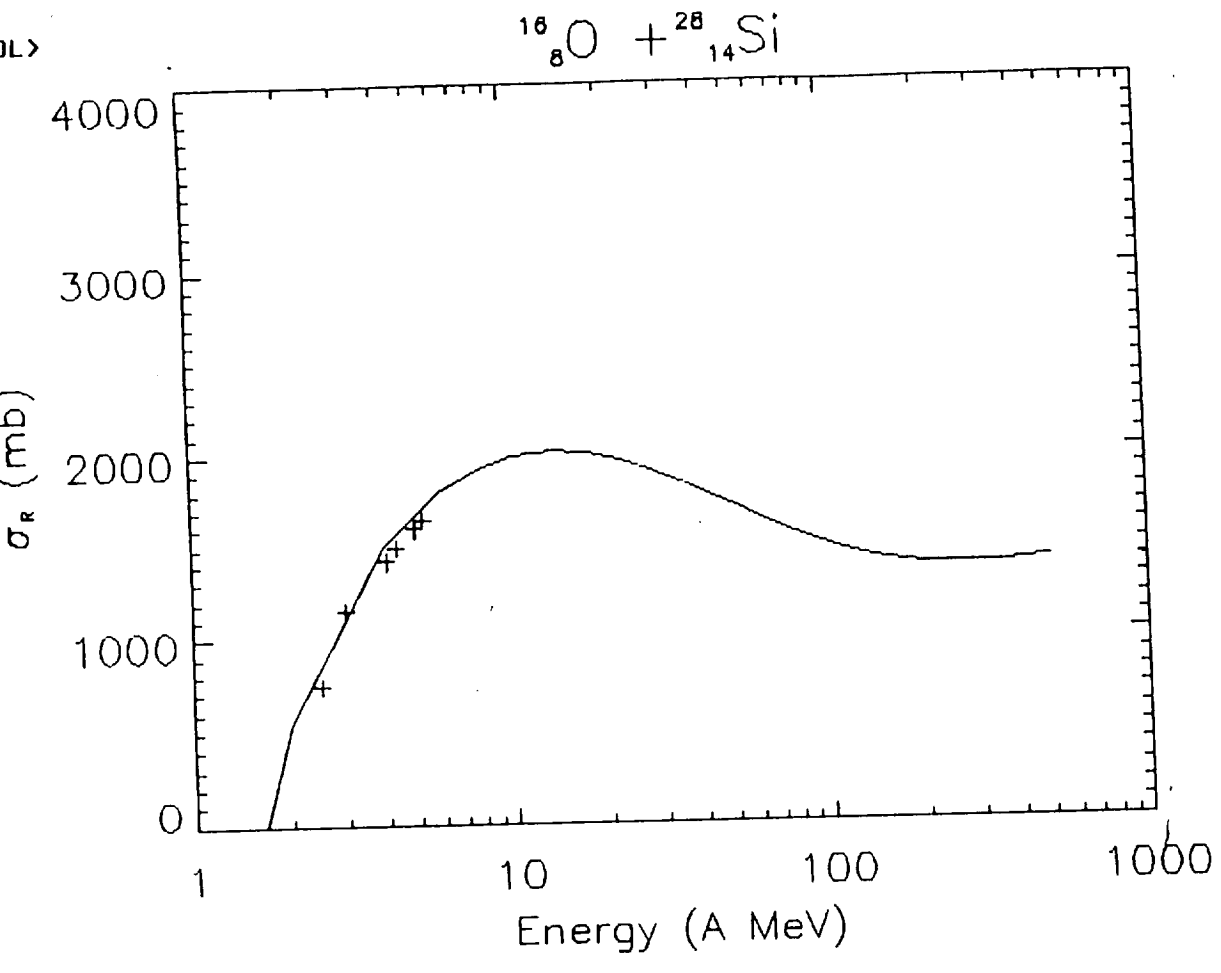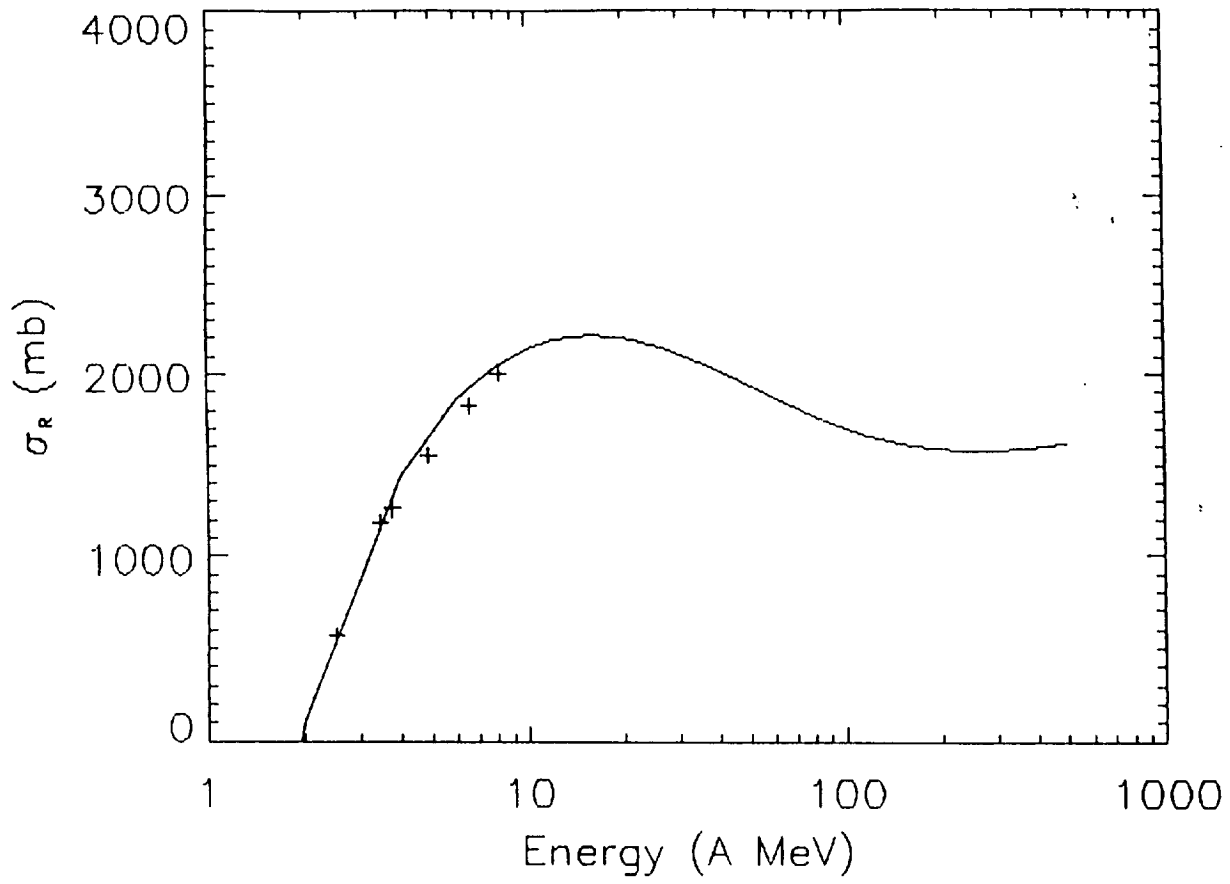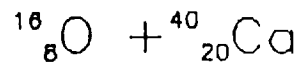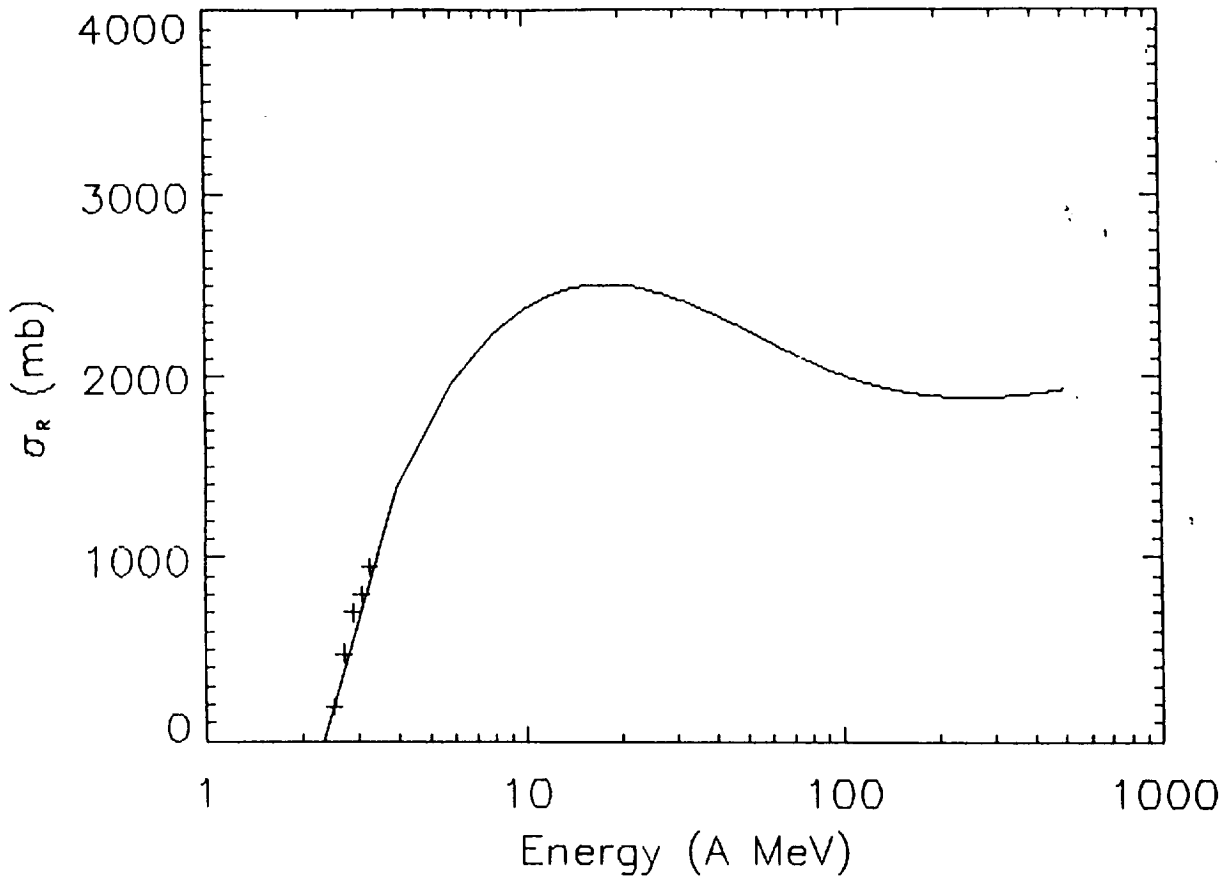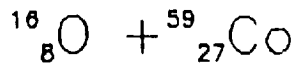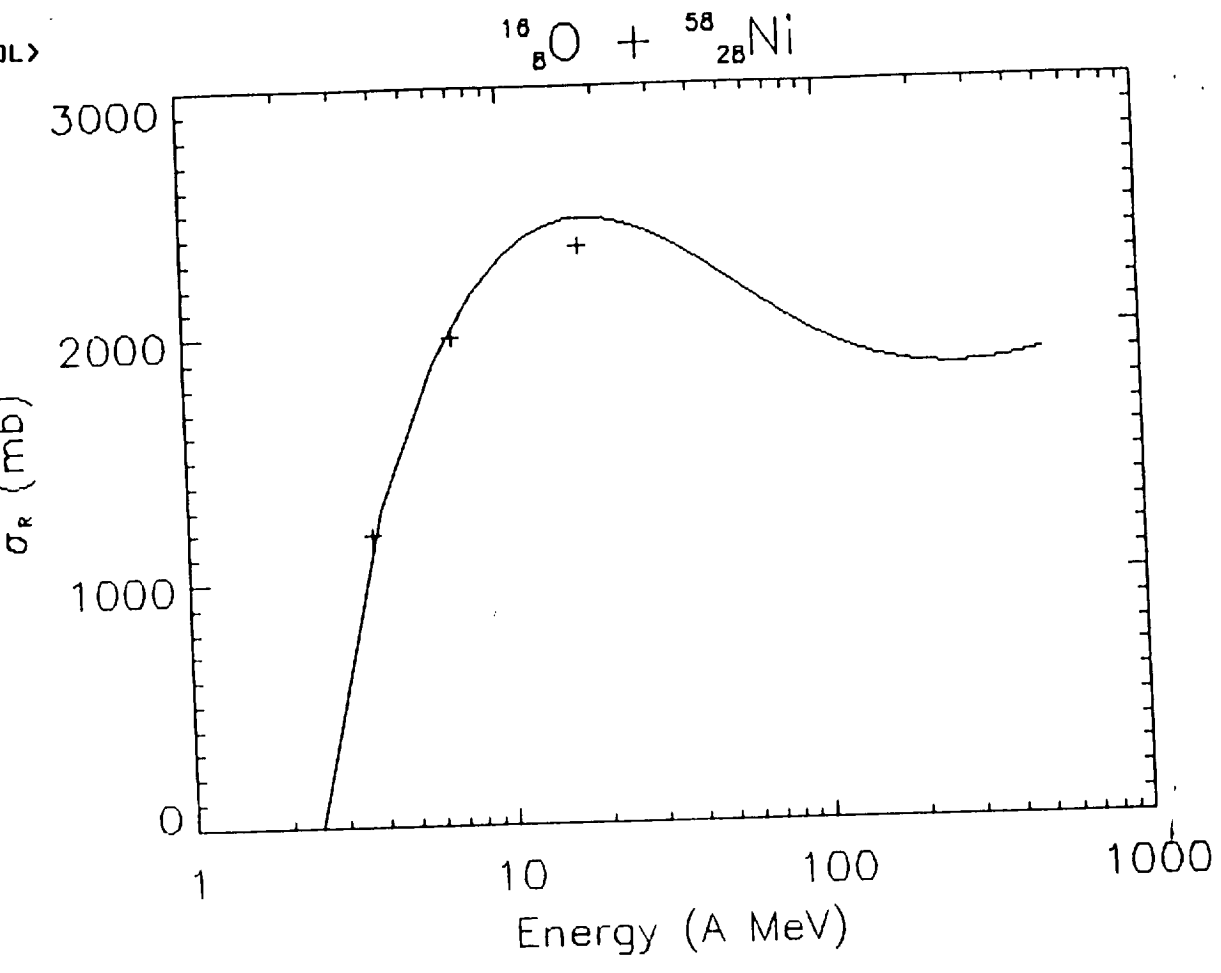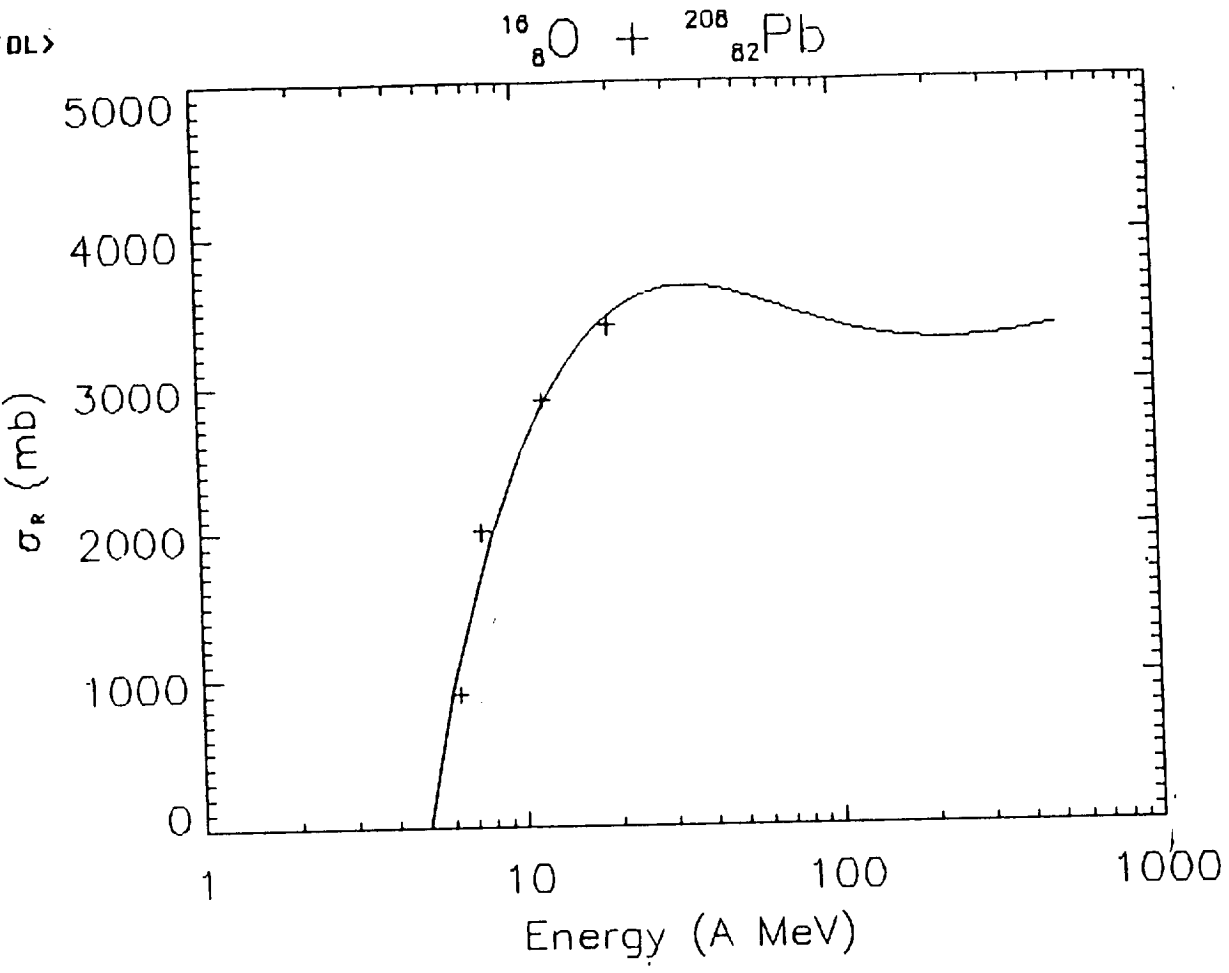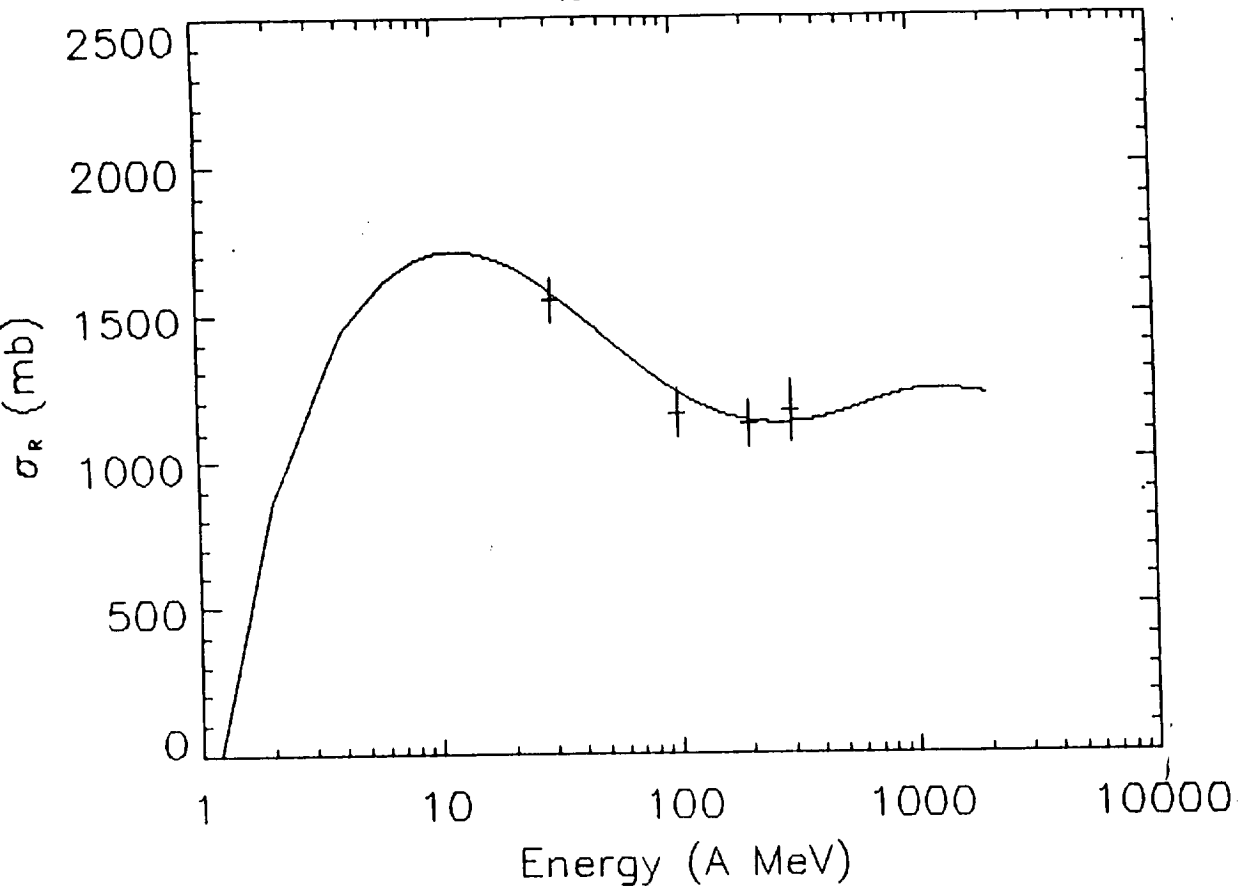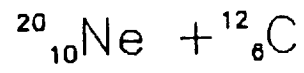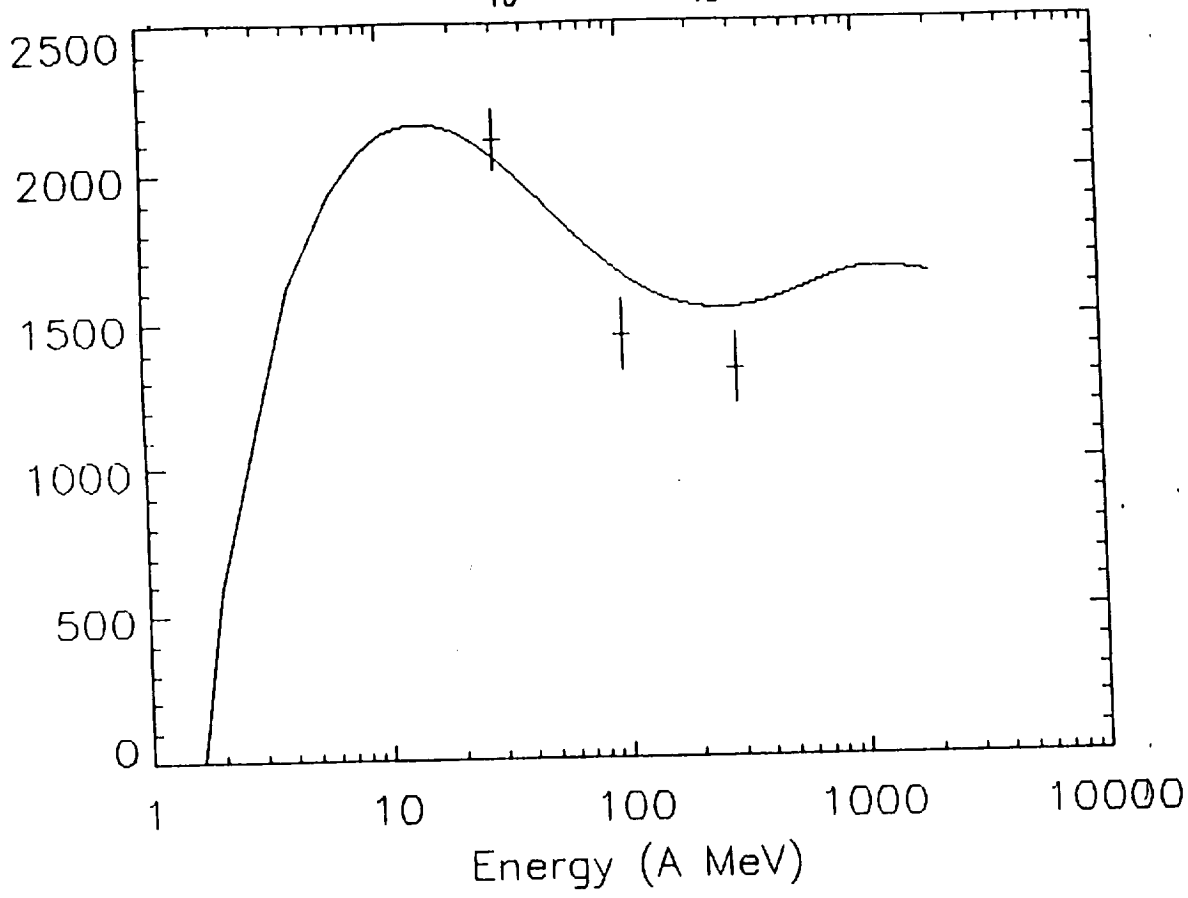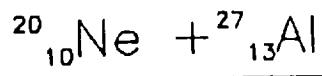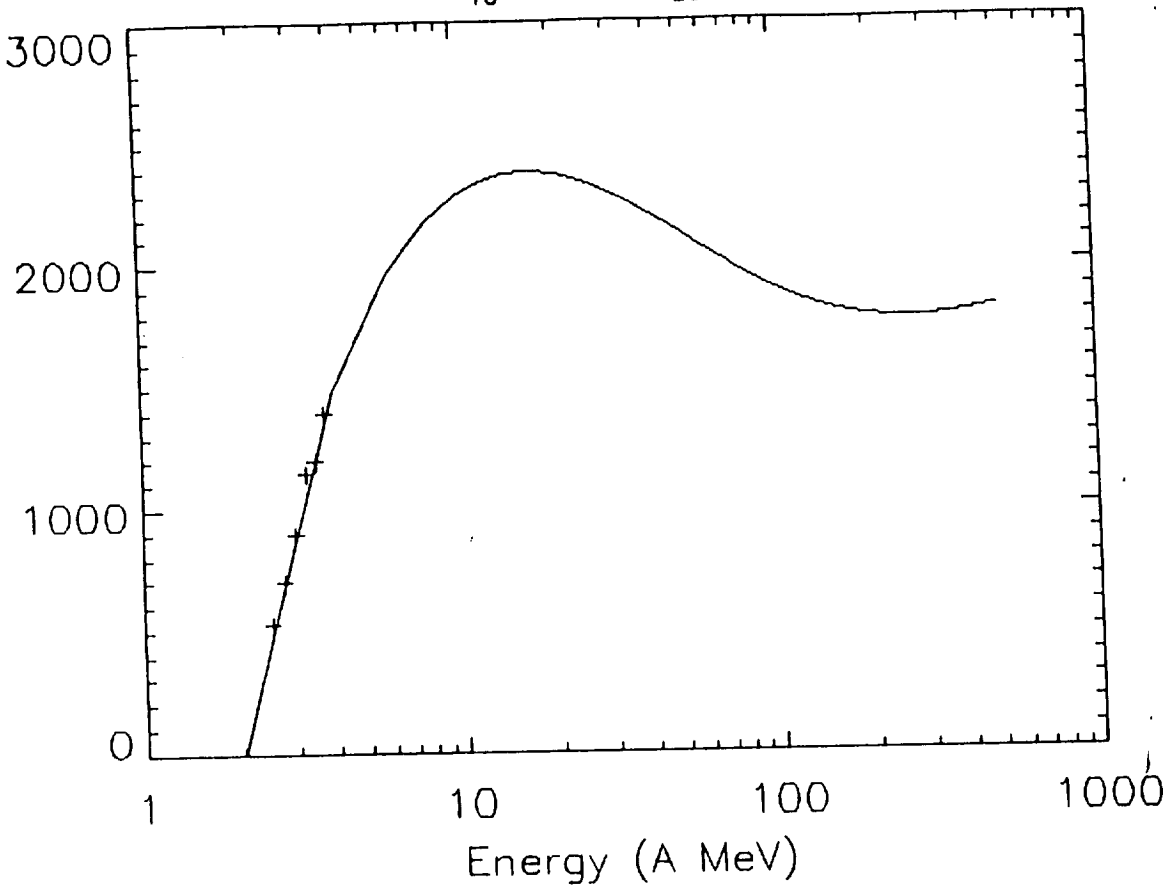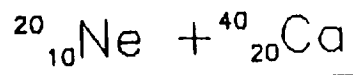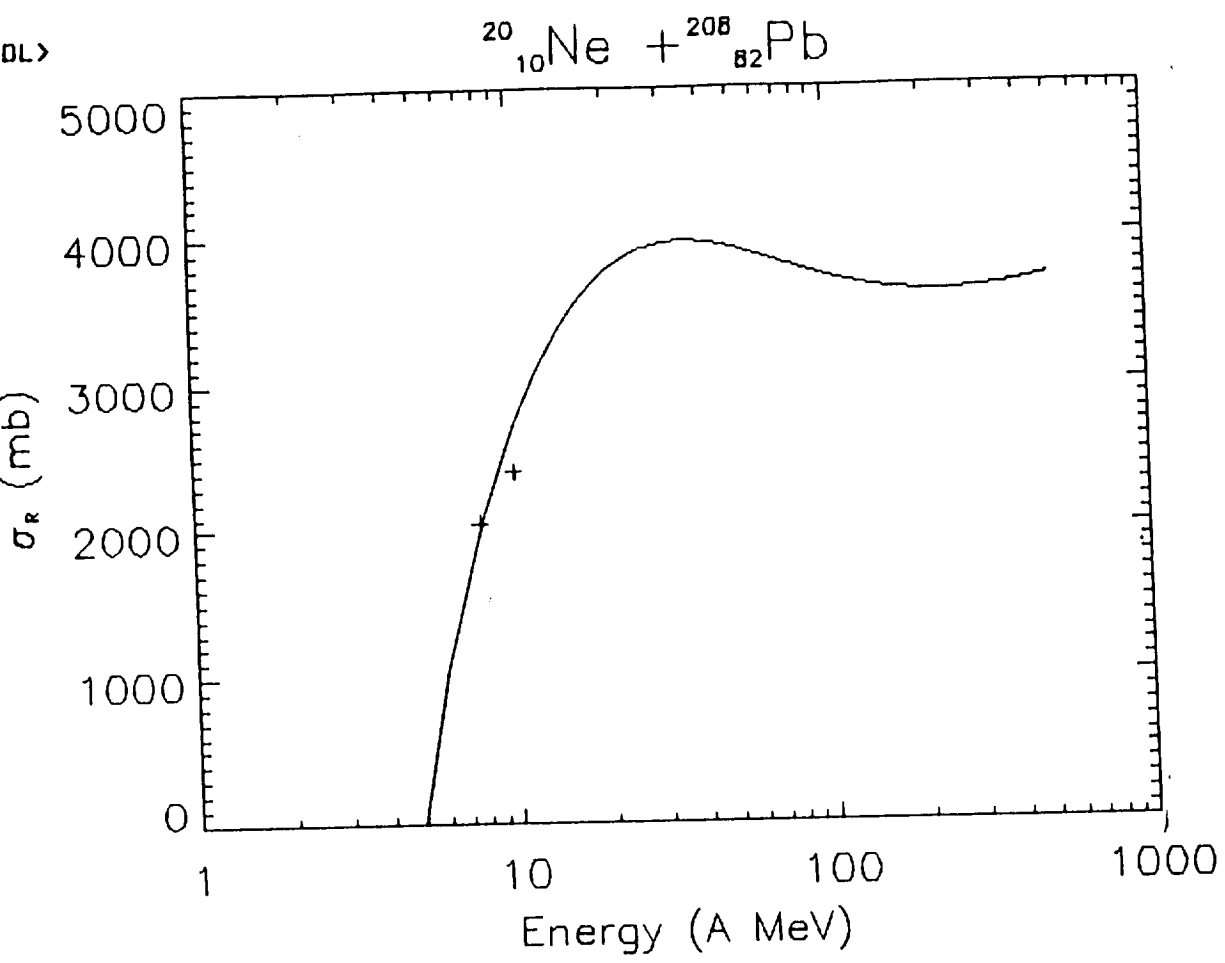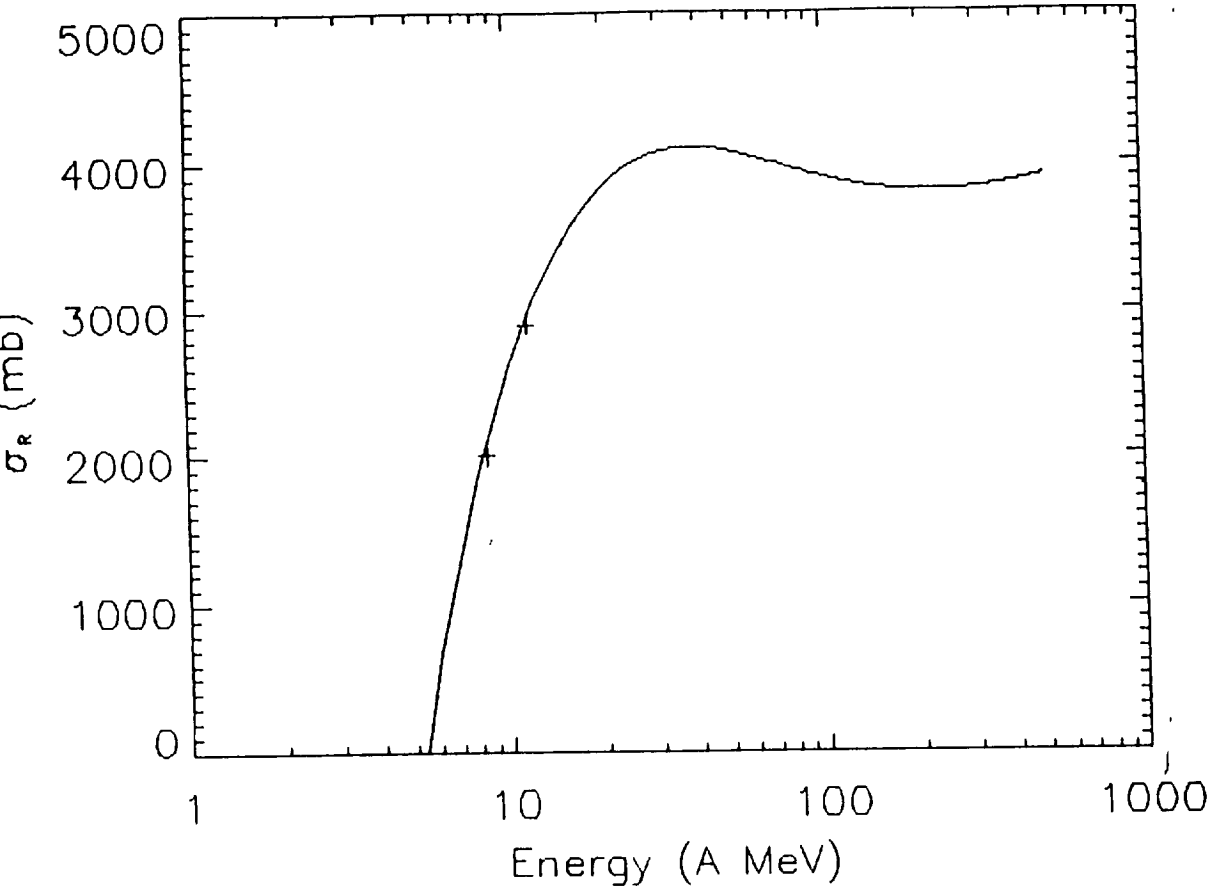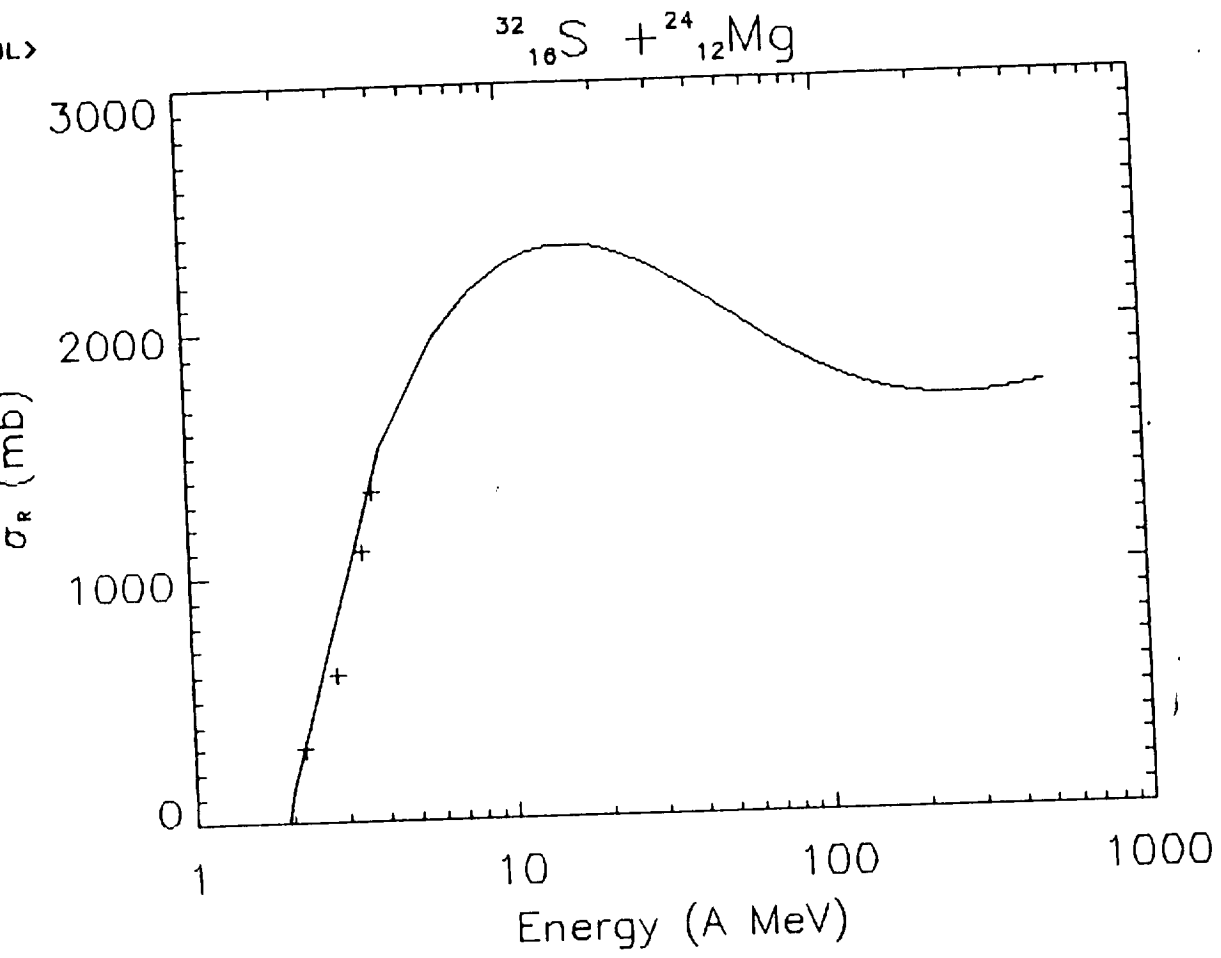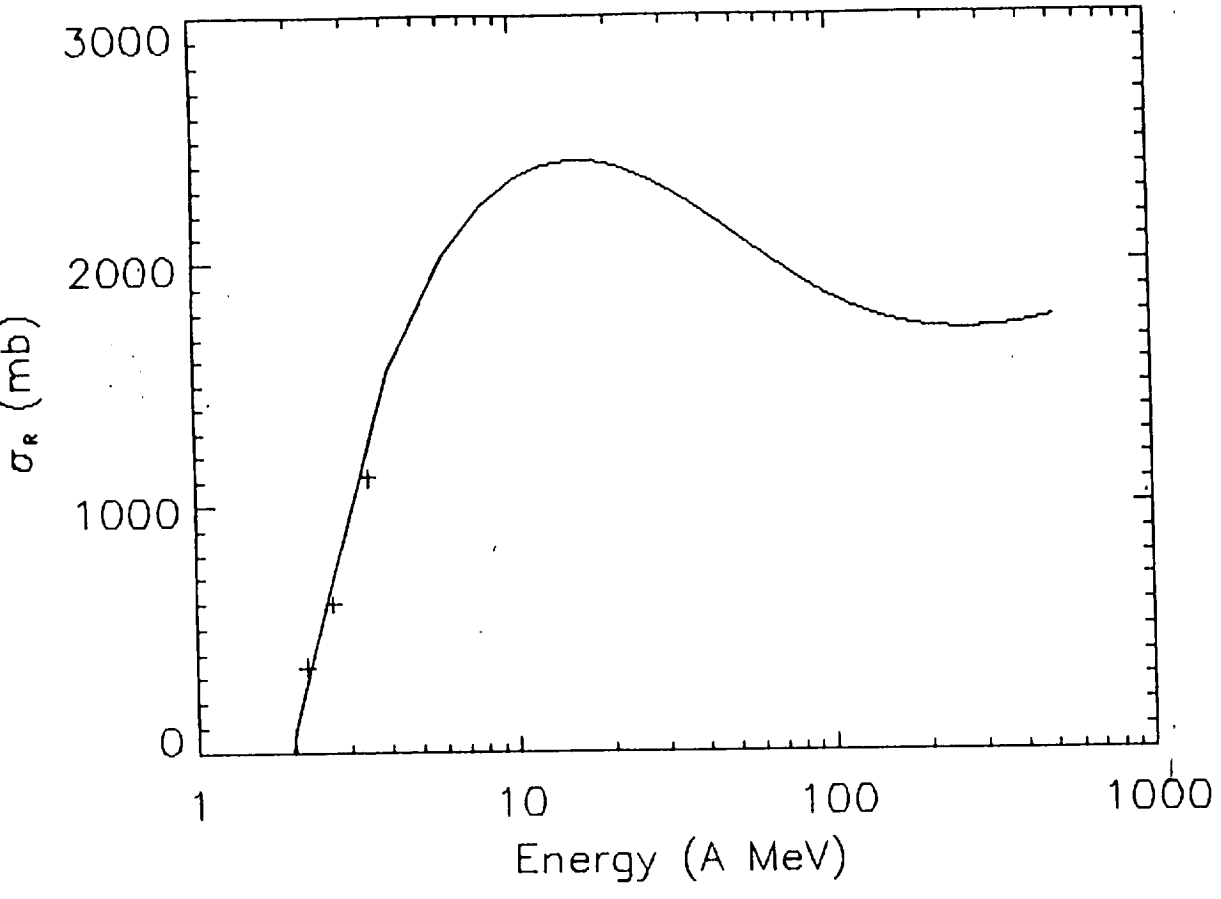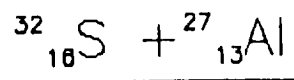
Fig. 45

Emission of light fragments as an indicator of equilibrated

populations in nuclear collisions

R. K. Tripathi
Department of Physics
Southern Illinois University
Carbondale, IL 62901
USA

and

L. W. Townsend
NASA Langley Research Center
Hampton, VA 23681-0001
USA

Abstract

A fully self-consistent, quantum statistical model is used to investigate the emission of light fragments from equilibrated nuclear systems with varying proton-to-neutron ratios over a range of internal excitation energies. A very strong correlation between the species of emitted fragments and the composition of the equilibrated system is found. This finding suggests that light fragments emitted by excited nuclear systems may serve as an indicator of the equilibrated population. We also note that a portion of the emitted alpha particle spectrum is condensed.

Obtaining information about nuclear matter under unusual conditions of density and temperature (excitation energy) has been a goal of research in nuclear physics for some time [1-12]. Because nuclear collisions may last for only a short period of time ($\sim 10^{-22}$ sec), the formation of unusual matter is often transitory. Because most observations are endpoint in nature, information about transitory behavior is often lost. In this letter, we suggest that studies of the distributions of light particles emitted from an equilibrated nuclear systems may be useful for ascertaining the composition of the emitting excited system. Although there is some debate concerning the existence of equilibrated systems in heavy ion collisions, there is general agreement, for the low energies considered herein, that at least a portion of the colliding matter does become equilibrated.

In the work described herein, we show that an unequivocal correlation exists between the abundances of the emitted light fragments and the overall composition of the equilibrated system. This correlation is strong enough that the light fragment abundances may be used as indicators of the transitory composition of the nuclear collision

participants. We also note that a measurable fraction of the emitted alpha particles are condensed.

To begin, consider an assembly of A nucleons consisting of N_o neutrons and Z_o protons in a volume of V_o. Let the proton-to-neutron ratio be denoted by $\gamma (= Z_o/N_o)$. Allow the system of A nucleons to evolve in thermodynamic equilibrium at temperature T and density ρ, and to emit light particles: neutrons (n), protons (p), deuterons (d), tritons (t), ^{3}He (h), and alphas (α). Besides their sets of intrinsic properties (spin, mass, etc.) which differ for each particle, we also classify them in terms of γ so that they can be related to the total equilibrium population A. Specific values for each are (γ in parentheses): n (0), t (0.5), d (1), α (1), and ^{3}He (2). For protons, γ is infinite since we are dividing by zero. In the model, charge and baryon number are conserved by requiring that

$$\sum_i n_i N_i = N_o$$

$$\sum_i z_i N_i = Z_o \tag{1}$$

where the N_i refer to the number of particles of species i. The system evolves in chemical equilibrium, which implies that for any species i, the chemical potential is

$$\mu_i = z_i \mu_p + n_i \mu_n + \varepsilon_i \tag{2}$$

where z_i and n_i are the number of protons and neutrons in the ith species,

and ϵ_i is its binding energy. The distribution of fermions is given by [13]

$$N_i = 2 g_i V_o \pi^{-1/2} \lambda_i^{-3} F_{FD}\left(\mu_i / k_B T\right) \tag{3}$$

where $g_i = 2 S_i + 1$ is the spin degeneracy, μ_i is the chemical potential λ_i is

the thermal wavelength for the ith particle of mass m_i

$$\lambda_i = 2 \pi \hbar \left(2\pi m_i k_B T\right)^{-1/2} \tag{4}$$

where k_B is Boltzmann's constant, and the species index is i (= p, n, h, t) as

appropriate. Values for the Fermi-Dirac integral functions are tabulated in

the literature [14]. For bosons [13, 15, 16], we have

$$N_i = \left[\exp\left(-\mu_i / k_B T\right) - 1\right]^{-1} + g_i V_o \lambda_i^{-3} F_{BE}\left(-\mu_i k_B T\right), \tag{5}$$

where the first term on the right side of Eq. (5) gives the number of

condensed bosons, the second term is the number of noncondensed

bosons, and the species index is i (= d, α). The Bose-Einstein integral

functions appearing in Eq. (5) haven been extensively studied elsewhere

[13, 15].

The evolution of the system is studied as follows: for a given

temperature T, density ρ (= A/V_o), and proton/neutron ratio γ, Eqs. (1) - (5)

are solved self-consistently until a convergent solution is found. The

density is then incrementally increased, for the same T and γ, until another self-consistent solution is found. The set of calculations is stopped at any density for which no self-consistent solution can be found. The calculations for increasing density are repeated for different temperatures, and then the entire process is again carried out for different γ values.

To illustrate, consider systems with $A = 80$ and $\gamma = 1.0, 0.5,$ and 0.25, respectively. These choices for the proton/neutron ratio span most systems of interest in nuclear and astrophysics studies. The total number of equilibrated nucleons ($A = 80$) is reasonable for collisions involving heavier nuclear systems where some but possibly not all of the nucleons may be in equilibrium. Temperature of 1, 2.5, 5, and 7.5 MeV are assumed. At higher temperatures, the alphas and other composite species will undergo significant breakup.

The results of the model calculations are displayed in figures 1 to 3. For $\gamma = 1$ (fig. 1) the most abundant light fragment species is the alpha particle which also has a proton/neutron ratio of $\gamma = 1$. Note that the distributions of alpha particles are very similar for all excitation energies (temperatures) considered. For lower densities and high temperatures

(5 and 7.5 MeV), deuterons (also with $\gamma = 1$) appear. The abundances of other species with $\gamma \neq 1$ are rare.

Figure 2 displays model predictions for a proton-to-neutron ratio of 0.5. Here, the most abundant fragment produced is the triton (^{3}H), which also has $\gamma = 0.5$. The next most abundant fragment species is the neutron ($\gamma = 0$), followed by the alpha particle ($\gamma = 1$) and deuteron ($\gamma = 1$). Again, as was the case with Fig. 1, the most abundant fragment species is that which has the same proton-neutron ratio as the total equilibrated population.

Next, we consider the extreme case for a proton-neutron ratio of $\gamma = 0.25$. Among the emitted species considered herein, none have this value of γ. Based on the results displayed in figs., 1 and 2, however, we would expect that the most likely emitted fragment species would be one with a low γ value, such as the neutron ($\gamma = 0$). From fig. 3, we observe that this is the case. Neutrons are the most abundant species – followed by the triton ($\gamma = 0.5$). Other species which appear (barely) are those with $\gamma = 1$.

Among the light nuclear fragments considered here, the alpha particle is the most-tightly bound. Therefore, from binding energy considerations, one would expect alpha production to dominate -- irrespective of the assumed equilibrium conditions. Instead, our

calculations indicate that particle emissions from equilibrated systems are dictated by the actual composition (γ values) of the source regions rather than by binding energy considerations. This finding may be useful for monitoring the transitory equilibrated population in heavy ion collisions.

This study also provides indications of another interesting phenomena regarding the population of emitted alpha particle -- namely that a measurable fraction of the emitted alphas are condensed. This effect, as expected, is a maximum for the $\gamma = 1$ equilibrium population which favors alpha particle production. In fact, for every temperature and density considered when $\gamma = 1$, most of the emitted alphas are condensed. These results are shown in fig. 4, where the number of condensed alpha particles is displayed as a function of density, temperature, and γ value. Note that condensed alpha particles are also present for $\gamma \neq 1$. For $\gamma = 0.5$, the trends in alpha particle emission as a function of density and temperature are similar to those for $\gamma = 1$, where an increase in the number of condensed alphas with increasing system density is observed at each temperature. For $\gamma = 0.25$, however, we note that very few condensed alphas are produced -- irrespective of system density and/or temperature.

Since we are unable, a priori, to determine the actual composition of the population in thermal equilibrium for any nuclear collision, experimental detection of condensed alphas might be enhanced by selecting the most favorable conditions. From fig. 4, this appears to be lower temperatures (T = 1, 2.5 MeV) and lower densities (ρ < 0.5 normal nuclear matter). It is satisfying to note that these conditions are similar to those found at the surface of a finite nucleus where, at T = 0 MeV, alpha particles are naturally present. Some years ago, an analysis of nuclear matter at T = 0 MeV by Mueller and Clark [17] also predicted the presence of alpha particles at densities lower than that of normal nuclear matter.

In this letter, we have demonstrated that the distributions of light particles emitted from thermalized, equilibrated nuclear systems are mainly dictated by the proton-to-neutron ratio of the equilibrated source, rather than by binding energy. This finding may be useful for monitoring the presence of transitory equilibrium in heavy ion collisions. Although more realistic calculations should be performed to confirm these results, it is anticipated that the general conclusions presented here would not be substantially altered.

References

[1]   Csernai LP 1985 *Phys. Rev. Lett.* **54** 639

[2]   Cugnon J 1984 *Phys, Lett* **135B** 374

[3]   Bauer W Bertsch GF and Shultz H 1992 *Phys. Rev. Lett.* **69** 1888

[4]   Subramarian PR et al 1981 *J. Phys. G* **7** L241

[5]   Csernai LP and Kapusta J 1986 *Phys. Rep.* **131** 223

[6]   Zimanyi J Fai G Jakobson B 1979 *Phys. Rev. Lett.* **43** 1705

[7]   Panagiotou AD Curtin MW Toki H Scott DK and Siemens PJ 1984

       Phys Rev. Lett. **52** 496

[8]   Minnich RW et al 1982 *Phys. Lett.* **118B** 458

       Hirsch AS et al 1984 *Phys. Rev. C* **29** 508

[9]   Li GQ Faessler A and Huang SW 1993 *Prog. Part. Nucl. Phys.* **31** 159

       Bertsch GF and Das Gupta S 1988 *Phys. Rep.* **16** 189

[10]   Stöcker H and Greiner W 1986 *Phys. Rep.* **137** 227

[11]   Tripathi RK 1982 *Phys. Rev. C* **25** 1114

[12]   Boal DH 1987 *Ann. Rev. Nucl. Part. Sci.* **37** 1

       Lynch WG 1987 *ibid* **37** 493

[13]   Walecka JD 1989 *Fundamentals of Statistical Mechanics* (Stanford:

       Stanford University Press)

[14]   Beer AC Chase MN Choquard PF 1955 *Helv. Phys. Acta* **28** 529

[15]   Robinson JE 1951 *Phys. Rev.* **83** 678

[16]   London F 1954 *Superfluids* Vol. II (New York: Wiley)

[17]   Mueller GP and Clark JW 1970 *Nucl. Phys.* **A155** 561c

Figure Captions

Figure 1. Distributions of emitted particles for A = 80 and $\gamma = 1$

($N_o = Z_o = 40$) as a function of temperature and density ratio

($\rho_o = 0.17$ fm^{-3}). Curves for the more abundant fragment species are the

only ones displayed.

Figure 2. Distributions of emitted particles for A = 80 and $\gamma = 0.5$

($N_o = 53$, $Z_o = 27$) as a function of temperature and density ratio

($\rho_o = 0.17$ fm^{-3}). Curves for the more abundant fragment species are the

only ones displayed.

Figure 3. Distributions of emitted particles for A = 80 and $\gamma = 0.25$

($N_o = 64$, $Z_o = 16$) as a function of temperature and density ratio

($\rho_o = 0.17$ fm^{-3}). Curves for the more abundant fragment species are the

only ones displayed.

Figure 4. Number of condensed alpha particles as a function of

temperature and density ratio ($\rho_o = 0.17$ fm^{-3}) for different compositions

($\gamma = 1, 0.5, 0.25$) of equilibrated matter.
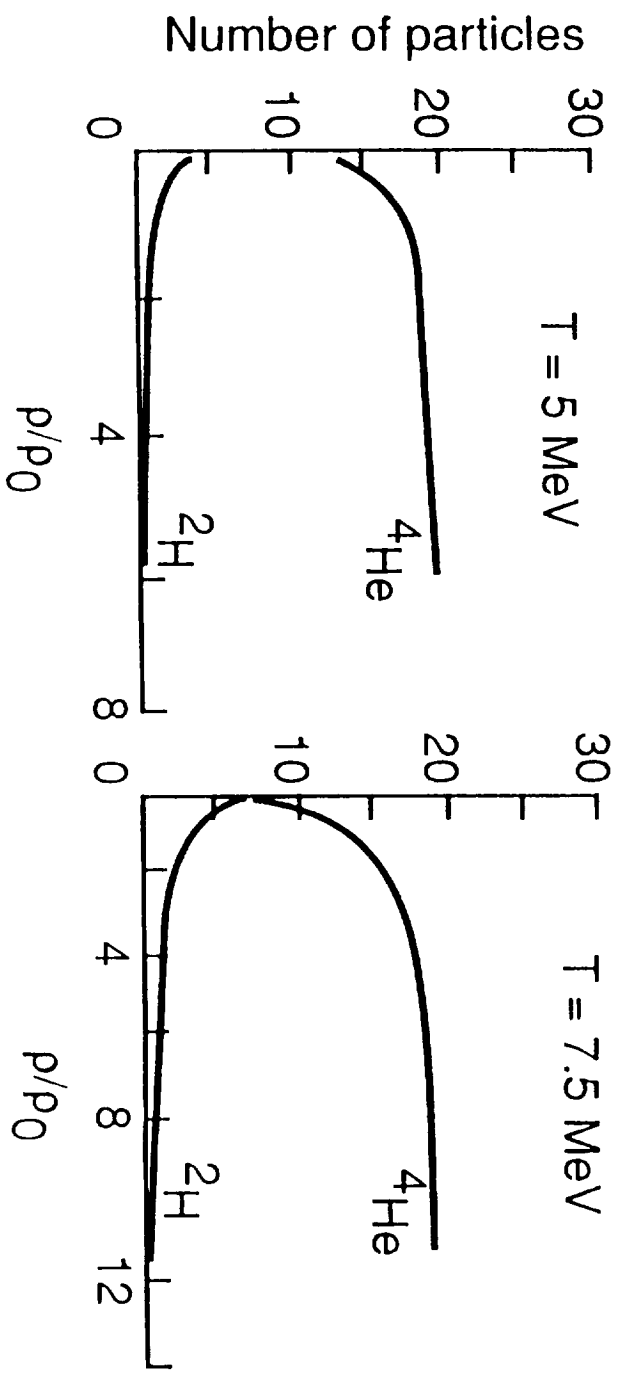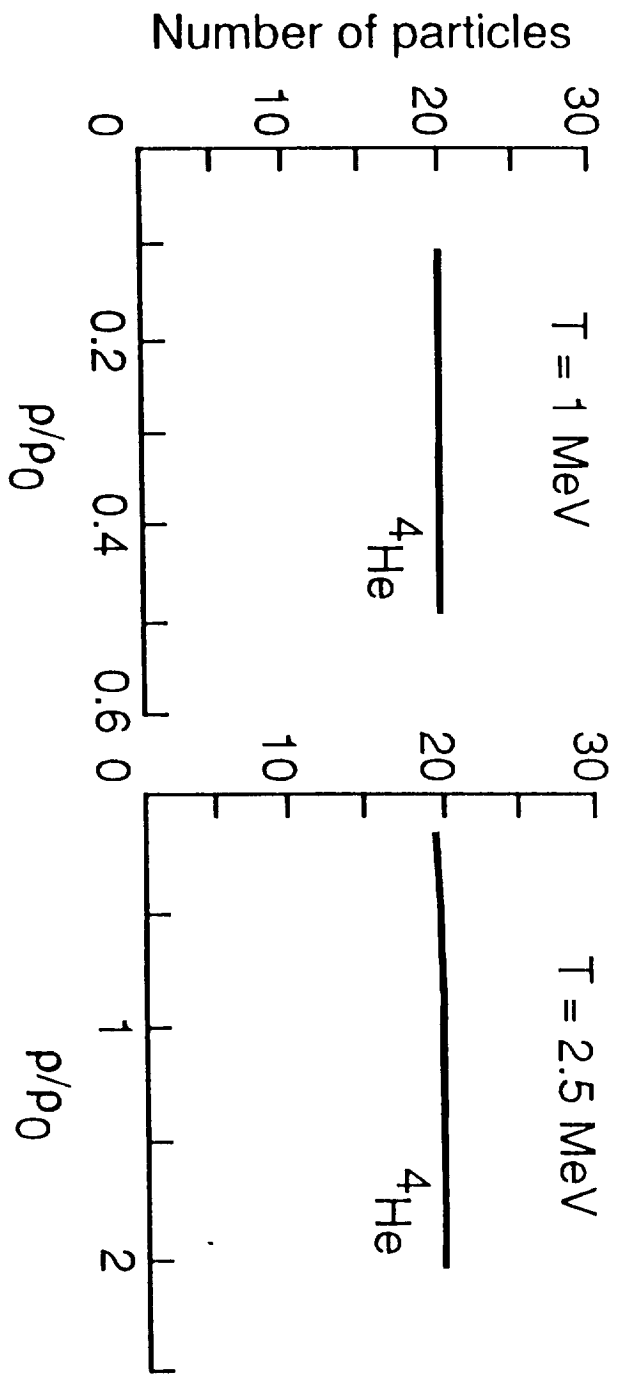
Fig. 1 – Tripathi / Townsend
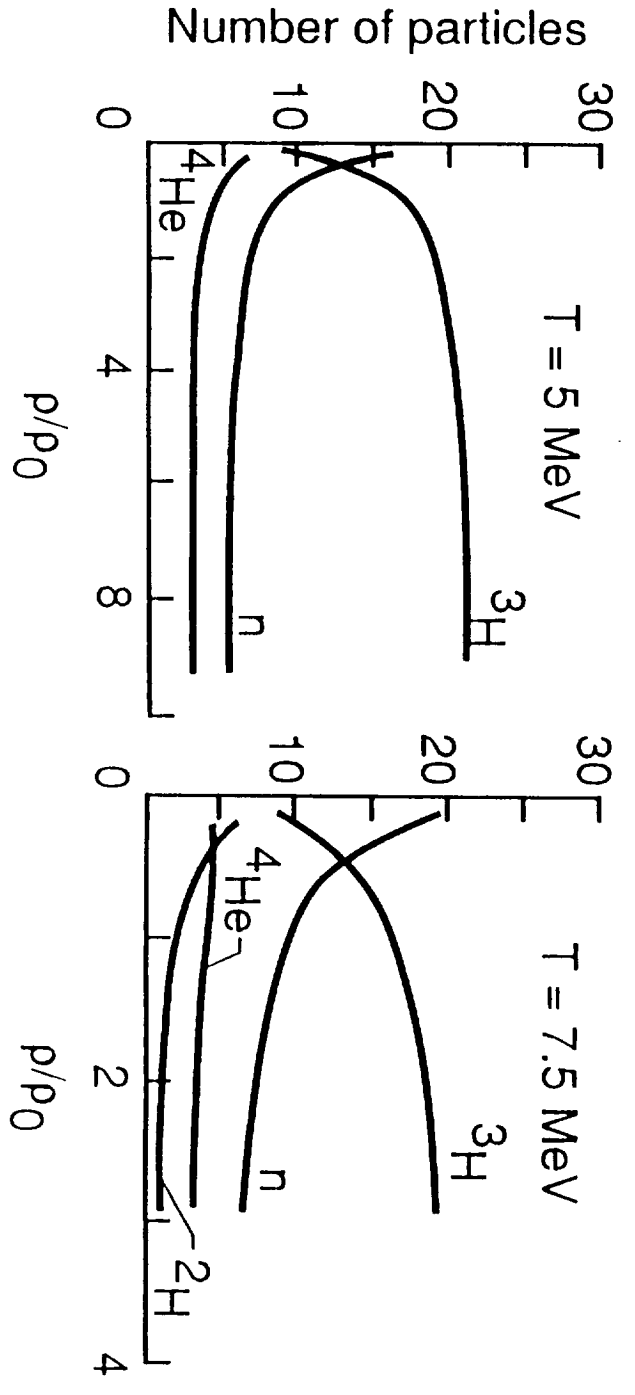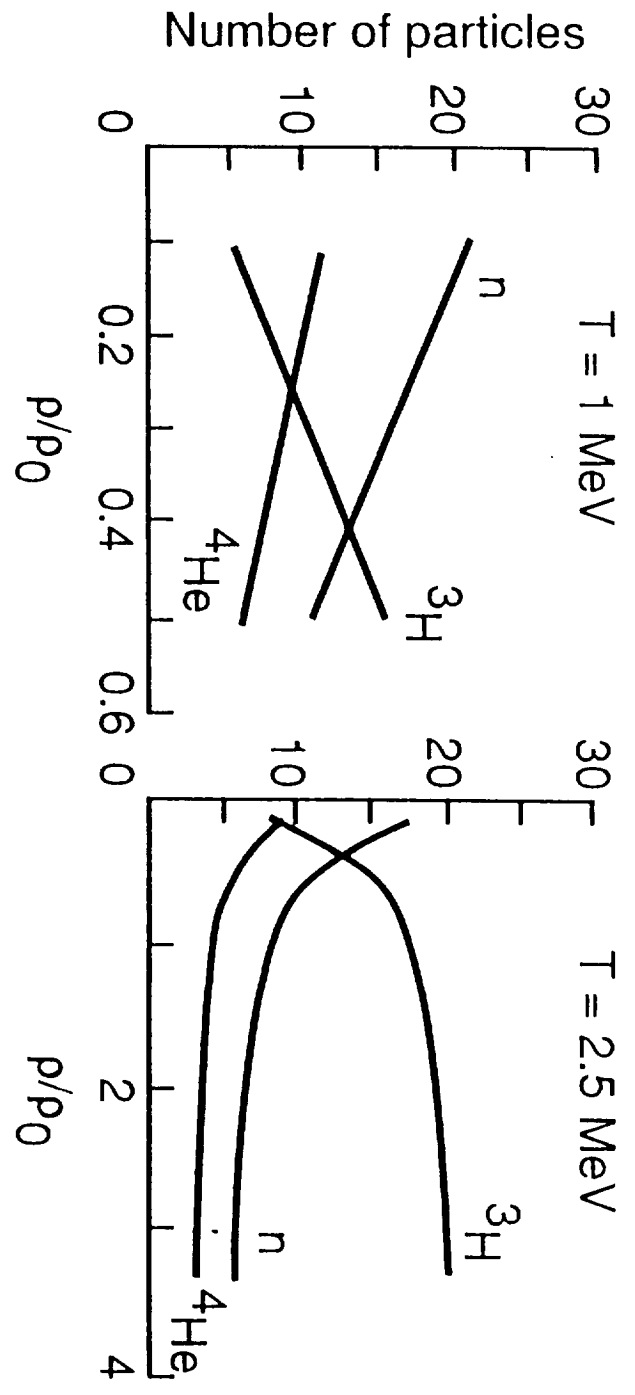
Fig. 2 – Tripathi / Townsend
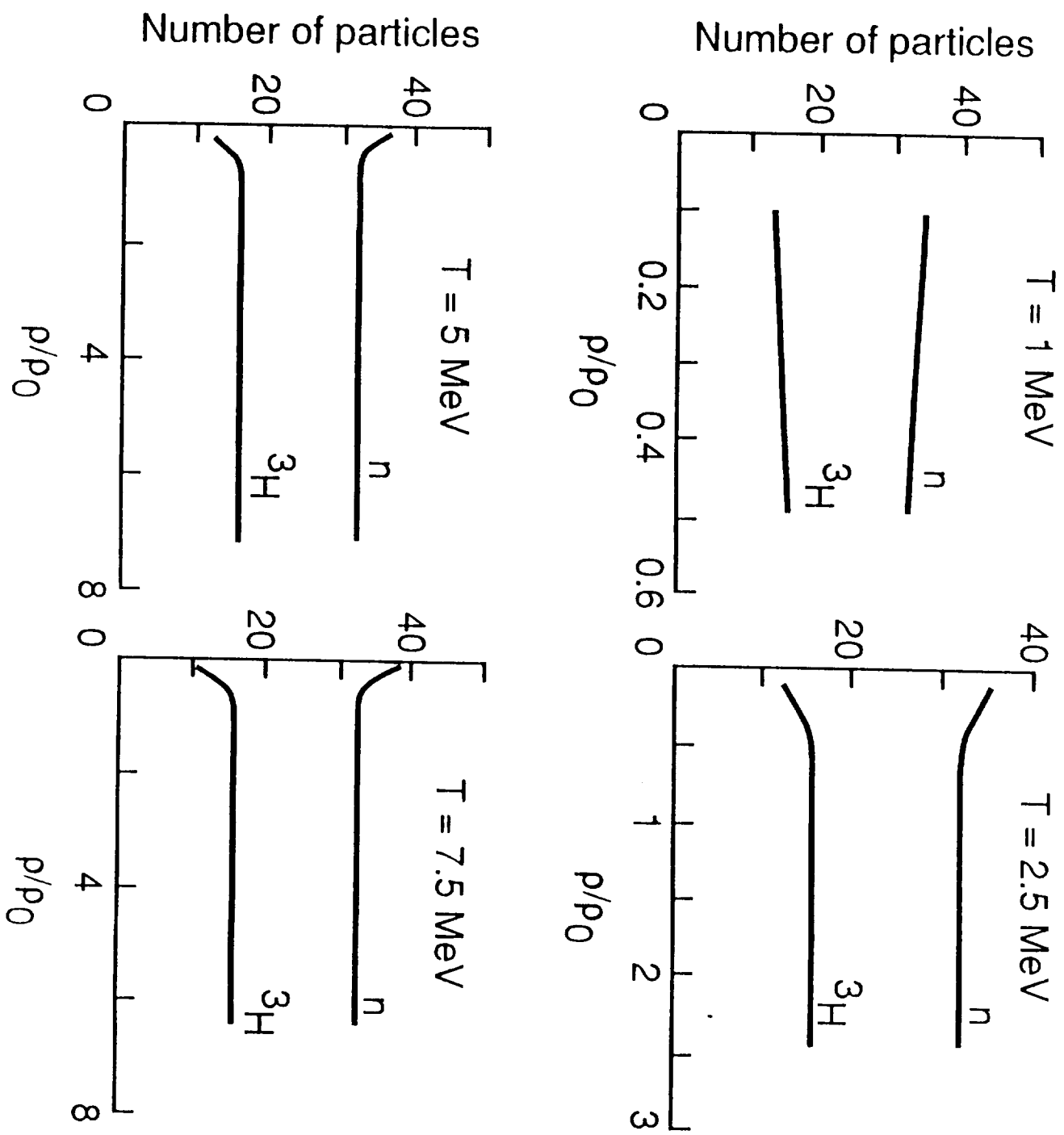
Fig. 3— Tripathi / Townsend
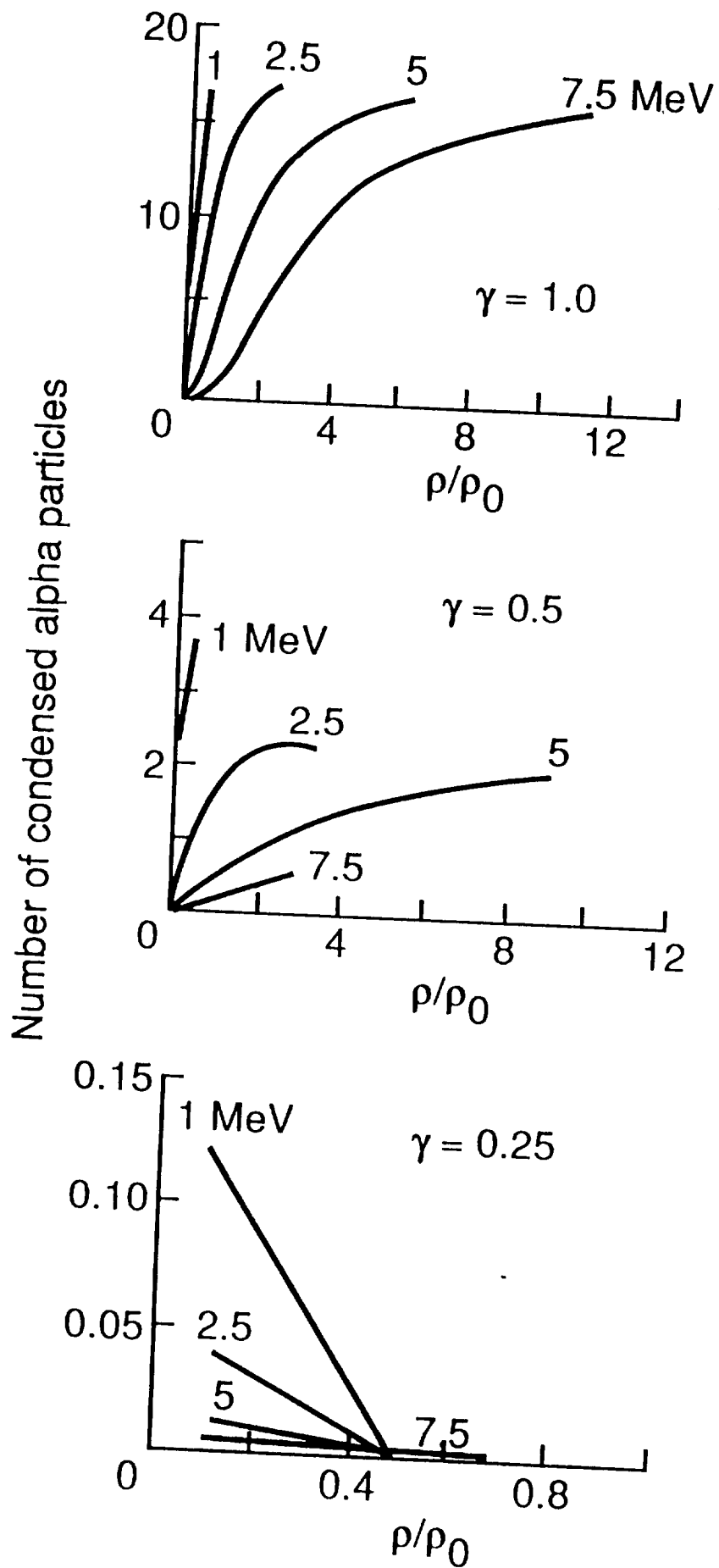
Fig. 4 — Tripathi / Townsend

Transport of Light Ions in Matter

J. W. Wilson, F. A. Cucinotta, H. Tai, and J. L. Shinn
NASA Langley Research Center
Hampton, VA 23681-0001

S. Y. Chun
Old Dominion University
Norfolk, VA 23581

R. K. Tripathi
University of Southern Illinois
Carbondale, IL 62901

L. Sihver
GSI
Darmstadt, Germany

Number of copies submitted: 4
Number of pages: 9
Number of figures: 6
Number of tables: 1

Transport of Light Ions in Matter

J. W. Wilson, F. A. Cucinotta, H. Tai, and J. L. Shinn
NASA Langley Research Center
Hampton, VA 23681-0001

S. Y. Chun
Old Dominion University
Norfolk, VA 23581

R. K. Tripathi
University of Southern Illinois
Carbondale, IL 62901

L. Sihver
GSI
Darmstadt, Germany

Abstract

A recent set of light ion experiments are analyzed using the GRNTRN transport code and the NUCFRG2 fragmentation database generator code. Although the NUCFRG2 code reasonably represents the fragmentation of heavy ions, the effects of light ion fragmentation requires a more detailed nuclear model including shell structure and short range correlations appearing as tightly bound clusters in the light ion nucleus. The NUCFRG2 code is augmented with a quasielastic alpha knockout model and semiempirical adjustments in the fragmentation process allowing reasonable agreement with the experiments to be obtained. A final resolution of the appropriate cross sections must await the full development of a coupled channel reaction model in which shell structure and clustering can be accurately evaluated.

Introduction

The need for accurate transport methods and corresponding atomic/nuclear database for protection against radiations in space was demonstrated in a recent review of issues in space radiation protection (1). Although the earliest efforts in code validation experiments were placed on the relatively light ion beam of neon because of the potential importance of that beam to radiation therapy (2–5), the first beam studied specifically for space radiation protection was the iron beam which is the single most important species in long term space exposures (6, 7). Among the specific issues in the iron beam experiments are the production cross sections for light fragments which were in doubt and in fact the reason for development of the NUCFRG code (8). Recent experiments at the GSI accelerator in preparation for medical therapy has recently provided data on the transport in water of the light ions of carbon, nitrogen and oxygen (9–11). Aside from the fact that the most abundant ions in the space environment with charge of three or more is the CNO group produced in abundance in star interiors, these are also interesting ions for which the NUCFRG code (based on a liquid drop model) is expected to be least appropriate (12–14). Hence, the current data set is an important test for the fragmentation database used in space studies.

In the present report, we give a brief review of the current state of the transport formalism and application to the analysis of the GSI beam data. The initial results from the NUCFRG2 database are found to be in error by 30–40 percent. It is surmised that the fault lies in the liquid drop assumption. The nuclear interaction viewed as a combination of inelastic, quasielastic, and nonelastic events leads us to assume the main quasielastic event in which specific particles or clusters are removed from a reasonably stable core cannot be accomadated within a liquid drop formalism (13, 14) while the highly nonelastic events in which the mass removed from the projectile is fully dissociated is well represented by the NUCFRG2 code. One can see these dynamic differences in the $^{12}C/^{13}C$ ratio in the fragmentation of ^{40}Ar (ratio of 1) in comparison with the value for

fragmentation of ^{16}O (ratio of 2.3) as measured by Tull (15) and Olson et al. (16) respectively. The cluster effect for ^{16}O projectiles is taken herein from the work of Cucinotta and Dubey (13, 14) and some additional ad hoc adjustments are made to the liquid drop model representing the non elastic events until a more complete cluster code is available. The resultant database is an improvement over the NUCFRG2 code but Li and Be fragments remain untested by the GSI experiments. In the absence of such data the further development of the cluster model is our best hope of resolving these cross sections.

Transport Methods

In the domain of a spatially uniform beam, the Boltzmann transport equation assuming a straight-ahead approximation is useful in evaluating many field quantities in high-energy ion transport. Even for narrow and directed ion beams, angular and spectral corrections have been applied successfully as multiplicative factors (3–5). The ion flux of type j at x with energy E (AMeV) is given as (17)

$$\varphi_j(x,E) = \frac{S_j(E_j)\,P_j(E_j)}{S_j(E)\,P_j(E)}\,\phi_j(0,E_j)$$

$$+ \sum_k \int_E^{E_j} dE'\,\frac{A_j\,P_j(E')}{S_j(E)\,P_j(E)}\int_{E'}^{\infty} dE''\,\sigma_{jk}(E',E'')\varphi_k\big[x + R_j(E) - R_j(E'),E''\big]$$

$$(1)$$

where $S_j(E)$ is the stopping power, $P_j(E)$ is the nuclear attenuation coefficient given as

$$P_j(E) = \exp\left[-\int_0^E \sigma_j(E')A_j\,dE'/S_j(E')\right] \qquad (2)$$

$E_j = R_j^{-1}\left[x + R_j(E)\right]$ is the energy at the boundary for an ion j at x with residual energy E, and $R_j(E)$ is the residual range, $R_j^{-1}\left[R_j(E)\right] = E$. We may rewrite the solution in terms of the Green's function as

$$\varphi_j(x,E) = \sum_k \int_0^\infty G_{jk}(x,E,E_o)\varphi_k(0,E_o)dE_o \tag{3}$$

where $G_{jm}(x,E,E_o)$ satisfies an integral equation similar to Eq. (1) as

$$G_{jm}(x,E,E_o) = \frac{S_j(E_j)\,P_j(E_j)}{S_j(E)\,P_j(E)}\,G_{jm}(0,E_j,E_o) + \sum_k \int_E^{E_j} dE' \frac{A_j\,P_j(E')}{S_j(E)\,P_j(E)}$$
$$\int_{E'}^\infty dE''\, \sigma_{jk}(E',E'')\,G_{km}\left[x + R_j(E) - R_j(E'),E'',E_o\right] \tag{4}$$

where

$$G_{jm}(0,E,E_o) = \delta_{jm}\,\delta(E - E_o) \tag{5}$$

We use the Neuman expansion as a perturbative series

$$G_{jm}(x,E,E_o) = \sum_{i=0}^\infty G_{jm}^{(i)}(x,E,E_o) \tag{6}$$

where the leading term is

$$G_{jm}^{(o)}(x,E,E_o) = \frac{S_j(E_j)\,P_j(E_j)}{S_j(E)\,P_j(E)}\,\delta_{jm}\,\delta(E_j - E_o) \tag{7}$$

and the higher order terms are given by

$$G_{jm}^{(i)}(x,E,E_o) = \sum_k \int_E^{E_j} dE' \frac{A_j\,P_j(E')}{S_j(E)\,P_j(E)}\int_{E'}^\infty dE''\, \sigma_{jk}(E',E'')$$
$$G_{km}^{(i-1)}\left[x + R_j(E) - R_j(E'),E'',E_o\right] \tag{8}$$

The first iterate of Eq. (8) is given as

$$G_{jm}^{(1)}(x, E, E_o) = \sum_k \int_E^{E_j} dE' \frac{A_j P_j(E')}{S_j(E) P_j(E)} \int_{E'}^{\infty} dE'' \, \sigma_{jk}(E', E'')$$

$$\frac{S_k(E'_k) P_k(E'_k)}{S_k(E'') P_k(E'')} \, \delta_{km} \, \delta(E'_k - E_o)$$

(9)

where

$$E'_k = R_k^{-1}\left[x + R_j(E) - R_j(E') + R_k(E'')\right]$$

(10)

If we make the usual assumption that the interaction is dominated by perpherial processes then

$$\sigma_{jm}(E', E'') = \sigma_{jm}(E'') \, \delta(E' - E'')$$

(11)

for which the second term of the Neuman series becomes

$$G_{jm}^{(1)}(x, E, E_o) = \frac{A_j}{S_j(E)} \frac{\upsilon_j}{|\upsilon_m - \upsilon_j|} \frac{P_j(E')}{P_j(E)} \, \sigma_{jm}(E') \frac{P_m(E_o)}{P_m(E')}$$

(12)

for values of E such that

$$\frac{\upsilon_m}{\upsilon_j}\left[R_m(E_o) - x\right] < R_j(E) < \frac{\upsilon_m}{\upsilon_j} R_m(E_o) - x$$

(13)

where v_j is the range scaling parameter $\left(v_i \approx Z_j^2 / A_j\right)$. It was shown by Chun et al. (18) that the second term can be approximated by a linear function of energy as

$$
\begin{aligned}
G_{jm}^{(i)}(x,E,E_o) &= \frac{1}{2}\left[G_{jm}^{(i)}(x,E,E_{o\,min}) + G_{jm}^{(i)}(x,E,E_{o\,max})\right] \\
&\quad + \left[\frac{G_{jm}^{(i)}(x,E,E_{o\,max}) - G_{jm}^{(i)}(x,E,E_{o\,min})}{E_{o\,max} - E_{o\,min}}\right]\left(E - \frac{E_{o\,max} + E_{o\,min}}{2}\right)
\end{aligned}
\tag{14}
$$

where $E_{o\,max}$ and $E_{o\,min}$ are associated with the allowed range in relation (13). Eq. (14) allows a simple numerical evaluation of the ion flux spectra (5, 18). The higher order terms we evaluate using the nonperturbative method discussed elsewhere (5).

Comparison With Experiment

Experiments were performed at the GSI accelerator using beams of ^{12}C, ^{14}N, and ^{16}O at energies of 674($\pm$2) MeV/u in which the transmitted flux of charge 5 to 8 were measured behind a water target of variable thickness (9–11). The measured transmitted flux of the same charge (open circles) is shown in fig. 1 along with the solution for the primary beam flux (dashed curve) and the calculated flux of all ions of charge equal to the initial beam (solid curve). It appears that the total absorption and neutron removal cross sections of the NUCFRG2 are reasonably correct. The measured flux with a single charge removed (open circles) is shown in fig. 2. The NUCFRG2 code (filled circles) tends to overestimate the single charge removal cross section for ^{12}C and ^{16}O projectiles and underestimates the cross section for ^{14}N projectiles. This unsystematic behavior is indicative of structure dependent effects and perhaps results from the fact that the carbon and oxygen nuclei consist of integral numbers of highly stable alpha particles and nitrogen does not. Results for the revised NUCRFG cross sections are also shown as the first collision term (dashed) and the complete solution (solid) which is in reasonable agreement

with the experiments. The measured removal of two charge units from the initial beams of ^{14}N and ^{16}O (open circles) is shown in fig. 3 with the NUCFRG2 results (filled circles). NUCFRG2 underestimates the charge 2 removal from ^{16}O and overestimates for ^{14}N. The effects of alpha clustering is most apparent in the alpha knockout process for ^{16}O collisions (fig. 3b). The carbon isotope distribution in highly nonelastic collisions are equally distributed between ^{12}C and ^{13}C as can be seen in ^{40}Ar fragmentation (15). In distinction, the fragmentation of ^{16}O shows the single alpha knockout cross section to cause an excess of ^{12}C fragments being produced (16). The addition of the alpha knockout cross section leaving the ^{12}C core in the ground state to the NUCFRG2 nonelastic cross section (solid curve) brings good agreement with the GSI oxygen beam data. The carbon fragments produced on the first collision is shown as the dashed curve in the figure. The only triple charge removal data is for the ^{16}O ion beam as shown in fig. 4 for which the NUCFRG2 is in reasonable agreement.

As a result of the present comparison the NUCFRG2 code has been modified to include Cucinotta's alpha knockout cross sections for ^{16}O projectiles on all targets giving satisfactory agreement with the measurements of Heckman et al. (17) as shown in fig. 5. Although the inclusion of this cluster effect is important in filling the gap between experiment and theory, additional ad hoc adjustments were made in the NUCFRG2 code to better fit the GSI data. The final NUCFRG2 cross sections are shown in comparison with those measured at GSI in table 1. The use of these cross sections in evaluation of the transport result are shown in figs. 2–4 as dashed curve for the first collision flux and the solid curve including all the higher order collision terms using nonperturbative theory. Still, the Li and Be production cross sections are not represented in these latest measurements and are left uncertain. Further development of the cluster model calculations will be helpful in resolving these cross sections and such results will hopefully be available in the near future. Most important in this respect is the strong energy dependence in the cluster knockout cross sections as seen in fig. 6 for several

targets. There is expected to be a large α knockout cross section for other 4n nuclei such as ^{20}Ne, ^{24}Mg, and ^{28}Si which are important contributors to galactic cosmic ray exposures (14). Also, the knockout of other light clusters will become important heavy ion fragmentation for all nuclei which have large spectroscopic constants for clusters outside closed subshells in the ground state of the projectile or target. There is strong energy dependence from the nuclear form factors and the effects of pion production as clearly shown in the few hundred MeV to one GeV region in fig. 6. Other structure dependent effects are expected to show strong energy variations. Fortunately the energy dependence is less severe in light targets and low energy which is helpful in developing medical therapy beams.

Concluding Remarks

The value of having transport experiments to guide semiempirical models used to generate nuclear databases for estimation of shielding properties is aptly demonstrated in the present paper. The resulting revisions in the NUCFRG2 code will increase its usefulness in future studies. It is clear from the present study that a final database generator will require cluster models for the light ions. Partial results of such models was , instrumental in correcting some of the deficiencies in the revised NUCFRG2 code presented herein. Clearly future versions should use exclusively cluster models for the light ions.

References

1. J. W. Wilson, M. Kim, W. Schimmerling, F. F. Badavi, S. A. Thibeault, F. A. Cucinotta, J. L. Shinn and R. Kiefer: Issues in space radiation protection: galactic cosmic rays. *Health Phys.*, **68**, 50–58 (1995).

2. W. Schimmerling, J. Miller, M. Wong, M. Rapkin, J. Howard, H. G. S. Spieler and B. V. Jarret: The fragmentation of 670A MeV neon-20 as a function of depth in water. I. Experiment. *Radiat. Res.*, **120**, 36–71 (1989).

3. M. R. Shavers, S. B. Curtis, J. Miller and W. Schimmerling: The fragmentation of 670A MeV neon-20 as a function of depth in water. II. One-generation transport theory. *Radiat. Res.*, **124**, 117–130 (1990).

4. M. R. Shavers, K. Frankel, J. Miller, W. Schimmerling, L. W. Townsend and J. W. Wilson: The fragmentation of 670A MeV neon-20 as a function of depth in water. III. Analytical multigeneration transport theory. *Radiat. Res.*, **136**, 1–14 (1993).

5. J. W. Wilson, M. R. Shavers, F. F. Badavi, J. Miller, J. L. Shinn and R. C. Costen, Nonperturbative methods in HZE propagation. *Radiat. Res.*, **140**, 241–248 (1994).

6. J. L. Shinn, J. W. Wilson, F. F. Badavi, E. V. Benton, I. Csige, A. L. Frank, E. R. Benton: HZE beam transport in multilayered materials. *Radiat. Measurement*, **23**, 57–64 (1994).

7. F. A. Cucinotta, J. W. Wilson, R. E. J. Mitchell, and A. Trivedi: Multistage carcinogenesis models and cosmic ray exposure. COSPAR, Hamburg, July 11–21, 1994.

8. J. W. Wilson, L. W. Townsend and F. F. Badavi: Galactic HZE propagation through the earth's atmosphere. *Radiat. Res.*, **109**, 173–183 (1987).

9. I. Schall: Untersuchung der kernfragmentation leichter ionen im hinblick auf die strahlentherapie. Dissertation, Technischen Hochschule Darmstadt, 1994.

10. D. Schardt, I. Schall, H. Geissel, H. Irnich, G. Kraft, A. Magel, M. F. Mohar, G. Münzenberg, F. Nickel, C. Scheidenberger, W. Schwab and L. Sihver. Nuclear fragmentation of high-energy heavy ions in water. COSPAR, Hamburg, July 11–21, 1994.

11. L. Sihver, C. H. Tsao, R. Silberberg, A. F. Barghouty, and T. Kanai: Calculations of depth-dose distributions, cross sections, and momentum loss. COSPAR, Hamburg, July 11–21, 1994.

12. J. W. Wilson, R. K. Tripathi, F. A. Cucinotta, J. L. Shinn, F. F. Badavi, S. Y. Chun, J. W. Norbury, C. J. Zeitlin, L. H. Hielbronn and J. Miller, NUCFRG2: An evaluation of the semiempirical nuclear fragmentation database. NASA TP-3533, 1995.

13. F. A. Cucinotta and R. R. Dubey: Alpha-cluster description of excitation energies in ^{12}C (^{12}C, 3α) X at 2.1A GeV. *Phys. Rev.*, **C50**, 979–984 (1994).

14. F. A. Cucinotta, Cluster abrasion of large fragments in relativistic heavy ion fragmentation. *Bull. Am. Phys. Soc.*, **48**, 1401 (1994).

15. C. E. Tull: Relativistic heavy ion fragmentation at HISS, University of California, LBL 29718, Oct. 1990.

16. D. L. Olson, B. L. Berman, D. E. Greiner, H. H. Heckman, P. J. Lindstrom and H. J. Crawford, Factorization of fragment-production cross sections in relativistic heavy-ion collisions. *Phys. Rev.*, **C28**, 1602–1613 (1983).

17. J. W. Wilson: Analysis of the theory of high-energy ion transport. NASA TN D-8381, 1977.

18. S. Y. Chun, G. S. Khandelwal, J. W. Wilson and F. F. Badavi: Development of a fully energy dependent HZE Green's function. In *Proceedings of the Eighth International Conference on Radiation Shielding*, American Nuclear Society, La Grange Park, IL, 1994, pp. 625–632.

Table 1. Augmented NUCFRG2 charge changing cross sections (mbn) and experimental values in a water target (9)

Projectile	Fragment Charge	NUCFRG2	Experiments
676A MeV ^{12}C	6	103	----------
	5	225	215 ± 3
	4	129	----------
	3	95	----------
303A MeV ^{14}N	7	87	----------
	6	362	383 ± 18
	5	147	----------
	4	90	----------
	3	82	----------
674A MeV ^{14}N	7	84	----------
	6	337	340 ± 12
	5	143	137 ± 6
	4	93	----------
	3	85	----------
300A MeV ^{16}O	8	138	----------
	7	284	290 ± 7
	6	290	296 ± 6
	5	129	----------
	4	72	----------
	3	65	----------
469A MeV ^{16}O	8	134	----------
	7	283	262 ± 9
	6	281	272 ± 12
	5	131	109 ± 5
	4	75	----------
	3	68	----------
672A MeV ^{16}O	8	131	----------
	7	281	269 ± 5
	6	276	274 ± 6
	5	132	129 ± 5
	4	79	----------
	3	71	----------

676A MeV $^{12}C \rightarrow C$
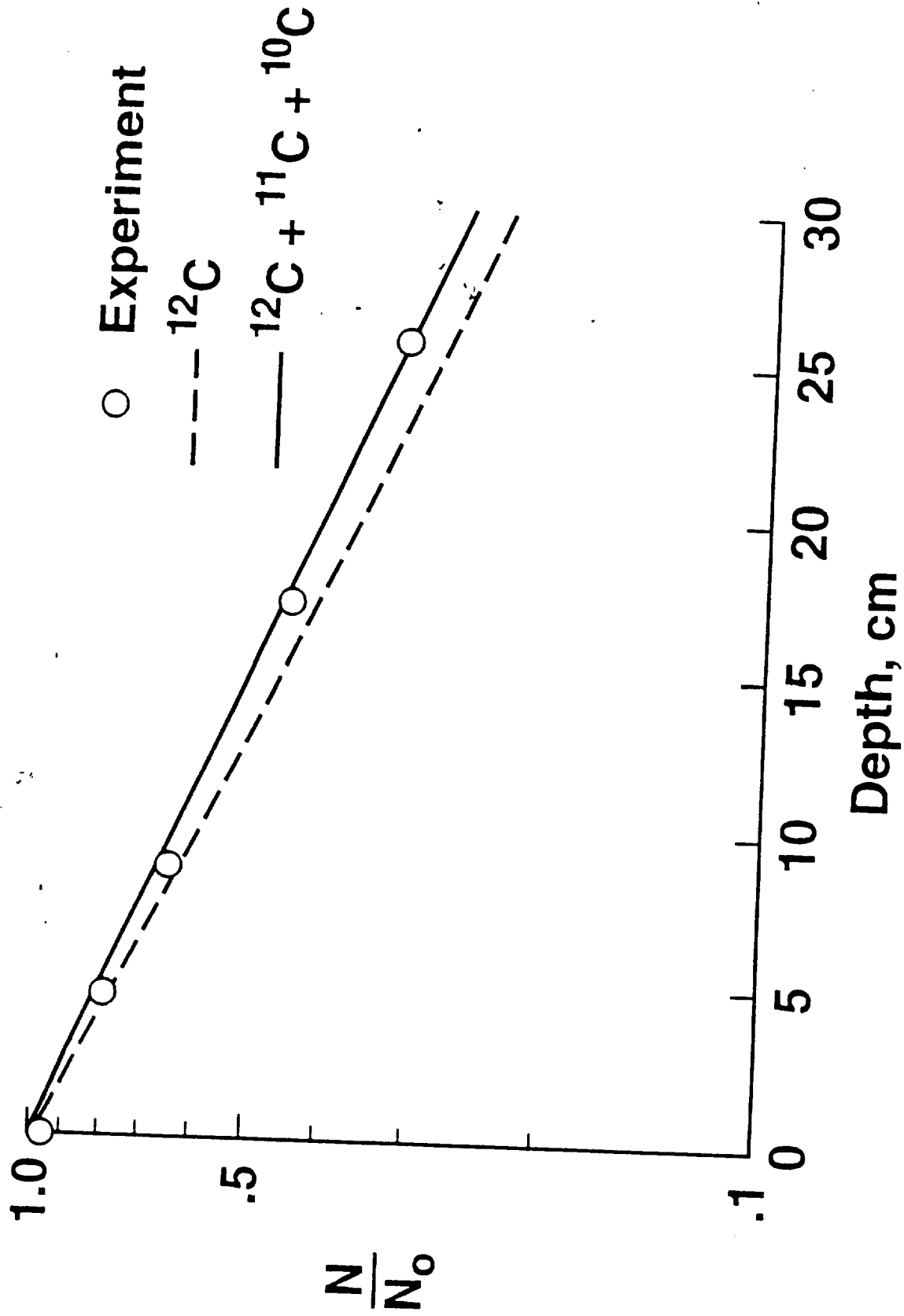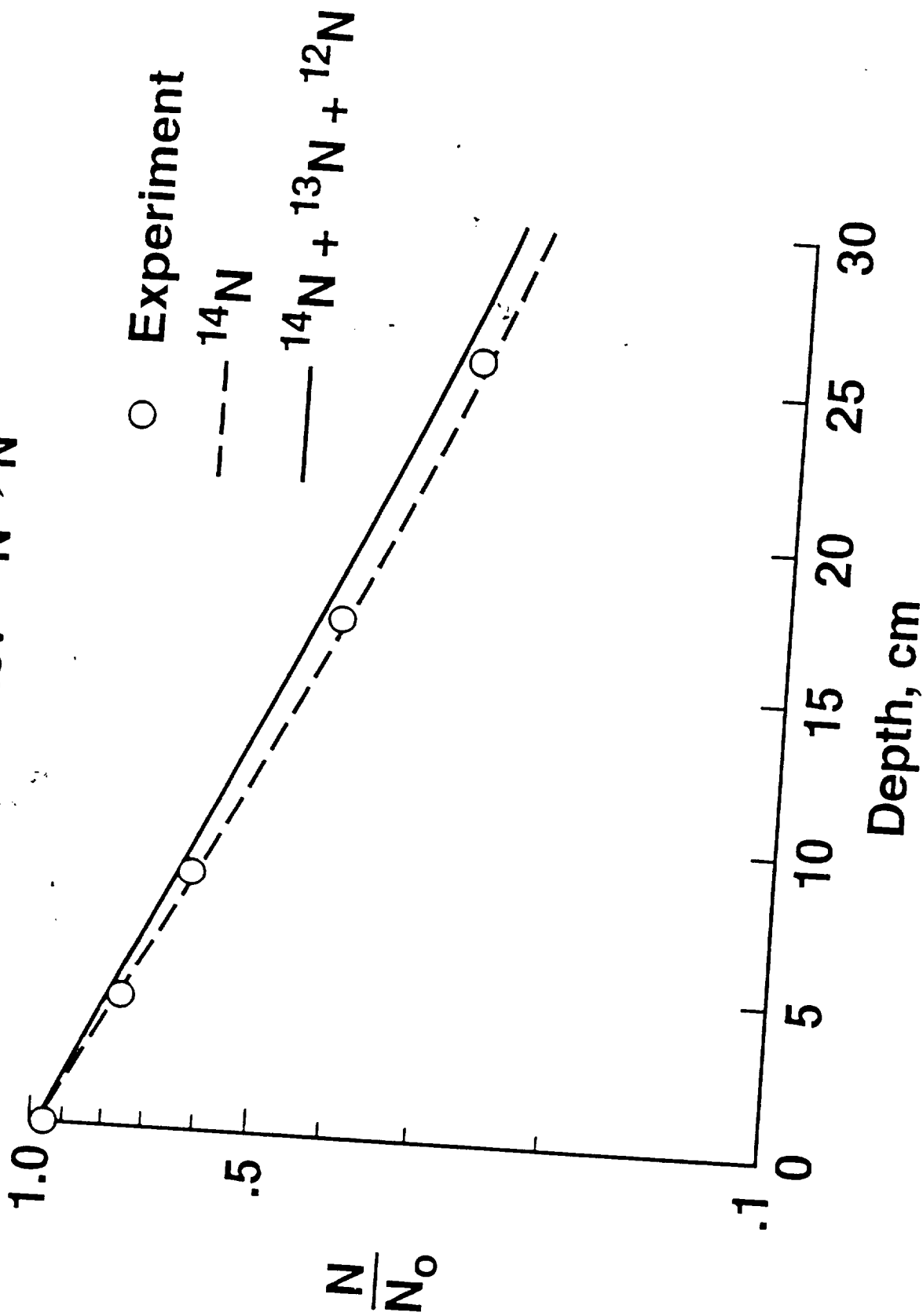
○ Experiment

-- ^{12}C

— $^{12}C + ^{11}C + ^{10}C$

$\frac{N}{N_o}$

Depth, cm

674A MeV $^{14}N \rightarrow N$

○ Experiment
- - - ^{14}N
—— $^{14}N + ^{13}N + ^{12}N$

$\dfrac{N}{N_o}$

Depth, cm

672A MeV $^{16}O \rightarrow O$

○ Experiment

- - - ^{16}O

—— $^{16}O + {}^{15}O + {}^{14}O$

$\frac{N}{N_o}$

Depth, cm

1.0   .5   .1

0   5   10   15   20   25   30

676A MeV $^{12}C \rightarrow B$

N/N$_o$ vs Depth, cm

○ Experiment
--- 1st term
— All
● Old

674A MeV ^{14}N→C

Experiment ○
1st term ---
All —
Old ●

$\frac{N}{N_o}$

Depth, cm

G/N-CI95-789

672A MeV $^{16}O \rightarrow N$

$\frac{N}{N_o}$ vs Depth, cm

Experiment ○
1st term - - -
All ——
Old ●

674A MeV ^{14}N → B

Legend:
- ○ Experiment
- – – – 1st term
- —— All
- ● Old

Axes: $\frac{N}{N_o}$ vs Depth, cm

672A MeV $^{16}O \rightarrow C$

$\frac{N}{N_o}$

Depth, cm
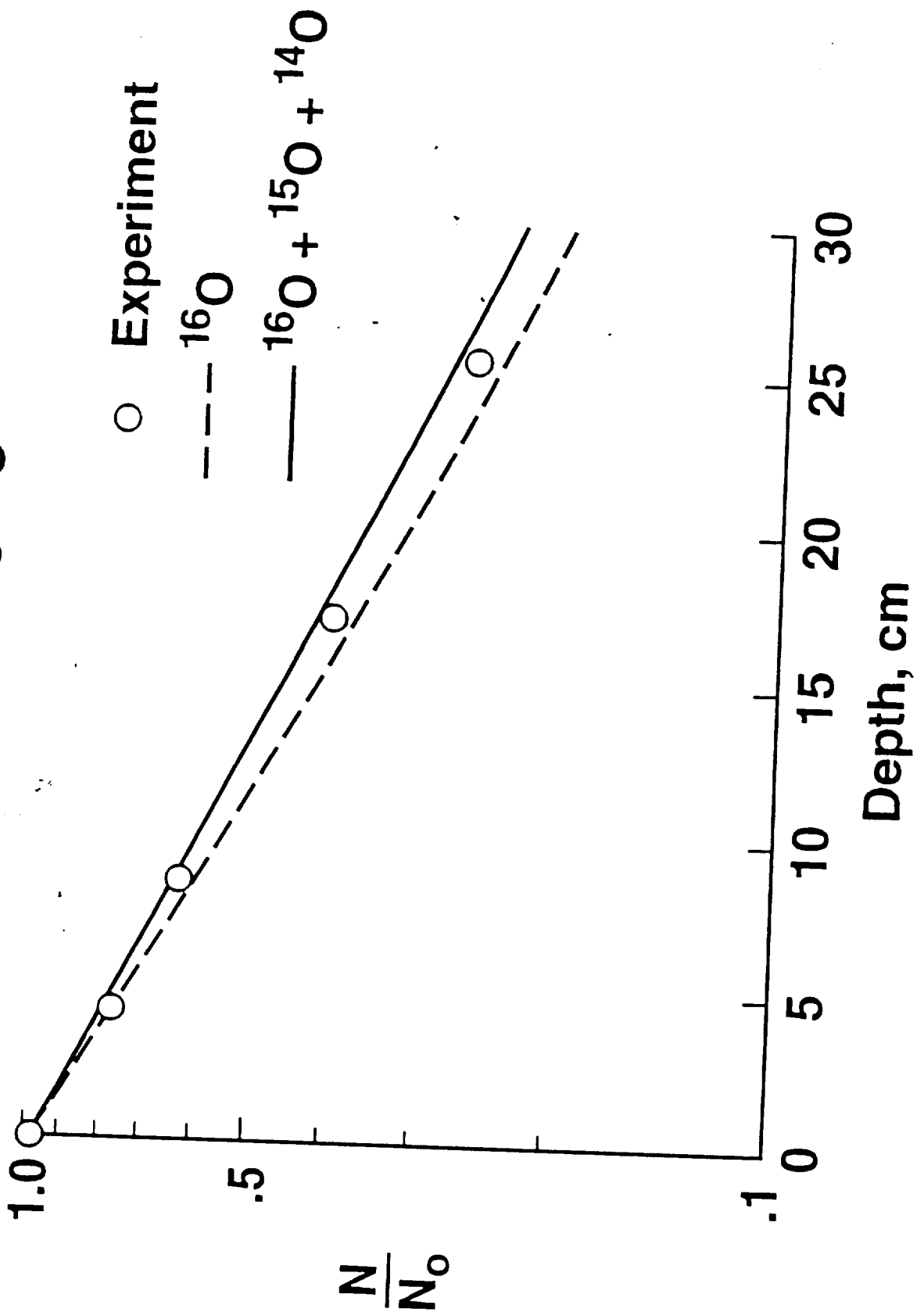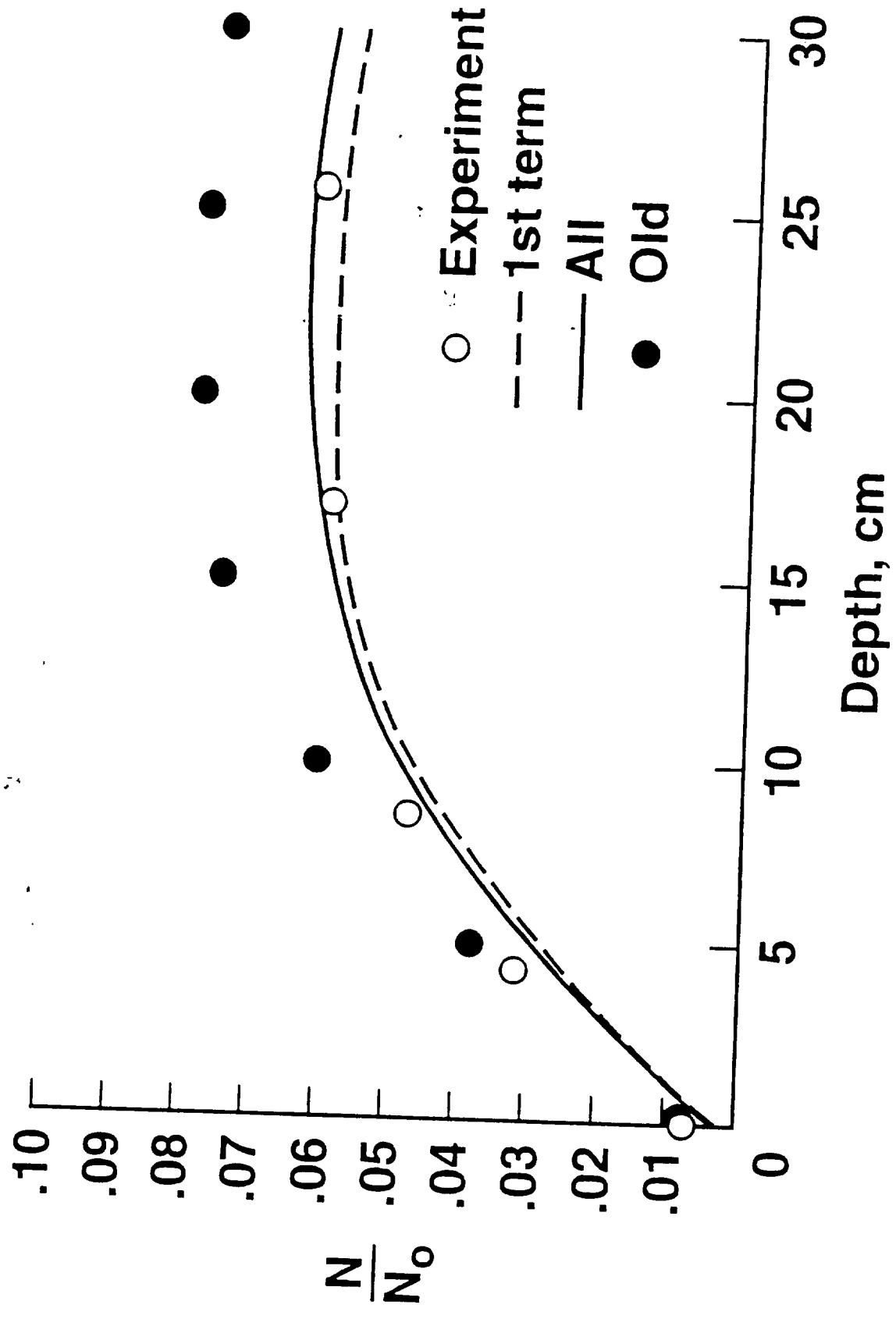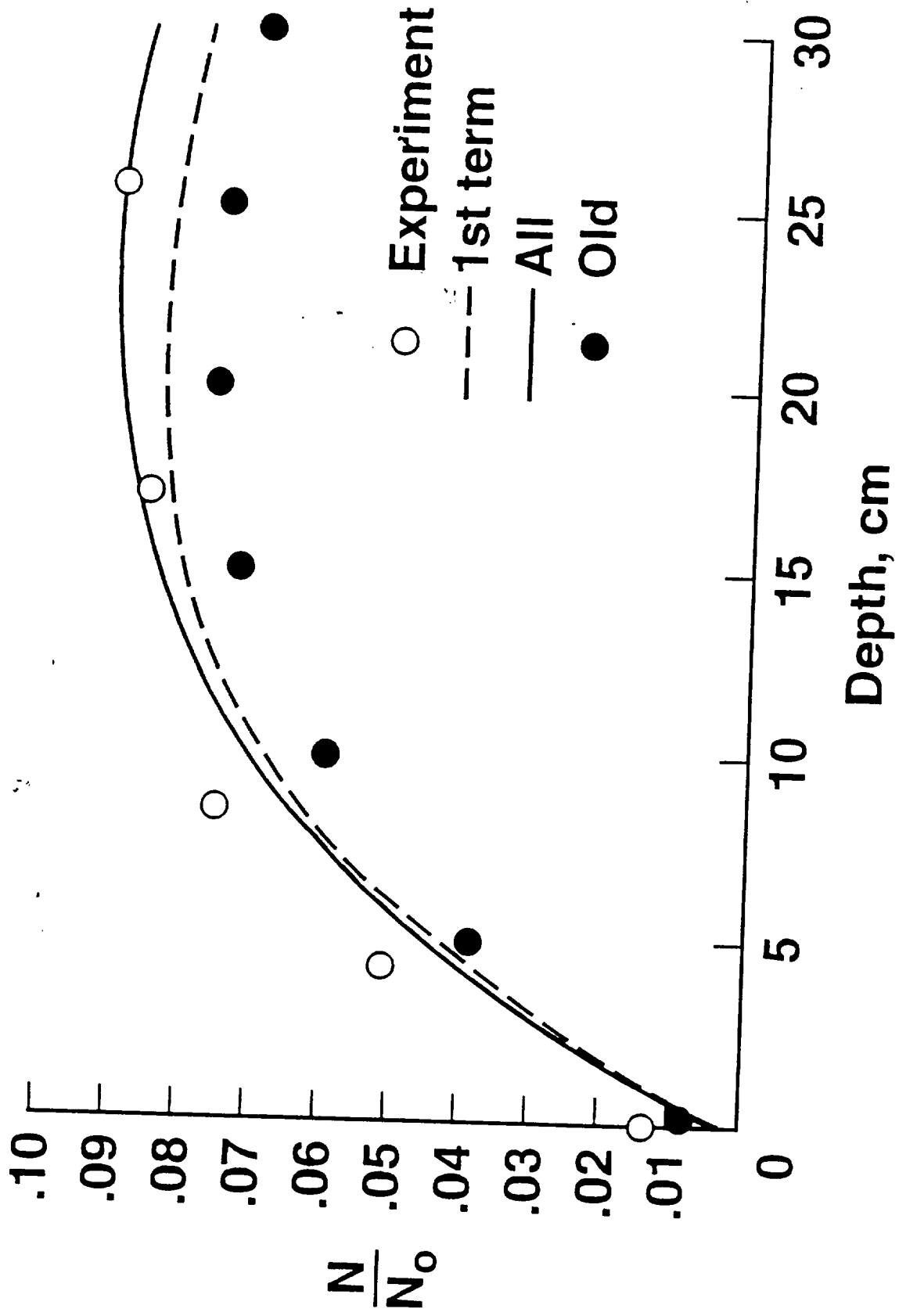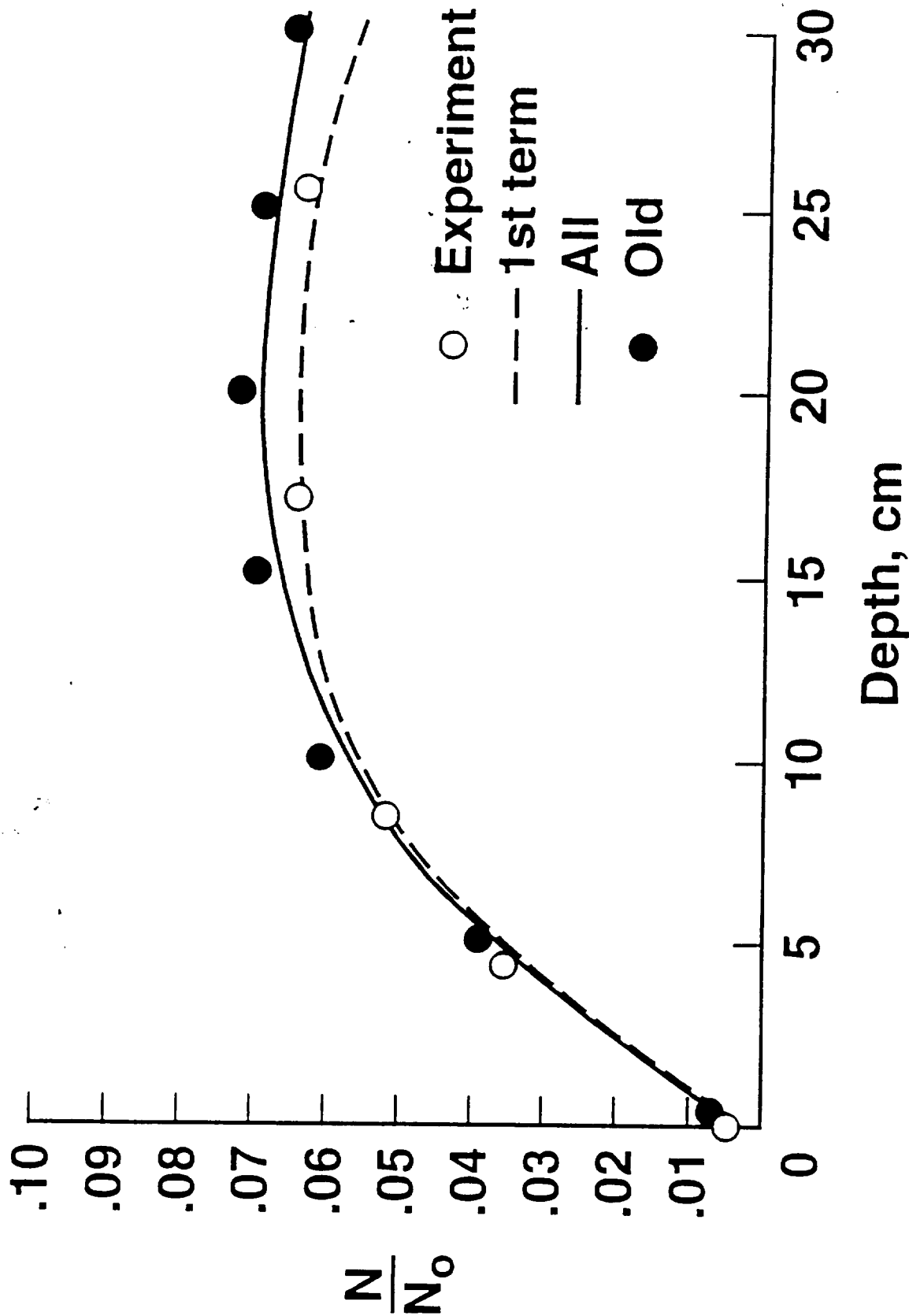
○ Experiment
- - - 1st term
—— All
● Old

672A MeV ^{16}O→B

Legend:
- ○ Experiment
- - - - 1st term
- ——— All
- ● Old

X-axis: Depth, cm (0, 5, 10, 15, 20, 25, 30)

Y-axis: $\frac{N}{N_o}$ (.01, .02, .03, .04, .05, .06, .07, .08, .09, .10)

2.1 A GeV $^{16}O \rightarrow ^{12}C$

.... NUCFRG2
— · — · Alpha knockout
——— Total
□ Expt. (LBL)

σ, mb

Target mass number
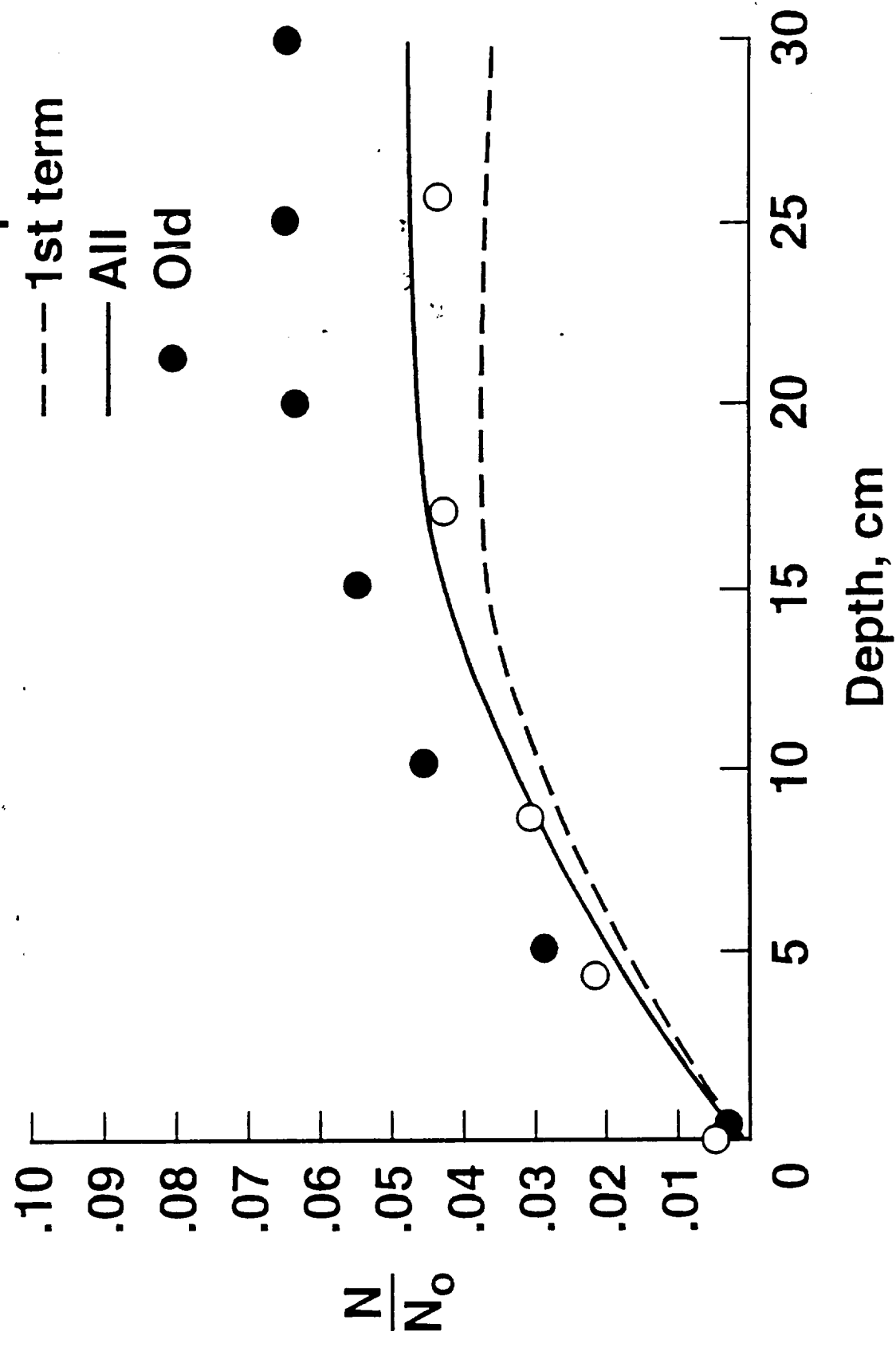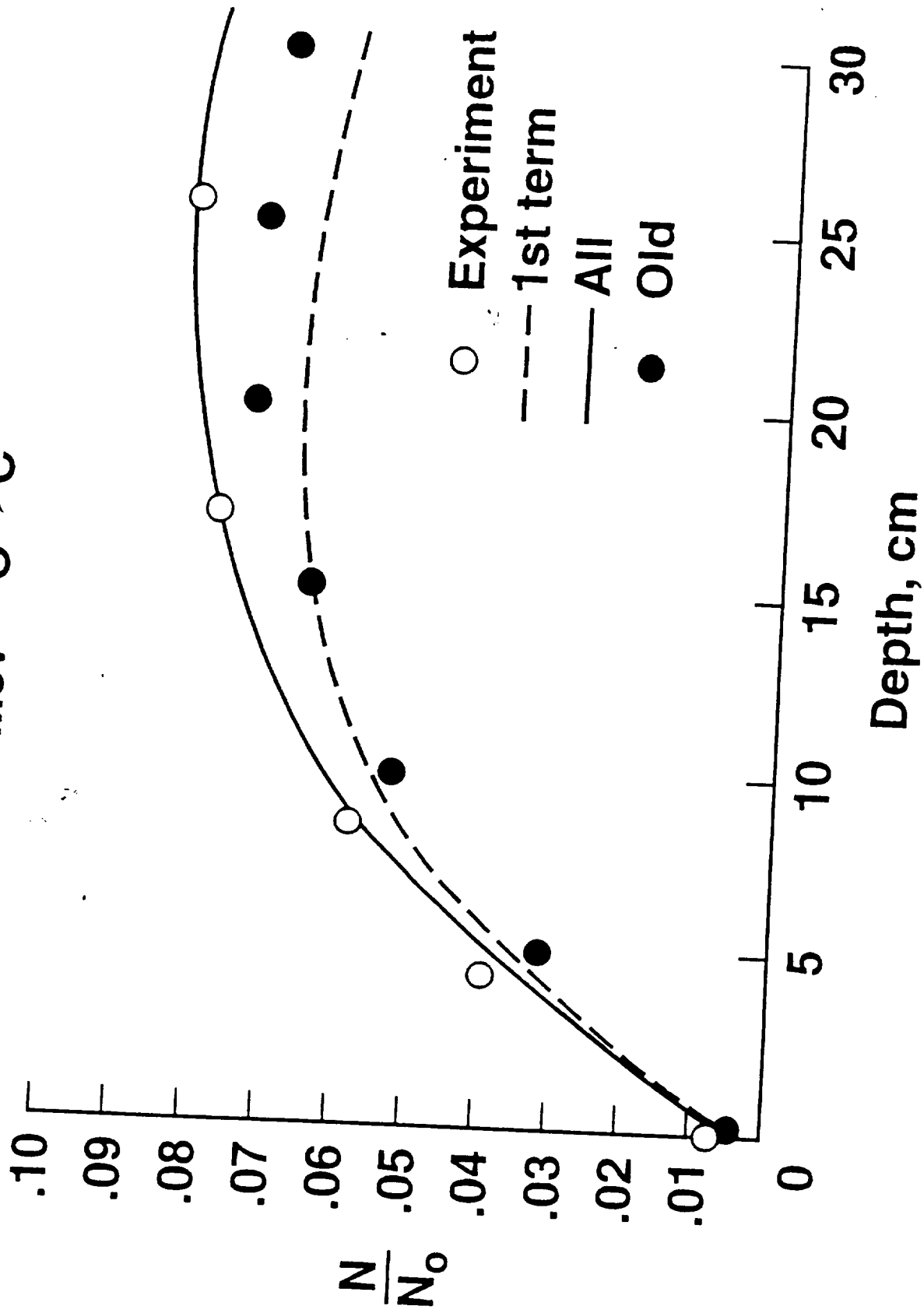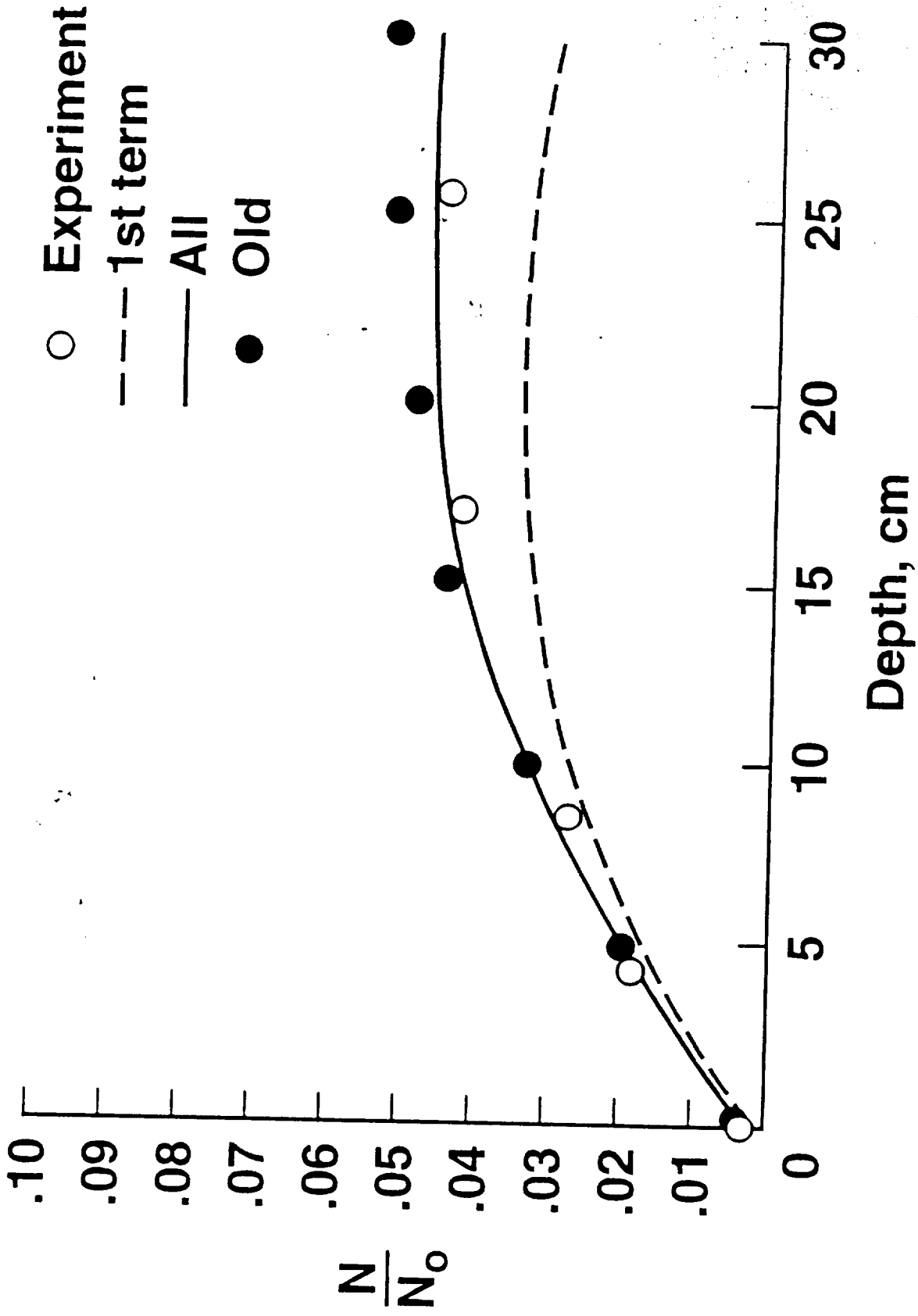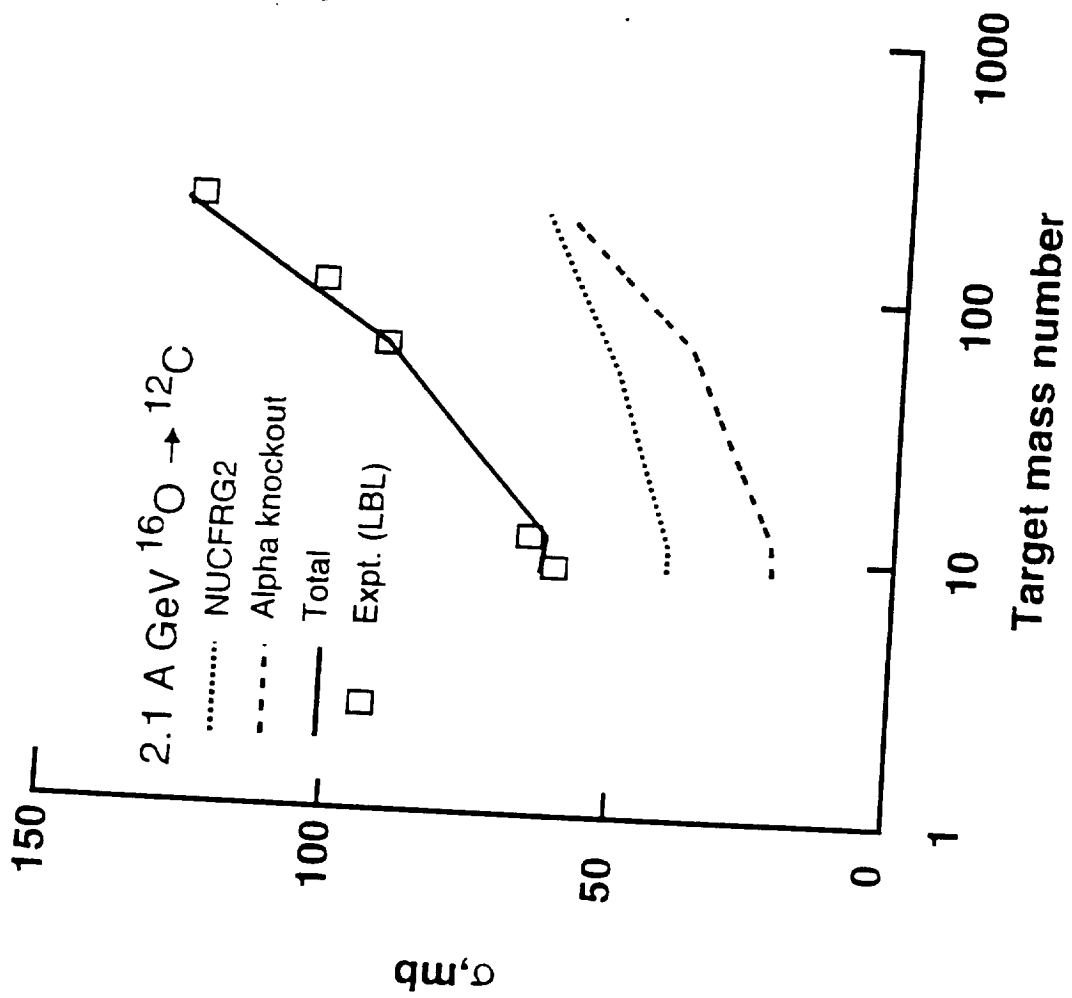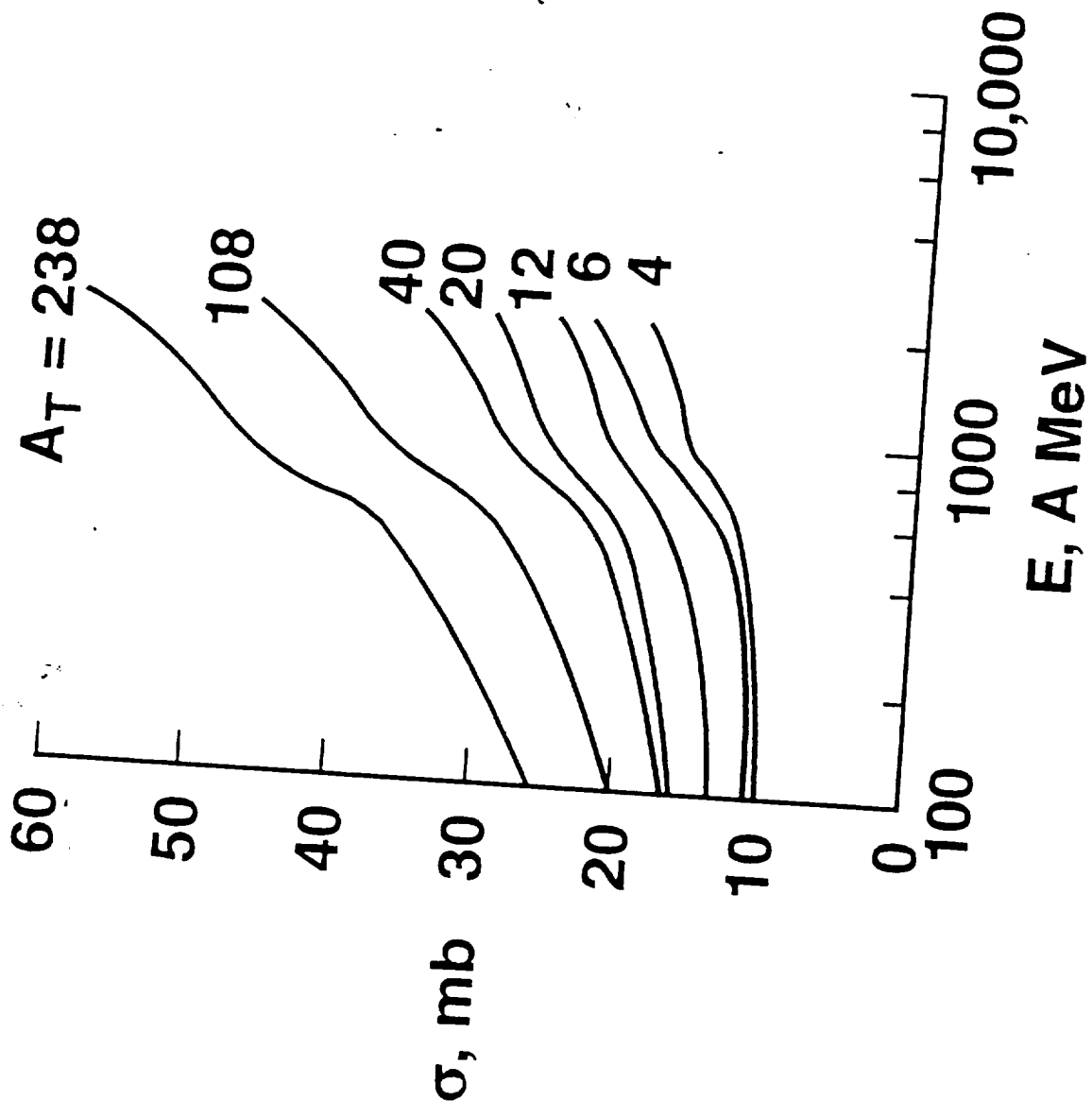
BOSE-EINSTEIN CONDENSATION OF NUCLEI

L. W. Townsend

NASA Langley Research Center

Hampton, Virginia 23681-0001, USA

R. K. Tripathi

Department of Physics

Southern Illinois University

Carbondale, IL 62901, USA

1. INTRODUCTION

Obtaining information about nuclear matter under unusual conditions of density and temperature (or excitation energy) has been a goal of research in nuclear physics for nearly two decades [1-12]. In particular, there has been an intrinsic interest in Bose-Einstein condensation of particles with a concomitant phase transition in nuclear collisions. Studies of multifragmentation reactions may provide information about liquid-vapor and other types of nuclear phase transitions, and ultimately information about the nuclear matter equation of state. Because nuclear collisions may last for only a short period of time ($\sim 10^{-22}$ sec), the formation of unusual nuclear matter may be highly transitory. Since most experimental observations are endpoint in nature (e.g., cross sections or yields), information about transitory behavior is often lost or overlooked. In previous work [13] we demonstrated the possibility that Bose-Einstein condensation of nuclei is just such a transient phenomenon, which has thus far been undetected. Over a decade ago, Bose condensation of pions was predicted to occur in the expansion phases of nuclear collisions and other forms of matter [4-6]. To date, none have been observed. There is a significant difference, however, between Bose-Einstein condensation of nuclei and that of pions. To form nuclei, matter must have some minimum density because several nucleons must be in close physical and momentum proximity. On the other hand, pion production is generally a one-nucleon phenomenon and therefore does not depend upon a minimum density of nuclear matter. Hence, Bose condensation of pions should be observable in end-point measurements but

condensation of nuclei will not. Its observation must be related to pre-ultimate stages of the reaction (e.g., compression). Bose-Einstein condensation has been a well-known phenomenon in condensed matter physics and has recently become a vigorous area of research in atomic physics [14, 15]. There is no reason for this fundamental phenomenon to be absent from nuclear physics.

We begin the paper by briefly reviewing the quantum statistical model used to investigate the Bose-Einstein condensates [13]. Theoretical results for symmetric $(Z_o = N_o)$ and asymmetric $(Z_o \neq No)$ nuclear systems are presented (Z_o (N_o) refers to the number of protons (neutrons) initially present). Then some interesting aspects of light fragment emissions from equilibrium nuclear systems are discussed. Finally, possible experimental signatures of these Bose condensed nuclei are described.

2. THEORY

Since our initial focus was on the possible existence of Bose condensate nuclei, a simple model based upon quantum statistics was assumed [13]. It ignores interactions between the particles, which should be a reasonable assumption for the low densities and temperatures being considered. More detailed and reliable predictions should incorporate the effects of particle interactions. In principle, we know how to do this [11]; such complexities, however, are left for future work. The present, simple model will suffice to demonstrate the possible existence of the phenomenon and to investigate qualitatively some of its features.

2.1 Quantum Statistical Model

To begin, consider an assembly of A nucleons consisting of N_o neutrons and Z_o protons in a volume V_o. The smallness of the finite volumes could mask a clear signal of any phase transition. However, by exercising care, experimental evidence of Bose condensation may be observable. Assume that the system of A nucleons is evolving in thermodynamic equilibrium at a temperature T and density ρ to form the light ions: ^{12}C, ^{11}B, ^{10}B, ^{9}Be, ^{7}Li, ^{6}Li, ^{4}He(α), ^{3}He(h), ^{3}H(t), ^{2}H(d), together with protons (p) and neutrons (n). Although there is some debate concerning the existence of fully equilibrated systems in heavy ion collisions, there is general agreement that at least a portion of the colliding matter does become equilibrated, and can be described by

equilibrium thermodynamics. In the model, charge and baryon number are conserved by requiring that

$$\sum_i n_i N_i = N_o$$

$$\sum_i z_i N_i = Z_o, \tag{1}$$

where the N_i refer to the number of particles of species i. The system evolves in chemical equilibrium, which implies that the chemical potential is

$$\mu_i = z_i \mu_p + n_i \mu_n + \epsilon_i, \tag{2}$$

where z_i and n_i are the number of protons and neutrons in the ith species, and ϵ_i is its binding energy. For convenience, the particles are treated as point particles moving in a reduced volume given by

$$V_{pt} = V_o - \sum_i N_i V_i, \tag{3}$$

where V_i is the eigenvolume of the ith particle. The number density is

$$\rho_o = A/V_o, \tag{4}$$

and the density of point particles is

$$\rho_{pt} = A/V_{pt}. \tag{5}$$

The distribution of fermions, from quantum statistics, is given by [16]

$$N_i = 2g_i V_{pt} \pi^{-1/2} \lambda_i^{-3} F_{FD}(\mu_i/k_B T), \tag{6}$$

where $g_i = 2S_i + 1$ is the spin degeneracy and λ_i is the thermal wavelength for the ith particle of mass m_i

$$\lambda_i = 2\pi h \, (2\pi m_i k_B T)^{-1/2} \tag{7}$$

where k_B is Boltzmann's constant and the species index is $i = (p, n, h, t, ^7\text{Li}, ^9\text{Be}, ^{11}\text{B})$ as appropriate. Values for the Fermi-Dirac integrals

$$F_{FD}(\nu) = \int_o^\infty \frac{x^{1/2}}{1 + e^{x-\nu}} \, dx \tag{8}$$

are well documented in the literature [17]. For bosons quantum statistics yields [16]

$$N_i = g_i [\exp(-\mu/k_B T) - 1]^{-1} + g_i V_{pt} \lambda_i^{-3} F_{BE}(-\mu_i/k_B T), \tag{9}$$

where the first term on the right side of Eq. (9) gives the number of condensed bosons, the second term is the number of noncondensed bosons, the species index is $i(= d, \alpha, {}^6\mathrm{Li}, {}^{10}\mathrm{B}, {}^{12}\mathrm{C})$, and the Bose-Einstein integrals [18] are

$$F_{BE}(\nu) = \int_0^\infty \frac{x^{1/2}}{e^{x+\nu} - 1} \, dx. \tag{10}$$

2.2 Calculational Methods

The evolution of the system is studied as follows: for a given temperature T, density ρ_{pt}, and proton-to-neutron ratio $\gamma(= Z_0/N_0)$, Eqs. (6) and (9) are solved self-consistently, while simultaneously satisfying Eqs. (1) and (2), until a convergent solution is found. The density is then incrementally increased, for the same T and γ, until another self-consistent solution is found. The set of calculations is stopped at any density for which no self-consistent solution can be found. This occurs when the magnitude of the chemical potential for one of the bosonic species is at a minimum. The calculations for increasing density are repeated for different temperatures, and then the entire procedure is again carried out for another value of γ.

3. RESULTS

We have studied systems with $\gamma = 1.0, 0.5,$ and 0.25, and with $A = 80, 160, 320, 640,$ and 1280. These choices for γ span most systems of interest in nuclear and astrophysics studies. The smallest number of equilibrated nucleons ($A = 80$) is reasonable for collisions involving heavier nuclear systems where some but possibly not all of the nucleons may be in equilibrium. The largest value of A ($A = 1280$) is a computationally reasonable ensemble of nucleons for representing stellar interiors or infinite nuclear matter. Temperatures of 2.5 and 5 MeV were assumed. At higher temperatures, the excitation energy would be near or above the average binding energy per nucleon and significant breakup of the composite species being formed could occur.

3.1 Results for Symmetric ($\gamma = 1$) Systems

Representative results of model calculations for symmetric systems with $A = 160$ and 1280 at $T = 2.5$ MeV are displayed in figures 1 to 3. Results for $A = 80$ at $T = 2.5$ MeV and 5 MeV were presented elsewhere [13]. Figure 1 displays particle distributions as a function of the density ratio ρ_{pt}/ρ_{nm} where $\rho_{nm} = 0.17$ fm^{-3} is the
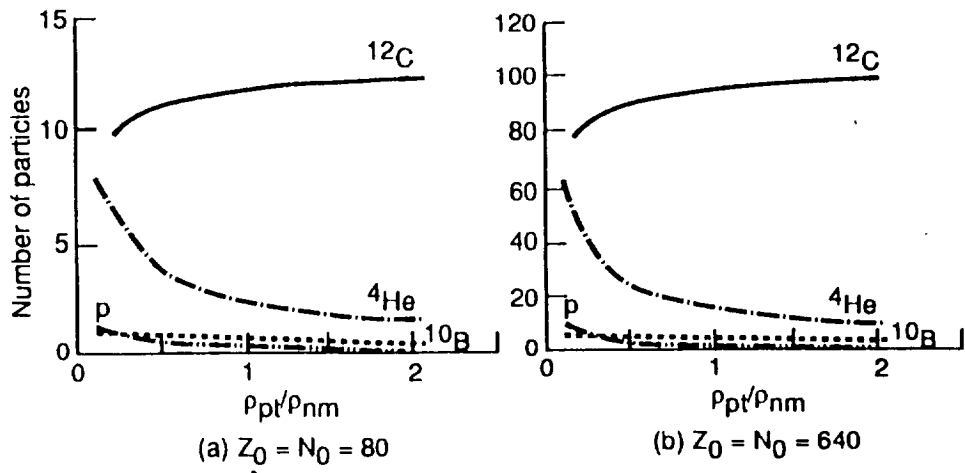
Fig. 1. Distribution of most abundant particles for symmetric ($\gamma = 1$) systems at T = 2.5 MeV. Other species have abundances which are smaller than the lowest curves shown here.
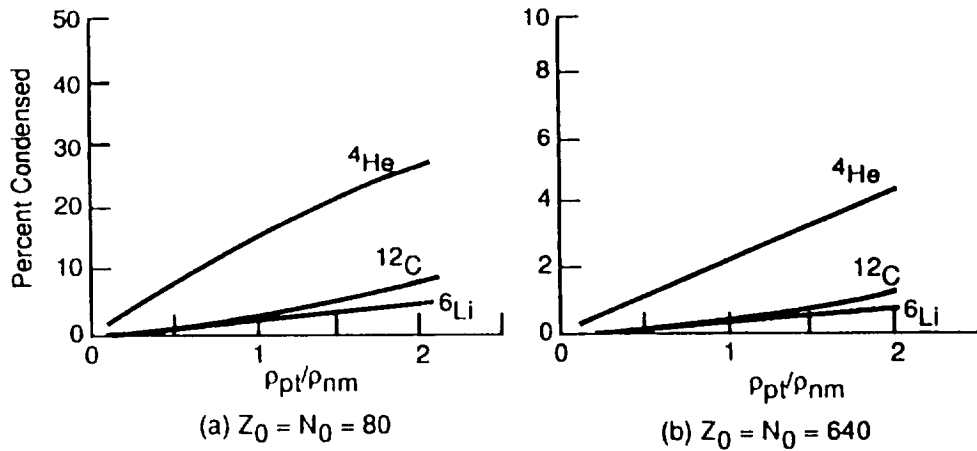
Fig. 2. Percent of condensed bosons for symmetric ($\gamma = 1$) systems at T = 2.5 MeV. Other bosons have values smaller than those displayed.
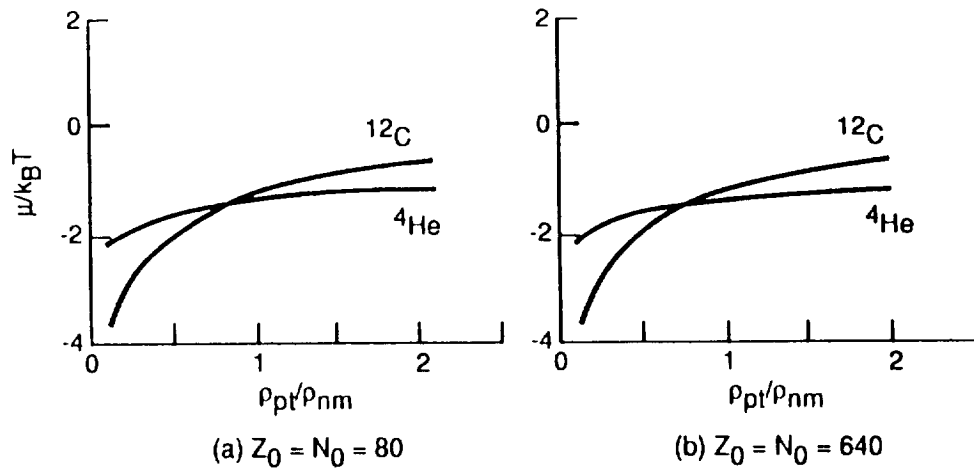
Fig. 3. Chemical potentials for the most abundant bosons for symmetric ($\gamma = 1$) systems at T = 2.5 MeV. Other bosons have values smaller than those displayed.

usual nuclear matter value. Note that bosons are more abundant than fermions. The most abundant ion species are ^{12}C and ^{4}He, both with $\gamma = 1$. Note also that the distributions scale with the total mass number A such that for each density ratio, the number of particles for a particular species when $A = 1280$ is eight times larger than when $A = 160$. This same scaling is present for the other A values and for $T = 5$ MeV. Figure 2 displays the percentage of condensed bosons. From these results, it is apparent that there is a finite probability of producing detectable numbers of condensed alpha particles and carbon nuclei at densities which typically occur in heavy ion collisions ($\rho \leq 2 \rho_{nm}$). Note that the percentage of condensed bosons increases with increasing density, but the percentages decrease with increasing A. Hence there is no simple scaling with mass number. Finally, figure 3 displays the chemical potentials for the most abundant bosons (^{12}C and ^{4}He). All other boson species have values which are smaller (more negative) than those shown in the figure. Here we note that the chemical potentials are nearly identical for both A values. This result holds for all calculated A values and is not unexpected since Eq. (2) has no A dependence. Similar features are observed for the $T = 5$ MeV calculations.

3.2 Results for Asymmetric ($\gamma \neq 1$) Systems

Results of model calculations for asymmetric systems with $\gamma = 0.5, A = 160$ and 1280, and $T = 2.5$ MeV are displayed in figures 4 to 6. From figure 4, we note that fermions are more abundant than bosons, which is the opposite trend to that which occurs for symmetric systems. However, as was the case for symmetric systems, the particle distributions do scale with total mass number A. Naively, one would expect that the most abundant species should be those which are most tightly bound (^{12}C or ^{4}He). Instead, these results indicate that the most frequent species that are produced are those which have γ values close to the value of the overall equilibrated system. In this case, the most abundant species are ^{3}H ($\gamma = 0.5$) and neutrons ($\gamma = 0$). The total number of bosons produced is quite small.

Figure 5 displays the percentages of condensed bosons. These percentages are comparable to those displayed in figure 2 for symmetric systems. However, because of the small number of bosons produced, the number of condensed bosons is probably too small to detect in asymmetric systems.

Figure 6 displays chemical potentials for the bosons in the $\gamma = 0.5$ system. Note again that there is little or no A dependence. Note also that the magnitudes for this system ($\gamma = 0.5$) are much larger than for the symmetric case ($\gamma = 1$) displayed in figure 3.
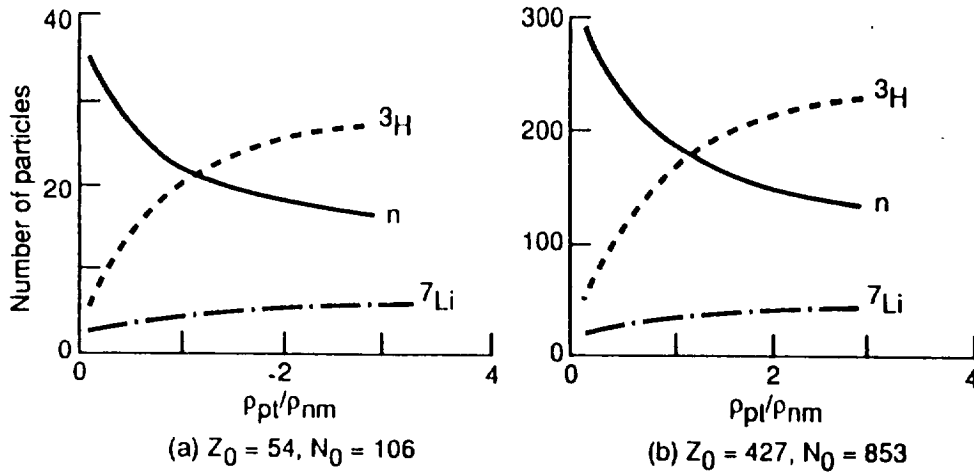
Fig. 4. Distribution of most abundant particles for asymmetric ($\gamma = 0.5$) systems at T = 2.5 MeV. Other species have abundances which are smaller than the lowest curves shown here.
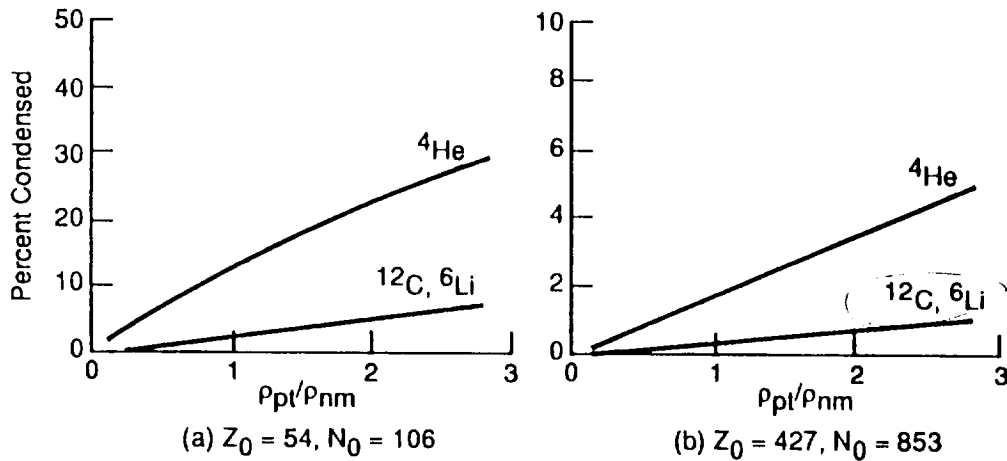
Fig. 5. Percent of condensed bosons for asymmetric ($\gamma = 0.5$) systems at T = 2.5 MeV. Other bosons have values smaller than those displayed.
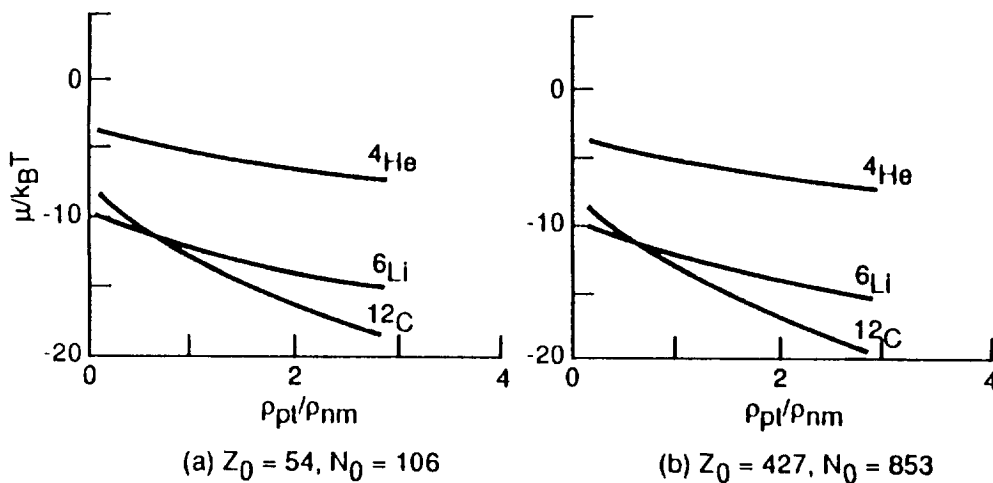
Fig. 6. Chemical potentials for the most abundant bosons for asymmetric ($\gamma = 0.5$) systems at T = 2.5 MeV. Other bosons have values smaller than those displayed.

3.3 Summary of Results

The two main findings described in the previous sections were: (1) Bose-Einstein condensation of nuclei, such as ^{4}He or ^{12}C, is a real possibility in equilibrated nuclear systems composed of equal or nearly equal numbers of protons and neutrons; and (2) the distributions of light particles emitted from thermalized, equilibrated nuclear systems are mainly dictated by the proton-to-neutron ratio of the equilibrated source, rather than by binding energy. Therefore, the composition of the light fragments emitted in the collision may be an indicator of the composition of the equilibrium population of nucleons in the source.

4. EXPERIMENTAL DETECTION OF BOSE-EINSTEIN CONDENSATION

Because we are unable, a priori, to determine the actual composition of the population in thermal equilibrium for any nuclear collision, experimental detection of condensed nuclei might be enhanced by selecting the most favorable production conditions. From the previous section, this appears to be symmetric collision systems ($Z_o = N_o = A/2$), low temperatures ($T = 2.5$ MeV or lower) and low densities ($\rho < 1.0\ \rho_{nm}$). It is satisfying to note that these conditions are similar to those found near the surface of a finite nucleus where, at $T = 0$ MeV, alpha particles are naturally present. Some years ago, an analysis of nuclear matter at $T = 0$ MeV by Mueller and Clark [19] also predicted the presence of alpha particles at densities lower than that of normal nuclear matter.

The critical question is how to observe Bose condensate nuclei once they are produced. For any distribution of reaction products, total yields or cross sections are most commonly measured. A measurement of this type, however, would neither confirm nor deny the existence of condensed nuclei. Figure 1 indicates that the total yields of bosons (sums of condensed and noncondensed) vary with temperature and density. Figure 2 indicates that the percentages of condensed bosons also vary. Therefore, experimental observations must be able to distinguish between condensed and noncondensed particles. The most promising method appears to be measurements of the momentum distributions of each boson species. In the collision center-of-mass system, condensed bosons will be produced with zero/near-zero momenta. The noncondensed bosons will have much larger momentum values in that coordinate system. Therefore, it appears that the clearest, most unambiguous signal that

Bose-Einstein condensation has occurred is to detect bosons with near-zero momenta in the center-of-mass system. In the laboratory, the condensed bosons would be detected at $0°$ to the beam with a momentum equal to that of the collision system center of mass.

5. CONCLUDING REMARKS

In this paper we have used a fully self-consistent quantum statistical model to investigate the phenomenon of Bose-Einstein condensation of nuclei in symmetric and asymmetric ensembles of nucleons in thermal and chemical equilibrium. It is found that Bose condensation of nuclei is favored in symmetric or nearly symmetric, equilibrated nuclear systems, at low temperatures ($T = 2.5$ MeV or below) and low densities (densities at or below normal nuclear matter). The most direct evidence of their existence is to experimentally detect bosons with little or no momenta in the system's center-of-mass frame.

We also found that the distributions of light particles emitted from thermalized, equilibrated nuclear systems are mainly dictated by the proton-to-neutron ratio of the equilibrated source, rather than by binding energy. This finding may be useful for monitoring the presence of transitory equilibrium in heavy ion collisions.

Finally, we emphasize that the findings presented in this work, although definitive, deserve further study using more sophisticated models. Nevertheless, the specific experimental signature of Bose-Einstein condensation of nuclei proposed in our work will not be substantially altered by the use of improved theoretical models. In view of the importance of the phenomenon to fundamental physics, experimental verification of its existence or nonexistence should be a high priority.

REFERENCES
1. L. P. Csernai, *Phys. Rev. Lett.* 54, 639 (1985).
2. J. Cugnon, *Phys. Lett.* 135B, 374 (1984).

3. L. P. Csernai and J. Kapusta, *Phys. Rep.* 131, 223 (1986).

4. A. B. Migdal, *Rev. Mod. Phys.* 50, 107 (1978).

5. J. Zimanyi, G. Fai, and B. Jakobson, *Phys. Rev. Lett.* 43, 1705 (1979).

6. R. K. Tripathi, A. Faessler, and A. Shimuzu, Z. *Phys.* A297, 275 (1980).

7. P. J. Siemens, Nature 305, 410 (183).

8. R. W. Minich, et al., *Phys. Lett.* 118B, 458 (1982).

9. G. F. Bertsch and S. Das Gupta, *Phys. Rep.* 16, 109 (1988).

10. H. Stöcker and W. Grenier, *Phys. Rep.* 137, 227 (1986).

11. R. K. Tripathi, *Phys. Rev.* C25, 1114 (1982).

12. D. H. Boal, *Annu. Rev. Nucl. Part. Sci.* 37, 1 (1987).

13. R. K. Tripathi and L. W. Townsend, *Phys. Rev.* C50, R7 (1994).

14. J. M. Doyle, J. C. Sandberg, I. A. Yu, C. L. Cesar, D. Kleppner, and T. J. Greytak, *Phys. Rev. Lett.* 67, 603 (1991).

15. M. Edwards and K. Burnett, *Phys. Rev.* A51, 1382 (1995).

16. J. D. Walecka, Fundamentals of Statistical Mechanics (Stanford University Press, 1989).

17. A. C. Beer, M. N. Chase, and P. F. Choquard, *Helv. Phys. Acta* 28, 529 (1955).

18. J. E. Robinson, *Phys. Rev.* 83, 678 (1951).

19. G. P. Mueller and J. W. Clark, *Nucl. Phys.* A155, 561c (1970).

THEORETICAL MODEL OF HZE PARTICLE FRAGMENTATION BY HYDROGEN TARGETS

L. W. Townsend,* F. A. Cucinotta,* R. Bagga** and R. K. Tripathi***

* *NASA Langley Research Center, Hampton, VA 23681-0001, U.S.A.*
** *Old Dominion University, Norfolk, VA 23529, U.S.A.*
*** *Southern Illinois University, Carbondale, IL 62901, U.S.A.*

ABSTRACT

The fragmenting of high energy, heavy ions (HZE particles) by hydrogen targets is an important, physical process in several areas of space radiation research. In this work quantum mechanical optical model methods for estimating cross sections for HZE particle fragmentation by hydrogen targets are presented. The cross sections are calculated using a modified abrasion-ablation collision formalism adapted from a nucleus-nucleus collision model. Elemental and isotopic production cross sections are estimated and compared with reported measurements for the breakup of neon, sulphur, and iron, nuclei at incident energies between 400 and 910 MeV/nucleon. Good agreement between theory and experiment is obtained.

INTRODUCTION

There is a need for reliable methods of accurately estimating cross sections for high-energy heavy ion breakup by hydrogen for a variety of space radiation applications. In astrophysics, interstellar hydrogen comprises the major type of material encountered by galactic cosmic rays (GCR) as they travel through the universe. Hence, accurate cross sections are crucial for understanding cosmic-ray propagation and source abundances. Hydrogen is also a major constituent of human tissue and appears to be the most effective GCR shield material per unit mass for long duration, manned space missions /1, 2/. Therefore, accurate cross sections are needed for proper risk assessment of critical organ exposures of astronauts. Typically, cross sections used in many of these studies have been obtained from semiempirical parameterizations /3, 4/ which have various fitting parameters. In this paper we present fundamental, quantum-mechanical,optical model methods for estimating these cross sections using a knockout (abrasion) - ablation collision formalism obtained from nuclear scattering theory /5, 6/. The model has no arbitrary fitting parameters. Predictions of element and isotope production cross sections are in good agreement with recently reported measurements /7/.

THEORY

In an abrasion-ablation model, the projectile nuclei, moving at relativistic speeds, collide with stationary target nuclei. In the abrasion step (particle knockout), those portions of the nuclear volumes that overlap are sheared away by the collision. The remaining projectile piece, called a prefragment, continues its trajectory with essentially its precollision velocity. Because of the dynamics of the abrasion process, the prefragment is highly excited and subsequently decays by the emission of gamma radiation or nuclear particles. This step is the ablation stage. The resultant isotope is the nuclear fragment whose cross section is measured.

Although a picture of overlapping nuclear volumes being sheared off may be reasonable for heavier nuclei colliding with each other, it is not reasonable for a single nucleon striking another nucleus. Instead, a more reasonable physical picture involves individual collisions between the projectile constituents and the target proton. Some struck projectile nucleons exit the fragmenting nucleus without further interaction, and some interact one or more times with the remaining constituents before departing. These interactions are called frictional-spectator interactions (FSI). The remaining nucleus (prefragment), in an excited state because of the energy deposited during the collision, then de-excites by particle- or gamma-emission processes. This picture is easily described by an abrasion-ablation-FSI model where the abrasion stage is described by a quantum-mechanical, optical model knockout formalism, and the ablation stage is modeled with cascade-evaporation techniques. There is no excess surface area energy. Instead, the prefragment excitation energy is assumed to be provided by FSI contributions from the abraded nucleons.

In the optical potential knockout (abrasion) formalism /6/, the cross section for producing a prefragment of charge Z_{PF} and mass A_{PF}, because of collision with a hydrogen target, is given by equations (1) - (3) of ref. /5/ with $A_T = 1$ and $\rho_T(\xi_T) = \delta(\xi_T)$.

Prefragment excitation energies are estimated from the FSI energy contribution which is calculated with a modified form of the model of Rasmussen /8/. In the modified model, the average energy deposited in the prefragment for each FSI is

$$< E_{FSI} > \approx 8.5R\ MeV \tag{1}$$

where the nuclear radius is $R = 1.29\ R_{rms}$.

Therefore, the cross section for a prefragment species (Z_{PF}, A_{PF}) which has undergone frictional spectator interactions is obtained from eq. (5) of ref. /5/ and, the final hadronic cross section for production of the type i isotope is obtained from eq. (6) of ref. /5/. Finally, the elemental production cross sections are obtained by summing all isotopes of a given element according to

$$\sigma_{nuc}\left(Z_i\right) = \sum_{A_i} \sigma_{nuc}\left(Z_i, A_i\right) \tag{2}$$
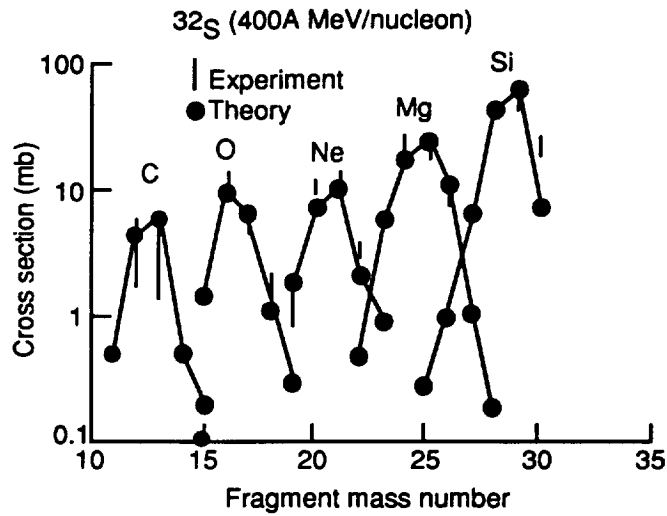
Fig. 1. Isotope production cross section for ^{32}S at 400 MeV/nucleon fragmenting in hydrogen targets. For clarity only even - Z (charge number) isotopes are displayed. Also displayed are recently reported experimental measurements /7/.
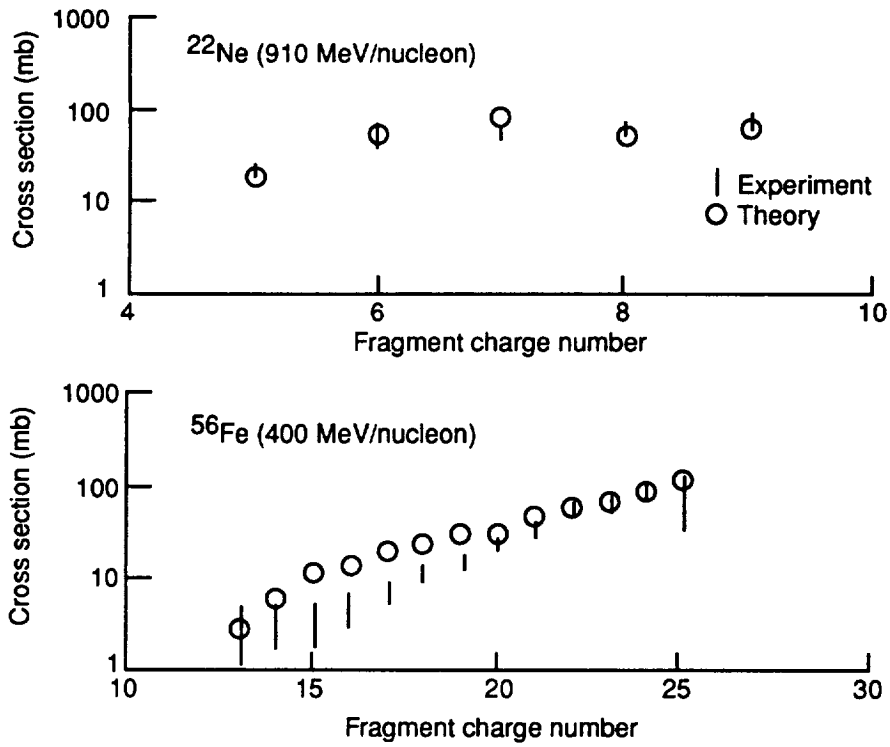
Fig. 2. Element production cross section for ^{22}Ne at 910 MeV/nucleon and for ^{56}Fe at 400 MeV/nucleon fragmenting in hydrogen targets. Also displayed are recently reported experimental measurements /7/.

RESULTS

Figure 1 shows isotope production cross sections for ^{32}S beams at 400 MeV/nucleon fragmenting in hydrogen targets. The figure also shows recent experimental measurements /7/. For brevity, only the even - Z (charge number) fragment isotopes are shown. Element production cross sections are displayed in Figure 2 for ^{22}Ne beams at 910 MeV/nucleon, and for ^{56}Fe beams at 400 MeV/nucleon. The figure also shows recent experimental measurements /7/. For these collisions, the agreement between theory and experiment is good, especially considering that no arbitrary fitting parameters are in the theory.

CONCLUSION

A simple optical potential knockout-ablation fragmentation model has been presented for use in studies of high-energy heavy ion breakup by proton. The model has no arbitrarily adjusted parameters. Model predictions are in good agreement with reported laboratory measurements of fragment production cross sections for the fragmenting of sulfur, neon, and iron beams by hydrogen targets.

REFERENCES

1. L. W. Townsend and J. W. Wilson, Galactic Heavy Ion Propagation Through Spacecraft, in Proceedings of the Natural Space Radiation and VLSI Technology Conference, NASA CP-10023, II-3-1 to II-3-10 (1987).

2. J. R. Letaw, R. Silberberg, and C. H. Tsao, Radiation Hazards on Space Missions Outside the Magnetosphere, *Adv. Space Res.*, **9**, (10) 285- (10) 291 (1989).

3. R. Silberberg, C. H. Tsao, and M. M. Shapiro, Semiempirical Cross Sections and Applications to Nuclear Interactions of Cosmic Rays, in Spallation Nuclear Reactions and Their Applications, ed. B. S. P. Shen and M. Merker, pp. 49-81, Reidel Publishing Co., Dordrecht, Holland, 1976.

4. W. R. Webber, J. C. Kish, and D. A. Schrier, Formula for Calculating Partial Cross Sections for Nuclear Reactions of Nuclei With E ≥ 200 MeV/Nucleon in Hydrogen Targets, *Phys. Review C*, **41**, 566-571 (1990).

5. L. W. Townsend, and F. A. Cucinotta, this issue.

6. L. W. Townsend, Optical Model Analyses of Heavy Ion Fragmentation in Hydrogen Targets, *Phys. Review C*, **49**, 3158-3161 (1994).

7. J. G. Guzik, et al., A Program to Measure New Energetic Particle Nuclear Interaction Cross Sections, *Adv. Space Res.*, **14**, (10) 825 - (10) 830 (1994).

8. L. F. Oliveira, R. Donangelo, J. O. Rasmussen, Abrasion-Ablation Calculations of Large Fragment Yields From Relativistic Heavy Ion Reactions, *Phys. Review C*, **19**, 826-833 (1979).

LIQUID DROP MODEL CONSIDERATIONS IN HZE PARTICLE FRAGMENTATION BY HYDROGEN

L.W. Townsend[1], R.K. Tripathi[2], F.A. Cucinotta[3], and R. Bagga[4]

[1]*Department of Nuclear Engineering, The University of Tennessee, Knoxville, TN 37996-2300, USA*
[2]*Physics Department, Southern Illinois University, Carbondale, IL 62901, USA*
[3]*Materials Division, NASA Langley Research Center, Hampton, VA 23681, USA*
[4]*Physics Department, Old Dominion University, Norfolk, VA 23529, USA*

ABSTRACT

The fragmenting of high energy, heavy ions by hydrogen targets is an important physical process in several areas of space radiation protection research. Quantum mechanical, optical model methods for calculating cross sections for particle fragmentation by hydrogen have been developed from a modified abrasion-ablation collision formalism. The abrasion stage is treated as a knockout process which leaves the residual prefragment in an excited state. In the ablation stage the prefragment deexcites to produce the final fragment. The prefragment excitation energies are estimated from a combination of liquid drop model considerations and frictional-spectator interaction processes. Estimates of elemental and isotopic production cross sections are in good agreement with published cross section measurements.

INTRODUCTION

Reliable methods of accurately and quickly estimating cross sections for the breakup of high-energy heavy ions (HZE particles) by hydrogen targets are needed for a variety of space radiation protection applications including risk assessment and shielding of astronauts from galactic cosmic rays (GCR). Many hydrogen target cross sections used in these studies are obtained from the semiempirical parameterizations of Silberberg et al (1976) and Webber et al (1990), which have various fitting parameters. In previous work (Townsend 1994, 1996) we have taken a more fundamental approach using a knockout-ablation collision formalism based upon quantum-mechanical, optical model methods obtained from nuclear scattering theory. The model had no arbitrary fitting parameters. In this work we improve the model by incorporating previously-neglected excitation energy contributions from liquid drop model considerations. The improved model is used to estimate element and isotope production cross section for a variety of projectiles ions colliding with hydrogen targets.

THEORY

In the knockout-ablation fragmentation model, the projectile nuclei, moving at relativistic speeds, collide with stationary target protons. In the knockout step individual collisions between the projectile constituents and target proton occur. Some of the struck projectile nucleons exit the fragmenting nucleus

v.ithout further interaction, and some interact one or more times with the remaining constituents before departing. These interactions are called frictional-spectator interactions (FSI). The remaining nucleus, called a prefragment or spectator is in an excited state because of the energy deposited during the collision. The prefragment subsequently decays by particle - or gamma - emission processes to produce the final fragment species whose cross section is measured.

In the optical potential knockout formalism (Townsend 1994) the cross section for producing a prefragment of charge Z_{PF} and mass A_{PF}, because of collision with a hydrogen target, is given by

$$\sigma_{abr}(Z_{PF}, A_{PF}) = \binom{N}{n}\binom{Z}{z} \int d^2b \left[1 - T(b)\right]^{n+z} \left[T(b)\right]^{A_{PF}} \tag{1}$$

where

$$T(b) = \exp\left\{-\sigma(e)\left[2\pi B(e)\right]^{-3/2} \int dz_o \int d^3y \rho_P(b + z_o + y)\exp\left[-y^2/2B(e)\right]\right\} \tag{2}$$

In Eqs. (1) and (2), b is the impact parameter vector, e is the two-nucleon kinetic energy in their center-of-mass frame, z_o is the target proton position in the projectile nucleus rest frame, y is the projectile-nucleon-target proton relative separation vector, ρ_P is the projectile nucleus ground state number density distribution, $\sigma(e)$ is the constituent - averaged nucleon-nucleon cross section, and B(e) is diffractive nucleon-nucleon scattering slope parameter. Equation (1) assumes a hypergeometrical charge dispersion model to describe the distribution of knocked-out nucleons z out of Z projectile protons and n out of N projectile neutrons are knocked out, Note that $N + Z = A_P$ and $A_{PF} = A_P - n - z$ where A_P is the projectile nuclear mass number.

Prefragment excitation energies are computed from $E_{exc} = E_{LD} + E_{FSI}$. E_{FSI} denotes the FSI energy contribution which is calculated using a modified form of the model of Oliveira et al (1979). In the modified model, the average energy deposited for each FSI is $<E_{FSI}> \approx 5R$ MeV where the nuclear radius is $R = 1.29\ R_{rms}$. The liquid drop model energy E_{LD} is estimated by considering the differences in volume energy, surface energy and coulomb energy between the prefragment and the incident projectile nucleus. For ^{56}Fe it is approximately 2 MeV/knockout. For ^{32}S it is about 4 MeV/knockout.

Depending upon the magnitude of its excitation energy, the prefragment decays by particle and/or photon emission. The probability $\alpha_{ij}(q)$ that a prefragment species j, which has undergone q FSI, decays to produce a final species i is obtained using the EVA Monte Carlo cascade-evaporation computer code (Morrissey 1979). Therefore, the final cross section for producing fragment species i is

$$\sigma_{nuc}(Z_i, A_i) = \sum_j \sum_{q=0}^{n+z} \alpha_{ij}(q)\sigma_{abr}\left(Z_j, A_j, q\right) \tag{3}$$

where the summation over j accounts for contributions from different prefragment isotopes j, and the summation over q accounts for the effects of different FSI excitation energies. Finally, the elemental production cross sections are obtained by summing over all isotopes of a given element according to

$$\sigma_{nuc}(Z_i) = \sum_{A_i} \sigma_{nuc}(Z_i, A_i) \tag{4}$$

RESULTS AND CONCLUSION

Table 1 lists element production cross sections for ^{56}Fe beams at 400A MeV fragmenting in hydrogen targets. Results for the previous model (Townsend 1996) and the current work are displayed along with the experimental measurements of Guzik et al (1994). Note that the current model predictions are in much better agreement with the experimental data. Table 2 displays predicted isotope production cross sections for ^{32}S beams at 600A MeV fragmenting in hydrogen targets. The agreement between theory and experiment is reasonably good, especially considering the lack of arbitrary fitting parameters in the theory.

ACKNOWLEDGMENTS

REFERENCES

Guzik, J.G., S. Albergo, C.X. Chen, S. Costa, H.J. Crawford, et al., A Program to Measure New Energetic Particle Nuclear Interaction Cross Sections, *Adv. Space Res.*, 14, (10)825 (1994).

Morrissey, D.J., L.F. Oliveira, J.O. Rasmussen, G.T. Seaborg, Y. Yariv, and Z. Fraenkel, Microscopic and Macroscopic Model Calculations of Relativistic Heavy-Ion Fragmentation Reactions, *Phys. Rev. Lett.*, 43, 1139 (1979).

Oliveira, L.F., R. Donangelo, and J.O. Rasmussen, Abrasion-Ablation Calculations of Large Fragment Yields From Relativistic Heavy Ion Reactions, *Phys. Rev. C.*, 19, 826 (1979).

Silberberg, R., C.H. Tsao, and M.M. Shapiro, Semiempirical Cross Sections and Applications to Nuclear Interactions of Cosmic Rays, in *Spallation Nuclear Reactions and Their Applications*, edited by B.S.P. Shen and M. Merker, pp. 49-81, Reidel Publishing Co., Dordrecht, Holland (1976).

Townsend, L.W., Optical Model Analyses of Heavy Ion Fragmentation in Hydrogen Targets, *Phys. Rev. C.*, 49, 3158 (1994).

Webber, W.R., J.C. Kish, and D.A. Schrier, Formula for Calculating Partial Cross Sections for Nuclear Reactions of Nuclei With E $\geq$ 200 MeV/Nucleon in Hydrogen Targets, *Phys. Rev. C.*, 41, 566 (1990).

Table 1. Element Production Cross Sections For 400A MeV Iron Beams Colliding With Hydrogen. Experimental Data Are From Guzik et al (1994). Previous Work Refers to Townsend et al (1996).

Element Produced	Experiment	Cross Section (in millibarns)	
		Previous Work	This Work
Mn	117.47 ± 70.54	166	195
Cr	108.54 ± 6.21	115	120
V	72.98 ± 4.25	85	84
Ti	65.25 ± 3.46	83	82
Sc	40.14 ± 2.92	57	59
Ca	29.12 ± 2.40	35	33
K	17.74 ± 2.12	36	28
Ar	13.43 ± 2.00	26	18
Cl	7.36 ± 1.99	19	13
S	5.74 ± 2.41	16	9.3
P	3.25 ± 2.76	9	4.6
Si	3.86 ± 2.08	6.8	2.5
Al	2.51 ± 2.73	2.5	1.5

Table 2. Isotope Production Cross Sections For 600A MeV ^{32}S Beams Colliding With Hydrogen. For Brevity Only Even-Charge Number Isotopes Are Displayed. Experimental Data Are From Guzik et al (1994).

Isotope Produced	Cross Section (in millibarns)	
	Experiment	This Work
^{30}Si	18.63 ± 2.14	21.7
^{29}Si	40.01 ± 3.11	55.7
^{28}Si	38.10 ± 3.20	44.1
^{27}Si	4.98 ± 1.04	10.6
^{26}Mg	13.43 ± 2.21	9.7
^{25}Mg	27.58 ± 3.14	22.7
^{24}Mg	25.90 ± 3.05	18.5
^{23}Mg	2.76 ± 0.96	4.9
^{22}Ne	7.39 ± 1.95	3.1
^{21}Ne	14.63 ± 2.86	9.7
^{20}Ne	11.16 ± 2.07	5.9
^{19}Ne	1.27 ± 1.16	1.0
^{18}O	3.37 ± 2.35	1.1
^{17}O	6.78 ± 1.83	3.7
^{16}O	11.81 ± 2.60	7.1
^{15}O	2.09 ± 0.81	2.6

NUCFRG2: An Evaluation of the Semiempirical Nuclear Fragmentation Database

J. W. Wilson, R. K. Tripathi, F. A. Cucinotta, J. L. Shinn, F. F. Badavi, S. Y. Chun, J. W. Norbury, C. J. Zeitlin, L. Heilbronn, and J. Miller

NUCFRG2: An Evaluation of the Semiempirical Nuclear Fragmentation Database

J. W. Wilson
Langley Research Center • Hampton, Virginia

R. K. Tripathi
University of Southern Illinois • Carbondale, Illinois

F. A. Cucinotta and J. L. Shinn
Langley Research Center • Hampton, Virginia

F. F. Badavi
Christopher Newport University • Newport News, Virginia

S. Y. Chun
Old Dominion University • Norfolk, Virginia

J. W. Norbury
University of Wisconsin • LaCrosse, Wisconsin

C. J. Zeitlin, L. Heilbronn, and J. Miller
Lawrence Berkeley Laboratory • Berkeley, California

Abstract

A semiempirical abrasion-ablation model has been successful in generating a large nuclear database for the study of high charge and energy (HZE) ion beams, radiation physics, and galactic cosmic ray shielding. The version reported herein has coulomb trajectory corrections, improved transmission factors, improved surface energy corrections, and light fragment emission was added. The cross sections that are generated are compared with measured HZE fragmentation data from various experimental groups. A research program for improvement of the database generator is discussed.

Introduction

An adequate and reliable nuclear database that assesses the quality of heavy ion beams for various technological efforts is needed. For example, the nuclear fragmentation properties of shielding materials can alter the protection of astronauts by an order of magnitude through the selection of appropriate shield materials (refs. 1 and 2). The radiation quality of heavy ions, which is related to the ability to cause biological injury, is an essential parameter in high altitude commercial aviation, radiotherapy, microelectronic signal processing, and information storage. Understanding single event upset damage to microelectronic systems is becoming more important as more aircraft and spacecraft control functions are handled by microprocessors. This damage is of special concern for miniature spacecraft in which reduced telemetry requires intensive onboard processing by low power microprocessors with large memory. Such small scale devices are very sensitive to single event upsets and evaluation of onboard shield worth is critical to an adequate design. The specification of the nuclear fragmentation cross sections is critical in all these applications.

Over the years the theoretical description of nuclear fragmentation in heavy ion collisions has been described with abrasion-ablation models (refs. 3 to 11 and recent work by Cucinotta, Townsend, and Wilson of Langley Research Center). In these models, fragmentation occurs in two stages. In the fast abrasion stage, the projectile and the target overlap and matter is sheared away from both nuclei. The remnants of the colliding nuclei are called the prefragments (projectile or target) and are assumed to be left in a state of excitation. The ablation stage is the description of the decay of the prefragment nuclei. The emphasis of these models is typically the prediction of inclusive mass yields of the final fragments that are observed. In the semiempirical descriptions of these reactions (refs. 3 to 6), the overlap volume of projectile and target is esti-

mated by using a classical approach. The excitation energy of the prefragments is estimated by using a surface distortion model with correction terms and energy transfer across the interface of the interaction zone. These models provide reasonable overall agreement with measured data; however, they lack a description of nuclear structure effects and a description of the nuclear diffuseness related to skin thickness. A fundamental and more complex problem is the degree to which the distribution of levels of prefragment nuclei must be considered to provide the correct description (ref. 5).

Hüfner, Schäfer, and Schürmann used the Glauber model in a first attempt at formulating a quantum mechanical abrasion-ablation model (ref. 7). In this model, closure is made on the final states of the target in describing the projectile fragmentation and the unobserved nucleons abraded from the projectile. Energy conservation is also ignored and a final closure approximation is assumed for the prefragment states that occur following the removal of a fixed number of nucleons. The advantageous factorization properties in the Glauber model of the nuclear amplitude then allow closed-form expressions for the abrasion cross sections to be found. The Glauber model of the abrasion cross section can then be shown to correspond closely to the semiempirical models when the abrasion cross section for a given product relates to the volume of the projectile and the target removed in their overlap. A study of the closed-form expression for the nuclear absorption cross section in the eikonal form of the first-order optical potential model led to a recasting of the abrasion model as an optical model by using the binomial distribution (refs. 8, 9, 12, and 13). A comparison of the abrasion cross sections (ref. 7) with the optical models (refs. 8, 9, and 12) reveals that the two differ only by the assumptions of coherence and closure in the projectile intermediate states. The optical models being preferred for the sum rule on the abrasion cross sections to satisfy unitarity.

The Glauber model or the optical model of abrasion began to employ sophisticated evaporation or cascade/evaporation codes to describe the ablation stage. These codes rely on a correct average excitation energy to be used to start the evaporation process. A major shortcoming in the physical description results from the use of closure on the prefragment final states in the Glauber model (ref. 7). In the Glauber model, all information on the distribution of the actual levels excited from abrasion in the prefragment state is lost and is replaced by an average state that is described uniquely by the abrasion cross section and average excitation energy. For light prefragments (mass number (A) is less than 16) where nuclear structure effects are large and resonance levels separated by several MeV, the use of an average prefragment state is highly questionable.

The use of a cascade model in the ablation stage is also noted. In the abrasion stage, nucleons in the projectile are knocked into the continuum by the target. These escaping nucleons will multiple scatter inside the projectile and cause further nucleon knockout. This process may be described as final state interaction (FSI) with the Moller operator and is expected to be highly dependent on the trajectory of the initial cascading nucleon (ref. 14). In the optical model (ref. 12) and the semiempirical model (refs. 5 and 6), a final state interaction correction to the prefragment excitation energy has been used to mimic the cascade effect of projectile knockouts. It is unclear whether the cascade effects described by the Monte-Carlo codes for describing ablation are distinct from the FSI corrections that describe prefragment nuclei. It was further found in the semiempirical model that statistical fluctuations in the FSI correction must be considered (ref. 5).

In a more recent formulation of the abrasion-ablation model that uses the Glauber amplitude, three major improvements are made (refs. 10 and 11 and recent work by Cucinotta, Townsend, and Wilson of Langley Research Center). First, energy conservation is treated in describing nuclear abrasion. Second, the treatment of the excitation of specific levels in the prefragments is considered for the first time. Here the prefragment excitation is considered as a core excitation during the knockout stage of abrasion. By using fractional parentage coefficients to couple nucleons to the core (prefragment) in the projectile ground state, we expect that for many nuclei the complex configurations of the nuclear ground state that result in virtual states of relative excitation are such that the core excitation is dominated by diagonal transitions to excited states of the prefragment. As the number of nucleons lost in abrasion

becomes large, the use of parentage coefficients to form the prefragment level spectrum will become intractable. For many nucleon knockouts, off-diagonal coupling is expected to become more dominant and statistical methods will become necessary to determine the distribution of prefragment levels. The preequilibrium models developed by Feshbach et al. (ref. 15), Griffin (ref. 16), and Tamura, Udagawa, and Lenske (ref. 17) may be amenable to the description of the heating of prefragment nuclei in heavy ion collisions. The third development in the reformulation of the abrasion-ablation model is the description of cluster knockout in nuclear abrasion. This description allows the treatment of nuclear structure effects in nuclear abrasion, which is important for many projectile and target nuclei of interest (C, O, and Ne). The reformulation also considers the momentum distribution for nucleon production from abrasion (ref. 18) as well as ablation (ref. 19). Although this more systematic approach will ultimately meet the need for a high quality nuclear database, current interaction studies rely on the semiempirical model.

The genesis of the semiempirical model is in the abrasion-ablation model of Bowman, Swiatecki, and Tsang (ref. 4) as discussed in references 5 and 6. In the development of the model, the transmission factors of a projectile and target were averaged and included to account for the mean free path in nuclear matter (ref. 6). Then, a semiempirical higher order correction was given to the surface deformation energy of the abrasion products (ref. 6) and the energy transfer across the interaction zone boundary was treated as a two-valued distribution (ref. 5). The final charge distribution of the fragmentation products was approximated by Rudstam's formalism (ref. 6). The available experimental nuclear fragmentation data were very limited at the time of the first reporting of the model (ref. 6). The model agreed with experimental data to the extent that the experimentalists agreed among themselves.

Since the inception of the NUCFRG model, additional experimental fragmentation cross sections (refs. 20 to 23) and thick target fluence data (refs. 24 and 25) have become available for validation of the database. Incremental improvements have been made by including the coulomb dissociation contribution (ref. 26), an energy-dependent nuclear mean free path (ref. 27) based on the analysis of Dymarz and Kohmura (ref. 28), and the nuclear radii extracted from experimental charge distributions (ref. 27). These improvements were included in the publicly released version of the HZEFRG1 code (ref. 27). In addition to these improvements, the version of the code described herein

also includes the following. A coulomb trajectory correction that includes the effects of an energy downshift has been added (ref. 29). The transmission factor is evaluated at the maximum overlap in the interaction zone. The spectator nucleons in the interaction zone are now assumed to be poorly bound to the spectators of the abraded fragment outside the interaction zone and undergo pre-equilibrium emission. A unitarity correction is made for targets with $A > 63$. Finally, a correction to the semiempirical excess surface distortion energy is made for light projectiles.

In the report presented herein, the model database is compared with available experimental data. Weaknesses within the model are thereby uncovered and a research program for database improvement is outlined.

Semiempirical Fragmentation Model

The equation of motion for a low energy ion in a nuclear coulomb field is given by energy conservation as

$$E_{\text{tot}} = \frac{1}{2}\mu\dot{r}^2 + \frac{\ell^2}{2\mu r^2} + \frac{Z_P Z_T e^2}{r} \qquad (1)$$

where E_{tot} is the total energy in the center of mass, r is the relative distance between the charge centers with time derivative $\dot{r}$, μ is the reduced mass, ℓ is the angular momentum, Z_P and Z_T are the atomic numbers of the projectile nucleus and target nucleus, respectively, and e is the electric charge. (That is, $e^2 = 2R_y a_o$, where R_y is the Rydberg constant and a_o is the Bohr radius.) The angular momentum is given as

$$\ell^2 = 2\mu E_{\text{tot}} b^2 \qquad (2)$$

The distance of closest approach is given by equation (1) for $\dot{r} = 0$ as

$$E_{\text{tot}} = \frac{E_{\text{tot}} b^2}{r^2} + \frac{Z_P Z_T e^2}{r} \qquad (3)$$

which is written as

$$b^2 = r(r - r_m) \qquad (4)$$

where

$$r_m = \frac{Z_P Z_T e^2}{E_{\text{tot}}} \qquad (5)$$

Note that r_m is the distance of closest approach for zero impact parameter.

At a given impact parameter, there is a distance of closest approach r for which the interaction takes place. When r is large, the interaction is dominated

by coulomb excitation, which is discussed by Norbury et al. (ref. 30). At smaller distances, the overlap of the nuclear densities strongly interact and mass is removed from the projectile and the target.

Abrasion Process Description

The strength of the interaction varies over the interaction zone. The projected interaction potential on the impact plane is given as

$$\int V(\mathbf{R} + \mathbf{z})dz \approx \sigma\rho_P \, C_P(\mathbf{R}) \, \rho_T \, C_T(\mathbf{R}) \qquad (6)$$

where $\mathbf{R}$ is a position vector in the impact plane, $\mathbf{z}$ is the longitudinal position component, σ is the two-body cross section that includes Pauli blocking, ρ_P and ρ_T are the projectile and target mass density, respectively, and $C_P(\mathbf{R})$ and $C_T(\mathbf{R})$ are the projectile and target chord, respectively, at position $\mathbf{R}$ along $\mathbf{z}$. (See ref. 31.) The amount of nuclear material removed from the projectile in the collision at a given impact separation is the volume of the overlap region times an attenuation factor that is evaluated at the maximum product of the chords in equation (6). The formula for the number of participating projectile constituents in the interaction zone is

$$\Delta_{\text{abr}} = FA_P[1 - \exp(-C_T/\lambda)] \qquad (7)$$

where A_P is projectile mass number, λ is mean free path, and C_T is the value of $C_T(\mathbf{R})$ that maximizes equation (6) and is given for $r_T > r_P$ as

$$C_T = \left\{ \begin{array}{ll} 2\sqrt{r_T^2 - x^2} & x > 0 \\ 2\sqrt{r_T^2 - r^2} & x \leq 0 \end{array} \right\} \qquad (8)$$

where

$$x = (r_P^2 + r^2 - r_T^2)/(2r) \qquad (9)$$

and r_P and r_T are the projectile and target radius, respectively, and are related to the root-mean-square charge radius (r_{rms}) of electron scattering $\left(r_j \approx 1.29\sqrt{r_{\text{rms}}^2 - 0.84^2}\right)$ (ref. 31). When $r_P > r_T$, the chord C_T is given as

$$C_T = \left\{ \begin{array}{ll} 2\sqrt{r_T^2 - x^2} & x > 0 \\ 2r_T & x \leq 0 \end{array} \right\} \qquad (10)$$

in which

$$x = (r_T^2 + r^2 - r_P^2)/(2r) \qquad (11)$$

The quantity F in equation (7) is the fraction of the projectile in the interaction zone as given in the

appendix (refs. 5, 6, 32, and 33). (The b in ref. 5 is replaced by the r in the equations presented herein.) The number of projectile spectator constituents in the interaction zone is given as

$$\Delta_{\text{spc}} = A_P F \, \exp(-C_T/\lambda) \qquad (12)$$

The spectator constituents are assumed to be only loosely bound to the projectile constituents outside the interaction zone. The nuclear mean free path is taken as

$$\lambda = 16.6/E^{0.26} \qquad (13)$$

where E is the projectile energy in MeV/nucleon. (See refs. 27 and 28.) The charge ratio of the removed nucleons is assumed to be that of the initial projectile nucleus, an assumption that ignores polarization effects.

Surface Distortion and Collisional Excitation

The projectile constituents outside the interaction zone (spectators) retain the same relation among themselves after the collision as before the collision. (This retention of relationship is a sudden approximation that is strictly applicable at higher energies.) The mass removed by the interaction has altered the overall stability of the spectators. This instability is related to the reduced binding energy when the nuclear surface is other than its minimum energy spherical configuration.

The excess surface area is given as

$$\Delta S = 4\pi r_P^2 [1 + P - (1 - F)^{2/3}] \qquad (14)$$

The functions F and P are defined in the appendix. (See ref. 32.) For small surface distortions ΔS in units of fm^2, the excitation energy E_S' in units of MeV is approximated by

$$E_S' = 0.95 \, \Delta S \qquad (15)$$

At the impact separations $r \ll r_P + r_T$, the projectile spectator group is left far from equilibrium and the 0.95 MeV/fm^2 coefficient requires correction that is taken herein as a semiempirical parameter f given by

$$f = 1 + 5F + [1500 - 320(A_P - 12)] \, F^3 \qquad (16)$$

where the quantity in the square brackets is limited to values between 0 and 1500. The cubic coefficient F^3 provides a correction for light projectiles that are unstable because of large surface distortions. The semiempirical surface excitation energy is then

$$E_S = E_S' \, f \qquad (17)$$

Note that the correction factor approaches 1 as Δ_{abr} becomes small. As before, we assume that fragments with a mass number of 5 are unbound, 90 percent of fragments with a mass number of 8 are unbound, and 50 percent of fragments with a mass number of 9 are unbound.

A second source of excitation energy is the transfer of kinetic energy of relative motion across the intersecting boundaries of the two ions. The rate of energy loss of a nucleon when passing through nuclear matter is taken as 13 MeV/fm (ref. 34). The energy deposit is assumed to be symmetrically dispersed about the azimuth so that at the interface 6.5 MeV/fm per nucleon is the average rate of energy transferred into excitation energy. This energy is transferred in single particle collisions. In half the events, the energy is transferred to excitation energy of the projectile and in the remaining events, the projectile excitation energy remains unchanged. The estimate of this contribution is made by using the length of the longest chord C_ℓ in the projectile surface interface. This chord length is the maximum distance traveled by any target constituent through the projectile interior and is given by

$$C_\ell = \begin{cases} 2(r_P^2 + 2rr_T - r^2 - r_T^2)^{1/2} & (r > r_T) \\ 2r_P & (r \leq r_T) \end{cases} \qquad (18)$$

The number of other target constituents in the participant and spectator interface may be found by estimating the maximum chord transverse to the projectile velocity that spans the projectile surface interface C_t which is given by

$$C_t = 2(r_P^2 - b_P^2)^{1/2} \qquad (19)$$

where

$$b_P = (r_P^2 + r^2 - r_T^2)/(2r) \qquad (20)$$

The total excitation energy transferred across the participant and spectator interface is then

$$E_x' = 13 \, C_\ell + \frac{1}{3} \, 13 \, C_\ell (C_t - 1.5) \qquad (21)$$

where the second term contributes only if $C_t > 1.5$ fm. The effective longitudinal chord length for these remaining nucleons is assumed to be one third the maximum chord length.

Nuclear Ablation

The decay of highly excited nuclear states is dominated by heavy particle emission. In the present

4

model, a nucleon is assumed to be removed for every 10 MeV of excitation energy and is determined by

$$\Delta_{abl} = (E_s + E_x)/10 + \Delta_{spc} \qquad (22)$$

where Δ_{spc} are the loosely bound projectile spectators in the interaction zone that are emitted prior to the equilibrium deexcitation process. (See ref. 4.) In accordance with the previously discussed directionality of the energy transfer, the E_x is double valued as

$$E_x = \begin{Bmatrix} E_x' & \left(P_x = \tfrac{1}{2}\right) \\ 0 & \left(P_{\bar{x}} = \tfrac{1}{2}\right) \end{Bmatrix} \qquad (23)$$

where P_j is the corresponding probability of occurrence for each value of E_x in the collision.

Nuclear Abrasion-Ablation Model

The number of nucleons removed through the abrasion-ablation process is given as a function of impact parameter b as

$$\Delta A = \Delta_{abr}(b) + \Delta_{abl}(b) \qquad (24)$$

The impact parameter is related to the impact separation r by equation (4) for a coulomb trajectory.

A second correction to the trajectory calculation comes from the transfer of kinetic energy into binding energy during the release of particles from the projectile. (Obviously, energy is also lost in releasing particles from the target, which we do not yet calculate.) The total kinetic energy in passing through the reaction zone is reduced to

$$E_f = E_i - 10\,\Delta A \qquad (25)$$

which assumes that 10 MeV is the average binding energy. The kinetic energy used in the closest approach calculation is the average of the initial and the final energies and is given as

$$E_{tot} = \frac{1}{2}(E_i + E_f) = E_i - \frac{1}{2}(10\,\Delta A) \qquad (26)$$

Obviously, E_{tot} as given by equation (26) is very crude and substantial improvements can be made. The values of ΔA for carbon projectiles on a copper target and for copper projectiles on a carbon target are shown in figure 1 for high energies. A real collision would be given by a statistical distribution between the limits shown by these two curves. The average event will be calculated as if the two extremes occurred with equal probability as noted in equation (23).
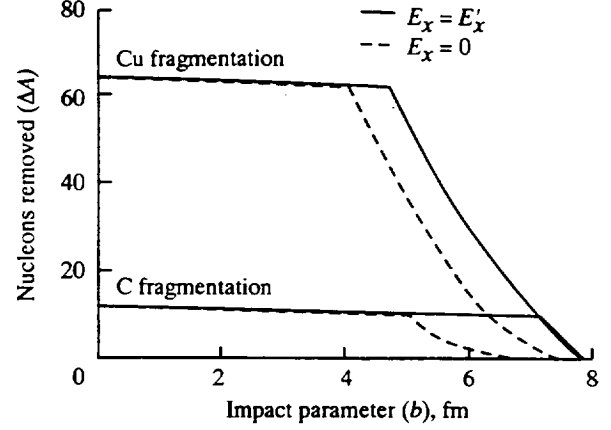
Figure 1. Nucleon removal number as a function of impact parameter in carbon-copper collisions.

The nuclear fragmentation cross sections discussed herein are approximated as the abrasion-ablation model of Bowman, Swiatecki, and Tsang (ref. 4). The cross section for removal of ΔA nucleons is estimated as

$$\sigma(\Delta A) = \pi b_2^2 - \pi b_1^2 \qquad (27)$$

where b_2 is the impact parameter for which the volume of intersection of the projectile contains Δ_{abr} nucleons and the resulting excitation energies release Δ_{abl} additional nucleons at the rate of 1 nucleon for every 10 MeV of excitation so that

$$\Delta_{abr}(b_2) + \Delta_{abl}(b_2) = \Delta A - \frac{1}{2} \qquad (28)$$

and similarly for b_1

$$\Delta_{abr}(b_1) + \Delta_{abl}(b_1) = \Delta A + \frac{1}{2} \qquad (29)$$

The charge distributions of the final projectile fragments are strongly affected by nuclear stability. We expect that the charge distribution given by Rudstam (ref. 35) for a given $\sigma(\Delta A)$ to be reasonably correct as

$$\sigma(A_F, Z_F) = F_1 \exp\left[-R|Z_F - SA_F + TA_F^2|^{3/2}\right]\sigma(\Delta A) \qquad (30)$$

where the values of $R = 11.8/A_F^D$, $D = 0.45$, $S = 0.486$, and $T = 3.8 \times 10^{-4}$ are taken from Rudstam and F_1 is a normalizing factor so that

$$\sum_{Z_F} \sigma(A_F, Z_F) = \sigma(\Delta A) \qquad (31)$$

5

The formula of Rudstam for $\sigma(\Delta A)$ was not used because his ΔA dependence is too simple and is not useful for heavy targets. For fragments with a mass of 9, the cross sections were reduced by a factor of 2.6, and for fragments with a mass of 7, cross sections were increased by a factor of 1.25 and distributed between ^{7}Li and ^{7}Be with factors of 0.52 and 0.48, respectively.

The charge of the removed nucleons ΔZ is calculated according to charge conservation

$$\Delta Z = Z_P - Z_F \qquad (32)$$

where Z_F is the charge of the fragment and Z_P is the charge of the projectile. The charge is divided according to the following rules among the nucleons and the light nuclei produced by the interaction. The abraded nucleons are those removed from the portion of projectile in the overlap region. Therefore, the abraded nucleon charge is assumed to be proportional to the charge fraction of the projectile nucleus and is given as

$$Z_{\mathrm{abr}} = Z_P \Delta_{\mathrm{abr}}/A_P \qquad (33)$$

This assumption, of course, ignores the charge separation due to the giant dipole resonance model of Morrissey et al. (ref. 33). The charge release in the ablation is then given as

$$Z_{\mathrm{abl}} = \Delta Z - Z_{\mathrm{abr}} \qquad (34)$$

which conserves the remaining charge. Similarly, mass is conserved to obtain A_{abl}.

The alpha particle is unusually tightly bound in comparison to other nucleon arrangements. Because of this unusually tight binding, the helium production is maximized in the ablation process as

$$N_\alpha = [\mathrm{Int}(Z_{\mathrm{abl}}/2), \mathrm{Int}(A_{\mathrm{abl}}/4)]_{\mathrm{minimum}} \qquad (35)$$

where $\mathrm{Int}(x)$ denotes the integer part of x. The other light isotopes are likewise maximized from the remaining ablated mass and charge numbers in the order of decreasing binding energy. The number of protons produced is given by charge conservation as

$$N_p = Z_{\mathrm{abl}} - \sum_i Z_i N_i \qquad (36)$$

Similarly, mass conservation requires the number of neutrons produced to be

$$N_n = A_{\mathrm{abl}} - N_p - \sum_i A_i N_i \qquad (37)$$

where the term i ranges over the mass numbers 2, 3, and 4 for ablated particles.

The calculation is performed for $\Delta A = 1$ to $\Delta A = A_P - 1$ for which the cross section associated with $\Delta A > A_P - 0.5$ is missed. This missed region corresponds to the central collisions for which it is assumed that the projectile disintegrates into single nucleons if $r_P < r_T$ then

$$N_p = Z_P \qquad (38)$$

and

$$N_n = A_P - Z_P \qquad (39)$$

Otherwise, this missed region is ignored. The energetic target fragments are being ignored as well as the mesonic components. The peripheral collisions with $\Delta A < 0.5$ are also missing. The most important process in these collisions with large impact separations will be the coulomb dissociation process (ref. 30).

Electromagnetic Dissociation

The total electromagnetic cross section for one nucleon removal that results from electric dipole ($E1$) and electric quadrupole ($E2$) interaction is written as

$$\begin{aligned} \sigma_{\mathrm{em}} &= \sigma_{E1} + \sigma_{E2} \\ &= \int [N_{E1}(E)\sigma_{E1}(E) + N_{E2}(E)\sigma_{E2}(E)]\,dE \end{aligned} \qquad (40)$$

where the virtual photon spectra of energy E produced by the target nucleus are given by

$$N_{E1}(E) = \frac{1}{E}\frac{2}{\pi}Z^2\alpha\frac{1}{\beta^2}\left[\xi K_0 K_1 - \frac{1}{2}\xi^2\beta^2(K_1^2 - K_0^2)\right] \qquad (41)$$

for the dipole field and by

$$N_{E2}(E) = \frac{1}{E}\frac{2}{\pi}Z^2\alpha\frac{1}{\beta^4}\left[2(1-\beta^2)K_1^2 \right. \\ \left. + \xi(2-\beta^2)^2 K_0 K_1 - \frac{1}{2}\xi^2\beta^2(K_1^2 - K_0^2)\right] \qquad (42)$$

where α is the fine structure constant for the quadrupole field. (See ref. 36.) The terms $\sigma_{E1}(E)$ and $\sigma_{E2}(E)$ are the corresponding photonuclear reaction cross sections for the fragmenting projectile nucleus. The terms K_0 and K_1 in the expression for N_{E1} and N_{E2} are modified Bessel functions of the second kind and are also functions of the parameter ξ with

$$\xi = \frac{2\pi E b_{\mathrm{min}}}{\gamma\beta\hbar c} \qquad (43)$$

6

where E is the virtual photon energy, $b_{\min}$ is the minimum impact parameter below which the collision dynamics are dominated by nuclear interactions (rather than electromagnetic (EM) interactions), β is the speed of the target (measured from the projectile rest frame) as a fraction of the speed of light c, $\hbar$ is Planck's constant, and γ is the Lorentz factor from special relativity that is given by $\gamma = (1 - \beta^2)^{-1/2}$. The minimum impact parameter is given by

$$b_{\min} = (1 + x_d)\, b_c + \frac{\pi \alpha_0}{2\gamma} \qquad (44)$$

where $x_d = 0.25$ and

$$\alpha_0 = \frac{Z_P Z_T e^2}{m_0 \beta^2 c^2} \qquad (45)$$

allows for deviation of the trajectory from a straight line (ref. 37). The critical impact parameter for single nucleon removal is

$$b_c = 1.34 \left[A_P^{1/3} + A_T^{1/3} - 0.75 \left(A_P^{1/3} + A_T^{1/3} \right) \right] \qquad (46)$$

where b_c is in units of fm and A_P and A_T are the projectile and the target nucleon mass numbers, respectively.

The photonuclear cross sections $\sigma_{E1}(E)$ and $\sigma_{E2}(E)$ are Lorentzian shaped and somewhat sharply peaked in energy. Therefore, the photon spectral functions can be taken outside the integral of equation (40) to yield an approximate form given by (ref. 36)

$$\sigma_{\text{em}} \approx N_{E1}(E_{\text{GDR}}) \int \sigma_{E1}(E)\, dE$$
$$+ N_{E2}(E_{\text{GQR}})\, E_{\text{GQR}}^2 \int \sigma_{E2}(E)\, \frac{dE}{E^2} \qquad (47)$$

where E_{GDR} and E_{GQR} are the energies at the peaks of the giant dipole resonance (GDR) and giant quadrupole resonance (GQR) photonuclear cross sections, respectively. These integrals of photonuclear cross sections over energy are evaluated with the following sum rules:

$$\int \sigma_{E1}(E)\, dE = 60\, \frac{N_P Z_P}{A_P} \qquad (48)$$

which is expressed in units of MeV-mb and

$$\int \sigma_{E2}(E) \frac{dE}{E^2} = 0.22\, f Z_P A_P^{2/3} \qquad (49)$$

which is expressed in units of μb/MeV. (See ref. 36.)

In equations (48) and (49), N_P is the number of neutrons, Z_P is the number of protons, and A_P is the mass number of the projectile nucleus. The fractional exhaustion of the energy weighted sum rule in equation (49) is (ref. 34)

$$f = \begin{cases} 0.9 & (A_P > 100) \\ 0.6 & (40 < A_P \leq 100) \\ 0.3 & (40 \leq A_P) \end{cases} \qquad (50)$$

In equation (47) E_{GDR} and E_{GQR} are the energies at the peaks of the GDR and GQR photonuclear cross sections. For the dipole term it is

$$E_{\text{GDR}} = \frac{\hbar c}{2\pi} \left[\frac{m^* c^2 R_0^2}{8J} \left(1 + u - \frac{1 + \varepsilon + 3u}{1 + \varepsilon + u} \varepsilon \right) \right]^{-1/2} \qquad (51)$$

which is expressed in units of MeV with

$$u = \frac{3J}{Q'} A_P^{-1/3} \qquad (52)$$

and

$$R_0 = r_0 A_P^{1/3} \qquad (53)$$

where $\varepsilon = 0.0768$, $Q' = 17$ MeV, $J = 36.8$ MeV, $r_0 = 1.18$ fm, and m^* is 7/10 of the nucleon mass. (See ref. 34.) For the quadrupole term, it is simply given by

$$E_{\text{GQR}} = \frac{63}{A_P^{1/3}} \qquad (54)$$

which is expressed in units of MeV.

Finally, the single proton or single neutron removal cross sections are obtained from σ_{em} (eq. (47)) with proton and neutron branching ratios g_p and g_n, respectively, as

$$\sigma(i) = g_i \sigma_{\text{em}} \qquad (i = p \text{ or } n) \qquad (55)$$

The proton branching ratio has been parameterized by Westfall et al. as

$$g_p = \min \left[\frac{Z_P}{A_P}, 1.95\, \exp(-0.075 Z_P) \right] \qquad (56)$$

where Z_P is the number of protons, and the minimum value of the two quantities in square brackets is taken. (See ref. 34.) This parameterization is satisfactory for heavier nuclei ($Z_P > 14$). For light nuclei, however, the following branching ratios are used:

$$g_p = \begin{cases} 0.5 & (Z_P < 6) \\ 0.6 & (6 \leq Z_P \leq 8) \\ 0.7 & (8 < Z_P < 14) \end{cases} \qquad (57)$$

For neutrons, the branching ratio is given by

$$g_n = 1 - g_p \qquad (58)$$

Database Evaluation

Measurements have been made for carbon ion beams on carbon target at the four energies of 250 A MeV (ref. 38), 600 A MeV (ref. 22), 1.05 A GeV (ref. 39), and 2.1 A GeV (ref. 39) and are shown in figure 2 with results from NUCFRG2. These fragmentation cross sections are among the best known (ref. 40). The effects of the coulomb trajectory are clearly apparent in the energy dependence of the lighter mass fragment cross sections of Li and Be below 100 A MeV. These coulomb effects will be even more important for projectiles and targets with greater charge. Figure 3 shows the NUCFRG2 model at very low energy (11.7 A MeV) for ^{16}O projectiles onto an ^{92}Mo target where coulomb trajectory corrections are very important (ref. 40). The cross sections of the resulting charge removal seem well represented by NUCFRG2 even at such low energies. The addition of exchange poles to the model would bring the cross sections of $\Delta Z = 0$ into agreement, which can be judged by the proton exchange pole contribution for $\Delta Z = -1$ as shown in figure 3. Clearly, the model gives a far better result than expected.

There are three projectile and target combinations for which two groups, 1.55 A GeV (ref. 20) and 1.88 A GeV (ref. 34) have measured cross sections at nearly the same energy. On the basis of NUCFRG2, very small cross section differences are expected at these energies. (See fig. 2.) The cross sections from NUCFRG2 tend to agree more closely with the experiments of Westfall et al. (ref. 34) and are 10 to 50 percent higher than those measured by Cummings et al. (ref. 20) as shown in figures 4 to 6. However, for charges between 10 to 13, NUCFRG2 agrees more closely with the data of Cummings et al.

To better quantify the comparison of results shown in figures 4 to 6, a chi square analysis is used. A comparison of NUCFRG2 model with the experiments of Westfall et al. (ref. 34) and Cummings et al. (ref. 20) is shown in table 1 for iron projectiles on three targets. Shown in table 1 are the total chi square value and the average chi square contribution per degree of freedom n. Clearly, the data for producing Al fragments in the Westfall et al. experiments show large systematic errors and is the dominant contribution to the chi square value. Except for the Al datum, the model shows good agreement with the data of Westfall et al. for carbon and copper
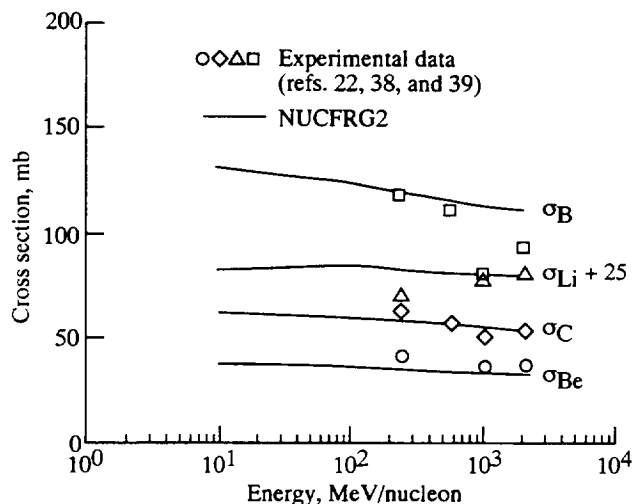
Figure 2. Charge removal cross sections for carbon ions on a carbon target as a function of projectile energy.
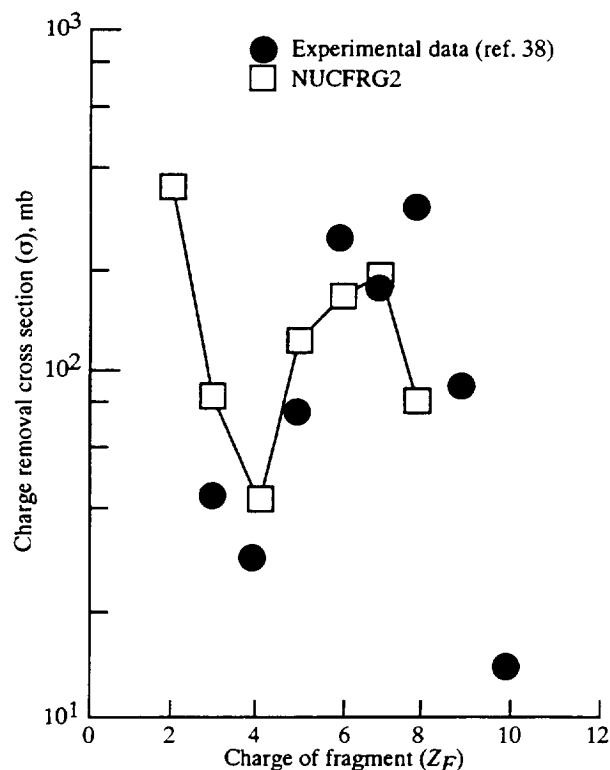
Figure 3. Charge-removal cross sections for 11.7 A MeV ^{16}O projectiles onto ^{92}Mo targets.

targets. The greater discrepancy for the lead targets surely results from simplified nuclear matter distribution in NUCFRG2. A diffuse model instead of the uniform spheres of the NUCFRG2 computation

O Experimental data at 1.55 A GeV (ref. 20)
+ Experimental data at 1.88 A GeV (ref. 34)
□ NUCFRG2
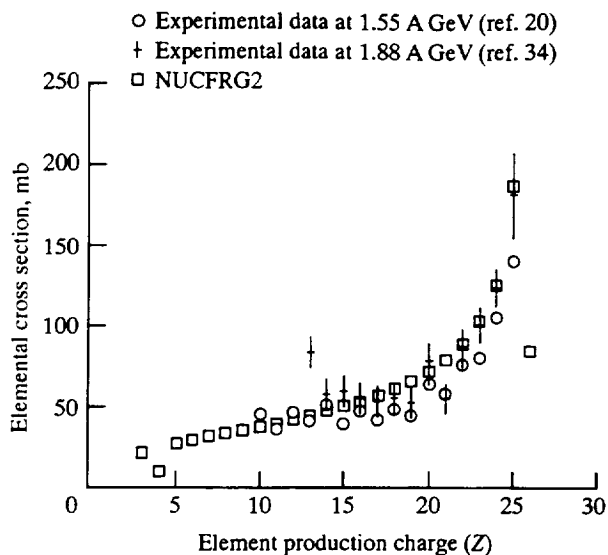
Figure 4. Charge removal cross sections for Fe ions on a carbon target compared with measurements by Westfall et al. and Cummings et al.

O Experimental data at 1.55 A GeV (ref. 20)
+ Experimental data at 1.88 A GeV (ref. 34)
□ NUCFRG2

Figure 5. Charge removal cross sections for Fe ions on a copper target compared with measurements by Westfall et al. and Cummings et al.

is recommended. This growing discrepancy with increasing target mass leads to a lack of unitarity given by the condition

$$A_P \, \sigma_{\text{abs}} = \sum A_i \sigma_i \qquad (59)$$

O Experimental data at 1.55 A GeV (ref. 20)
+ Experimental data at 1.88 A GeV (ref. 34)
□ NUCFRG2

Figure 6. Charge removal cross sections for Fe ions on a lead target compared with measurements by Westfall et al. and Cummings et al.

In generating nuclear data for transport studies, a correction is applied to targets with a charge number greater than 29 to ensure mass conservation. Comparing the NUCFRG2 model with the data of Cummings et al. shows similar trends with target mass, but the overall agreement with the data of Cummings et al. is inferior to agreement with the data of Westfall et al. as we have noted in the discussion of figures 4 to 6.

The chi square analysis has been used to compare how well one experimental group compares with the results of another group. These results are shown in table 2. From table 2, it is clear that the NUCFRG2 model better represents the two sets of experimental data than either experimental data set represents the other. The systematic errors led to a chi square per datum of 10 to 15, which might be used as a measure of goodness of fit of the NUCFRG2 model.

The fragmentation cross section for several projectile species on carbon targets at several energies are shown in table 3 (refs. 19 to 22, 34, 38, and 41). In the table, cross sections for the fragment charge, the mass for isotopic measurements, the statistical uncertainty, the results of NUCFRG2, and the chi square per datum are shown. If the error in the experimental data were only statistical, then a chi square per datum value of 1 to 2 would be appropriate and a data set with near zero would be viewed with suspicion. Clearly, large values of chi square per datum indicate possible systematic errors or errors in the NUCFRG2

model and it is difficult to make a clear judgment in all cases. Although the ^{12}C projectile isotonic breakup cross sections fit the data perhaps too well, the isotopic distributions of NUCFRG2 are distinctly different from the experiments in most cases.

Unlike the ^{12}C projectiles, the isotonic and the isotopic fragmentations of ^{16}O are outside the statistical uncertainty of the experiments. The ^{23}Na and ^{24}Mg fragmentations show a strong even-odd effect on fragment charge, which are not well represented in the results of the NUCFRG2 model. The more massive projectiles of ^{40}Ar and ^{56}Fe are better represented by the NUCFRG2 model for the isotope distributions. The isotonic fragmentation cross sections for ^{56}Fe on carbon targets are represented well by the NUCFRG2 model.

The isotopic distributions of light fragments shown in table 4 are improperly distributed in the breakup of ^{12}C projectiles on numerous targets. In particular, the isotopes of B are produced in disproportionate numbers for all targets. We also note that the cross sections from the NUCFRG2 model for heavier targets are systematically low and probably result from the assumption of uniform spheres in the nucleus (ref. 31). This error is corrected in the model presented herein by applying a renormalization factor N_R to individual fragment cross sections

$$N_R = A_p \; \sigma_{\text{abs}} / \sum_j A_j \; \sigma_j \qquad (60)$$

where p denotes the projectile and j the fragment. This unitarity factor is used in the final database but is not included in tables 1 to 7.

The light fragment distributions through carbon isotopes are examined best by comparing the ^{16}O breakup cross sections. We again suspect significant nuclear structure effects that are not well represented by the Rudstam formalism. Heavier targets show larger differences with the NUCFRG2 model presented herein because of effects of the diffuseness at the nuclear surface. The poor representation of the isotopic distribution of light fragments persists in the ^{42}Ar fragmentation in KCl shown in table 6.

The remaining ^{56}Fe fragmentation data in table 7 are the measurements of Westfall et al. (ref. 34) and Cummings et al. (ref. 20). Generally the NUCFRG2 model agrees with the two experiments (at least to the degree that they agree with each other) except for the few spurious data points in the data of Westfall et al. The model is most accurate for light targets.

The variation of chi square per n over the available experimental data is summarized in table 8. Re-

call that the estimate of systematic experimental error obtained by comparing the Westfall et al. iron data with that of Cummings et al. gives the experimental chi square per n of 4 to 12. The corresponding model chi square per n for NUCFRG2 for these experimental data sets is from 2 to 7, which shows that NUCFRG2 tends to split the difference between the two experiments. The iron fragmentation for targets below sulfer show comparable model chi square per n between 2.3 and 7.4. The model chi square per n for targets above sulfer indicate systematic model errors, which need to be resolved. Clearly, the current experimental data are adequate as a measure of model improvement. However, current experimental accuracy is inadequate to evaluate the resulting nuclear database to the accuracy required for shield design.

More recently, fragmentation cross sections were measured at the Lawrence Berkeley Laboratory for 600 A MeV iron beams on 2-cm-thick polyethylene $(CH_2)_x$ targets (ref. 41). The results are shown in figure 7. A systematic error was introduced by an electronic trigger inefficiency to fragments lighter than Ne. The chi square per datum for fragments heavier than Ne is 3×10^{-4}, while for the complete data set the chi square per datum is 6×10^{-4}.
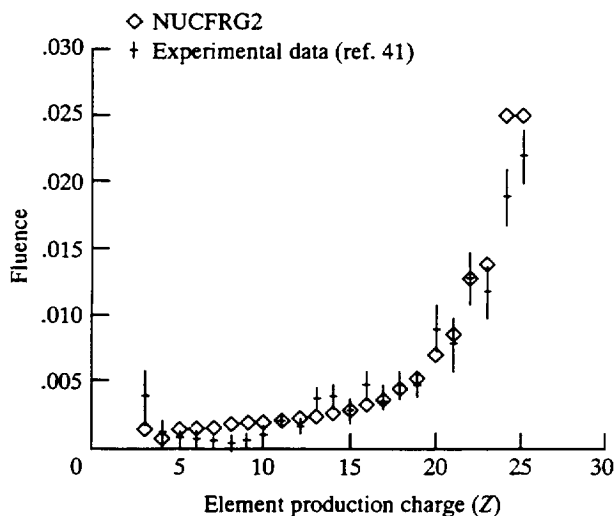
Figure 7. Charge removal cross sections for Fe ions at 600 A MeV in polyethylene.

The comparison of the NUCFRG2 model with the measured fragmentation cross sections mainly tests the dependence of $\sigma(\Delta A)$ and the applicability of the formalism of Rudstam for the charge distribution. A more sensitive test of the model representation of the ablation process is to compare the numbers and the types of particles produced. The multiplicities of the charged reaction products were measured by
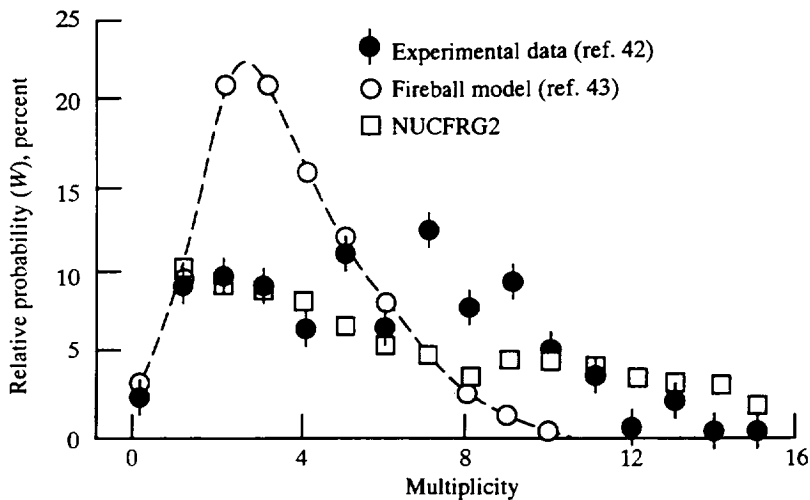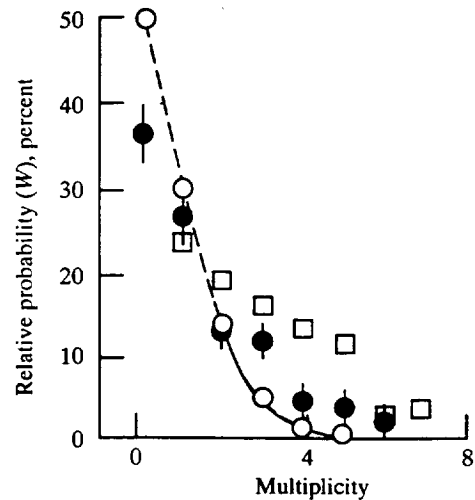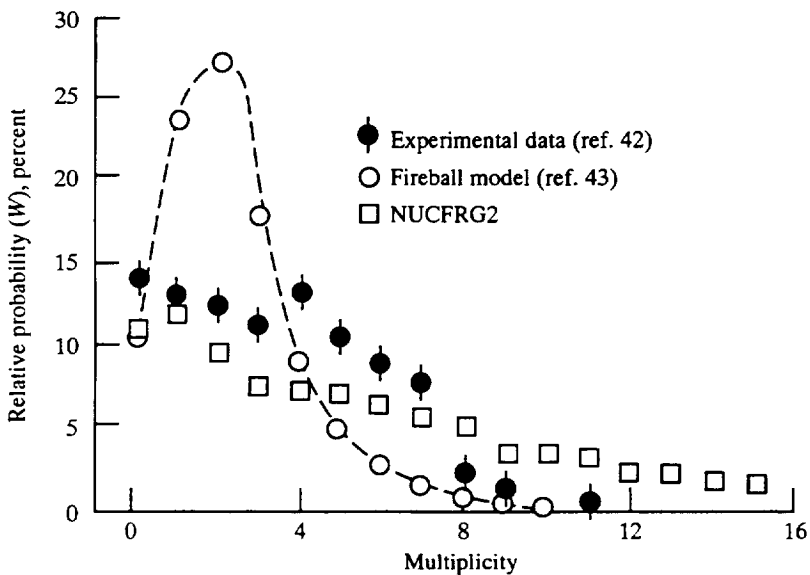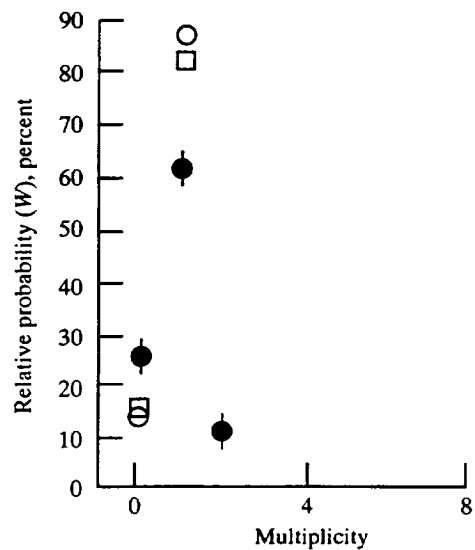
Figure 8. Relative probabilities for multiplicity of various charge states for ^{56}Fe ion beams in nuclear emulsion.

Dudkin et al. (ref. 42) and are shown in figure 8 for comparison with calculations with the fireball model (ref. 43) and the version of NUCFRG2 presented herein. The primary difference between the two models is the semiempirical correction to the excitation energy required by the NUCFRG2 model to fit the atmospheric air shower data (ref. 42) and the implementation of the deexcitation process.

As shown by Dudkin et al., the fireball model shows even qualitative differences in the frequency distribution of multiplicities in nuclear emulsion when compared with the experimental results

(ref. 42). In general, the fireball model overestimates the events of low multiplicity and correspondingly underestimates the high multiplicity events. The NUCFRG2 model gives a much improved distribution of events, although the predicted number of high multiplicity events appears greater than is seen experimentally. However, the resolution of the multiplicity when many high-energy secondaries are produced at one apex is not good. Clearly, if some of the observed several prong events were in fact of higher multiplicity, then good agreement between the NUCFRG2 model and the experiments is conceivable.

11

Concluding Remarks

The analysis of experimental data of iron beam interactions in polyethylene and aluminum targets has resulted in an improved semiempirical model for nuclear database generation. However, this analysis is still unable to unambiguously resolve differences between various experimental groups that use the same projectile and target combinations. Further improvements to the basic model have been made as a result of the presented evaluation. These improvements are correcting the charge distributions in the formulation of Rudstam for light nuclei where shell structure effects cause important deviations from simple systematic behavior. Even with these improvements, there is need for improved target mass dependence where the skin diffuseness is suspected to require further correction.

There are two approaches to improve the generation code of the NUCFRG2 nuclear database. The first is incremental improvements to the semiempirical model. The second approach is more radical and involves the further development of quantum based methods. Ultimately, model development is still limited by the systematic errors in the experimental fragmentation data and the paucity of experimental data.

The semiempirical model is first limited by the assumed uniform nuclear matter distribution. This assumption is the main source of nonconservation of mass and charge for massive targets that is temporarily corrected by forcing unitarity; however, a fully correct description must replace the uniform sphere model with realistic nuclear density distributions. Although ad hoc corrections have been made for structure effects in the low mass fragments (mass number less than 10), errors remain in the isotope distributions lighter than Ne. Improved methods for representing the distribution of excitation energy and corrections to Rudstam's distribution will be required. The distribution of mass and charge in the final ablation products depends on the excitation energy. Although the multiplicities are reasonable and are greatly improved over the fireball model, the agreement with atmospheric air shower data might be improved.

The microscopic description of nuclear fragmentation proceeds from a multiple-scattering theory (MST), a description that uses the Glauber or eikonal approximation of the multiple-scattering series, which results from a systematic reduction of relativistic MST or a nonrelativistic MST. A relativistic or nonrelativistic model may be cast as a distorted-wave series by using an average optical potential for elastic transitions.

A very difficult task still remains in treating multiple inelastic transitions that occur in heavy ion fragmentation. The difficulty arises first because of the many irreducible diagrams that contribute to any integral equation that would be formulated. Typically, integral equations of six or more dimensions will occur for inelastic transitions. This occurence of six or more dimensions is in comparison with the 3-dimensional integral equations that appear in the optical model formulation of elastic heavy ion scattering. Also, a perturbative approach becomes difficult because of the large number of terms required for heavy ion scattering and the complexity of summing over intermediate state variables.

A more practical approach is to use the forward scattering assumptions of the eikonal model, which is expected to be valid at high energies. This approach allows for closed-form expressions to be derived for the multistep processes. Here, the eikonal approximation can be applied in both the nonrelativistic MST or a relativistic MST. A relativistic eikonal model could allow the effects of negative-energy states on nuclear fragmentation to be considered. A study of the one- and two-step contributions to fragmentation could be made in the relativistic or nonrelativistic models to provide a test of the validity of the eikonal approximation and the neglecting of off-shell effects. In all of the approaches mentioned, a treatment of meson and antinucleon production in the MST should be considered.

An alternative to the use of an MST or the Glauber model in formulating the fragmentation process is to derive transport equations from an MST. In the MST, it is difficult to include the cascade of projectile knockouts through the projectile prefragments. In nucleon-nucleus scattering, the number of cascade particles is small at low to medium energies that are typical of the relative energy expected between knockouts and prefragments. However, the multiple-scattering cascade terms will depend strongly on the initial trajectory of the knockouts, which will lead to a heavy computational burden. A derivation of the simple final state interaction (FSI) corrections may help to simplify an MST approach. The transport models are a more tractable approach to the cascade problem. These models are usually used to study the knockout spectrum of nucleons. In some cases, the spectrum of residual energies after the cascade is used to predict the final fragment mass yields. The reliance upon classical methods that ignore quantum effects and the use of Monte-Carlo simulations that require large

computational times may limit the usefulness of this approach.

In describing the abrasion-ablation process, the dynamical model of choice should be used to formulate the creation of the prefragment state in an arbitrary configuration. The description of the prefragment configuration requires the variables mass and charge number, the distribution of excitation energies, and the spin to be complete. This description should distinguish whether the creation of the prefragment occured after multistep nucleon removal or cluster removal and predict the correct yields and the energy spectrum of light fragments in the reaction. Such a description would require a large amount of nuclear structure input. For example, the study of cluster abrasion requires a more detailed description of the nuclear ground state than the independent particle model. The development of the formalism for overlap function of the nuclear ground state for competing cluster configurations is required to aid the description of the abrasion process. Clearly, nuclear shell effects will be more correctly described in such a formalism. Much information on the level densities and decay modes of nuclei is well known, although the treatment of extremely high excitation energies is less understood. Also less understood is whether there is a one-to-one correspondence between the decay of excited prefragments produced in heavy ion fragmentation and the equilibrium decay treated by statistical methods. Further studies in these areas should be made.

NASA Langley Research Center
Hampton, VA 23681-0001
July 7, 1995

Appendix

Abrasion Model Formula

Two functions F and P used in the formalism given in the text are described in this appendix. For $r_T > r_P$, where r_T is target radius and r_P is projectile radius, we have

$$P = 0.125(\mu\nu)^{1/2}\left(\frac{1}{\mu} - 2\right)\left(\frac{1-\beta}{\nu}\right)^2 - 0.125\left[0.5(\mu\nu)^{1/2}\left(\frac{1}{\mu} - 2\right) + 1\right]\left(\frac{1-\beta}{\nu}\right)^3 \qquad \text{(A1)}$$

and

$$F = 0.75(1-\nu)^{1/2}\left(\frac{1-\beta}{\nu}\right)^2 - 0.125[3(1-\nu)^{1/2} - 1]\left(\frac{1-\beta}{\nu}\right)^3 \qquad \text{(A2)}$$

with

$$\nu = r_P/(r_P + r_T) \qquad \text{(A3)}$$

$$\beta = b/(r_P + r_T) \qquad \text{(A4)}$$

and

$$\mu = (1/\nu) - 1 = r_T/r_P \qquad \text{(A5)}$$

(See ref. 32.) Equations (A1) and (A2) are valid when the collision is peripheral (i.e., the two nuclear volumes do not completely overlap). In this case, the impact separation r is restricted so that

$$r_T - r_P \leq r \leq r_T + r_P \qquad \text{(A6)}$$

If the collision is central, then the projectile nucleus volume completely overlaps the target nucleus volume ($r < r_T - r_P$), and all the projectile nucleons are abraded. In this case, equations (A1) and (A2) are replaced by

$$P = -1 \qquad \text{(A7)}$$

and

$$F = 1 \qquad \text{(A8)}$$

and there is no ablation of the projectile, because it was destroyed by the abrasion.

For the case where $r_P > r_T$ and the collision is peripheral, equations (A1) and (A2) become

$$P = 0.125(\mu\nu)^{1/2}\left(\frac{1}{\mu} - 2\right)\left(\frac{1-\beta}{\nu}\right)^2 - 0.125\left\{0.5\left(\frac{\nu}{\mu}\right)^{1/2}\left(\frac{1}{\mu} - 2\right)\right.$$
$$\left. - \left[(1/\nu)(1-\mu^2)^{1/2} - 1\right]\frac{[(2-\mu)\mu]^{1/2}}{\mu^{1/2}}\right\}\left(\frac{1-\beta}{\nu}\right)^3 \qquad \text{(A9)}$$

and

$$F = 0.75(1-\nu)^{1/2}\left(\frac{1-\beta}{\nu}\right)^2 - 0.125\left\{\frac{3(1-\nu)^{1/2}}{\mu}\right.$$
$$\left. - \frac{[1-(1-\mu^2)^{3/2}][1-(1-\mu)^2]^{1/2}}{\mu^3}\right\}\left(\frac{1-\beta}{\nu}\right)^3 \qquad \text{(A10)}$$

where the impact separation is restricted so that

$$r_P - r_T \leq r \leq r_P + r_T \qquad \text{(A11)}$$

14

(See ref. 33.) For a central collision $(r < r_P - r_T)$ with $r_P > r_T$, equations (A9) and (A10) become

$$P = \left[\frac{1}{\nu}(1 - \mu^2)^{1/2} - 1 \right] \left[1 - \left(\frac{\beta}{\nu} \right)^2 \right]^{1/2} \tag{A12}$$

and

$$F = \left[1 - (1 - \mu^2)^{3/2} \right] \left[1 - \left(\frac{\beta}{\nu} \right)^2 \right]^{1/2} \tag{A13}$$

References

1. Wilson, John W.; Thibeault, Sheila A.; Nealy, John E.; Kim, Myung-Hee; and Kiefer, R. L.: Studies in Space Radiation Shield Performance. *Proceedings of the Engineering & Architecture Symposium*, Prairie View A&M Univ., 1993, pp. 169–176.

2. Kim, Myung-Hee Y.; Wilson, John W.; Thibeault, Sheila A.; Nealy, John E.; Badavi, Francis F.; and Kiefer, Richard L.: *Performance Study of Galactic Cosmic Ray Shield Materials*. NASA TP-3473, 1994.

3. Eisenberg, Y.: Interaction of Heavy Primary Cosmic Rays in Lead. *Phys. Rev.*, vol. 96, no. 5, Dec. 1954, pp. 1378–1382.

4. Bowman, J. D.; Swiatecki, W. J.; and Tsang, C. F.: *Abrasion and Ablation of Heavy Ions*. LBL-2908, Univ. of California, July 1973.

5. Wilson, John W.; Townsend, Lawrence W.; and Badavi, F. F.: A Semiempirical Nuclear Fragmentation Model. *Nucl. Instrum. & Methods Phys. Res.*, vol. B18, no. 3, Feb. 1987, pp. 225–231.

6. Wilson, John W.; Townsend, Lawrence W.; and Badavi, Forooz F.: Galactic HZE Propagation Through the Earth's Atmosphere. *Radiat. Res.*, vol. 109, no. 2, Feb. 1987, pp. 173–183.

7. Hüfner, J.; Schäfer, K.; and Schürmann, B.: Abrasion-Ablation in Reactions Between Relativistic Heavy Ions. *Phys. Rev. C*, vol. 12, no. 6, Dec. 1975, pp. 1888–1898.

8. Bleszynski, M.; and Sander, C.: Geometrical Aspects of High-Energy Peripheral Nucleus-Nucleus Collisions. *Nucl. Phys. A*, vol. 326, nos. 2–3, Sept. 1979, pp. 525–535.

9. Townsend, L. W.: Abrasion Cross Section for ^{20}Ne Projectiles at 2.1 GeV/Nucleon. *Canadian J. Phys.*, vol. 61, no. 1, Jan. 1983, pp. 93–98.

10. Cucinotta, Francis A.; and Dubey, Rajendra R.: Alpha-Cluster Description of Excitation Energies in $12C(12C,3\alpha)X$ at 2.1A GeV. *Phys. Rev. C: Nucl. Phys.*, vol. 50, no. 2, Aug. 1994, pp. 1090–1096.

11. Cucinotta, F. A.; and Dubey, R. R.: Cluster Abrasion of Large Fragments in Relativistic Heavy Ion Fragmentation. *Bull. Am. Phys. Soc.*, vol. 39, no. 5, Oct. 1994, p. 1401.

12. Oliveira, Luiz F.; Donangelo, Raul; and Rasmussen, John O.: Abrasion-Ablation Calculations of Large Fragment Yields From Relativistic Heavy Ion Reactions. *Phys. Rev. C*, vol. 19, no. 3, Mar. 1979, pp. 826–833.

13. Wilson, John W.: Composite Particle Reaction Theory. Ph.D. Diss., College of William and Mary, June 1975.

14. Cucinotta, Francis A.; and Dubey, Rajendra R.: *Final State Interactions and Inclusive Nuclear Collisions*. NASA TP-3353, 1993.

15. Feshbach, Herman; Kerman, Arthur; and Koonin, Steven: The Statistical Theory of Multi-Step Compound and Direct Reactions. *Ann. Phys.*, vol. 125, 1980, pp. 429–476.

16. Griffin, J. J.: Statistical Model of Intermediate Structure. *Phys. Rev. Lett.*, vol. 17, no. 9, Aug. 1966, pp. 478–481.

17. Tamura, T.; Udagawa, T.; and Lenske, H.: Multistep Direct Reaction Analysis of Continuum Spectra in Reactions Induced by Light Ions. *Phys. Rev. C*, vol. 26, no. 2, Aug. 1982, pp. 379–404.

18. Cucinotta, Francis A.: Forward Production of Protons in Relativistic 12C–Nucleus Collisions. *J. Phys. G: Nucl. Part. Phys.*, vol. 20, 1994, pp. 1803–1815.

19. Cucinotta, Francis A.; Townsend, Lawrence W.; and Wilson, John W.: *Description of Alpha-Nucleus Interaction Cross Sections for Cosmic Ray Shielding Studies*. NASA TP-3285, 1993.

20. Cummings, J. R.; Binns, W. R.; Garrard, T. L.; Israel, M. H.; Klarmann, J.; Stone, E. C.; and Waddington, C. J.: Determination of the Cross Sections for the Production of Fragments From Relativistic Nucleus-Nucleus Interactions. I. Measurements. *Phys. Rev. C*, vol. 42, no. 6, Dec. 1990, pp. 2508–2529.

21. Tull, C. E.: *Relativistic Heavy Ion Fragmentation at HISS*. LBL-29718, Univ. of California, Oct. 1990.

22. Webber, W. R.; Kish, J. C.; and Schrier, D. A.: Individual Isotopic Fragmentation Cross Sections of Relativistic Nuclei in Hydrogen, Helium, and Carbon Targets. *Phys. Rev. C: Nucl. Phys.*, vol. 41, no. 2, Feb. 1990, pp. 547–565.

23. Webber, W. R.; Kish, J. C.; and Schrier, D. A.: Individual Charge Changing Fragmentation Cross Sections of Relativistic Nuclei in Hydrogen, Helium, and Carbon Targets. *Phys. Rev. C: Nucl. Phys.*, vol. 41, no. 2, Feb. 1990, pp. 533–546.

24. Shavers, Mark R.; Frankel, Kenneth; Miller, Jack; Schimmerling, Walter; Townsend, Lawrence W.; and Wilson, John W.: The Fragmentation of 670A MeV Neon-20 as a Function of Depth in Water. III. Analytical Multigeneration Transport Theory. *Radiat. Res.*, vol. 136, no. 1, Oct. 1993, pp. 1–14.

25. Shinn, J. L.; Wilson, J. W.; Badavi, F. F.; Benton, E. V.; Csige, I.; Frank, L.; and Benton, E. R.: HZE Beam Transport in Multilayered Materials. *Radiat. Meas.*, vol. 23, no. 1, Jan. 1994, pp. 57–64

26. Badavi, F. F.; Townsend, L. W.; Wilson, J. W.; and Norbury, J. W.: An Algorithm for a Semiempirical Nuclear Fragmentation Model. *Comput. Phys. Commun.*, vol. 47, nos. 2–3, Nov.–Dec. 1987, pp. 281–294.

27. Townsend, Lawrence W.; Wilson, John W.; Tripathi, Ram K.; Norbury, John W.; Badavi, Francis F.; and Khan, Ferdous: *HZEFRG1: An Energy-Dependent Semiempirical Nuclear Fragmentation Model*. NASA TP-3310, 1993.

28. Dymarz, R.; and Kohmura, T.: *The Mean Free Path of Protons in Nuclei and the Nuclear Radius*. Ref: 58/82, Nuclear Physics Lab., Oxford Univ., 1982.

29. Wilson, John W.; Chun, Sang Y.; Badavi, Francis F.; and John, Sarah: *Coulomb Effects in Low-Energy Nuclear Fragmentation*. NASA TP-3352, 1993.

16

30. Norbury, John W.; Cucinotta, F. A.; Townsend, L. W.; and Badavi, F. F.: Parameterized Cross Sections for Coulomb Dissociation in Heavy-Ion Collisions. *Nucl. Instrum. & Methods Phys. Res.*, vol. B31, no. 4, June 1988, pp. 535–537.

31. Wilson, J. W.; and Townsend, L. W.: An Optical Model for Composite Nuclear Scattering. *Canadian J. Phys.*, vol. 59, no. 11, Nov. 1981, pp. 1569–1576.

32. Gosset, J.; Gutbrod, H. H.; Meyer, W. G.; Poskanzer, A. M.; Sandoval, A.; Stock, R.; and Westfall, G. D.: Central Collisions of Relativistic Heavy Ions. *Phys. Rev. C*, vol. 16, no. 2, Aug. 1977, pp. 629–657.

33. Morrissey, D. J.; Marsh, W. R.; Otto, R. J.; Loveland, W.; and Seaborg, G. T.: Target Residue Mass and Charge Distributions in Relativistic Heavy Ion Reactions. *Phys. Rev. C*, vol. 18, no. 3, Sept. 1978, pp. 1267–1274.

34. Westfall, G. D.; Wilson, Lance W.; Lindstrom, P. J.; Crawford, H. J.; Greiner, D. E.; and Heckman, H. H.: Fragmentation of Relativistic ^{56}Fe. *Phys. Rev. C*, vol. 19, no. 4, Apr. 1979, pp. 1309–1323.

35. Rudstam, G.: Systematics of Spallation Yields. *Zeitschrift fur Naturforschung*, vol. 21a, no. 7, July 1966, pp. 1027–1041.

36. Bertulani, Carlos A.; and Baur, Gerhard: Electromagnetic Processes in Relativistic Heavy Ion Collisions. *Phys. Rep.*, vol. 163, nos. 5 & 6, June 1988, pp. 299–408.

37. Aleixo, A. N. F.; and Bertulani, C. A.: Coulomb Excitation in Intermediate-Energy Collisions. *Nucl. Phys.*, vol. A505, no. 2, Dec. 1989, pp. 448–470.

38. Kidd, J. M.; Lindstrom, P. J.; Crawford, H. J.; and Woods, G.: Fragmentation of Carbon Ions at 250 MeV/Nucleon. *Phys. Rev. C*, vol. 37, no. 6, June 1988, pp. 2613–2623.

39. Olson, D. L.; Berman, B. L.; Greiner, D. E.; Heckman, H. H.; Lindstrom, P. J.; and Crawford, H. J.: Factorization of Fragment-Production Cross Sections in Relativistic Heavy-Ion Collisions. *Phys. Rev. C*, vol. 28, no. 4, Oct. 1983, pp. 1602–1613.

40. Lefort, Marc: Mass Distribution in Dissipative Reactions—The Frontier Between Fusion and Deep Inelastic Transfers. *Deep-Inelastic and Fusion Reactions With Heavy Ions*, W. von Oertzen, ed., Volume 117 of *Lecture Notes in Physics*, Springer-Verlag, 1980, pp. 25–42.

41. Zeitlin, C. J.; Frankel, K. A.; Gong, W.; Heilbronn, L.; Lampo, E. J.; Leres, R.; Miller, J.; and Schimmerling, W.: A Modular Solid State Detector for Measuring High Energy Heavy Ion Fragmentation Near the Beam Axis. *Radiat. Meas.*, vol. 23, no. 1, Jan. 1994, pp. 65–81.

42. Dudkin, V. E.; Kovalev, E. E.; Nefedov, N. A.; Antonchik, V. A.; Bogdanov, S. D.; Ostroumov, V. I.; Crawford, H. J.; and Benton, E. V.: Multiplicities of Secondaries in Interactions of 1.8 GeV/Nucleon ^{56}Fe Nuclei With Photoemulsion and the Cascade Evaporation Model. *Nucl. Phys.*, vol. A509, no. 4, Mar. 1990, pp. 783–799.

43. Westfall, G. D.; Gosset, J.; Johansen, P. J.; Poskanzer, A. M.; Meyer, W. G.; Gutbrod, H. H.; Sandoval, A.; and Stock, R.: Nuclear Fireball Model for Proton Inclusive Spectra From Relativistic Heavy-Ion Collisions. *Phys. Rev. Lett.*, vol. 37, no. 18, Nov. 1976, pp. 1202–1205.

Table 1. Chi Square Analysis of Iron Fragmentation Model

System	NUCFRG2 and Westfall et al.				NUCFRG2 and Cummings et al.	
	χ^2	χ^2 without Al data	χ^2/n	χ^2/n without Al data	χ^2	χ^2/n
Fe + C	50.2	16.0	5	1.8	48.3	3.7
Fe + Cu	200.6	22.9	20	2.5	78.4	6.0
Fe + Pb	177.4	56.2	18	6.2	83.1	6.7

Table 2. Chi Square Analysis of Iron Fragmentation Experiments

System	Westfall et al. and Cummings et al.				Cummings et al. and Westfall et al.			
	χ^2	χ^2 without Al data	χ^2/n	χ^2/n without Al data	χ^2	χ^2 without Al data	χ^2/n	χ^2/n without Al data
Fe + C	85.6	43.3	8.6	4.8	54.6	33.6	5.5	3.7
Fe + Cu	424.4	108.4	42.4	12.0	160.3	69.4	16.0	7.7
Fe + Pb	348.8	79.5	34.9	8.8	143.1	55.8	14.3	6.2

Table 3. Chi Square Analysis of Fragmentation Cross Sections of Projectile Ions on Carbon Targets

[See page 32 for footnotes]

Projectile	Fragment charge	Fragment mass number	Experiment cross section, mb	Experiment uncertainty, mb	NUCFRG2 cross section, mb	Chi square per degree of freedom (n)
^{11}B 326 A MeV[a]	4		105.9	1.59	99.31	
	3		30.1	.45	56.84	
						6.508
^{12}C 250 A MeV[b]	6	11	55.97	4.06	56.19	
	6	10	5.33	.81	.37	
	5	11	65.61	2.55	56.33	
	5	10	47.50	2.42	57.46	
	4	10	5.88	9.70	3.47	
	4	9	10.44	.85	14.21	
	4	7	22.64	1.49	20.37	
	3	8	1.33	1.00	.11	
	3	7	17.19	3.00	20.07	
	3	6	26.35	2.10	30.80	
						8.504
^{12}C 403 A MeV[a]	5		106.0	1.59	114.62	
	4		29.6	.89	40.79	
						.929
^{12}C 418 A MeV[a]	5		111.2	1.67	114.50	
	4		32.1	.96	40.66	
						.949
^{12}C 561 A MeV[a]	5		108.7	1.63	113.07	
	4		30.3	.91	40.16	
						1.295
^{12}C 600 A MeV[c]	6	11	53.6	.80	54.1	
	6	10	2.1	.11	.3	
	5	11	70.7	1.06	54.3	
	5	10	38.6	.58	55.3	
	4	10	5.6	.28	3.3	
	4	9	9.6	.29	13.52	
	4	7	15.5	.47	19.53	
						3.092
^{12}C 693 A MeV[a]	5		110.1	1.65	112.41	
	4		34.9	1.05	39.76	
						0.321

Table 3. Continued

Projectile	Fragment charge	Fragment mass number	Experiment cross section, mb	Experiment uncertainty, mb	NUCFRG2 cross section, mb	Chi square per degree of freedom (n)
^{12}C 915 A MeV[a]	5		109.4	1.64	111.1	
	4		33.6	1.01	39.0	
						0.387
^{12}C 1016 A MeV[a]	5		113.2	1.70	110.8	
	4		36.8	1.10	39.0	
						.072
^{12}C 1050 A MeV[d]	6	11	44.70	2.80	52.7	
	6	10	4.44	.24	.4	
	5	11	48.60	2.40	52.9	
	5	10	27.90	2.20	54.4	
	4	10	5.34	.29	3.2	
	4	9	10.70	.50	13.1	
	4	7	18.60	.90	19.0	
	3	8	2.40	.18	.1	
	3	7	21.50	1.10	20.5	
	3	6	27.10	2.20	28.5	
	2	6	1.83	.19	.4	
						10.836
^{12}C 1572 A MeV[a]	5		103.9	1.56	109.2	
	4		35.6	1.07	38.1	
						.211
^{12}C 2100 A MeV[d]	6	11	46.50	2.30	51.3	
	6	10	4.11	.22	.3	
	5	11	53.80	2.70	51.6	
	5	10	35.10	3.40	53.7	
	4	10	5.81	.29	3.2	
	4	9	10.63	.53	12.7	
	4	7	18.61	.93	18.5	
	3	8	2.18	.15	.1	
	3	7	21.50	1.10	20.0	
	3	6	30.00	2.40	27.9	
	2	6	2.21	.22	.4	
						9.456
^{14}N 516 A MeV[a]	6		169.2	2.54	124.0	
	5		63.1	1.89	85.8	
	4		27.9	.84	33.8	
						7.828

Table 3. Continued

Projectile	Fragment charge	Fragment mass number	Experiment cross section, mb	Experiment uncertainty, mb	NUCFRG2 cross section, mb	Chi square per degree of freedom (n)
^{16}O 441 A MeV[a]	7		162.9	2.44	133.8	
	6		160.2	2.40	111.3	
	5		60.7	1.82	75.7	
	4		13.6	.65	32.9	
						9.718
^{16}O 491 A MeV[a]	7		146.4	2.20	133.3	
	6		146.2	2.19	110.6	
	5		54.7	1.64	75.5	
	4		13.4	.67	32.8	
						7.491
^{16}O 669 A MeV[a]	7		158.5	2.38	131.7	
	6		159.6	2.39	109.3	
	5		56.5	1.69	74.7	
	4		17.3	.87	32.3	
						10.661
^{16}O 903 A MeV[a]	7		154.4	2.32	130.4	
	6		152.9	2.29	108.2	
	5		52.4	1.57	73.9	
	4		20.3	1.02	32.1	
						8.331
^{16}O 1563 A MeV[a]	7		125.3	1.88	128.4	
	6		123.2	1.85	106.1	
	5		46.6	1.40	72.8	
	4		18.2	.91	31.7	
						4.500
^{16}O 2100 A MeV[d]	8	15	42.90	2.30	57.6	
	8	14	1.67	.12	.6	
	7	15	54.20	2.90	58.0	
	7	14	41.80	3.30	61.7	
	7	13	8.06	.42	6.9	
	7	12	.73	.07	.3	
	6	14	4.71	.31	10.8	
	6	13	27.70	1.40	47.7	
	6	12	65.10	5.20	40.3	
	6	11	18.46	.92	6.0	
	6	10	2.51	.16	.2	
	5	13	.44	.05	.4	
	5	12	2.44	2.15	4.3	
	5	11	26.0	1.30	32.7	

Table 3. Continued

Projectile	Fragment charge	Fragment mass number	Experiment cross section, mb	Experiment uncertainty, mb	NUCFRG2 cross section, mb	Chi square per degree of freedom (n)
^{16}O 2100 A MeV[d]	5	10	20.3	1.60	32.3	
	4	11	.19	.03	.17	
	4	10	3.9	.30	1.9	
	4	9	9.0	.51	9.8	
	4	7	22.3	1.10	16.5	
	3	8	2.5	.18	.09	
	3	7	26.3	1.30	17.9	
	3	6	35.9	2.90	26.2	
	2	6	2.0	.21	.3	
						8.018
^{20}Ne 468 A MeV[a]	9		106.3	1.60	129.9	
	8		181.0	2.72	136.0	
	7		134.5	4.04	103.5	
	6		135.1	4.05	85.9	
	5		53.7	2.69	70.9	
						12.132
^{20}Ne 599 A MeV[a]	9		91.6	.14	128.8	
	8		150.6	2.26	134.7	
	7		111.1	3.33	102.6	
	6		125.9	3.78	85.2	
	5		52.6	2.63	72.2	
						7.607
^{20}Ne 608 A MeV[a]	9		96.9	1.45	128.7	
	8		159.5	2.39	134.6	
	7		118.8	3.56	102.4	
	6		120.2	3.61	85.2	
	5		53.6	2.68	70.2	
						6.655
^{20}Ne 1057 A MeV[a]	9		87.6	1.31	126.2	
	8		140.1	2.10	132.1	
	7		103.0	3.09	100.7	
	6		119.8	3.59	83.7	
	5		57.2	2.86	69.3	
						6.003
^{23}Na 461 A MeV[a]	10		132.3	1.98	179.7	
	9		62.1	1.86	118.0	
	8		106.1	3.18	94.1	
	7		89.3	2.68	79.8	
	6		101.2	3.04	70.5	
						11.007

22

Table 3. Continued

Projectile	Fragment charge	Fragment mass number	Experiment cross section, mb	Experiment uncertainty, mb	NUCFRG2 cross section, mb	Chi square per degree of freedom (n)
^{24}Mg 309 A MeV[a]	11		147.8	2.22	112.2	
	10		133.0	2.00	147.0	
	9		58.1	1.74	109.3	
	8		136.6	2.05	89.8	
	7		89.3	2.68	77.6	
	6		114.3	3.43	69.1	
	5		39.8	1.99	59.0	
						14.072
^{24}Mg 481 A MeV[a]	11		124.3	1.86	110.5	
	10		111.0	1.67	139.5	
	9		56.3	1.69	107.2	
	8		119.7	1.80	88.5	
	7		89.4	2.68	76.5	
	6		120.4	3.61	68.4	
	5		48.1	2.41	58.3	
						12.297
^{24}Mg 739 A MeV[a]	11		116.1	1.74	108.7	
	10		102.2	1.53	137.3	
	9		48.7	1.46	105.8	
	8		103.5	1.55	87.2	
	7		75.9	2.28	75.7	
	6		108.6	3.26	67.6	
	5		45.6	4.56	58.0	
						10.124
^{24}Mg 1455 A MeV[a]	11		116.4	1.75	106.6	
	10		101.5	1.52	134.0	
	9		48.0	1.44	103.8	
	8		106.5	1.60	85.7	
	7		73.8	2.21	74.4	
	6		106.6	3.20	66.8	
	5		48.6	2.43	57.6	
						9.857
^{27}Al 582 A MeV[a]	12		182.1	2.73	163.7	
	11		95.6	1.43	123.5	
	10		89.4	1.34	97.7	
	9		37.6	1.88	82.8	
	8		81.5	2.44	72.8	
	7		60.2	1.81	65.3	
	6		74.1	3.71	59.3	

Table 3. Continued

Projectile	Fragment charge	Fragment mass number	Experiment cross section, mb	Experiment uncertainty, mb	NUCFRG2 cross section, mb	Chi square per degree of freedom (n)
^{27}Al 582 A MeV[a]	5		37.6	3.76	51.5	
						5.330
^{40}Ar 600 A MeV[c]	18	39	146.4	2.20	63.7	
	18	38	72.3	1.08	68.8	
	18	37	8.4	.43	29.7	
	17	39	39.1	.59	63.7	
	17	38	34.9	.52	9.5	
	17	37	59.3	.89	35.9	
	17	36	38.0	.57	49.1	
	17	35	12.3	.61	28.2	
	16	38	.8	.08	.1	
	16	37	5.1	.26	1.2	
	16	36	19.3	.58	4.6	
	16	35	32.6	.49	22.6	
	16	34	51.0	.77	39.8	
	16	33	15.3	.46	28.0	
	16	32	1.1	.11	5.8	
	15	35	1.2	.12	.6	
	15	34	6.3	.32	2.7	
	15	33	23.8	.36	14.7	
	15	32	35.9	1.80	33.4	
	15	31	24.0	1.20	27.9	
	15	30	2.2	.22	6.9	
	14	32	4.1	.21	1.7	
	14	31	17.6	.53	9.6	
	14	30	40.1	.60	28.2	
	14	29	27.6	.41	27.6	
	14	28	9.2	.46	8.3	
	13	30	1.2	.12	1.1	
	13	29	11.8	.35	6.2	
	13	28	20.5	1.03	23.9	
	13	27	33.1	.50	26.6	
	13	26	4.2	.42	10.0	
	12	27	4.1	.21	3.9	
	12	26	23.0	.35	20.0	
	12	25	23.1	.35	25.7	
	12	24	12.7	.38	11.5	
	12	23	1.0	.10	1.2	
						9.591
^{40}Ar 1650 A MeV[e]	17	39	79.50	19.50	61.89	
	17	38	8.10	4.05	9.33	
	17	37	27.00	8.85	34.92	

24

Table 3. Continued

Projectile	Fragment charge	Fragment mass number	Experiment cross section, mb	Experiment uncertainty, mb	NUCFRG2 cross section, mb	Chi square per degree of freedom (n)
^{40}Ar 1650 A MeV[e]	17	36	49.50	16.60	47.71	
	17	35	51.00	19.50	27.34	
	17	34	12.00	6.45	4.93	
	16	38	4.35	1.50	.15	
	16	37	11.70	2.70	1.19	
	16	36	12.40	3.00	4.48	
	16	35	24.00	5.40	21.83	
	16	34	49.50	10.80	38.49	
	16	33	31.50	7.05	27.31	
	16	32	10.60	3.00	5.74	
	16	31	.54	.42	.99	
	15	36	.615	.195	.06	
	15	35	2.10	.33	.58	
	15	34	5.85	.825	2.67	
	15	33	18.00	1.80	14.36	
	15	32	27.00	2.70	32.65	
	15	31	21.00	2.10	27.26	
	15	30	3.90	.63	6.83	
	15	29	.315	.195	1.05	
	14	34	.01	.07	.02	
	14	33	1.32	.24	.30	
	14	32	3.00	.24	1.71	
	14	31	11.00	1.80	9.40	
	14	30	37.50	3.15	27.76	
	14	29	25.50	3.00	26.96	
	14	28	13.00	1.95	8.17	
	14	27	.69	.285	1.11	
	13	32	.129	.111	.01	
	13	31	.705	.21	.15	
	13	30	3.00	.405	1.10	
	13	29	10.40	2.25	6.08	
	13	28	19.50	2.40	23.48	
	13	27	25.50	2.85	26.25	
	13	26	7.20	1.28	9.85	
	13	25	.315	.165	1.17	
	12	30	.165	.126	.01	
	12	29	.66	.21	.01	
	12	28	2.10	.495	.71	
	12	27	6.75	1.02	3.86	
	12	26	24.00	2.85	19.77	
	12	25	22.50	3.45	25.33	
	12	24	14.20	1.80	11.46	
	12	23	.96	.315	1.25	
	11	27	.36	.135	.03	

Table 3. Continued

Projectile	Fragment charge	Fragment mass number	Experiment cross section, mb	Experiment uncertainty, mb	NUCFRG2 cross section, mb	Chi square per degree of freedom (n)
^{40}Ar 1650 A MeV[c]	11	26	2.40	0.51	0.45	
	11	25	7.90	1.05	2.42	
	11	24	12.60	2.10	15.91	
	11	23	22.50	3.15	24.49	
	11	22	8.25	1.65	13.13	
	11	21	.255	.123	1.38	
	10	25	.21	.146	.02	
	10	24	1.80	.45	.27	
	10	23	4.80	.54	1.53	
	10	22	12.30	2.25	12.49	
	10	21	16.50	2.55	22.93	
	10	20	8.55	1.80	14.72	
	10	19	.705	.36	1.61	
	9	22	.765	.285	.15	
	9	21	4.35	.81	.98	
	9	20	7.20	1.95	9.46	
	9	19	11.70	2.25	21.69	
	9	18	5.40	1.32	15.93	
	9	17	.345	.315	1.88	
	8	20	.33	.088	.09	
	8	19	3.60	.645	.64	
	8	18	6.75	1.44	6.81	
	8	17	9.75	2.40	20.31	
	8	16	14.20	3.45	16.71	
	8	15	1.23	.615	2.18	
	8	14	.086	.111	.16	
	7	18	.60	.24	.04	
	7	17	2.25	.57	.41	
	7	16	4.65	1.30	4.65	
	7	15	18.00	5.10	18.79	
	7	14	8.70	2.70	17.23	
	7	13	.75	.48	2.52	
	6	16	.375	.165	.02	
	6	15	1.17	.675	.25	
	6	14	4.35	1.50	3.03	
	6	13	10.00	3.00	17.25	
	6	12	10.20	3.30	17.45	
	6	11	1.215	.555	2.88	
	6	10	.18	.24	.11	
	5	13	1.455	.555	.14	
	5	12	2.25	.855	1.86	
	5	11	7.80	2.70	15.64	
	5	10	4.05	1.485	17.18	
	5	9	.495	.27	1.29	

Table 3. Continued

Projectile	Fragment charge	Fragment mass number	Experiment cross section, mb	Experiment uncertainty, mb	NUCFRG2 cross section, mb	Chi square per degree of freedom (n)
^{40}Ar 1650 A MeV[c]	5	8	0.21	0.255	0.01	
						5.313
^{56}Fe 330 A MeV[a]	25		244.3	7.33	196.8	
	24		182.7	5.48	132.3	
	23		121.1	3.63	107.7	
	22		110.7	3.32	92.2	
	21		89.2	2.68	81.4	
	20		79.6	2.39	73.4	
	19		51.6	2.58	67.2	
	18		44.4	2.22	62.0	
	17		38.2	1.91	57.5	
	16		42.4	2.12	53.5	
						5.471
^{56}Fe 434 A MeV[a]	25		223.8	3.36	194.8	
	24		175.1	2.63	131.2	
	23		116.1	3.48	106.7	
	22		116.0	3.48	91.4	
	21		79.8	2.39	80.8	
	20		73.9	2.22	73.0	
	19		52.3	2.62	66.8	
	18		48.2	2.41	61.7	
	17		39.5	1.98	57.3	
	16		44.3	2.22	53.4	
	15		24.89	2.49	49.9	
	14		45.7	4.57	47.0	
						4.355
^{56}Fe 520 A MeV[a]	25		206.2	3.09	193.6	
	24		163.4	2.45	130.2	
	23		115.2	3.46	105.9	
	22		112.3	3.37	91.2	
	21		76.7	2.30	80.4	
	20		71.3	2.14	72.7	
	19		51.8	2.59	66.7	
	18		52.8	2.64	61.5	
	17		40.6	2.03	57.3	
	16		41.7	2.09	53.3	
	15		29.5	1.48	49.9	
	14		48.6	4.86	46.9	
						2.960

Table 3. Continued

Projectile	Fragment charge	Fragment mass number	Experiment cross section, mb	Experiment uncertainty, mb	NUCFRG2 cross section, mb	Chi square per degree of freedom (n)
^{56}Fe 600 A MeV[c]	26	55	164.3	2.46	67.1	
	26	54	28.2	.85	14.7	
	26	53	3.0	.30	3.3	
	25	55	53.7	.81	64.3	
	25	54	66.9	1.00	64.3	
	25	53	64.0	.96	45.5	
	25	52	21.6	.65	14.5	
	25	51	3.9	.39	3.3	
	24	54	4.7	.24	6.6	
	24	53	16.0	.48	20.5	
	24	52	63.6	.95	42.3	
	24	51	60.7	.91	39.5	
	24	50	30.5	.46	16.2	
	24	49	5.1	.15	3.6	
	23	52	1.1	.11	3.4	
	23	51	8.3	.25	11.3	
	23	50	33.1	.50	30.8	
	23	49	43.0	.65	35.7	
	23	48	24.7	.37	18.4	
	23	47	4.9	.49	4.0	
	22	50	1.6	.16	1.9	
	22	49	8.4	.25	6.5	
	22	48	30.5	.46	22.6	
	22	47	40.6	.61	32.0	
	22	46	23.3	.35	20.3	
	22	45	4.0	.40	5.0	
	22	44	.6	.60	1.2	
	21	48	.3	.30	1.1	
	21	47	2.7	.27	3.9	
	21	46	12.8	.38	16.1	
	21	45	28.3	.42	28.7	
	21	44	21.5	.32	22.0	
	21	43	6.9	.34	6.3	
	20	45	2.7	.27	2.6	
	20	44	10.6	.32	11.2	
	20	43	22.6	.34	25.0	
	20	42	22.0	.33	23.0	
	20	41	10.9	.55	7.9	
	20	40	1.3	.13	1.6	
	19	44	.7	.07	.4	
	19	43	2.8	.28	1.8	
	19	42	8.1	.08	7.5	
	19	41	16.6	.50	21.5	
	19	40	14.6	.43	23.2	

Table 3. Continued

Projectile	Fragment charge	Fragment mass number	Experiment cross section, mb	Experiment uncertainty, mb	NUCFRG2 cross section, mb	Chi square per degree of freedom (n)
^{56}Fe 600 A MeV[c]	19	39	7.3	0.37	9.8	
	19	38	1.0	.10	1.8	
	18	41	1.7	.17	1.2	
	18	40	8.0	.40	4.9	
	18	39	17.9	.54	17.8	
	18	38	19.1	.57	22.7	
	18	37	6.1	.31	11.8	
	18	36	1.1	.11	2.1	
	17	39	.9	.09	.8	
	17	38	3.4	.34	3.1	
	17	37	12.5	.38	14.3	
	17	36	13.5	.41	22.0	
	17	35	9.6	.48	13.6	
	17	34	.9	.09	2.6	
	16	37	.6	.06	.5	
	16	36	2.2	.22	2.1	
	16	35	8.0	.40	10.8	
	16	34	14.6	.44	20.5	
	16	33	11.1	.33	15.1	
	16	32	5.6	.28	3.3	
	16	31	1.6	.16	.6	
						3.751
^{56}Fe 662 A MeV[a]	25		191.6	2.87	192.3	
	24		163.2	2.45	129.2	
	23		114.3	3.43	105.3	
	22		105.3	3.16	90.3	
	21		68.9	2.07	80.0	
	20		69.6	2.09	72.3	
	19		49.8	2.49	66.3	
	18		52.9	5.29	61.5	
	17		41.8	2.09	57.1	
	16		45.8	2.29	53.3	
	15		32.0	3.20	49.8	
	14		48.3	4.83	46.9	
						2.562
^{56}Fe 724 A MeV[a]	25		166.5	1.75	191.9	
	24		130.9	1.96	128.5	
	23		91.5	2.75	105.1	
	22		87.7	2.63	90.1	
	21		66.1	1.98	79.7	
	20		62.0	1.86	72.3	
	19		45.4	2.27	66.3	

Table 3. Continued

Projectile	Fragment charge	Fragment mass number	Experiment cross section, mb	Experiment uncertainty, mb	NUCFRG2 cross section, mb	Chi square per degree of freedom (n)
^{56}Fe 724 A MeV[a]	18		47.8	2.39	61.3	
	17		35.5	1.78	57.0	
	16		39.6	1.98	53.3	
	15		29.3	2.93	49.8	
	14		44.3	4.43	46.9	
						3.243
^{56}Fe 944 A MeV[a]	25		177.8	2.67	190.2	
	24		130.4	1.96	127.8	
	23		86.7	2.61	104.2	
	22		85.3	2.56	89.6	
	21		66.7	2.00	79.2	
	20		60.2	1.81	71.9	
	19		41.4	2.07	66.0	
	18		43.4	2.17	61.1	
	17		37.6	1.88	56.9	
	16		43.9	2.19	53.1	
	15		29.8	2.98	49.9	
	14		43.7	4.37	46.7	
						3.231
^{56}Fe 1086A MeV[a]	25		157.7	2.37	189.3	
	24		113.3	1.70	127.3	
	23		77.9	2.34	103.8	
	22		76.4	2.29	89.3	
	21		56.4	1.69	79.1	
	20		57.8	1.73	71.8	
	19		40.7	2.04	65.8	
	18		42.1	2.10	61.1	
	17		35.4	1.77	56.8	
	16		40.6	2.03	53.1	
	15		28.5	2.85	49.9	
	14		44.1	4.41	46.6	
	13		27.2	2.72	44.0	
	12		35.9	3.57	41.7	
						4.831
^{56}Fe 1409A MeV[a]	25		162.2	2.43	188.1	
	24		106.8	1.60	126.3	
	23		73.5	2.21	103.0	
	22		72.7	2.18	88.8	
	21		53.3	1.60	78.7	
	20		56.9	1.71	71.6	
	19		40.8	2.04	65.6	

Table 3. Continued

Projectile	Fragment charge	Fragment mass number	Experiment cross section, mb	Experiment uncertainty, mb	NUCFRG2 cross section, mb	Chi square per degree of freedom (n)
^{56}Fe 1409A MeV[a]	18		40.3	2.02	60.8	
	17		35.7	1.79	56.8	
	16		42.3	2.11	53.1	
	15		34.6	3.46	49.8	
	14		42.3	4.23	46.7	
	13		28.4	2.84	44.0	
	12		33.6	3.36	41.7	
						4.851
^{56}Fe 1512 A MeV[a]	25		160.2	2.40	187.7	
	24		102.4	1.54	125.9	
	23		79.5	2.39	103.0	
	22		79.3	2.38	88.7	
	21		57.1	1.71	78.6	
	20		55.7	1.67	71.5	
	19		41.3	2.07	65.5	
	18		39.5	1.98	60.9	
	17		33.6	1.68	56.7	
	16		39.7	1.99	53.0	
	15		31.1	3.11	49.8	
	14		40.9	4.09	46.6	
	13		28.5	2.85	44.1	
	12		34.2	3.42	41.6	
						4.871
^{56}Fe 1570 A MeV[f]	25		140.73	3.36	187.7	
	24		105.33	2.69	126.0	
	23		79.32	2.31	102.8	
	22		75.17	2.23	88.5	
	21		57.29	1.92	78.6	
	20		63.37	2.01	71.3	
	19		43.62	1.64	65.7	
	18		47.65	1.72	60.7	
	17		41.45	1.59	56.7	
	16		46.47	1.68	53.0	
	15		39.45	1.53	49.8	
	14		50.99	1.75	46.8	
	13		41.23	1.55	44.0	
	12		45.45	1.62	41.6	
	11		35.83	1.42	39.4	
	10		44.79	1.59	37.0	
						3.094

31

Table 3. Concluded

Projectile	Fragment charge	Fragment mass number	Experiment cross section, mb	Experiment uncertainty, mb	NUCFRG2 cross section, mb	Chi square per degree of freedom (n)
^{56}Fe 1615 A MeV[a]	25		150.6	2.26	187.5	
	24		99.7	1.50	125.9	
	23		74.7	2.24	102.7	
	22		73.7	2.21	88.5	
	21		54.5	1.64	78.5	
	20		54.8	1.64	71.5	
	19		38.4	1.92	65.6	
	18		38.6	1.93	60.6	
	17		33.7	1.69	56.8	
	16		36.0	1.80	53.1	
	15		28.1	2.81	49.7	
	14		38.3	3.83	46.8	
	13		25.7	2.57	44.0	
	12		28.9	2.87	41.6	
						6.499
^{56}Fe 1880 A MeV[g]	25		181.0	27.0	186.8	
	24		124.0	13.0	125.3	
	23		100.0	11.0	102.5	
	22		87.0	11.0	88.3	
	21		54.0	9.0	78.3	
	20		78.0	11.0	71.2	
	19		52.0	7.0	65.5	
	18		55.0	9.0	60.7	
	17		53.0	7.0	56.7	
	16		54.0	10.0	53.0	
	15		59.0	10.0	49.7	
	14		57.0	10.0	46.9	
	13		83.0	11.0	44.1	
						3.864

[a]From reference 23.
[b]From reference 36.
[c]From reference 22.
[d]From reference 39.
[e]From reference 21.
[f]From reference 20.
[g]From reference 34.

Table 4. Chi Square Analysis of Fragmentation Cross Sections of Carbon Projectile Ions on Targets Other Than Carbon

[See page 36 for footnote]

Target	Fragment charge	Fragment mass number	Experiment cross section, mb	Experiment uncertainty, mb	NUCFRG2 cross section, mb	Chi square per degree of freedom (n)
^{9}Be 1050 A MeV[a]	6	11	44.70	2.60	52.88	
	6	10	4.02	.23	.35	
	5	11	50.70	3.20	52.99	
	5	10	28.80	2.30	55.01	
	4	10	5.08	.39	3.32	
	4	9	11.60	.76	13.14	
	4	7	17.80	.90	19.03	
	3	9	.75	.08	.03	
	3	8	2.36	.14	.10	
	3	7	23.40	1.20	20.61	
	3	6	24.80	2.00	29.03	
	2	6	2.09	.17	.37	
						10.026
^{9}Be 2100 A MeV[a]	6	11	46.70	2.30	51.51	
	6	10	4.20	.21	.34	
	5	11	53.20	2.90	51.64	
	5	10	31.10	2.60	53.81	
	4	10	5.97	.31	3.25	
	4	9	10.98	.55	12.85	
	4	7	18.91	.95	18.66	
	3	9	.92	.08	.03	
	3	8	2.52	.16	.10	
	3	7	22.80	1.10	20.23	
	3	6	33.10	2.70	28.37	
	2	6	2.54	.25	.36	
						11.964
^{27}Al 1050 A MeV[a]	6	11	57.80	3.90	59.27	
	6	10	5.06	.37	.38	
	5	11	64.50	5.30	60.09	
	5	10	30.40	3.50	59.66	
	4	10	6.49	.48	3.60	
	4	9	13.90	.90	14.34	
	4	7	19.90	1.10	20.80	
	3	9	.82	.16	.04	
	3	8	2.87	.27	.11	
	3	7	28.50	1.40	22.53	
	3	6	24.90	2.90	31.62	
	2	6	2.00	.29	.40	
						13.464

Table 4. Continued

Target	Fragment charge	Fragment mass number	Experiment cross section, mb	Experiment uncertainty, mb	NUCFRG2 cross section, mb	Chi square per degree of freedom (n)
^{27}Al						
2100 A MeV[a]	6	11	59.50	3.10	58.69	
	6	10	4.99	.34	.37	
	5	11	65.20	4.80	59.84	
	5	10	36.40	4.80	58.27	
	4	10	7.02	.40	3.52	
	4	9	12.74	.71	14.02	
	4	7	25.80	1.30	20.43	
	3	9	.88	.12	.04	
	3	8	2.79	.23	.11	
	3	7	27.30	1.40	22.14	
	3	6	36.30	2.90	30.64	
	2	6	2.82	.27	.39	
						13.846
^{63}Cu						
1050 A MeV[a]	6	11	78.10	8.10	70.91	
	6	10	7.53	.70	.43	
	5	11	80.10	7.90	73.88	
	5	10	36.40	9.90	67.08	
	4	10	7.69	.61	4.05	
	4	9	14.30	1.20	16.29	
	4	7	25.00	1.90	23.08	
	3	9	1.05	.38	.04	
	3	8	3.99	.70	.12	
	3	7	32.60	1.90	25.00	
	3	6	33.10	6.00	35.91	
	2	6	3.01	.68	.46	
						23.774
^{63}Cu						
2100 A MeV[a]	6	11	81.40	6.30	72.59	
	6	10	5.38	.55	.42	
	5	11	84.40	9.00	77.16	
	5	10	43.70	9.80	66.28	
	4	10	8.57	.70	4.00	
	4	9	16.10	1.30	15.88	
	4	7	33.70	2.30	22.85	
	3	9	1.38	.36	.04	
	3	8	3.89	.47	.12	
	3	7	31.90	2.30	24.75	
	3	6	47.30	4.50	35.30	
	2	6	3.21	.47	.45	
						23.436

Table 4. Continued

Target	Fragment charge	Fragment mass number	Experiment cross section, mb	Experiment uncertainty, mb	NUCFRG2 cross section, mb	Chi square per degree of freedom (n)
^{107}Ag 1050 A MeV[a]	6	11	98.00	13.00	83.18	
	6	10	7.70	1.00	.47	
	5	11	110.00	15.00	89.42	
	5	10	43.00	12.00	74.01	
	4	10	8.40	1.20	4.47	
	4	9	23.70	2.70	17.35	
	4	7	21.60	2.70	25.05	
	3	9	1.15	.49	.04	
	3	8	2.80	1.20	.14	
	3	7	42.10	3.40	27.14	
	3	6	38.10	7.60	38.30	
	2	6	3.60	1.40	.49	
						19.443
^{107}Ag 2100 A MeV[a]	6	11	101.90	9.60	89.88	
	6	10	7.03	.88	.47	
	5	11	109.00	13.00	100.17	
	5	10	65.00	17.00	73.03	
	4	10	8.81	.91	4.41	
	4	9	18.60	1.70	17.10	
	4	7	41.20	3.30	24.63	
	3	9	1.20	.33	.04	
	3	8	3.27	.53	.13	
	3	7	40.30	3.30	26.68	
	3	6	46.10	5.60	37.56	
	2	6	3.50	1.10	.48	
						19.202
^{208}Pb 1050 A MeV[a]	6	11	128.00	22.00	106.46	
	6	10	10.90	1.70	.54	
	5	11	149.00	25.00	120.13	
	5	10	51.00	18.00	83.37	
	4	10	10.90	1.80	5.04	
	4	9	22.20	3.70	19.68	
	4	7	37.80	4.70	28.02	
	3	9	1.76	.81	.05	
	3	8	4.90	1.60	.16	
	3	7	45.20	4.80	30.36	
	3	6	51.00	13.00	42.94	
	2	6	7.30	2.70	.55	
						42.293

Table 4. Concluded

Target	Fragment charge	Fragment mass number	Experiment cross section, mb	Experiment uncertainty, mb	NUCFRG2 cross section, mb	Chi square per degree of freedom (n)
^{208}Pb 2100 A MeV[a]	6	11	145.00	17.00	128.19	
	6	10	7.80	1.50	.53	
	5	11	155.00	23.00	153.25	
	5	10	74.00	25.00	82.40	
	4	10	10.00	1.40	4.98	
	4	9	22.50	2.60	19.36	
	4	7	47.90	4.90	27.44	
	3	9	1.43	.53	.05	
	3	8	3.40	.82	.15	
	3	7	45.90	4.60	29.73	
	3	6	60.00	8.50	43.42	
	2	6	4.20	1.10	.55	
						21.363

[a]From references 37 and 39.

Table 5. Chi Square Analysis of Fragmentation Cross Sections of Oxygen Projectile Ions on Targets Other Than Carbon

[See page 39 for footnote]

Target	Fragment charge	Fragment mass number	Experiment cross section, mb	Experiment uncertainty, mb	NUCFRG2 cross section, mb	Chi square per degree of freedom (n)
^{9}Be 2100 A MeV[a]	8	15	43.00	2.20	57.60	
	8	14	1.60	.10	.60	
	7	15	54.10	2.70	57.80	
	7	14	49.50	4.00	63.00	
	7	13	8.01	.40	7.04	
	7	12	.66	.05	.33	
	6	14	5.21	.30	11.10	
	6	13	28.60	1.40	48.20	
	6	12	60.80	4.90	40.91	
	6	11	21.00	1.10	6.08	
	6	10	2.81	.17	.21	
	5	13	.50	.04	.41	
	5	12	2.75	.15	4.36	
	5	11	27.50	1.40	32.95	
	5	10	19.20	1.50	33.02	
	4	10	3.92	.27	1.99	
	4	9	9.79	.50	9.91	
	4	7	22.00	1.10	16.83	
	3	7	27.00	1.40	18.24	
	3	6	33.50	2.70	26.60	
						5.722
^{27}Al 2100 A MeV[a]	7	15	66.00	4.30	69.48	
	6	14	6.29	.46	12.59	
	6	13	31.40	2.00	55.56	
	5	12	3.61	.24	5.03	
	5	11	31.00	1.60	37.64	
	4	9	11.22	.68	11.34	
	3	7	34.80	1.80	21.12	
						3.021
^{63}Cu 2100 A MeV[a]	8	15	74.00	7.80	85.47	
	8	14	2.14	.42	.78	
	7	15	98.20	9.80	92.10	
	7	14	72.00	14.00	82.02	
	7	13	14.70	1.60	9.22	
	7	12	.42	.18	.43	
	6	14	7.76	.92	14.45	
	6	13	35.80	3.70	63.11	
	6	12	92.00	14.00	53.65	
	6	11	27.00	2.60	7.91	
	6	10	4.45	.52	.27	

Table 5. Continued

Target	Fragment charge	Fragment mass number	Experiment cross section, mb	Experiment uncertainty, mb	NUCFRG2 cross section, mb	Chi square per degree of freedom (n)
^{63}Cu 2100 A MeV[a]	5	13	0.82	0.17	0.54	
	5	12	2.98	.38	5.72	
	5	11	35.90	2.90	42.91	
	5	10	35.20	5.50	42.64	
	4	11	.30	.13	.21	
	4	10	6.51	.86	2.57	
	4	9	12.30	1.10	12.94	
	4	7	32.00	2.50	21.79	
	3	8	3.63	.47	.11	
	3	7	38.70	2.90	23.60	
	3	6	61.20	7.90	33.87	
						14.183
^{107}Ag 2100 A MeV[a]	8	15	99.00	13.00	108.69	
	8	14	2.20	.58	.85	
	7	15	121.00	15.00	123.72	
	7	14	68.00	23.00	89.42	
	7	13	18.60	2.20	10.16	
	7	12	1.11	.34	.47	
	6	14	7.50	1.30	15.75	
	6	13	39.40	5.10	69.55	
	6	12	104.00	18.00	58.14	
	6	11	37.80	3.80	8.70	
	6	10	4.20	1.20	.30	
	5	13	.65	.28	.60	
	5	12	4.04	.58	6.20	
	5	11	43.60	3.90	47.16	
	5	10	26.60	6.30	47.09	
	4	10	5.65	.77	2.84	
	4	9	13.80	1.50	14.16	
	4	7	36.40	3.20	23.80	
	3	7	39.80	3.50	25.79	
	3	6	49.40	8.50	38.06	
						12.336
^{208}Pb 2100 A MeV[a]	8	15	135.00	22.00	162.79	
	8	14	2.80	1.50	.96	
	7	15	202.00	26.00	199.79	
	7	14	71.00	22.00	100.65	
	7	13	17.00	3.20	11.48	
	6	14	12.30	2.20	17.73	
	6	13	45.40	8.30	78.53	
	6	12	126.00	25.00	66.34	
	6	11	36.90	5.70	9.90	
	6	10	7.20	1.40	.34	

Table 5. Concluded

Target	Fragment charge	Fragment mass number	Experiment cross section, mb	Experiment uncertainty, mb	NUCFRG2 cross section, mb	Chi square per degree of freedom (n)
^{208}Pb 2100 A MeV[a]	5	13	0.70	0.44	0.68	
	5	12	3.98	.75	7.07	
	5	11	52.90	5.90	53.67	
	5	10	35.70	11.00	52.95	
	4	10	6.80	1.10	3.20	
	4	9	15.30	2.10	16.36	
	4	7	43.30	6.40	27.84	
	3	7	39.70	4.30	30.17	
	3	6	56.00	13.00	42.04	
						17.217

[a]From references 37 and 39.

Table 6. Chi Square Analysis of Fragmentation Cross Sections of Argon Projectile Ions on Targets Other Than Carbon

[See page 41 for footnote]

Target	Fragment charge	Fragment mass number	Experiment cross section, mb	Experiment uncertainty, mb	NUCFRG2 cross section, mb	Chi square per degree of freedom (n)
KCl 1650 A MeV[a]	17	34	17.00	10.00	6.05	
	17	35	38.00	15.00	33.26	
	17	36	6.80	3.80	57.01	
	17	37	42.00	31.00	41.18	
	17	39	56.00	29.00	87.56	
	16	31	1.90	1.50	1.23	
	16	32	20.00	6.30	7.08	
	16	33	41.00	8.50	33.54	
	16	34	50.00	11.00	47.23	
	16	35	32.00	8.60	26.56	
	16	36	29.00	6.00	5.35	
	16	37	19.00	4.10	1.40	
	16	38	9.90	2.70	.18	
	15	29	.42	.33	1.33	
	15	30	7.40	1.70	8.53	
	15	31	21.00	3.80	33.93	
	15	32	25.00	3.00	40.25	
	15	33	22.00	5.70	17.64	
	15	34	2.10	1.50	3.27	
	15	35	2.80	.93	.71	
	15	36	.20	.07	.07	
	14	27	1.40	.60	1.42	
	14	28	15.00	2.80	10.41	
	14	29	38.00	5.20	33.97	
	14	30	43.00	5.20	34.70	
	14	31	14.00	9.00	11.70	
	14	32	1.50	1.80	2.11	
	14	33	.54	.89	.37	
	14	34	.16	.10	.03	
	13	25	.86	.44	1.53	
	13	26	8.00	1.30	12.57	
	13	27	37.00	4.30	33.54	
	13	28	18.00	4.70	29.91	
	13	29	22.00	5.30	7.66	
	13	30	1.50	.49	1.38	
	13	31	.58	.32	.19	
	12	23	.40	.18	1.62	
	12	24	21.00	3.50	14.83	
	12	25	26.00	3.90	33.08	
	12	26	29.00	3.20	25.24	
	12	27	10.00	4.70	4.93	
	12	28	.42	.80	.90	

Table 6. Concluded

Target	Fragment charge	Fragment mass number	Experiment cross section, mb	Experiment uncertainty, mb	NUCFRG2 cross section, mb	Chi square per degree of freedom (n)
KCl 1650 A MeV[a]	12	29	0.68	0.34	0.09	
	11	21	.76	.80	1.84	
	11	22	12.00	2.20	17.37	
	11	23	30.00	5.90	31.67	
	11	24	19.00	4.30	20.60	
	11	25	5.20	2.90	3.17	
	11	26	1.70	1.40	.57	
	10	19	.46	.24	2.16	
	10	20	14.00	3.30	19.69	
	10	21	25.00	4.50	30.40	
	10	22	16.00	2.70	16.52	
	10	23	5.50	1.70	1.98	
	10	24	1.40	.51	.35	
	9	18	5.80	2.00	21.65	
	9	19	16.00	3.30	29.02	
	9	20	9.10	1.90	12.66	
	9	21	4.60	1.70	1.30	
	9	22	2.20	.93	.20	
	8	15	2.00	1.10	3.02	
	8	16	24.00	6.10	23.14	
	8	17	17.00	3.80	27.18	
	8	18	8.30	2.50	9.26	
	8	19	6.10	1.40	.86	
	8	20	.99	.30	.11	
	7	13	1.20	.76	3.57	
	7	14	12.00	5.30	24.04	
	7	15	27.00	7.00	26.01	
	7	16	7.70	3.10	6.44	
	7	17	4.80	.73	.56	
	6	10	.48	.55	.16	
	6	11	1.50	.67	4.16	
	6	12	14.00	6.00	24.66	
	6	13	13.00	4.20	24.42	
	6	14	4.00	2.70	4.23	
	6	15	2.80	.98	.35	
	5	9	1.20	.88	1.89	
	5	10	5.60	1.80	24.83	
	5	11	11.00	3.70	22.55	
	5	12	1.60	1.70	2.63	
	5	13	1.90	2.00	.21	
						14.886

[a]From reference 21.

Table 7. Chi Square Analysis of Fragmentation Cross Sections of Iron Projectile Ions on Targets Other Than Carbon

[See page 45 for footnotes]

Target	Fragment charge	Fragment mass number	Experiment cross section, mb	Experiment uncertainty, mb	NUCFRG2 cross section, mb	Chi square per degree of freedom (n)
^{7}Li 1880 A MeV[a]	25		141.00	18.00	187.66	
	24		98.00	7.00	127.29	
	23		88.00	7.00	104.06	
	22		75.00	6.00	89.86	
	21		67.00	6.00	79.78	
	20		64.00	6.00	72.48	
	19		56.00	5.00	66.76	
	18		55.00	6.00	61.97	
	17		38.00	4.00	57.78	
	16		56.00	6.00	54.16	
	15		57.00	6.00	50.95	
	14		57.00	5.00	47.82	
	13		50.00	5.00	45.25	
						2.973
^{9}Be 1880 A MeV[a]	25		156.00	21.00	186.66	
	24		111.00	9.00	126.30	
	23		88.00	9.00	103.18	
	22		83.00	9.00	88.97	
	21		77.00	8.00	79.10	
	20		68.00	7.00	71.98	
	19		65.00	7.00	66.03	
	18		54.00	7.00	61.34	
	17		54.00	7.00	57.35	
	16		63.00	8.00	53.52	
	15		57.00	8.00	50.33	
	14		75.00	8.00	47.23	
	13		50.00	7.00	44.68	
						2.338
^{27}Al 1569 A MeV[b]	25		174.04	4.46	210.00	
	24		127.60	3.23	137.75	
	23		91.05	2.70	113.32	
	22		84.12	2.58	97.92	
	21		73.41	2.40	87.22	
	20		68.92	2.31	79.57	
	19		52.89	2.01	73.26	
	18		52.72	2.01	68.26	
	17		45.24	1.85	64.01	
	16		52.27	1.98	60.22	
	15		43.47	1.80	56.78	
	14		58.21	2.08	53.58	

Table 7. Continued

Target	Fragment charge	Fragment mass number	Experiment cross section, mb	Experiment uncertainty, mb	NUCFRG2 cross section, mb	Chi square per degree of freedom (n)
^{27}Al						
1569 A MeV[b]	13		45.37	1.82	50.85	
	12		51.76	1.94	48.17	
	11		45.23	1.81	46.10	
	10		49.11	1.88	43.75	
						2.354
^{32}S						
1880 A MeV[a]	25		250.00	22.00	219.02	
	24		128.00	16.00	140.59	
	23		86.00	16.00	115.73	
	22		64.00	10.00	100.47	
	21		91.00	13.00	89.77	
	20		97.00	14.00	81.95	
	19		55.00	21.00	75.66	
	18		74.00	13.00	70.46	
	17		66.00	14.00	66.35	
	16		74.00	12.00	62.24	
	15		50.00	8.00	58.95	
	14		106.00	14.00	55.66	
	13		78.00	18.00	52.98	
						7.376
^{63}Cu						
1569 A MeV[b]	25		238.96	6.78	265.32	
	24		147.44	3.73	158.74	
	23		98.89	3.00	132.79	
	22		98.45	2.97	116.63	
	21		73.64	2.57	105.32	
	20		80.32	2.67	97.14	
	19		59.98	2.31	90.85	
	18		61.18	2.32	85.56	
	17		49.41	2.09	81.17	
	16		59.58	2.27	77.52	
	15		49.82	2.08	74.04	
	14		72.20	2.48	70.87	
	13		51.47	2.10	68.46	
	12		61.03	2.27	66.09	
	11		50.17	2.06	64.08	
	10		54.55	2.14	62.03	
						4.867
^{63}Cu						
1880 A MeV[a]	25		219.00	20.00	268.30	
	24		149.00	16.00	158.27	
	23		121.00	15.00	132.58	
	22		101.00	14.00	116.20	
	21		100.00	15.00	105.34	
	20		98.00	14.00	97.25	

Table 7. Continued

Target	Fragment charge	Fragment mass number	Experiment cross section, mb	Experiment uncertainty, mb	NUCFRG2 cross section, mb	Chi square per degree of freedom (n)
^{63}Cu 1880 A MeV[a]	19		88.00	14.00	90.84	
	18		95.00	15.00	85.56	
	17		86.00	13.00	81.40	
	16		56.00	11.00	77.47	
	15		88.00	15.00	74.00	
	14		72.00	11.00	70.95	
	13		179.00	27.00	68.58	
						15.432
^{107}Ag 1880 A MeV[a]	25		280.00	23.00	341.73	
	24		218.00	21.00	170.26	
	23		117.00	15.00	143.15	
	22		124.00	16.00	126.07	
	21		104.00	13.00	114.45	
	20		118.00	14.00	105.98	
	19		79.00	11.00	99.32	
	18		84.00	14.00	93.97	
	17		79.00	14.00	89.40	
	16		96.00	13.00	85.33	
	15		64.00	13.00	81.89	
	14		158.00	20.00	78.77	
	13		112.00	19.00	76.30	
						10.746
^{181}Ta 1880 A MeV[a]	26		56.00	82.00	659.47	
	25		457.00	34.00	472.04	
	24		206.00	22.00	184.56	
	23		150.00	19.00	156.03	
	22		152.00	19.00	137.52	
	21		129.00	18.00	125.26	
	20		107.00	17.00	116.49	
	19		111.00	20.00	109.34	
	18		100.00	18.00	103.61	
	17		101.00	18.00	99.05	
	16		109.00	17.00	94.48	
	15		133.00	20.00	91.22	
	13		81.00	14.00	85.37	
						44.585
^{208}Pb 1563 A MeV[b]	25		500.52	13.42	491.81	
	24		223.00	6.18	189.75	
	23		130.18	4.64	159.71	
	22		135.00	4.67	141.33	
	21		104.01	4.11	128.57	
	20		98.20	3.98	119.27	

Table 7. Concluded

Target	Fragment charge	Fragment mass number	Experiment cross section, mb	Experiment uncertainty, mb	NUCFRG2 cross section, mb	Chi square per degree of freedom (n)
^{208}Pb 1563 A MeV[b]	19		79.76	3.60	112.27	
	18		77.23	3.54	106.34	
	17		59.97	3.14	101.80	
	16		75.75	3.47	97.07	
	15		63.66	3.19	93.81	
	14		86.28	3.65	90.52	
	13		61.90	3.12	87.75	
	12		74.14	3.38	85.15	
	11		66.19	3.20	83.33	
						5.457
^{208}Pb 1880 A MeV[a]	25		509.00	40.00	522.88	
	24		242.00	25.00	189.22	
	23		142.00	20.00	159.56	
	22		148.00	22.00	141.41	
	21		111.00	17.00	128.62	
	20		144.00	22.00	119.33	
	19		90.00	19.00	112.31	
	18		73.00	15.00	106.64	
	17		90.00	19.00	101.65	
	16		116.00	19.00	97.65	
	15		78.00	16.00	93.67	
	14		119.00	22.00	90.71	
	13		191.00	37.00	87.82	
						13.641
^{238}U 1880 A MeV[a]	25		646.00	43.00	582.03	
	24		208.00	22.00	193.87	
	23		181.00	27.00	163.80	
	22		95.00	16.00	144.57	
	21		153.00	21.00	132.02	
	20		143.00	19.00	122.79	
	19		105.00	15.00	115.3	
	18		113.00	19.00	109.7	
	17		133.00	22.00	104.7	
	16		116.00	22.00	100.2	
	15		176.00	34.00	96.56	
	14		169.00	28.00	93.24	
	13		307.00	79.00	90.97	
						52.651

[a]From reference 34.
[b]From reference 20.

Table 8. Chi Square per n Values for Target and Projectile Atomic Numbers

Z_T	Chi square per n for Z_P of—									
	5	6	7	8	10	11	12	13	18	26
3										3.0
4		11.0		5.8						2.3
6	6.5	6.2	7.8	7.6	8.1	11.0	11.5	5.3	6.8	5.0
13		13.7		3.0						2.3
16										7.4
18									14.9	
29		23.6		14.2						10.2
47		19.3		12.3						10.7
73										44.9
82		31.5		17.2						21.2
92										52.7

REPORT DOCUMENTATION PAGE

Form Approved
OMB No. 0704-0188

1. AGENCY USE ONLY *(Leave blank)*	2. REPORT DATE October 1995	3. REPORT TYPE AND DATES COVERED Technical Paper

4. TITLE AND SUBTITLE
NUCFRG2: An Evaluation of the Semiempirical Nuclear Fragmentation Database

5. FUNDING NUMBERS
WU 199-45-16-11

6. AUTHOR(S)
J. W. Wilson, R. K. Tripathi, F. A. Cucinotta, J. L. Shinn, F. F. Badavi, S. Y. Chun, J. W. Norbury, C. J. Zeitlin, L. Heilbronn, and J. Miller

7. PERFORMING ORGANIZATION NAME(S) AND ADDRESS(ES)
NASA Langley Research Center
Hampton, VA 23681-0001

8. PERFORMING ORGANIZATION REPORT NUMBER
L-17470

9. SPONSORING/MONITORING AGENCY NAME(S) AND ADDRESS(ES)
National Aeronautics and Space Administration
Washington, DC 20546-0001

10. SPONSORING/MONITORING AGENCY REPORT NUMBER
NASA TP-3533

11. SUPPLEMENTARY NOTES
Wilson, Cucinotta, and Shinn: Langley Research Center, Hampton, VA; Tripathi: University of Southern Illinois, Carbondale, IL; Badavi: Christopher Newport University, Newport News, VA; Chun: Old Dominion University, Norfolk, VA; Norbury: University of Wisconsin, LaCrosse, WI; Zeitlin, Heilbronn, and Miller: Lawrence Berkeley Laboratory, Berkeley, CA.

12a. DISTRIBUTION/AVAILABILITY STATEMENT
Unclassified–Unlimited
Subject Category 93
Availability: NASA CASI (301) 621-0390

12b. DISTRIBUTION CODE

13. ABSTRACT *(Maximum 200 words)*
A semiempirical abrasion-ablation model has been successful in generating a large nuclear database for the study of high charge and energy (HZE) ion beams, radiation physics, and galactic cosmic ray shielding. The cross sections that are generated are compared with measured HZE fragmentation data from various experimental groups. A research program for improvement of the database generator is also discussed.

14. SUBJECT TERMS
Cosmic ray shielding; Nuclear cross sections; Radiation protection

15. NUMBER OF PAGES
47

16. PRICE CODE
A03

17. SECURITY CLASSIFICATION OF REPORT Unclassified	18. SECURITY CLASSIFICATION OF THIS PAGE Unclassified	19. SECURITY CLASSIFICATION OF ABSTRACT Unclassified	20. LIMITATION OF ABSTRACT

NSN 7540-01-280-5500

Standard Form 298 (Rev. 2-89)
Prescribed by ANSI Std. Z39-18
298-102

ATOMIC ELECTRON CORRELATION AND PARTICLE AND ANTI-PARTICLE INDUCED SINGLE- AND DOUBLE-IONIZATION

T. Das* and F. Bary Malik

Physics Department, Southern Illinois University, Carbondale, Illinois, 62901, U.S.A.
*Current Address: Shawnee Community College, Ullin, Illinois, 62992, U.S.A.

1. INTRODUCTION

In a series of experiments, Andersen et al. [1,2] have found that the ratio, R, of double-ionization of He to single-ionization of He, by incident proton and anti-proton differs substantially in the incident energy range of 0.3 to 40 MeV. In this energy range one expects the impulse approximation to be valid and that the ionization probabilities are well described by Lewis-Merzbacher (noted hereforth as LM) Theory [3] which predicts this ratio to be the same in both cases. According to this theory, the interaction V (LM) causing the transition is the potential between the incident projectile and two bound electrons and is given by (minus and plus signs are, respectively, for incident proton and anti-proton)

$$V(LM) = \pm \frac{e^2}{|R-r_1|} \pm \frac{e^2}{|R-r_2|} \tag{1}$$

where R, r_1, and r_2 are coordinates of the projectile, electron one and electron two, respectively. In Born approximation, the scattering amplitude $f_{LM}(\Theta)$ is simply proportional to the square of the matrix-element of (1)

$$f_{LM}(\Theta) \sim |\iiint exp \{i(k_o \hat{n}_o - k_1 \hat{n}_1)\} \psi_f(r_1,r_2) V(LM) \psi_o(r_1 r_2) dr_1 dr_2 dR|^2 \tag{2}$$

In (2) $\psi_f(r_1,r_2)$ and $\psi_o(r_1 r_2)$ are final and initial electronic wave functions, respectively. The incident and outgoing projectile wave functions are represented by plane waves of wave numbers $k_o \hat{n}_o$ and $k_1 \hat{n}_1$, respectively, $\hat{n}_o$ and $\hat{n}_1$ being appropriate unit vectors. Since the scattering amplitude is an absolute square of the matrix-element of V(LM), incident proton and anti-proton should yield the same cross section for single—as well as double-ionization.

Calculations of Reading and Ford [4-6] using forced impulse approximation use (1) as the basic interaction causing the transition but include correlation in electronic wave functions. Their calculated R agrees to some extent with the data for incident proton but falls short of the observation for incident anti-proton.

Das, in his thesis [7] has pointed out that the two electrons in the final channel are far apart both for single- and double-ionization and hence do not interact anymore. Thus, the interaction causing the transition is not given by (1) but the interaction between two electrons must be added to (1). In section 2 we derive the expression for scattering amplitudes starting from the Schroedinger equation of the system and then do systematic approximation to examine this point. We find that electronic interaction must be added to (1). The consequences for the inclusion of this term in the calculations are that single- and double-ionization of He by p^+ and p^- should, in principle, be different. This has been observed in the recent experiements of Hvelplund et al. [8] and Andersen et al. [9]. In section 3, we apply the theory to both single- and double-ionization at a few incident energies and find reasonable agreement with the data. Section 4 summarizes our conclusion.

2. THEORY

The Schroedinger equation for He-atom and an incident projectile in the center of mass system of incident projectile and He-nucleus is given by

$$[-\frac{\hbar^2}{2\mu}\nabla_R^2 - \frac{\hbar^2}{2m}(\nabla_1^2 + \nabla_2^2) - (\mp Ze^2/R) - Ze^2/r_1 - Ze^2/r_2 + e^2/r_{12} \mp \frac{e^2}{|R-r_1|} \mp \frac{e^2}{|R-r_2|} - E]\psi(r_1, r_2, R) = 0$$

(3)

In (3) μ and m are reduced masses of projectile and electrons, respectively. r_1, r_2, and R are, respectively, coordinates of electron one, two and projectile. Minus and plus sign refer, respectively, to incident proton and anti-proton. One may expand ψ in the following complete orthonormal set:

$$\psi(r_1, r_2, R) = \sum_n F_n(R)\psi_n(r_1, r_2)$$

(4)

where $\psi_n(r_1, r_2)$ is defined by the following Hermitian equation:

2

$$[-\frac{\hbar^2}{2m}(\nabla_1^2+\nabla_2^2)-\frac{Ze^2}{r_1}-\frac{Ze^2}{r_2}]\psi_n(r_1,r_2)=E_n\psi_n(r_1,r_2) \tag{5}$$

with $(\psi_n,\psi_m)=\delta_{nm}$

Equations for $F_n(R)$ may now be obtained by taking scaler products of (3) with ψ_n.

$$(\nabla_R^2+k_n^2\mp\frac{Ze^2}{R})F_n(R)=-\frac{2\mu}{\hbar^2}\int\int dr_1\,dr_2\psi_n^*(r_1,r_2)\,[\mp\frac{Ze^2}{|R-r_1|}\mp\frac{Ze^2}{|R-r_2|}+\frac{e^2}{r_{12}}]\sum_{m\cdot n}F_m(R)\psi_m(r_1,r_2) \tag{6}$$

One may formally now write down the expression for differential cross section for transition form an initial state to a state 'n':

$$\frac{d\sigma}{d\Omega}=\frac{4\pi^2\mu^2}{h^2}\frac{k_n}{k_o}|\int\int\int dr_1 dr_2 dRF_{no}^*(R)\psi_n^*(r_1,r_2)$$
$$H_{int}(r_1,r_2,R)\sum_{m\cdot n}F_m(R)\psi_m(r_1,r_2)|^2 \tag{7}$$

with

$$H_{int}(r_1 r_2 R)=\mp\frac{Ze^2}{|r_1-R|}\mp\frac{Ze^2}{|r_2-R|}+e^2/r_{12} \tag{8}$$

In (7) $F_{no}(R)$ is the solution of the homogeneous part of (6) with outgoing asymptotic condition. (7) is exact and clearly the e^2/r_{12} should be included in the calculation.

In Born approximation, incident and outgoing projectile are represented by plane waves which is equivalent to neglecting Ze^2/R term on the left side of (6). We make further the following approximation

$$\sum_m F_m(R)\psi_m(r_1,r_2)\approx F_o(R)\sum_m\psi_m(r_1,r_2) \tag{9a}$$

$$=F_o(R)\psi_g(r_1,r_2) \tag{9b}$$

where $F_o(R)$ is the incident projectile wave function and ψ_g is correlated ground state electronic wave function in the incident channel. In case $F_o(R)$ is approximated by plane wave

3

in the incident channel with wave number $k_o \hat{n}_o$, the differential cross section is given by

$$\frac{d\sigma}{d\Omega} = \frac{4\pi^2\mu^2}{\hbar^2}\frac{k_n}{k_o}|\int\int\int dr_1 dr_2 dR exp\{i(k_o\hat{n}_o - k_n\hat{n}).R\}\psi_n^*(r_1,r_2)[\mp\frac{Ze^2}{|R-r_1|} \mp \frac{Ze^2}{|R-r_2|} + \frac{e^2}{r_{12}}]\psi_g(r_1,r_2)|^2$$

(10)

The important thing in (8) and (10) is to note that the interaction responsible for the transition is not (1) but e^2/r_{12} term must be added to it. This conclusion does not depend on approximations (9a) and (9b) but is correct for the most general case given by (8). It is the consequence of the necessary asymptotic condition that in the final channel the asymptotic behavior of the wave function is given by a product of scattering amplitude, outgoing plane or coulomb wave function, intrinsic wave functions of ejected electron and He$^+$ for single-ionization (or intrinsic wave functions of two ejected electrons and wave functions and He^{++} for double-ionization).

Another important consequence of (8) is to note that one expects anti-proton induced single- and double-ionization probabilities to be greater than those by proton, in case matrix-elements have similar phases. The structure of (10) also implies that single- and double-ionization cross sections by anti-proton and proton are, in principle, different from each other, the extent of which depends on magnitude of matrix-elements of e^2/r_{12} relative to those of other two interaction terms.

The Lewis-Merzbacher approximation is obtained by (a) neglecting the e^2/r_{12} term in the interaction, (b) using products of hydrogenic type of wave functions for $\psi_n(r_1,r_2)$ and $\psi_g(r_1,r_2)$, and (c) representing incident and outgoing p$^+$ or p$^-$ wave function by plane waves.

3. APPLICATIONS

We present here calculations at a few incident energies for single- and double-ionization by p$^+$ and p$^-$ and the ratio R. The details of the calculation along with results for the entire energy range of 0.4 MeV to 4.0 MeV are presented in ref. [10].

3.1 Single-Ionization

In Fig. 1 we have plotted calculations done in (LM) approximation, along with the data

of Rudd et al. [9] for incident proton. In LM approximation, the initial ground state wave function $\psi_g(r_1 r_2)$ is uncorrelated and is taken to be a product of two hydrogenic type wave functions, each with an effective charge of 1.6875. The final state electronic wave function is a product of a bound hydrogenic wave function with charge 2.0 and a continuum Coulomb wave function in Sommerfeld representation with an effective charge of 1.09. The rational for using an effective charge is that the ejected electron, being far away, sees a nuclear charge shielded by the other electron. Although the calculated results are close to the data, there is some significant differences between them at a few tens of keV.

In Fig. 2, we have plotted calculations that include the e^2/r_{12} term in H_{int} and correlated electronic ground state wave function, for which we have adopted the following variational wave function due to Hylleraas [12]:

$$\psi_g(r_1, r_2) = Ne^{-(\gamma/a_o)(r_1 + r_2)}(1 + cr_{12}^2) \tag{11}$$

In (11) N and a_o are the normalization constant and, Bohr radius, respectively. γ and c are determined from variational principle and found to be respectively, 1.69 and 0.142. The variational ground state energy of -78.28 eV is very close to the observed value of -78.62 eV. The final electronic wave function is taken to be the same as the one in the LM approximation. Whereas, there is no discernable difference between these calculations and those done in the LM approximation at high energies, the calculated results at low energies differ. Calculations done in this approximation are in better agreement with the data compared to those done in the LM model.

In the approximation that include the e^2/r_{12} term and use (11) as ground state wave function, the single-ionization cross sections for incident proton and anti-proton are different which is the case experimentally [8, 9, 15]. The difference is significant both at a very low and high energies. In Table 1 we have compared our calculations with the observed data for a few energies. There is a general agreement.
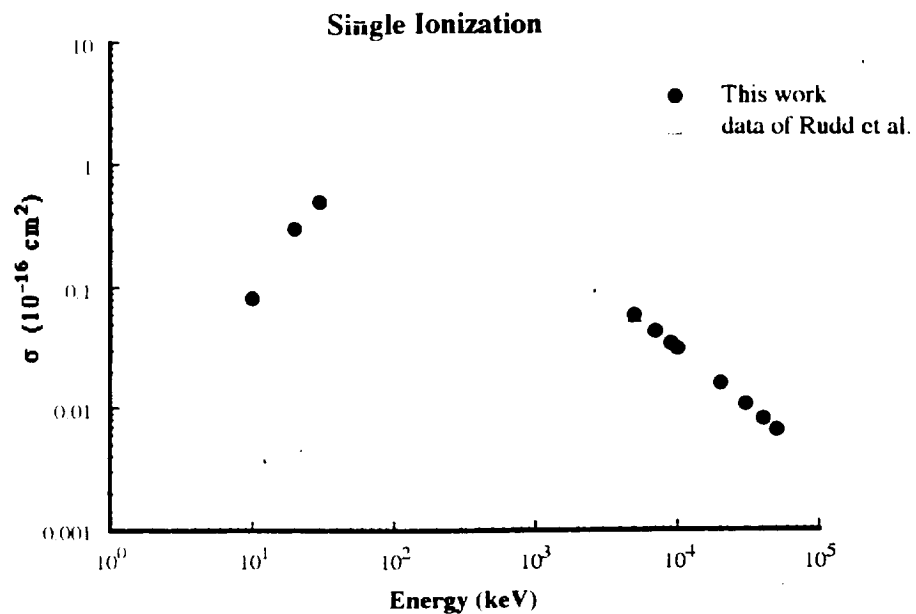
Fig. 1 Single-ionization cross sections calculated in LM approximation (solid dots) are compared with the data of Rudd et al. [11].
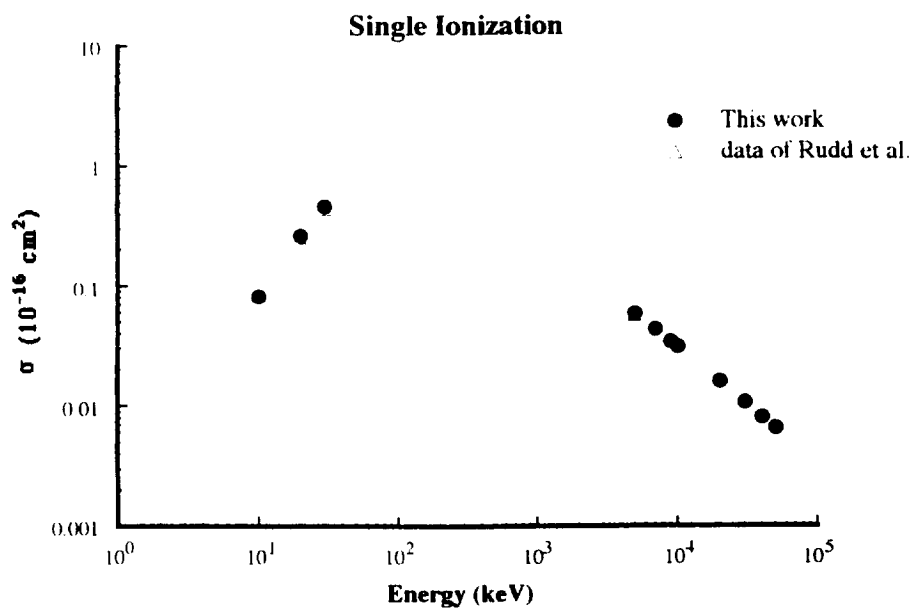

Fig. 2 Single-ionization cross sections calculated using (10) and (11) (solid dots) are compared with the data of Rudd et al. [11].

6

Table 1. Calculated single-ionization cross sections by p⁺ (column 2) and p⁻ (column 4) are compared with the data of ref. [15] for p⁺ (column 3) and of refs. [8, 9] for p⁻ (column 5).

Energy keV	$\sigma(p^+)$ in 10^{-16}cm²		$\sigma(p^-)$ in 10^{-16}cm²	
	th	expt	th	expt
10	0.082		0.106	
20	0.30	0.20	0.32	0.41
100	0.85	0.85	0.88	0.65
500	0.40		0.48	0.38
1000	0.24	0.23	0.26	
50000	0.0065		0.0293	

In the passing one may note that matrix-elements of e^2/r_{12} calculated by replacing ejected electron wave function by plane wave do not differ significantly from those calculated with Sommerfeld Coulomb function but the calculations simplify significantly.

3.2 Double-Ionization

In the LM approximation, double-ionization cross section for the case of incident proton and anti-proton should be the same but the measurements indicate them to be different [8, 9] and hence we are not presenting any calculation of double-ionization in the LM approximation.

We present here calculations using (10) for both cases. Because of the e^2/r_{12} term in the interaction, we expect the double-ionization probabilities for proton and anti-proton to be different. The initial ground stage $\psi_g(r_1,r_2)$ is again represented by (11) and the final electronic state $\psi_n(r_1,r_2)$ is taken to be a product of two Sommerfeld Coulomb function with charge Z=2, except for the matrix-elements of e^2/r_{12}, for which a product of two outgoing plane wave function is used. The latter is justified on the ground that actual calculations done in the case of single-ionization with Coulomb and plane wave show no significant difference in numerical values of matrix-elements of this term.
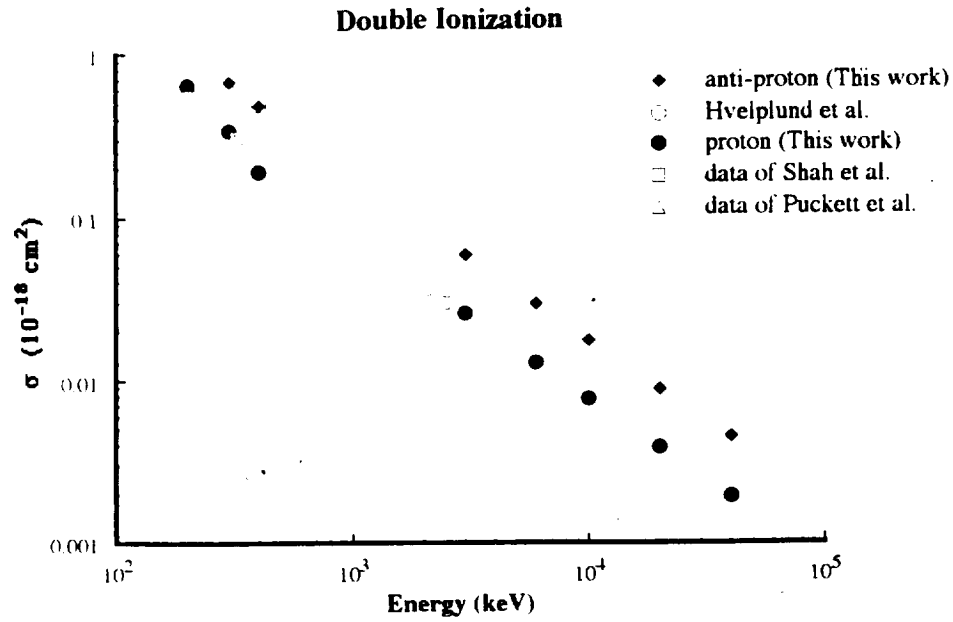
7

Double Ionization

Fig. 3   Calculated double-ionization cross sections for incident proton (solid dots) and anti-proton (solid diamonds) and experimental data for incident proton [13,14] and anti-proton [8,9] are plotted as a function of energy.
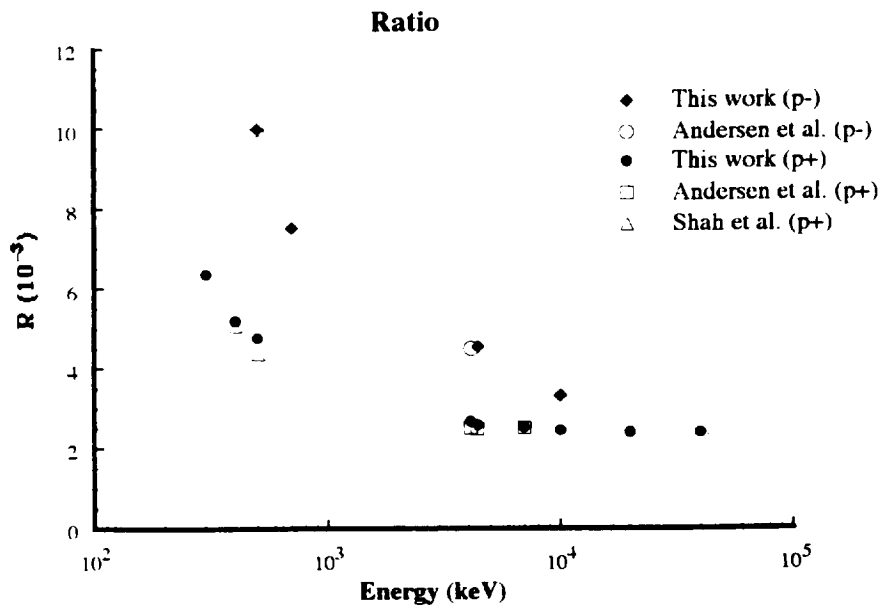
Ratio

Fig. 4   Calculated ratio for incident proton (solid dots) and anti-proton (solid diamonds) are compared to respective experimental observations for proton (open squares [1,2] and triangles [13] and anti-proton (open circles [1,2]).

8

Data for proton induced double-ionization taken by Shah and Gilbody [13] and Puckett and Martin [14], along with our calculations, are shown in Fig. 3. The agreement is satisfactory. In the same figure we also present our calculations for anti-proton induced double-ionization and compare them with the measurements of Hvelplund et al. [8, 9] and the agreement is good. Calculated cross sections for incident p̄ are larger than those for proton, as anticipated.

3.3 Ratio

In Fig. 4, we have plotted the ratio of double- to single-ionization cross section, R, for incident proton and anti-proton for a few tens of keV and a few tens of MeV. Our calculations both for incident proton and anti-proton are in agreement with the data of Shah and Gilbody [11] and Andersen et al. [1, 2]. The key factor responsible for the difference in two cases is the inclusion of e^2/r_{12} term in the interaction which makes double-ionization probabilities for the anti-proton substantially larger than those for the proton.

4. CONCLUSION

One may conclude that (a) the difference in measured R values for incident proton and anti-proton can in general be accounted for within the standard non-relativistic atomic physics, (b) In principle, one is to include two-electronic interaction in the calculation for both single- and double-ionization, (c) Single-ionization probabilities for incident proton and anti-proton are in principle different. This difference is pronounced at high energy and (d) double-ionization probabilities by anti-proton are substantially larger than those by protons from a few hundred keV to a few tens of MeV incident energies.

Lastly at low energies one expects the cross sections for the p̄ case to exhibit some structures originating from the quasi bound states in the attrafctive anti-proton-He potential [16]. These should be absent for incident proton because of the repulsive nature of proton-He potential. There are some indications of this in the data of [8, 9].

5. ACKNOWLEDGEMENT

REFERENCES

1. L. H. Andersen, P. Hvelplund, H. Knudsen, S. P. Møller, K. Elsner, K.-G. Rensfelt and E. Uggerhøj, Phys. Rev. Lett. $\underline{57}$, 2147 (1986).

2. L. H. Andersen, P. Hvelplund, H. Knudsen, S. P. Møller, A. H. Sorensen, K. Elsner, K. G. Rensfelt, and E. Uggerhøj, Phys. Rev. A. $\underline{36}$, 3612 (1987).

3. H. W. Lewis and E. Merzbacher, Handbuch der Physik, XXXIV, 166 (1958).

4. J. F. Reading and A. L. Ford, J. Phys. B. $\underline{20}$, 3747 (1987).

5. J. F. Reading and A. L. Ford, Phys. b. $\underline{21}$, L685, (1988).

6. J. F. Reading and A. L. Ford, Phys. Rev. Lett. $\underline{58}$, 543, (1987).

7. T. Das, Southern Illinois University at Carbondale, dissertation, (1994).

8. P. Hvelplund, H. Knudsen, U. Mikkelsen, E. Morenzoni, S. P. Møller, E. Uggerhøj and T. Worm, J. Phys. B $\underline{27}$, 925(1994).

9. L. H. Anderson, P. Hvelpund, H. Knudsen, S. P. Møller, J. O. P. Pedersen, S. Tang-Petersen, E. Uggerhøj, K. Elsener and E. Morenzoni, Phys. Rev. A $\underline{40}$, 7366 (1989); ibid $\underline{41}$, 6536 (1990).

10. T. Das and F. B. Malik, J. Physics B (to be submitted).

11. M. E. Rudd, R. D. DuBois, L. H. Toburen, C. A. Ratcliffe and V. Goffe, Phys. Rev. A. $\underline{28}$, 3244 (1983).

12. E. A. Hylleraas, Zeit. f. Physik, $\underline{65}$, 209 (1930).

13. M. B. Shah and H. B. Gilbody, J. Phys. B., $\underline{14}$, 2361 (1981).

14. L. J. Puckett and D. W. Martin, Phys. Rev. A., $\underline{1}$, 1432 (1970).

15. M. B. Shah and H. B. Gilbody, J. Phys. G $\underline{22}$, 3037 (1989); ibid $\underline{18}$, 899 (1985).

16. F. B. Malik, Condensed Matter Theories $\underline{7}$, 11 (1982).

On the ionization of He by proton and anti-proton: II. Double ionization and ratio

Trithnath Das* and F. Bary Malik
Physics Department, Southern Illinois University, Carbondale, Illinois 62901-4401, U.S.A.

*Presently at division of Mathematics and Science, Shawnee Community College, Ullin, Illinois 62992, U.S.A.

Abstract. We have calculated double ionization cross section of He by proton and anti-proton in the incident energy range of 50 keV to 20.0 MeV using a coupled channel approach restricted to two channels, incident and final. The projectiles have been represented by plane waves. The ground state wave function of He is taken to be a variational correlated one, and the final state wave functions of two ejected electron is taken to be Coulomb functions for calculating matrix elements of the electron-projectile interaction, and plane waves for calculating matrix elements of electron-electron interaction. The calculation satisfactorily accounts for the data on double ionization cross section and on the ratio of double to single ionization cross sections.

1

I. Introduction

In a series of experiments Andersen et al (1986, 1987) have found that the ratio R, of double to single ionization of He by proton and anti-proton differ significantly in the incident energy range of a few tens of keV to a few tens of MeV. Subsequently, measured single as well as double ionization cross sections of He by proton (Puckett and Martin 1970; Shah and Gilbody 1985, 1982a, b; Shah et al. 1989) are found to differ significantly from those by anti-proton (Andersen et al 1989, 1990 and Hvelplund et al 1994).

These findings are important because, within the framework of theories that represent projectiles by plane waves in the incident and outgoing channels and considering only electron-projectile interaction as perturbation, these ionization cross sections for incident proton and anti-proton and the ratio should be the same.

A number of theoretical approaches have been used to understand these phenomena. The relevant theories for single ionization are summarized in Das and Malik (1996) (This paper is termed as I).

Meng et al's (1993) calculations of single and double ionization cross sections of He for 500 keV incident proton and anti-proton using classical trajectory Monte Carlo method (Olson 1987) that includes electron-electron interaction approximately (noted henceforth as dCTMC) do not adequately explain the data. Reading and Ford (1987, 1988 and 1994) have calculated the double-ionization cross sections by incident proton and anti-proton only at three energies namely at 300, 1000 and 6000 keV and estimated them at 500, 3000 and 10000 keV using a time dependent approach termed as forced impulse approximation or FIM. Their calculated results for the 300, 500 and 1000 keV incident proton energies are in good agreement with the data of Shah and Gilbody (1994) taken at 326, 500 and 1000 keV/amu. However, their calculated cross sections for the 300 and 500 keV incident anti-proton differ about 10 to 20% from the data taken at 270, 326 and 503 keV incident energies (Andersen et al 1986, 1987 and Hvelplund et al 1994). No calculation has been reported for lower incident energies in the FIM. For a proper understanding of the underlying reaction mechanism associated with the ionization process, it is important to understand the low energy data at least in the 100 to 300 keV region.

Das (1994) in his thesis has calculated double ionization cross sections for incident p^+ and p^- in

the energy range of 100 keV to 20 MeV using coupled channel approach but restricting it to two

channels only. A few of these calculations at low and high energies have so far been reported

(Das and Malik 1995). In this paper we present calculated results for the double ionization and

the ratio in the energy range of a few tens of keV to 20 MeV and compare them with the

observed data for both incident proton and anti-proton. The theoretical ratios have been obtained

by using the calculated single ionization cross sections within the frame work of the same theory

in I. The outline of the theory, which is discussed in details in I, is presented in the following

section. Results and discussion, conclusions, and acknowledgment are presented in subsequent

sections.

2. Theory

In the coupled channel theory the equation governing the motion of proton or anti-proton

incident on He, is given by (Mott and Massey 1965 and I)

$$\left\{ \frac{h^2}{2\mu} \nabla^2 + k_n^2 \pm \frac{Ze^2}{R} \right\} F_n(R)$$

$$= - \int dr_1 dr_2 \sum_m \psi_{mn}^*(r_1,r_2) H_{int}(R,r_1,r_2) \sum_{m',n',\pm n} F_n(r_2) \psi_{m'n}(r_1,r_2) \tag{1}$$

In (1) μ is the reduced mass of the scattered particle with respect to He nucleus and R, r_1 and r_2

are, respectively, radius vectors of the projectile, electron 1 and electron 2 in the center of mass

system of incident projectile and He nucleus. $F_n(R)$ is the wave function of the projectile in

channel n. Minus and plus sign refer, respectively, to incident proton and anti-proton. k_n is the

wave number of the nth channel and related to total energy of the system E and the non-

interacting electron energies E_{nm} by $\hbar^2 k_n^2 = 2\mu(E-E_{nm})$. $\psi_{nm}(r_1, r_2)$ in the above expression is a

product of two hydrogen like wave functions in the states n and m including continuum states and

is eigenfunctions of the following equation:

3

$$\left[-\frac{\hbar^2}{2M}(\nabla_1^2+\nabla_2^2)-\frac{Ze^2}{r_1}-\frac{Ze^2}{r_2}\right]\psi_{nm}(r_1,r_2)=E_{nm}\psi_{nm}(r_1,r_2) \qquad (2)$$

with

$$(\psi_{nm},\psi_{n'm'})=\delta_{nn'}\delta_{mm'} \qquad (3)$$

The interaction energy in (1) is given by

$$H_{int}(R,r_1,r_2)=\mp\frac{Ze^2}{|r_1-R|}\mp\frac{Ze^2}{|r_2-R|}+\frac{e^2}{|r_1-r_2|} \qquad (4)$$

For single as well as double ionization, both electrons in the final channel are far apart from each other and represented by hydrogen-like eigenfunction of (2).

One may obtain the expression for differential cross section by imposing the asymptotic condition

$$\lim_{|R|\to\infty} F_n(R) = f_n(\theta,\phi)\frac{e^{i(k_n R-\eta\ln R)}}{R} \qquad (5)$$

where $\eta=\mu Ze^2/\hbar k_n$.

In (5) $f_n(\theta,\phi)$ is the scattering amplitude at angles (θ,ψ) defined with respect to the direction of incident momentum of the projectile. The expression for differential cross section is given by (Mott and Massey 1965)

$$\frac{d\sigma}{d\Omega} = |f_n(\theta,\varphi)|^2$$

$$=\frac{4\pi^2\mu^2}{h^4}\frac{k_n}{k_o}\left|\int\int\int dr_1 dr_2 dR\, F_{no}^*(R)\psi_{nm}^*(r_1,r_2)\,H_{int}(r_1,r_2 R)\sum_{m',n'\neq n}F_m(R)\psi_{n'm'}(r_1,r_2)\right|^2 \qquad (6)$$

Total cross section, σ_n, is then calculated by integrating over the solid angle $d\Omega$. $F_{no}(R)$ in (6)

4

is the solution of the homogeneous part of (1) with outgoing boundary condition (5).

The expression (6) is exact but represents an infinite set of coupled equations and approximations are to be made for numerical evaluation. Since the incident projectile energy of 10 keV to 20 MeV is considerably higher than the double ionization energy of He, it is reasonable to consider only two channels and use Born approximation in which the projectile in the incident and outgoing channels is described by plane wave. In this two-channel approximation, the summation over n' is replaced by one term denoted by 'o'. Hence

$$\sum_{n',n,m'} F_{n'}(R)\psi_{n'm'} \simeq F_o(R)\sum_{m'}\psi_{om'}(r_1,r_2) = F_o(R)\psi_g(r_1 r_2) \tag{7}$$

In (7) $\psi_g(r_1, r_2)$ is fully correlated wave function of the ground state of He. The differential cross section in this two channel plane wave Born approximation, denoted as 2cPWBA, is given by

$$\frac{d\sigma}{d\Omega} = \frac{4\pi^2\mu^2}{h^4}\left|\int\int\int dr_1 dr_2 dR \; exp\;(ik_o\hat{n}_o - ik_n\hat{n}_n)\psi_n^*(r_1,r_2)\;H_{int}(r_1,r_2 R)\psi_g(r_1,r_2)\right|^2 \tag{8}$$

In (8) $\hat{n}_o$ and $\hat{n}_n$ are, respectively, unit vectors in the directions of incident and outgoing wave numbers k_o and k_n.

It is important to note that the e^2/r_{12} term is to be included in H_{int} in principle This conclusion does not depend on the two-channel approximation and the approximation (7) but is correct for the most general expression (6) and is a consequence of the boundary condition that two electrons in the final channel do not interact asymptotically and each is represented by a one-body wave function of hydrogenic type in the final channel. This term does not cause any transition in the absence of projectile-electron interaction because in that case, the projectile wave functions are zero and hence the matrix elements of the term e^2/r_{12} are zero. In the single ionization case, the contribution of the matrix elements of the e^2/r_{12} term to the total cross section is not significant for incident energies greater than a few hundred keV.

The He-ground state wave function ψ_g is taken to be the following (Hylleraas 1930)

$$\psi_g(\boldsymbol{r_1},\boldsymbol{r_2}) = N \exp\left(-\gamma(r_1 + r_2)/a_o\right)(1 + cr_{12}^2) \qquad\qquad (9)$$

where N is the normalization constant and a_o, the Bohr radius . Parameters γ and c have been determined from the Raleigh-Ritz variation principle to be 1.69 and 0.142, respectively. The variational ground state energy of -78.28 eV is very close to the observed value of -78.62 eV.

The electronic wave function in the final channel, $\psi_n(\boldsymbol{r_1},\boldsymbol{r_2})$, is taken to be a product of two continuum Coulomb wave functions having two units of charge in the Sommerfeld representation (Bethe 1930; Lewis and Merzbacher 1958; Sommerfeld 1931) for calculating matrix elements of electron-projectile interaction and a product of two outgoing plane waves for calculating matrix elements of e^2/r_{12}. The latter approximation is motivated by the fact that in the case of single ionization, matrix elements of the e^2/r_{12} term calculated with the plane wave and Coulomb wave functions for the ejected electron yield about the same numerical value (Das and Malik 1996) in the entire energy range.

3. Results and Discussion

(a) *Proton induced double ionization and the ratio*

In Table 1 and Fig. 1 we have presented our calculated results for double ionization cross section in the incident proton energy range of about 50 keV to 20 MeV and compared them with the measurements of Shah and Gilbody (1985), Shah et al (1989) and Puckett and Martin (1970). The measurements extend from about 16 keV to 2400 keV, although the data below 50 keV have not been plotted. The calculation can account for the energy dependence and magnitude of observed cross section from 80 keV to 2400 keV very well. Below 80 keV the calculated values for the cross section seem to be slightly higher than the data which, however, have large errors. The observed cross section seem to be rather flat from 40 to 100 keV incident energy but not the calculated values.

Meng et al (1993) have calculated double ionization cross section in the dCTMC method at two energies. Their calculated values are 7.3 x 10^{-19} cm^2 and 4.1 x 10^{-19} cm^2 for 300 and 500 keV

incident energies, respectively, and are considerably larger than our calculated values and observed data. Calculations and estimates of Ford and Reading for the 300, 500, 1000 and 3000 keV incident energies are about 10% lower than our results and slightly lower than the observed values but their calculations for the 6.0 and 10.0 MeV agree with our results.

In Table 3 and Fig. 3 we have presented our calculated and the observed ratios of double to single ionization cross sections for incident proton using the values of single ionization calculation done in I in the 2cDWA, in the energy range of 50 keV to 20 MeV. The calculation reasonably accounts for the measured ratio in the entire energy range.

(b) *Anti-proton induced double ionization and the ratio*

We present the calculated double ionization cross section by incident anti-proton along with the observed data in the incident energy range of 40 keV to 50 MeV in Table 3 and have plotted them in Fig. 3. The calculation does account for the data in this large energy range and the observed fact that double ionization cross section by incident proton systematically lie lower than that by incident anti-proton in the energy range of 100 to 500 keV. The calculation predicts this trend to continue right up to 50 MeV. This is the consequence of the fact the three terms in (4) have the same sign for the anti-proton case but not for the proton case.

The ratio of double to single ionization cross section for incident anti-proton is calculated using the results of the single ionization cross section calculated in I in the 2cDWA. The calculated ratio is presented and compared to experimental observation in Table 3 and Fig. 3. The data cover a very large energy range from a few tens of keV to 20 MeV. The theoretical calculation can satisfactorily account for the data essentially in the entire energy range.

In I, the possibility of resonances or the formation of virtual (p^- - He) system has been raised. Such a physical situation would also influence double ionization cross section of He by anti-proton and hence the ratio. This process is estimated in I to occur at a few tens of keV. Kimura et al (1994) have incorporated such processes in their calculation of the ratio of incident energies below 50 keV and found them to be important. This process is absent for incident proton for which, on the other hand, the charge transfer channel becomes available. Kimura et al's calculations seem to explain the observed difference in R, for the two cases at energies below 50 keV. Incorporation of such phenomena is beyond the scope of our investigation which is,

therefore, restricted to incident energy grater than about 80 keV. At very low incident energy, Fermi-Teller effect (1947) might influence significantly the double-ionization cross section of He by anti-proton.

Satisfactory explanation of the observed data for double and single ionizations and their ratios for the incident energies above 80 keV indicates that the coupled channel method is a suitable one for describing ionization process. Because the perturbed potential (4) is different for double-ionization cross section for the two cases, theoretically, one predicts that the cross section for incident anti-proton will be higher than that by incident proton at incident energies greater than those used in current experiments. It would be interesting to verify this.

Theoretically, ionization cross sections by electron impact should have the same perturbation (4) for anti-proton, but has the additional complication of incorporating the Pauli principle which is important at lower incident energy (Malik and Trefftz 1961, Trefftz 1963). For He target, the effect of the Pauli principle on the cross section may not be critical for incident electron energies greater than 10 keV and the situation is then similar to that for incident anti-proton, except for the difference in masses. Hence, the energy dependence of the ratio should be qualitatively the same in both cases which is indeed the case, experimentally.

Within the framework of the 2cPWBA, alpha-induced ionization cross section should be similar to that by incident proton, except that the masses of two projectiles are different. This difference would cause the key features of the energy dependence of the cross sections such as maxima to occur at a different energy in the two cases but the general pattern should be the same, which is the case experimentally

4. Conclusion

The observed single and double cross sections and their ratio for incident proton and anti-proton can be well accounted for in the energy range of a few tens of keV to a few tens of MeV by the coupled channel method. It is important however to incorporate proper asymptotic condition in the incident as well as final channel.

5. Acknowledgment

References

Andersen L H, Hvelplund P, Knudsen H, Møller S P, Sørensen A H, Elsner K, Resnfelt K-G, and Uggerhøj E, 1987a *Phys. Rev. Lett.* **57** 2147

Andersen L H, Hvelplund P, Knudsen H, Møller S P, Sørensen A H, Elsner K, Resnfelt K-G, and Uggerhøj E, 1987b *Phys. Rev.* **A 36** 3612

Andersen L H, Hvelplund P, Knudsen H, Møller S P, Pedersen J O P, Tang-Petersen S, Uggerhøj E, Elsner K and Morenzoni E 1989a *Phys. Rev A.* **40** 7366

Andersen L H, Hvelplund P, Knudsen H, Møller S P, Pedersen J O P, Tang-Petersen S, Uggerhøj E, Elsner K and Morenzoni E 1989b *Phys. Rev A.* **41** 6536

Bethe H A 1930 *Annalen der Physik* **5** 325

Das T 1994 Dissertation, *Southern Illinois University at Carbondale, Illinois, U.S.A.*

Das T and Malik F B 1996 *Condensed Matter Theories* **11** (to be published)

Fermi E and Teller E 1947 *Phys. Rev.* **72** 399

Hvelplund P, Knudsen H, Mikkelsen U, Morenzoni E, Møller S P, Uggerhøj E and Worm T 1994 *J. Phys. B: At. Mol. Opt. Phys.* **27** 925

Hylleraas E A 1930 *Zeit. Physik* **65** 209

Kimura M, Shimamura I and Inokuti M 1994 *Phys. Rev.* **A 49** R4281

Lewis H W and Merzbacher E 1958 *Handbuch d. Physik* XXXIV 166

Malik F B and Trefftz E 1961 *Z. Naturforschg* **16a** 583

Puckett L J and Martin D W 1970 *Phys. Rev.* **A 1** 1432

Shah M B and Gilbody H B 1982a *J. Phys. B: At. Mol. Phys.* **15** 413

Shah M B and Gilbody H B 1982b *J. Phys. B: At. Mol. Phys.* **15** 3441

Shah M B and Gilbody H B 1985 *J. Phys. B: At. Mol. Phys.* **18** 899

Shah H B, McCallion P and Gilbody H B 1989 *J. Phys. B: At. Mol. Opt. Phys.* **22** 3037

Sommerfeld A 1931 *Ann. Physik* **9** 257

Trefftz E 1963 Proc. Roy. Soc. (Lond.) **A 271** 379

Table Caption

Table 1   Comparison between the calculated double ionization cross section of He by proton, σ (this work) and the selected observed ones, σ (Shad et al) and σ (puckett et al). Shah et al refers to (Shah and Gilbody 1985, 1982a, 1982b) and Puckett et al refers to (Puckett and Martin 1970).

Table 2   Comparison between the calculated double ionization cross section of He by anti-proton, σ (this work) and the selected observed data noted as σ (Aarhus). σ (Aarhus) refers to data in (Andersen et al 1987a, 1987b) and (Hvelplund et al 1994).

Table 3   Comparison between the calculated ratio of double to single ionization of He by proton and anti-proton noted in columns 2 and 5, respectively, and the corresponding data for incident proton and anti-proton noted in columns 3 and 6, respectively. Aarhus group refers to the selected date of (Andersen et al 1987a, 1987b, 1989a, 1989b) and (Hvelplund et al 1994). Shah et al refers to the selected data of (Shah and Gilbody 1985) and (Shah et al 1989).

12

Figure Caption

Fig. 1   Calculated double ionization cross section of He by proton noted as this work (p⁻)
          is plotted as a function of proton incident energy and compared to the selected
          data. References to the data are given in the caption of Table 1.

Fig. 2   Calculated double ionization cross section of He by anti-proton noted as this work
          (p⁻) is compared to the selected data. The references to the data are noted in the
          caption of Table 2.

Fig. 3   Calculated ratio of double to single ionization cross sections for incident proton,
          noted as this work (p⁻) and incident anti-proton, noted as this work (p⁻) are
          compared to the corresponding incident proton data, as noted Shah et al (p⁺) and
          incident anti-proton data, noted as Aarhus group (p⁻). References to these selected
          data are noted in the caption of Table 3.

Table 1:   Double Ionization cross section by proton.

Energy (keV)	σ (This work) (10^{-18} cm^2)	σ (Shah et al.) (10^{-18} cm^2)	σ (Puckett et al.) (10^{-18} cm^2)
50.00	1.49580		
58.46		0.920 ± 0.240	
60.00	1.25340		
70.00	1.07890		
70.56		0.910 ± 0.190	
80.00	0.94707		
80.67		1.057 ± 0.101	
84.67		0.870 ± 0.180	
90.00	0.84403		
100.00	0.86345		
100.79		0.890 ± 0.180*	
150.00			0.970
200.00	0.65856		0.678
201.59		0.560 ± 0.017	
300.00	0.35672		0.356
322.54		0.315 ± 0.022	
400.00	0.19341		0.242
403.18		0.236 ± 0.012	
500.00	0.15492		0.176
503.97		0.172 ± 0.008	
600.00	0.12921		0.146
645.08		0.127 ± 0.001	
700.00	0.11082		0.114
800.00	0.09701		0.0977
806.35		0.096 ± 0.0051	
900.00	0.086264		0.0828
1000.00	0.075660		0.0732
1007.90		0.0745 ± 0.0027	
1612.70		0.0454 ± 0.0037	

2000.00	0.037883	
2015.90		0.0365 ± 0.035
2398.90		0.0300 ± 0.021
3000.00	0.025934	
4000.00	0.019455	
5000.00	0.015566	
6000.00	0.012973	
7000.00	0.011121	
8000.00	0.0097309	
9000.00	0.0086501	
10000.00	0.0077853	
30000.00	0.0025956	
40000.00	0.0019468	
50000.00	0.0015574	

Table 2:   Double Ionization cross section by anti-proton.

Energy (keV)	σ (This work) (10^{-18} cm^2)	σ (Aarhus data) (10^{-18} cm^2)
50.00	3.5223	
53.90		2.011 ± 0.205
60.00	2.9594	
67.10		1.923 ± 0.156
70.00	2.4612	
80.00	2.2260	
80.40		1.543 ± 0.139
90.00	1.9555	
91.20		1.657 ± 0.145
100.00	1.8366	
101.60		1.577 ± 0.123
200.00	0.87739	
227.90		0.720 ± 0.039
270.10		0.696 ± 0.035
300.00	0.68717	
400.00	0.49127	
403.60		0.447 ± 0.023
500.00	0.36346	
503.60		0.410 ± 0.021
600.00	0.29580	
700.00	0.25284	
800.00	0.22134	
900.00	0.19682	
1000.00	0.17019	
2000.00	0.088013	
3000.00	0.059670	
4000.00	0.045388	
5000.00	0.036515	
6000.00	0.029799	
7000.00	0.025372	

8000.00	0.023202
9000.00	0.019736
10000.00	0.017763
30000.00	0.0059220
40000.00	0.0045416
50000.00	0.0035534

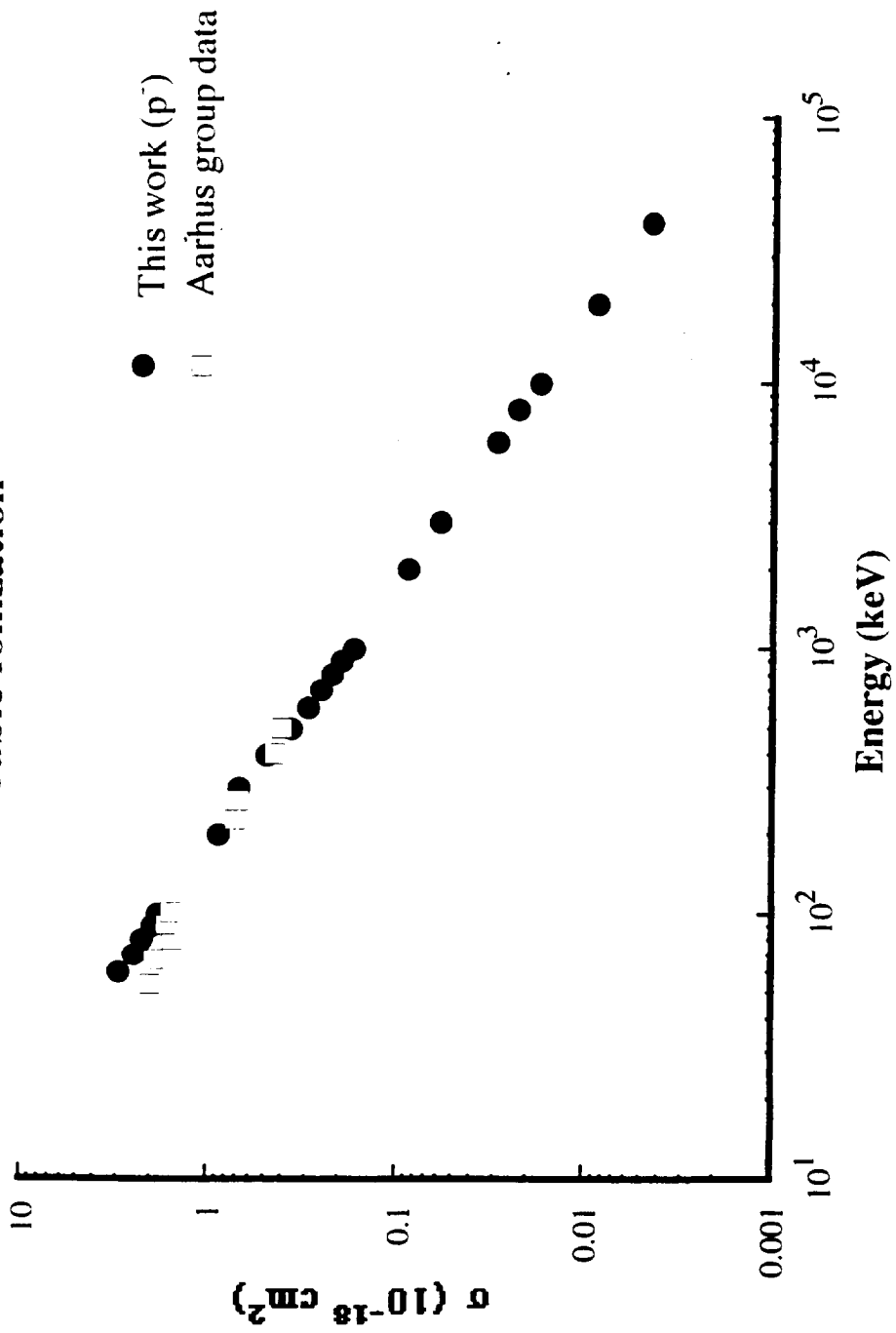# Table 3:   Ratio of double to single ionization cross sections.

Energy (keV)	This work (p+) (x 10-3)	Aarhus group. (p+) (x 10-3)	Shah et al. (p+) (x 10-3)	This Work (p-) (x 10-3)	Aarhus group. (p-) (x 10-3)
50.00	20.2300				
67.10					28.70 ± 2.30
70.00				28.5910	
80.67			12.70 ± 1.20		
100.00	10.1039			21.0229	
102.00					23.10 ± 1.10
200.00				13.2250	
227.90					14.46 ± 0.78
300.00	6.3632			11.7990	
326.30					13.00 ± 0.66
400.00	5.2785			10.9873	
403.18	5.2072		5.36 ± 0.28	10.5294	
403.60					11.32 ± 0.58
500.00	4.7762			9.9972	10.00 ± 0.60
503.97	4.7153		4.65 ± 0.27	8.5462	
667.00					8.50 ± 0.30
700.00	3.5231			7.5163	
800.00	3.4275			7.2449	
806.35	3.4144		3.60 ± 0.20	7.2074	
900.00	3.2343			6.9946	7.15 ± 0.25
1000.00	3.1818	3.22 ± 0.10		6.5322	
1007.90	3.1627		3.29 ± 0.16	6.5243	
1200.00	2.9642	3.12 ± 0.20		6.2312	
1370.00					6.40 ± 0.19
1612.70	2.9263		2.86 ± 0.21	6.0021	
1900.00	2.8859	2.80 ± 0.20		5.8296	5.80 ± 0.25
2000.00	2.8419	2.76 ± 0.06		5.6404	
2015.90	2.8326		2.82 ± 0.26	5.6212	
2100.00	2.8201			5.4923	
2260.00					5.10 ± 0.41

2398 90	2.8189		2.66 ± 0.18	5.3642	
3000 00	2.7759	2.64 ± 0.14		5.1364	
3200 00	2.6925	2.50 ± 0.20		5.0044	5.00 ± 0.25
3300 00	2.6473	2.50 ± 0.15		4 7049	4.50 ± 0.25
4400 00	2.6001	2.50 ± 0.10		4.5488	
7000 00	2.5230	2.51 ± 0.07		3.8582	
10000 00	2.5148	2.49 ± 0.10		3.3233	4.10 ± 0.41
20000 00	2.4498			2.3021	2.90 ± 0.20

Double Ionization

This work (p$^+$)
data of Shah et al.
data of puckett et el.

Energy (keV)

σ (10^{-18} cm^2)

Double Ionization

This work (p⁻)
Aarhus group data

Energy (keV)

σ (10⁻¹⁸ cm²)

Ratio

This work (p⁻)
Aarhus group. (p⁻)
This work (p⁺)
Aarhus group. (p⁺)
Shah et al. (p⁺)

Energy (keV)

R (10⁻³)
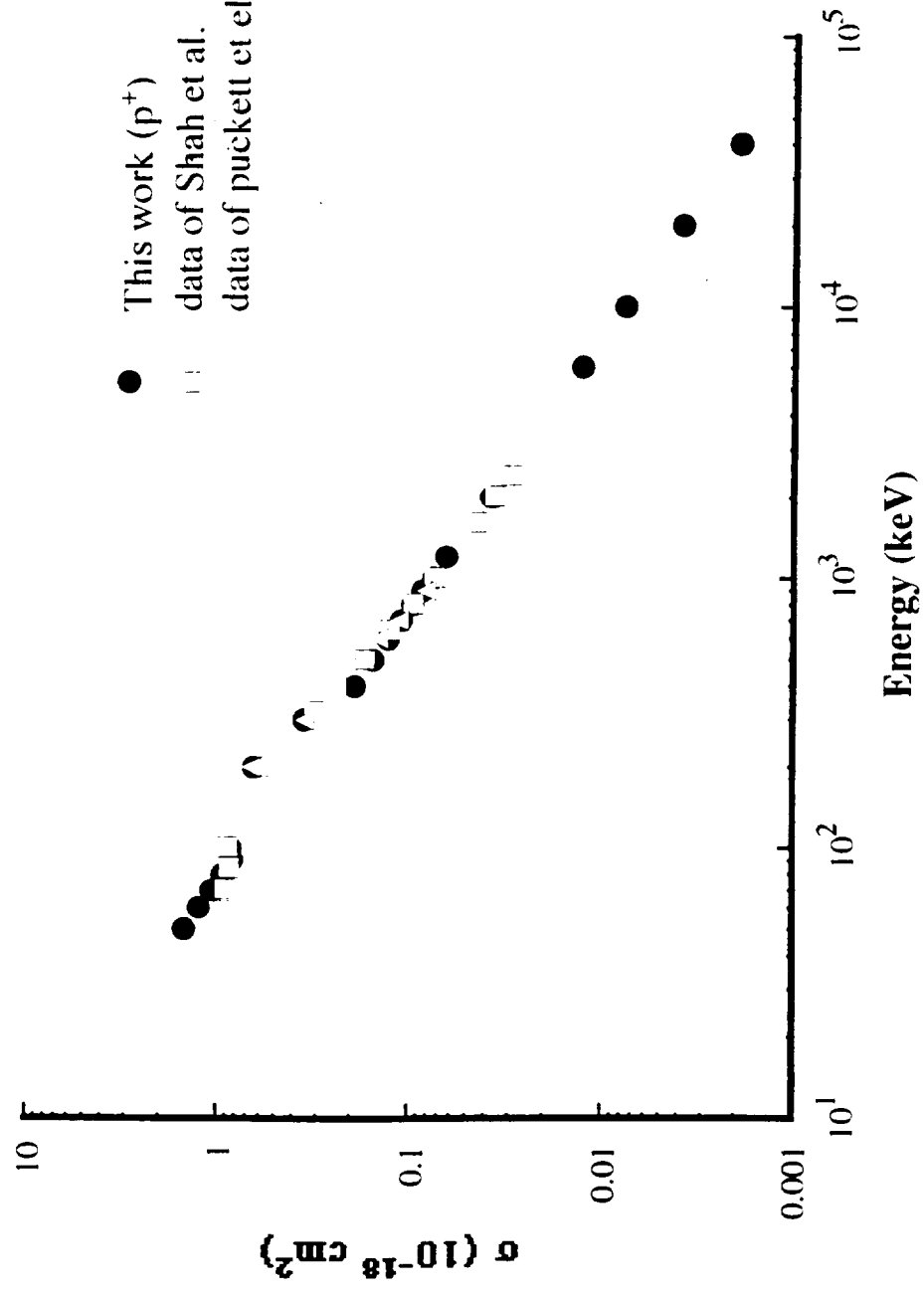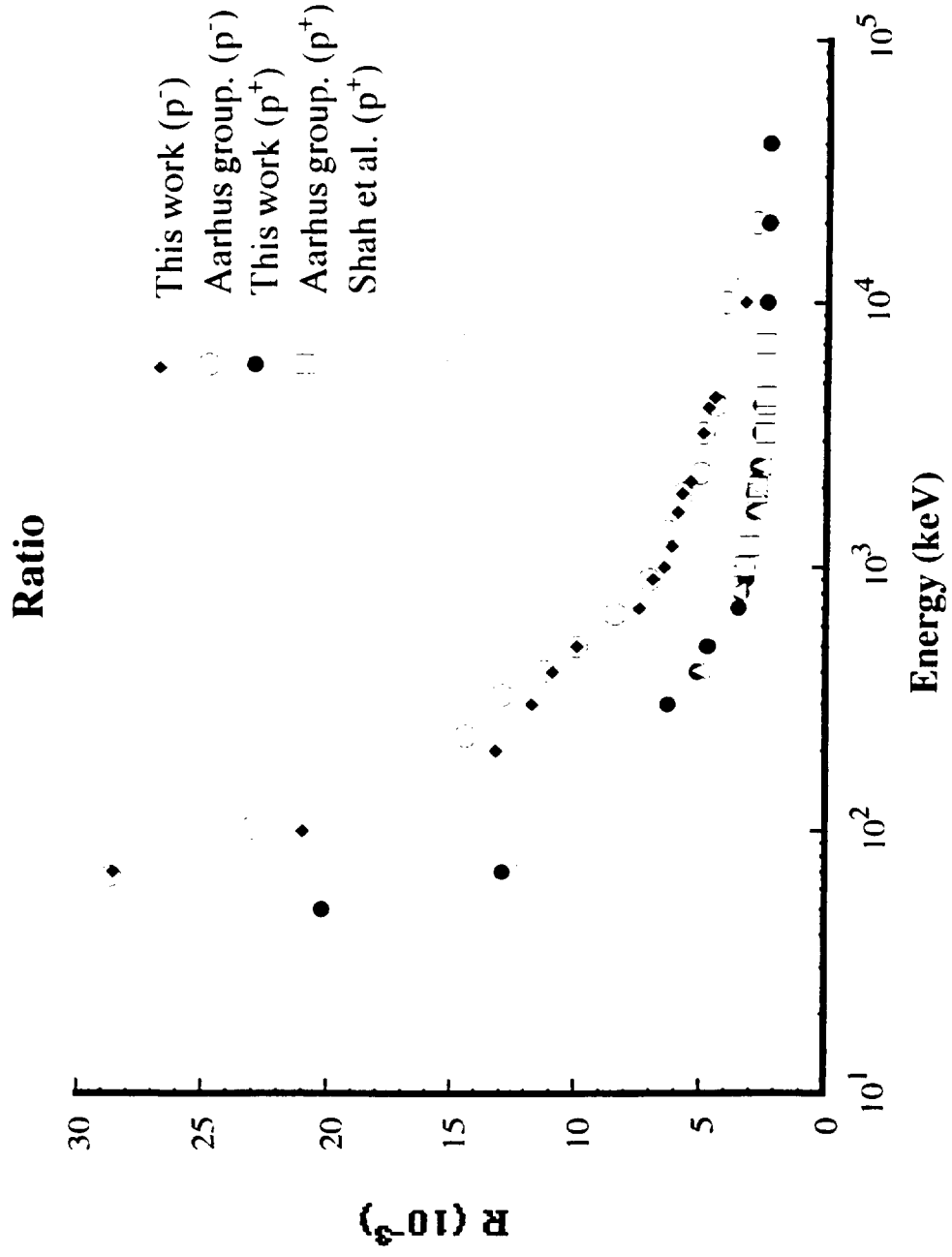
On the ionization of He by proton and anti-proton: I. Single ionization

Tirthanath Das* and F. Bary Malik
Physics Department, Southern Illinois University, Carbondale, IL 62901

*Presently at division of mathematics and science, Shawnee Community College, Ullin, IL 62922, U.S.A.

Abstract. We have presented here calculation of single ionization cross section of He by incident proton and anti-proton within the framework of a coupled channel theory restricted to two channels. The incident energy range considered is from 10 keV to 50 MeV. Projectile wave functions in initial and final channel are taken to be plane waves. The initial ground state wave function of He is taken to be a correlated variational one and the final channel electronic wave function is represented as an antisymmetrized product of a hydrogen-like bound (1s) and continuum Coulomb functions. The calculated results are in reasonable agreement with the observed data and explain the observed difference in cross sections for single ionization by incident proton and anti-proton. These results have been used in calculating the ratio of double to single ionization cross section by proton and anti-proton in a subsequent paper.

1. Introduction

In a series of experiments Andersen et al (1986, 1987) have revealed that the ratio, R, of double to single ionization cross sections of He by incident proton, p^- differs substantially from that by incident anti-proton p^-. Subsequent measurements of anti-proton induced single and double ionization cross sections of He by Andersen et al (1990) and Hvelplund et al (1994) indicate these to differ from those measured for incident p^+ (Shah and Gilbody 1981, 1985 and Shah et al 1989).

Before the series of investigations of single ionization by proton impact done by Shah and Gilbody using crossed-beam coincidence technique, there have been many previous measurements of proton induced single ionization of He using condenser plate technique which are referred to in the 1985 article of Shah and Gilbody. In particular, Rudd et al (1983) have measured single ionization cross section of He by incident protons in the energy range of a few keV to 4000 keV. Their measurements are in general agreement with those of Shah and Gilbody (1985) for energies above 200 keV. It is, therefore, well established that single ionization cross section of He is different for incident p^- and p^-. These findings are significant because, within the framework of Lewis-Merzbacher's theory (henceforth denoted as LM) using plane wave Born approximation (Lewis and Merzbacher 1956) and considering only projectile-electron interaction as perturbation one expects single ionization cross section of He by p^+ and p^- and ratio, R, to be the same.

In Coulomb-Born approximation, used by Trefftz (Trefftz 1963) to study ionization of OV and OVl by electron impact, the wave function of projectile in the final channel for the single ionization case should be represented by Coulomb function. In that case one expects, in principle, a difference in ionization cross section by p^+ and p^- because of the difference in signature of their charges in Coulomb function in the final channel. Similarly, in a distorted wave approximation used by Malik and Trefftz (1961) to study single ionization of OV by electron impact, the single ionization cross section of He by p^+ and p^- should, in principle, differ. In fact, the study of Fainstein et al (1987) using distortion of electron wave function due to incident projectile in eikonal approximation

and Coulomb wave function for ejected electron as well as projectile in the final channel (termed henceforth as CDW-EIS: Continuum-distorted-wave-eikonal-initial-state model) indicates different single ionization cross sections for incident proton and anti-proton, because of the difference of signature for charge of the projectile wave function in the final channel in the two cases. Their calculations for incident anti-proton reasonably account for the data from about 15 keV to 3000 keV (Hvelplund et al 1994). Their calculation for incident proton could reproduce the general trend of the observed cross section as a function of incident proton energy (Shah et al 1985, 1984) but differs by as much as 25% quantitatively (Andersen et al 1990). Unfortunately, no calculation of double ionization cross section of He in this approximation has been reported.

The theoretical calculation based on classical-trajectory-Monte Carlo (termed as CTMC) method (Olson 1987, Shultz 1989) does not provide satisfactory agreement with the data (Hvelplund et al 1990) for proton induced single ionization of He. Calculations of single ionization cross section, based on an improved version of this model (Montemayor and Sciwietz 1989 and Meng et al 1993) that includes correlation between two electrons in terms of screening potentials (the model is termed as dCTMC), give 0.404 and 0.293 Å^2 for 300 and 500 keV incident proton, respectively, and 0.327 and 0.251 Å^2 for incident anti-proton, respectively. The observed data for incident proton energies of 260, 320 and 500 keV/amu are, respectively, 0.587±0.011, 0.516±0.09 and 0.370±0.015 Å^2 (Shah and Gilbody 1985) and for incident anti-proton energies of 270.1, 326.3 and 503.6 keV are, respectively, 0.471±0.08, 0.437±0.08 and 0.354±0.08 Å^2 (Hvelplund et al 1994). Calculated double-ionization cross sections in this method overestimate significantly the proton induced double ionization data at these energies and slightly under estimate the corresponding anti-proton data.

Ford and Reading (1987a, b, 1989, 1994) have approached the problem from time-dependent view point. Their model, termed as forced-impulse method or FIM, breaks up the time development in small segments. Within a given segment, the electrons are treated in an uncorrelated fashion but between the segments the correlation is considered. Their earlier calculations done for incident energies higher than a few hundred keV

3

including s and p electron orbitals are in qualitative agreement with the proton data but falls short on the ratio of double to single ionization by p⁻. However, their latest calculation done only at 300, 500 and 1000 keV incident energies (Ford and Reading 1994) estimating the contributions of 9d orbitals to both single and double ionization are in reasonable quantitative agreement with the data around these energies. For example, their estimated cross sections for single ionization for incident proton are 0.498, 0.346 and 0.203 Å² at incident energies of 300, 500 and 1,000 keV, respectively, which are close to the observed values of 0.516±0.009, 0.370±0.015 and 0.226±0.008 Å² measured (Shah and Gilbody 1985) at incident energies of 320, 500 and 1000 keV/amu, respectively. Similarly, they estimate single ionization cross sections by incident anti-proton of energies 300, 500 and 1,000 keV to be 0.458, 0.331 and 0.188 Å², respectively. These are close to observed values (Hvelplund et al 1994, Andersen et al, 1990) of 0.471±0.02, 0.437±0.02, 0.354±0.02 and 0.195±0.01 Å² at incident energies of 270.1, 326.3, 503.6 and 1130 keV, respectively. So far, calculations at other energies, particularly lower ones have not been reported, although the measurements are available.

The early calculations of Bell and Kingston (1969) using plane wave Born approximation that approximates the electron-projectile interaction as dipole or the corresponding velocity operator (so called Bethe (1930) approximation) and uses a correlated ground state wave function do not agree with the data. In particular, the maximum of the cross section is not accounted for (Shah and Gilbody 1985). Of course, the anti-proton induced single ionization cross section is equal to that by proton in this approximation, and the observed difference in data in the two cases cannot be explained.

Toburen et al (1978) have calculated single ionization cross section at 300, 500 and 1000 keV incident proton energies in the LM approximation, except replacing initial hydrogenic He ground state wave function by Herman-Skillman's (1963) parameterized Hartree-Fock wave function and the Sommerfeld Coulomb wave function for ejected electron by a distorted wave (Manson et al 1975). Their calculated result agrees with the data of Rudd et al (1983) at 300 keV but is slightly higher than the data at 500 and 1000 keV, and differ significantly from the 100 keV data. Lewis and Merzbacher (1958) have

4

done calculation in the LM approximation up to about 200 keV incident proton energies, with limited agreement with the data.

Das and Malik (1994, 1995) have analyzed single and double ionization of He by proton and anti-proton using coupled channel approach (Mott and Massey 1965 or Malik and Trefftz 1961) restricting it to two channels, initial and final, and representing projectiles in both channels by plane waves. Their calculations for a few very low and very high energies are in very good agreement with the data for single and double ionization. In this paper we extend the calculation from 10 keV to 50 MeV for proton and anti-proton induced single ionization of Helium and compare them with the available data. We also present calculation in the LM approximation in this energy range. In a subsequent paper calculations for double ionization cross section and the ratio R for incident p⁺ and p⁻ will be presented for incident energies ranging from a few tens of keV to 20 MeV.

We present the theory in the following section and discuss the results in section 3. The conclusion and acknowledgment are presented in sections 4 and 5.

2. Theory

The Schroedinger equation for an incident projectile and a He-atom in the center of mass system of the incident particle and the nucleus of He may be written as

$$\left[-\frac{\hbar^2}{2\mu}\nabla_R^2 - \frac{-\hbar^2}{2m}(\nabla_1^2 + \nabla_2^2) - (\mp Ze^2/R) - Ze^2/r_1^2 - Ze^2/r_2 + e^2/r_{12} \mp \frac{e^2}{|R-r_1|} \mp \frac{e^2}{|R-r_2|} - E \right]\psi(R,r_1,r_2) = 0 \qquad (1)$$

In (1) μ and m are reduced masses of projectile and electrons with respect to He-nucleus, respectively. r_1, r_2 and R are coordinates of electrons 1 and 2 and the projectile, respectively. Minus and plus sign refer, respectively, to incident proton and anti-proton. In (1) $r_{12} = |r_1 - r_2|$, the interelectronic distance.

One may expand ψ (R, r_1, r_2) in the following orthonormal set

$$\psi(R,r_1,r_2) = \Sigma_n F_n(R)\Sigma_m \psi_{nm}(r_1,r_2) \qquad (2)$$

5

In view of the fact that the two electrons are far apart in the final channel and do not interact, we define the orthonormal set to be the eigenfunctions of the following hermitian Hamiltonian:

$$H_0 \psi_{nm} \equiv \left[-\frac{h^2}{2m} (\nabla_1^2 + \nabla_2^2) - \frac{Ze^2}{r_1} - \frac{Ze^2}{r_2} \right] \psi_{nm}(r_1, r_2) = E_m \psi_{nm}(r_1, r_2) \tag{3}$$

The above Hamiltonian represents accurately the asymptotic situation in the final channel where the ejected electron is far away from the He^+ ion and hence e^2/r_{12} term is negligible.

One may obtain the following equation for $F_n(\mathbf{R})$ by taking a scalar product of (1) with respect to ψ_{mn} and integrating over the coordinates r_1 and r_2:

$$\left\{ \frac{h^2}{2m} \nabla^2 + (E - E_n) \pm \frac{Ze^2}{R} F_n(\mathbf{R}) \right\} F_n(\mathbf{R})$$

$$= - \int dr_1 dr_2 \sum_m \psi_{mn}(r_1, r_2) \left\{ \mp \frac{Ze^2}{|R - r_1|} \mp \frac{Ze^2}{|R - r_2|} + \frac{e^2}{r_{12}} \right\} \sum_{n' \neq n} F_n(\mathbf{R}) \sum_m \psi_{m'n}(r_1 r_2) \tag{4}$$

The orthogonality condition on ψ_{nm} has been used in deriving (4). Using

$$k_n^2 = \frac{2m}{h^2} (E - E_n) \tag{5}$$

one gets

$$(\nabla_2 + k_n^2 \pm \frac{Ze^2}{R}) F_n(\mathbf{R})$$

$$= - \frac{2m}{h^2} \int dr_1 dr_2 \sum_m \psi_m^*(r_1, r_2) \left\{ \mp \frac{Ze^2}{|R - r_2|} \mp \frac{Ze^2}{|R - r_2|} + \frac{e^2}{r_{12}} \right\} \sum_{n' \neq n} F_n(\mathbf{R}) \sum_m \psi_{m'n}(r_1, r_2) \tag{6}$$

6

The equation (6) represents an infinite set of coupled channel equations and suitable approximations are needed before actual calculations could be carried out.

The above equation is now to be solved with the following boundary condition in the final channel

$$\lim_{|R| \to \infty} F_n(R) - f_n(\theta, \varphi) \frac{e^{i(k_n R - \eta \ell n R)}}{R}$$

(7)

with $\eta = \mu Z e^2 / \hbar k_n$, Z being the projectile charge. $f_n(\theta, \varphi)$ is the scattering amplitude in the channel n at angles (θ, φ) defined with respect to the direction of incident momentum. Following Mott and Massey (1965), one may obtain the expression of the differential cross section

$$\frac{d\sigma}{d\Omega} = |f_n \theta, \varphi|^2 = \frac{4\pi^2 \mu^2}{h^4} \frac{k^n}{k_o} \int\int\int dr_1 dr_2 dR F_{nh}^*(R) \sum_m \psi_{nm}^*(r_1, r_2)$$
$$H_{int}(R, r_1, r_2) \sum_{n'm'} F_n(R) \psi_m(r_1, r_2)|^2$$

(8)

with

$$H_{int}(R, r_1, r_2) = \mp \frac{Ze^2}{|r_1 - R|} \mp \frac{Ze^2}{|r_2 - R|} + \frac{e^2}{r_{12}}$$

(9)

k_o in (8) is the incident channel wave number and $F_{nh}^*(R)$ is the solution of the homogeneous part of (6) compatible with asymptotical boundary condition (7), i.e., outgoing Coulomb wave function for p^+ or p^-.

The total single ionization cross section, σ^+, is obtained by integrating over the solid angle $d\Omega$.

It is important to note that the expression (8) is exact and the e^2/r_{12} term is to be included in calculating matrix elements. In case electron-projectile interaction is switched off, the projectile wave function is zero and hence matrix elements of e^2/r_{12} and cross section are zero, i.e., there is no transition, as it should be.

7

Since the energy interval considered in this work is significantly larger than the ionization energy, we consider explicitly only two channels, the initial incident and the final. In this two-channel approximation the summation over n in (2) has two terms, the initial channel denoted by $F_o(\mathbf{R})$ and final channel noted $F_n(\mathbf{R})$. The summation over n' in (8) reduces to the following term:

$$\sum_{n'm'} F_{n'}(R)\psi_{n'm'}(R,r_1,r_2) \approx F_o(R)\sum_{m'} \psi_{om'}(r_1,r_2) = F_o(R)\psi_g(r_1,r_2) \tag{10}$$

ψ_g in (10) is the correlated ground state wave function of He.

In this approximation the differential cross section is given by

$$\frac{d\sigma}{d\Omega} = \frac{4\pi^2\mu^2}{h^4}\frac{k_n}{k_o}\Big| \int dr_1 dr_2 dR F_{nh}^{*}(R)\psi_n(r_1,r_2) $$
$$H_{int}(R,r_1,r_2)F_o(R)\psi_g(r_1,r_2)\Big|^2 \tag{11}$$

In case $F_{nh}(\mathbf{R})$ and $F_o(\mathbf{R})$ are taken, respectively, to be Coulomb and plane waves this approximation is equivalent to Coulomb Born approximation (CBA) used by Trefftz (1963) for single ionization of oxygen ions by electron.

The two channel plane wave Born approximation (2cPWBA) is obtained by replacing F_o and F_{nh} with plane wave function in respective channel. The differential cross section in the 2cPWBA is given by

$$\frac{d\sigma}{d\Omega} = \frac{4\pi^2\mu^2}{h^4}\frac{k_n}{k_o}\Big| \int dr_1 dr_2 dR \exp\big[i(k_o\hat{n}_o - k_n\hat{n})\cdot R\big]$$
$$\psi_n^{*}(r_1,r_2)H_{int}(R,r_1,r_2)\psi_g(r_1,r_2)\Big|^2 \tag{12}$$

Total cross section is obtained by integrating over $d\Omega$. In (12) $\hat{n}_o$ and $\hat{n}$ are unit vectors in the direction of momenta in incident and final channels, respectively.

The LM approximation is obtained by (i) replacing ψ_g with a product of two hydrogen-like (1s) wave functions, and (ii) neglecting e^2/r_{12} term in H_{int} $(\mathbf{R}, \mathbf{r}_1, \mathbf{r}_2)$.

The Bethe approximation or sometime denoted as zero-order or lowest-order Born

8

approximation is obtained by (i) omitting e^2/r_{12} from H_{int}, (ii) replacing ψ_g in (12) with a product of two (ls) hydrogen-like wave functions and (iii) keeping only terms up to dipole in the expansion of electron-projectile interaction.

Because H_{int} $(\mathbf{R}, \mathbf{r}_1, \mathbf{r}_2)$ given by (9) is different for incident proton and anti-proton, the calculated single ionization cross section in the 2cPWBA for the two cases differ, in principle, from each other. On the other hand, in the LM and Bethe approximations, they should be the same.

In the next section we present calculations in the LM approximation and the 2cPWBA.

Calculations in the LM approximation are done taking electronic wave function in the initial state to be a product of two hydrogenic (ls) functions, each having an effective charge 1.6875 and final state electronic wave function to be a product of a hydrogenic (ls) wave function with effective charge 2.0 and a continuum Coulomb wave function in Sommerfeld representation (Wentzel, 1929; Bethe, 1930; Sommerfeld, 1931) with an effective charge of 1.09.

The initial state wave function used in the 2cPWBA is the following correlated wave function due to Hylleraas (1930):

$$\psi_g(r_1, r_2) = N exp(-(\gamma/a_o)(r_1 + r_2))(1 + cr_{12}^2) \tag{13}$$

In (13) N and a_o are, respectively, the normalization constant and the Bohr radius. γ and c are determined from the Raleigh-Ritz variational principle to be 1.69 and 0.142, respectively. The variational ground state energy is -78.28eV which is very close to the observed value of -78.62 eV. The finale state wave function in the 2cPWBA is taken to be the same as the one in the LM approximation.

3. Results and Discussion

(a) *The LM approximation*

In table 1 we present our calculated results in the LM approximation in the incident energy range of 10 keV to 50 MeV for both incident proton and anti-proton. In the energy range of 10 keV to 200 keV, our calculations are in agreement with those of Lewis and Merzbacher (1958) which also serve as a check to our numerical code. In Fig. 1 the data of Shah and Gilbody (1981, 1982, 1985 and 1989) and Rudd et al. (1983) for the single ionization cross section of He by proton have been presented as a function of incident energies and compared to our calculation in the LM approximation. The theory can account for the data satisfactorily for incident energies greater than a few hundred of keV. At lower energies there is room for improvement.

(b) *2cPWBA for incident proton*

In table 1 we have also presented our calculation for single ionization cross section of He by incident protons in the energy range of 10 keV to 50 MeV in the two channel plane wave Born approximation. In general the calculated cross sections in the 2cPWBA are lower than those in the LM approximation. The difference is about 10% below 50 keV and above 30 MeV and only a few percent at other energies. In Fig. 2, we have compared our calculation with the data and the agreement is excellent in the entire energy range. In particular, the agreement between the theory and experiment has improved significantly at lower energies compared to those calculated in the LM approximation.

(c) *2cPWBA for incident anti-proton*

In table 2 we have presented our calculation in the 2cPWBA for incident anti-proton in the energy range of 10 keV and 50 MeV. They are compared to the observed single ionization cross section in Fig. 3. The calculation reproduces the general energy dependence of the cross section and the data quite well. However, the calculated values between 80 keV and 300 keV are somewhat higher than the data. Calculated cross section for incident anti-proton is always higher than those for proton but the difference is insignificant in the energy range of 70 to 2000 keV.

(d) *General discussion*

For the proton induced single ionization of He, our calculation can account for the observed cross section in the entire energy. The agreement between the data and our calculation is slightly better than the one between the data and the calculation of Fainstein et al. (1987) particularly below 150 keV and above 1000 keV. The Bethe approximation used by Bell and Kingston is inadequate at lower energies. The calculated values in the 2cPWBA agree with the data somewhat better than the calculations in the dCTMC (Meng et al 1993) and in the FIM approximations (Ford and Reading 1994). The LM approximation used by us is very similar to the method of Toburen et al (1975, 1978), except for the use of wave functions for initial electronic states, and the numerical numbers in the two cases are very close.

The contribution from the matrix elements of e^2/r_{12} term to cross section for the proton is only significant at low energies, i.e., below 100 keV. In Table 3, we have compared calculations in the 2cPWBA done using plane wave for the ejected electron instead of Coulomb wave function to compute matrix elements of the e^2/r_{12} term and they do not differ significantly. It is, therefore, sufficient to evaluate its matrix element using plane wave for the ejected electron, instead of Sommerfeld representation of Coulomb wave function. The use of plane wave for the ejected electron simplifies the calculation considerably.

For incident anti-proton the observed data agree very well with our calculation for incident energies greater than about 200 keV. At lower energies, the calculation of Fainstein et al (1987) are in somewhat better agreement with the data compared to ours. The data are in better agreement with our calculation compared to those done in the FIM (Ford and Reading 1994) and in dCTMC (Meng et al 1993).

The 2cPWBA theory predicts that at very high incident energies i.e., energies above a few MeV to non-relativistic energy the single ionization cross section of He by anti-proton should be higher than that by incident proton. This is the consequence of the difference in the perturbed potential, (9), in two cases. The data are available up to about 2.5 MeV for incident proton (Shah et al 1989) and 3.0 MeV for incident anti-proton

11

(Andersen et al 1990) and seem to borne out this theoretical calculations. It would certainly be most interesting to have data at higher incident energies.

At incident energies lower than about 100 keV, our calculated cross section for incident anti-proton lie a little higher than those for protons, whereas the data indicate the situation to be the opposite. At this incident energy region, the difference in Coulomb distortion in the two cases is likely to play an important role. In addition, the possibility of resonances for the anti-proton-Helium system may have to be considered. In the first approximation the location of such resonances is determined by the eigen-energies of the homogeneous part of (4) (Malik 1992). Clearly, there should be no resonance for the incident proton case since the (p$^-$ - He) system is unbound. On the other hand, the (p$^-$ - He) system has bound states, the energies of which are given by $E = -(20.0 \text{ keV})Z^2/n^2$ in the hydrogen-like approximation. Hence, the resonances could contribute to the cross section in the region of a few tens of keV for the anti-proton case and the spacing of these resonances should be from about a tenth to a few keV. It is interesting to note that the measured single-ionization cross section for the incident proton in the energy range of a few tens of keV is a smooth function of energy (Shah et al 1989) which is expected in the absence of resonances but the same for incident anti-proton seems to exhibit some structure (Hvelplund et al 1994) as expected in the presence of resonances. It would be most interesting to establish whether such structures are actually present for the anti-proton case.

4. Conclusion

The 2cPWBA can reasonably account for the energy dependence of the observed single ionization cross section of He by proton as well as anti-proton in the incident energy range of 10 keV to 3 MeV. The calculation has been presented up to 50 MeV incident energy with a view of using these results to calculate the ratio of double to single ionization in a subsequent paper. The data on the ratio are available in the MeV region. The inclusion of e^2/r_{12} term is not critical at energies higher than a few hundred keV and

lower than a few MeV but important at lower and higher energies. The success of the LM approximation, 2cPWBA and CDW-EIS in reproducing the data reasonably implies that the Coulomb distortion for the ejected electron must be included in calculation. Inclusion of ground state correlation in the initial electronic state of He is important at energies below a few hundred keV.

5. Acknowledgment

References

Andersen L H, Hvelplund P, Knudsen H, Møller S P, Elsner K, Rensfelt K G, and
Uggerhøj E 1986 *Phys. Rev. Lett.* **57** 2147

Andersen L H, Hvelplund P, Knudsen H, Møller S P, Sorensen A H, Elsner K, Rensfelt
K-G and Uggerhøj E 1987 *Phys. Rev.* **A 36** 3612

Andersen L H, Hvelplund P, Knudsen H. Møller S P, Pederson J O P, Tang-Podersen S,
Uggerhøj E, Elsner K and Morenzoni E 1989 *Phys. Rev.* **A 40** 7366

Andersen L H, Hvelplund P, Knudsen H, Møller S P, Pedersen J O P, Tang-Pedersen S,
Uggerhøj E, Elsner K, and Morenzoni E 1990 *Phys. Rev.* **A 41** 6536

Bethe H 1930 *Ann. D. Physik* **5** 325

Fainstein P D, Ponce V H and Riverola R D 1987 *Phys. Rev. A* **36** 3639

Ford A L and Reading J F 1988 *J. Phys. B: At. Mol. Opt. Phys.* **21** 3747

_____ 1994 *J. Phys. B: At. Mol. Opt. Phys.* **27** 4215

Herman F and Skillman S 1963 *Atomic structure calculations* (Prentice-Hall, Englewood
Cliffs, NJ, USA)

Hvelplund P, Knudsen H, Mikkelsen U, Morenzoni E, Møller S P, Ugggerhøj E and
Worm T 1994 *J. Phys. B: At. Mol. Opt. Phys.* **27** 925

Hylleraas E A 1930 *Zeit. Physik* **65** 209

Lewis H W and Merzbacher E 1958 *Handbach der Physik XXXIV* **166**

Malik F B and Trefftz E 1961 Z. Natwrforsch. *16a 583*

Malik F. B 1992 Condensed Matter Theories. **7** 11

Manson S T, Toburen L H, Madison D H and Stolterfohl N 1975 *Phys. Rev.* **A 12** 60

Mott N F and Massey H S W 1965 *The theory of atomic collision* (Third edition)
(Oxford Clarendon Press)

14

Olson R E 1987 *Phys. Rev.* **A 36** 1519

Puckett L J and Martin D W 1970 *Phys. Rev.* **A 1** 1432

Reading J F and Ford A L 1987a *Phys. Rev. Lett.* **58** 543

———————— 1987b *J. Phys. B: At. Mol. Phys.* **20** 3747

Rudd M E, DuBois R D, Toburen L H, Ratcliffe C A and Goffe T V 1983 *Phys. Rev.* **A 28** 3244

Schultz D R 1989 *Phys. Rev.* **A 40** 2330

Shah M B and Gilbody H B 1981 *J. Phys. B: At. Mol. Phys.* **14** 2361

———————— 1985 *J. Phys. B: At. Mol. Phys.* **18** 899

Shah M B, McCallion P and Gilbordy H B 1989 *J. Phys. B: At. Mol. Opt. Phys.* **22** 3037

Sommerfeld A 1931 *Ann. Physik* **9** 257

Toburen L H, Mason S T and Kim Y K 1978 *Phys. Rev.* **A 17** 148

Trefftz E 1963 *Proc. Roy. Soc.* (Lond) **A 271** 379

Wentzel G 1929 *Zeit. Physik* **58** 349

Table Caption

Table 1   Comparison of calculated single ionization cross section of He by proton in the LM approximation (column 2) and the 2cDWBA (column 3) with the selected observed ones in experiments of Shah and Gilbody (1981, 1985), Shah et al (1989) and Puckett et al (1970).

Table 2   Comparison of calculated single ionization cross section of He by anti-proton in the 2cDWBA with the selected observed data of the Aarhus group (Andersen et al, 1990 and Hvelplund et al 1994).

Table 3   Comparison between calculations of single ionization cross section of He by p^- done in the 2cPWBA (column 2) and the approximation where the plane wave function is used for ejected electron in evaluating the matrix element of e^2/r_{12} (column 1).

Figure Caption

Fig. 1   Comparison between the calculated single ionization cross section of He by proton done in the LM approximation and selected data. Shah et al refer to data reported in (Shah and Gilbody 1981, 1985 and Shah et al 1989). Rudd et al and Puckett et al refer to data from (Rudd et al 1983) and (Puckett and Martin 1970), respectively.

Fig. 2   Comparison between the calculated single ionization cross section of He by proton done in the 2cDWBA with selected data referred to in the caption of Fig. 1.

Fig. 3   Comparison between the calculated single ionization cross section of He by anti-proton done in the 2cDWBA and selected data of the group primarily based at Aarhus. Aarhus group data refer to (Andersen et al 1990) and (Hvelplund et al 1994).

Table 1:   Single ionization cross section by proton.

Energy (keV)	σ (LM) $(10^{-16} cm^2)$	σ (This work) $(10^{-16} cm^2)$	σ (Shah et al.) $(10^{-16} cm^2)$	σ (Puckett et al.) $(10^{-16} cm^2)$
10.00	0.087826	0.08098		
11.09			0.067 ± 0.003	
19.15			0.192 ± 0.006	
20.00	0.31223	0.29868		
28.22			0.340 ± 0.014	
30.00	0.51242	0.49882		
50.00	0.75246	0.73939		
64.51			0.750 ± 0.023	
70.00	0.84746	0.83285		
100.00	0.85942	0.84991		
100.79			0.845 ± 0.046	
131.03			0.809 ± 0.012	
150.00				0.880
200.00	0.70243	0.69203		0.718
200.59			0.693 ± 0.017	
300.00	0.57224	0.55834		0.510
400.00				0.429
403.18			0.441 ± 0.009	
500.00	0.41026	0.40160		0.350
503.97			0.370 ± 0.015	
600.00				0.314
700.00	0.32354	0.31343		0.273
900.00				0.227
1000.00	0.24879	0.23698		0.207
1000.79			0.226 ± 0.008	
2000.00	0.14394	0.13287		
2000.79			0.1295 ± 0.0011	
2398.90			0.1125 ± 0.0013	
5000.00	0.061243	0.058680		
7000.00	0.044078	0.042975		

9000.00	0.039741	0.033956
10000.00	0.032416	0.030742
30000.00	0.016347	0.010692
40000.00	0.0099929	0.0080732
50000.00	0.0072450	0.0064851

Table 2:   Single Ionization cross section by anti-proton.

Energy (keV)	σ (This work) (10^{-16} cm^2)	σ (Aarhus data) (10^{-16} cm^2)
10.00	0.10570	
12.90		0.199 ± 0.037
20.00	0.32337	
24.20		0.473 ± 0.038
30.00	0.52567	
34.60		0.591 ± 0.027
50.00	0.76732	
53.90		0.741 ± 0.030
70.00	0.86083	
100.00	0.87632	
101.60		0.645 ± 0.026
194.40		0.528 ± 0.020
200.00	0.71770	
270.10		0.471 ± 0.019
300.00	0.58235	
326.30		0.437 ± 0.017
500.00	0.42529	
645.00		0.310 ± 0.022
700.00	0.33639	
1000.00	0.26054	
1130.00		0.195 ± 0.014
2000.00	0.15604	
2470.00		0.105 ± 0.012
2918.00		0.099 ± 0.012
3000.00	0.11617	
5000.00	0.081557	
7000.00	0.065762	
9000.00	0.056724	
10000.00	0.053450	
30000.00	0.033468	
40000.00	0.030741	
50000.00	0.029239	

Table 3:

Energy (keV)	σ (plane wave) $(10^{-16}\,cm^2)$	σ (Sommerfeld) $(10^{-16}\,cm^2)$
10.00	0.08195	0.08098
20.00	0.30163	0.29868
30.00	0.50312	0.49882
50.00	0.74468	0.73939
70.00	0.83808	0.83285
100.00	0.85457	0.84991
200.00	0.69506	0.69203
300.00	0.56060	0.55834
500.00	0.40255	0.40160
700.00	0.31455	0.31343
1000.00	0.23779	0.23698
2000.00	0.13330	0.13287
3000.00	0.093427	0.093131
5000.00	0.058862	0.058680
7000.00	0.043107	0.042975
9000.00	0.034059	0.033956
10000.00	0.030835	0.030742
30000.00	0.010723	0.010692
40000.00	0.0080959	0.0080732
50000.00	0.0065040	0.0064851

Single Ionization

This work (p⁺)
data of Shah et al.
data of Rudd et al.
data of Puckett et al.

Energy (keV)

σ (10^{-16} cm^2)

Single Ionization

σ (10^{-16} cm^2)

Energy (keV)

● This work (p$^+$)
□ data of Shah et al.
△ data of Rudd et al.
▽ data of Puckett et al.

Single Ionization

This work (p⁻)
Aarhus group data

Energy (keV)

σ (10⁻¹⁶ cm²)